HIGH PRECISION THORIUM-230 AGES OF CORALS AND THE TIMING OF SEA LEVEL FLUCTUATIONS IN THE LATE QUATERNARY

Thesis by

R. Lawrence Edwards

In Partial Fulfillment of the Requirements

for the Degree of

Doctor of Philosopy

California Institute of Technology

Pasadena, California

1988

(Submitted January 7, 1988)

This work is dedicated to

Mom and Dad;

Margo, Joan, and Edith;

and

Melissa

ACKNOWLEDGMENTS

I thank Professor G.J. Wasserburg for his guidance. His ability to distill a problem into its most fundamental components and his energy in seeking solutions to each component have left a lasting impression on me. This work was possible only because of his efforts to design and redesign an appropriate physical and intellectual environment over the course of decades.

Dr. J.H. Chen welcomed me to work on a project which he had started and graciously divulged secrets which he had accumulated since the time when he himself was a graduate student. His excitement in trying new approaches, his attention to detail, and the companionship which he has provided will serve as an example for me.

Dr. D.A. Papanastassiou willingly shared his time and great knowledge of mass spectrometric and laboratory procedures. Others in the Lunatic Asylum contributed to my general well being. Dr. H.H. Ngo introduced me to chemical procedures. Paul Knust-Graichen lent technical support. David Pickett and Jay Banner added much needed good humor. Henry Shaw, Oded Navon, and Cheryl Brigham provided companionship and discourse often at odd hours. Priscilla Piano was sensitive to the needs of the inmates and insured the Asylum's smooth operation.

Ed Stolper served as my academic advisor and provided good advice at only the right times. Hugh Taylor held stimulating classes. Discussions with Kerry Sieh added perspective to this work.

I am particularly grateful to members of the scientific community

who contributed to this work. Fred Taylor provided expert guidance in the field and hours of stimulating discussion. Wally Broecker, Art Bloom, and Richard Ku shared ideas and enthusiasm. Karl Turekian provided valuable suggestions. R.K. Matthews and Paul Aharon contributed well documented carbonate samples. B.R. Constantz showed me techniques for etching and taking scanning electron photomicrographs of carbonates. C. Reimers and P.M. Williams assisted in collection of sea water.

Thanks are owed to Robin Chang for his continuing friendship, and special thanks to Missy McDonald for her support.

PREFACE

This thesis is composed, in part, of work that has been published elsewhere. The original articles and abstracts are in Appendices B and C. Included in these appendices is a study of the Nd and Sr isotopic systematics of mafic and ultramafic bodies in the Ural Mountains. This study is included because it introduced me to the world of isotope systematics and clean room chemical procedures. The uranium and thorium isotopic data for all the corals in this study can be found in the tables comprising Appendix A.

ABSTRACT

Mass spectrometric techniques for the measurement of ^{230}Th and ^{234}U have been developed. These techniques have made it possible to reduce the analytical errors in ^{230}Th dating of corals using very small samples. Samples of 8 X 10^7 atoms of ^{230}Th can be measured to an accuracy of ±130 °/oo (2 sigma), 6 X 10^8 atoms of ^{230}Th can be measured to an accuracy of ±29 °/oo, and 3 X 10^{10} atoms of ^{230}Th can be measured to an accuracy of ±2 °/oo. The time range over which useful data on corals can now be obtained ranges from 15 to 500,000 years. The error in age (based on analytical error) for a sample that is 18 years old is ±3 years (2 sigma). The error is ±5 years at 180 years, ±44 years at 8294 years, and ±1 ky at 123.1 ky. For young corals, this approach may be preferable to ^{14}C dating.

Fluctuations in climate result in changes in sea level because the ice stored in continental glaciers is ultimately derived from the ocean. Certain species of coral grow close to the sea surface. Fossils of these species therefore record the former height of the sea surface. The precision with which the age of a coral can now be determined makes it possible to determine, with some precision, the timing of sea level fluctuations in the late Quaternary. This record will allow a critical test of the Milankovitch hypothesis, which predicts the timing of Pleistocene climate fluctuations from changes in the distribution of solar insolation that result from changes in the earth's orbital geometry. Analyses of a number of corals that grew during the last interglacial period yield ages of 122 to 130 ky. The

ages coincide with or slightly postdate the summer solar insolation high at 65°N latitude, which occurred 128 ky ago. This supports the idea that changes in Pleistocene climate can be the result of orbital forcing.

Apparent fluctuations in sea level recorded on tectonically active shorelines are the result of both sea level change and vertical tectonic movement. If the record of sea level change is known (e.g., from the coral record in a stable area), this record can be subtracted from the record of apparent sea level change, in the tectonically active area, to yield a record of vertical tectonic movement. The precision with which coral ages can now be determined may allow us to resolve the ages of individual coseisimic uplift events and thereby date prehistoric earthquakes.

This possibility has been examined at two localities, northwest Santo Island and north Malekula Island, Vanuatu. Previous work (Taylor et al., 1980, 1985a, 1987) showed (using the counting of annual growth bands to determine ages) that the tops of partially emerged coral heads at each locality died at the same time as the last major earthquake at each locality (M_S=7.5, 1973, on northwest Santo; and M_S=7.5, 1965, on north Malekula). It was concluded that the tops of these coral heads were killed by coseismic uplift. At each locality, there were also completely emerged coral heads, which were inferred to have been killed by earlier coseismic uplift events. These could not be dated by growth band counting because the coral heads were completely dead.

The accuracy of ^{230}Th ages of very young corals was tested by dating portions of three corals whose ages were known from the counting

of growth bands. Within analytical error, the ^{230}Th ages were the same as the growth band ages for all three samples (dates of growth by counting growth bands - A.D. 1971 to 1973, A.D. 1935 to 1939, and A.D. 1804 to 1810; dates of growth from ^{230}Th measurements - A.D. 1969±3, A.D. 1932±5, and A.D. 1806 5 [2 sigma]) demonstrating that the ^{230}Th ages were accurate.

The ^{230}Th growth dates of the surfaces of adjacent emerged coral heads, collected from the same elevation (1.2 m) on northwest Santo Island, were, within analytical error, identical (A.D. 1866±4 and A.D. 1864±4). This indicates that the corals died at the same time and is consistent with the idea that they were killed by coseismic uplift. Similar adjacent coral heads on north Malekula Island yielded ^{230}Th growth dates of A.D. 1729±3 and A.D. 1718±5. The ages are similar but analytically distinguishable. The difference may be due to erosion of the outer, younger, portion of the latter coral head. Using the date of the large historical earthquake at each locality and the ^{230}Th growth date of the emerged corals at each locality, recurrence intervals of 108 years for northwest Santo and 236 years for north Malekula are calculated.

This experiment has shown that it is possible to date corals that grew in the past several centuries to accuracies of ±3 to ±5 years (2 sigma). The main problems with applying this approach to determine seismic histories will be associated with the preservation of fossil corals that have been killed by coseismic uplift and the ability to identify such features in the field.

TABLE OF CONTENTS

1. Introduction

The study of natural processes that have occurred in the geologically recent past is satisfying and important because (1) young features tend to be well preserved in the geologic record, (2) well constrained studies can be designed since parameters may be similar to their present day values, and (3) ongoing processes can be observed today and may be documented in the historical record. Thus, the study of Quaternary features provides a unique opportunity to examine natural processes in extreme detail.

The Quaternary is characterized by great fluctuations in the mass of continental glaciers. Evidence of these glaciations dominates the surface geology of a large portion of the northern hemisphere. The search for the causes of the glaciations has intrigued scientists ever since Agassiz (1840) first proposed the glacial theory. Sea level fluctuates as glaciers grow and decay because the ice stored in glaciers is ultimately derived from the ocean. Therefore the glacial record is preserved in features which record paleo-sea level. In this study, I wish to determine, with accuracy and precision, the timing of sea level fluctuations as a means of shedding light on the causes of the Quaternary glaciations.

Time is a fundamental variable, of great importance in geologic studies. A problem with many Quaternary studies is the inability to date materials in this time range. Conventional ^{14}C dating has a range of up to about 5×10^4 years. K-Ar techniques (Radicati di Brozolo et al., 1981; Bailey et al., 1976; Gillespie et al., 1984) and rarely Rb-Sr (Radicati di Brozolo et al., 1981; see Papanastassiou,

1970) have been used to date K-rich volcanics as young as about 10^5 years old, but the availability of such materials is limited and the analytical uncertainty is large. A number of nuclides in the ^{238}U, ^{235}U, and ^{232}Th decay series have half lives that are appropriate for dating Quaternary materials. The main problems with the so called disequilibrium dating schemes are unknown initial conditions, possible diagenetic alteration, and analytical uncertainty.

The purpose of this study is to develop a high precision technique to date corals that grew in the last half million years. Corals are dated by the method of ionium (^{230}Th) ingrowth, one of the disequilibrium dating schemes. The major advances discussed here are the development of high precision, high sensitivity techniques to measure ^{230}Th and ^{234}U abundances. Use of these techniques allows one to calculate ionium ages that have small errors (based on analytical uncertainty). The precision with which ^{230}Th and ^{234}U can be measured also allows one to examine, in some detail, diagenetic changes that may have altered the ionium clock. The ultimate goal is to determine the history of late Quaternary sea level fluctuations and vertical tectonic movements as a means of understanding the causes of global climate change and the nature of tectonic movement near the earth's surface.

2. The ^{238}U decay series and disequilibrium dating: a historical perspective

2.1 Secular equilibrium and ionium dating

^{238}U decays through a series of intermediate daughters to ^{206}Pb (figures 2.1 and 2.2). The parent, ^{238}U, has a mean life (6.449×10^9 y) which is much longer than the mean life of any of the intermediate daughters. In such a scheme, if a material remains closed to chemical exchange over time scales that are long compared to the mean lives of the intermediate daughters, then the nuclides in the series approach a state of secular equilibrium (Rutherford, 1905; Bateman, 1910). In this state, the activities of all the nuclides in the series are equal; i.e.:

$$N_1\lambda_1 = N_2\lambda_2 = N_3\lambda_3 = \cdots = N_n\lambda_n, \qquad (2.1)$$

where N_i is the number of atoms of nuclide i, λ_i is its decay constant, and the product $N_i\lambda_i$ is its activity. At secular equilibrium, the ratio of the activity of any of the daughters to the parent is unity ($N_i\lambda_i/N_1\lambda_1 = 1$). Imagine that such a system is disturbed (figure 2.3) and the activity ratio for nuclide i ($N_i\lambda_i/N_1\lambda_1$) is shifted from unity due to chemical fractionation of element i from element 1. At time t_o, the system becomes closed, with $N_i\lambda_i/N_1\lambda_1$ different from unity. With the passage of time, $N_i\lambda_i/N_1\lambda_1$ approaches unity again. The approach to unity is a function of time, which can be calculated by solving the equations of radioactive production and decay if the initial state of the system is known.

Figure 2.1. The uranium-238 decay scheme (Friedlander et al., 1981). The vertical axis is the number of protons; the horizontal axis is the number of neutrons. The times under the nuclides are mean-lives.

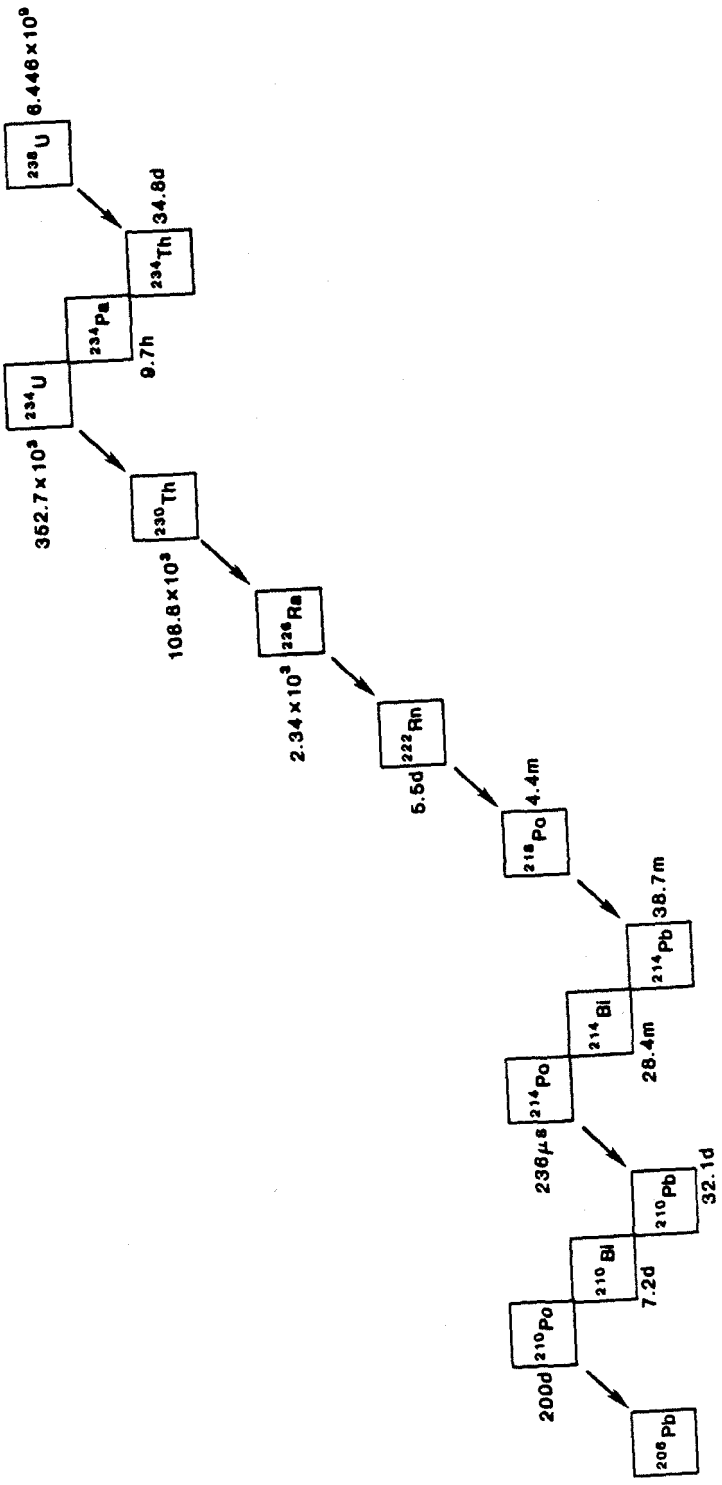
^{238}U 6.446×10⁹
^{234}Th 34.8d
^{234}Pa 9.7h
^{234}U 352.7×10³
^{230}Th 108.8×10³
^{226}Ra 2.34×10³
^{222}Rn 5.5d
^{218}Po 4.4m
^{214}Pb 38.7m
^{214}Bi 28.4m
^{214}Po 236μs
^{210}Pb 32.1d
^{210}Bi 7.2d
^{210}Po 200d
^{206}Pb

Figure 2.2. The uranium-238 decay scheme through thorium-230. The times underneath the nuclides are the mean lives used in this study. Note that the mean life of uranium-238 is much longer than the mean life of any of the intermediate daughters.

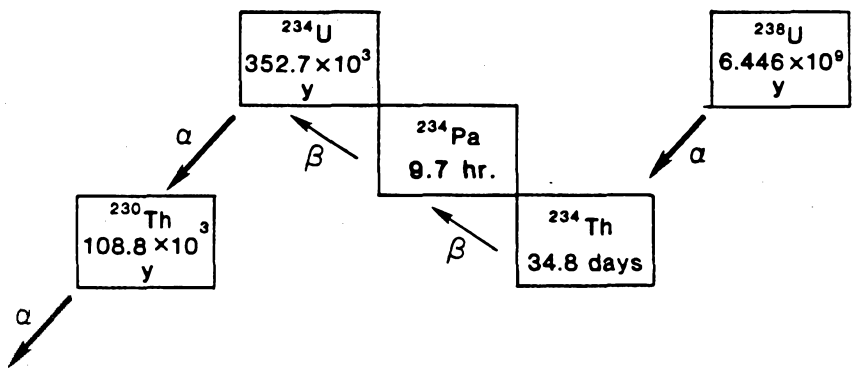
^{234}U
352.7×10^{3}
y
^{238}U
6.446×10^{9}
y
α
β
^{234}Pa
9.7 hr.
α
^{230}Th
108.8×10^{3}
y
β
^{234}Th
34.8 days
α

Figure 2.3. Daughter/parent activity ratio versus time illustrating how decay series isotopes can be used for age determinations. If the mean life of the parent is much longer than the mean life of any of the intermediate daughters, then the system approaches a state of secular equilibrium over time scales that are long compared to the mean lives of the daughters. In this state, all of the daughter/parent activity ratios are unity. An event that chemically fractionates a daughter nuclide from the parent nuclide changes this ratio. If the system becomes closed to chemical exchange, then the daughter/parent activity ratio will again approach unity as prescribed by the laws of radioactive production and decay. If the initial state of the system, immediately after the fractionation event, is known, then the time since the fractionation event can be determined from the measured daughter/parent ratio and the solution to the equations for radioactive production and decay. For thorium-230 dating of corals, the daughter/parent ratio is the $^{230}Th/^{238}U$ ratio; the chemical fractionation event is the weathering and transport of uranium to the ocean; the system becomes closed with initial $^{230}Th/^{238}U$ close to zero when coral aragonite crystallizes from seawater that has a low $^{230}Th/^{238}U$ ratio; and the $^{230}Th/^{238}U$ activity ratio approaches unity by radioactive decay.

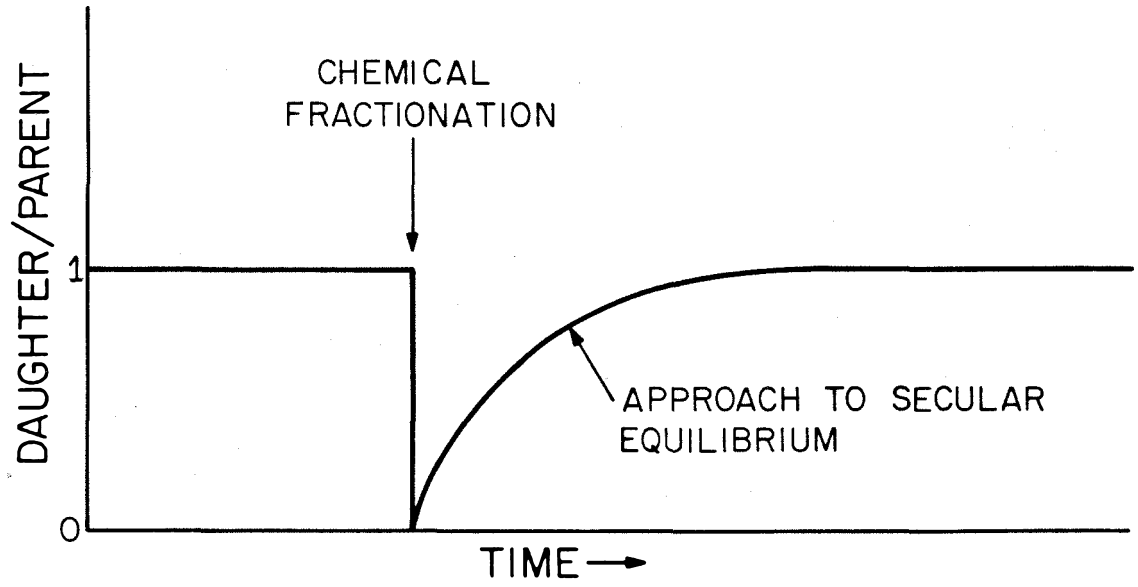
CHEMICAL
FRACTIONATION
DAUGHTER/PARENT
1
0
APPROACH TO SECULAR
EQUILIBRIUM
TIME

Thus, if the initial activity ratio at time t_o is known and the activity ratio at time t_1 can be measured, the interval of time t_1-t_o can be calculated. All disequilibrium dating schemes, including ionium dating, are based on these principles. For ionium dating of corals, it is assumed that the initial $^{230}Th/^{238}U$ ratio, when the coral grew, is zero. As time passes, if the coral skeleton remains closed to chemical exchange, the $^{230}Th/^{238}U$ activity ratio approaches unity. This is the basis for ionium dating of corals.

2.2 Early studies of ^{238}U and its daughters

The early studies of ^{238}U and its decay products led to an understanding of the nature of radioactivity. Becquerel (1896 a-e) discovered that uranium compounds darkened photographic plates that had not been exposed to sunlight. Curie and Curie (1898) showed that uranium and thorium compounds darkened photographic plates and ionized air and concluded that radioactivity was an atomic phenomenon. They also showed that some natural uranium minerals were more active than uranium metal and concluded that other radioactive substances must be present in these minerals. This observation led to the discovery of radium and polonium and, over the next decade, most of the nuclides in the ^{238}U, ^{235}U, and ^{232}Th decay chains. Rutherford and Soddy (1902) isolated ThX (^{224}Ra, half life = 3.6 days) and demonstrated that its activity decayed exponentially with time. Similar experiments on UX (^{234}Th) and radioactive "emanations" (^{220}Rn and ^{222}Rn) and observations of their decay and ingrowth after chemical separation led Rutherford and Soddy (1902) to conclude that radioactivity accompanies

change from one chemical atom to another and that changes must be occurring within the atom. Rutherford (1905) solved the equations of radioactive production and decay for a system with a parent and three intermediate daughters. Bateman (1910) later solved the same equations for an indefinite number of daughters with arbitrary initial state.

Ionium was discovered by Boltwood (1907a,b). The name refers to its ability to ionize air, a property which it shares with all alpha-emitters. Boltwood realized that ionium had chemical properties similar to those of thorium but refers to it as a new element. The concept of an isotope was put forward several years later.

An important early study (Joly, 1908) suggested that disequilibrium could exist in natural materials. He determined radium concentrations in deep sea sediments, which had been collected during the Challenger expedition, and discovered that radium (^{226}Ra) activity in deep sea sediments was extremely high. Because analytical capabilities to measure small amounts of uranium had not yet been developed, he could not unequivocably demonstrate that radium was out of equilibrium. He suggested, however, that the uranium (^{238}U) that was (the ultimate) parent of the radium was contained in ocean water. Joly's observation would eventually lead to an understanding that ionium is separated from uranium in seawater and that surficial deep sea sediments and seawater are complementary reservoirs. The sediments have $^{230}Th/^{238}U$ activity ratios much higher than unity; seawater has $^{230}Th/^{238}U$ ratios much lower than unity. The low $^{230}Th/^{238}U$ ratios in seawater are of fundamental importance in ionium

dating of corals because the assumption is made that the initial $^{230}Th/^{238}U$ ratio in corals is zero.

2.3 Quantitative measurements of decay series nuclides

After an initial decade of intense study, little was learned about disequilibrium in natural materials over the next three decades. This was largely due to analytical difficulties associated with measuring small amounts of U and Th decay series nuclides. One measurement that could be made was ^{226}Ra concentration. ^{222}Rn is the immediate daughter of ^{226}Ra and is a gas. ^{222}Rn emanating from a radium separate, could be collected, its activity measured, and the original ^{226}Ra concentration calculated. ^{226}Ra concentrations were determined in a number of natural materials in the 1930's (Piggot, 1933). These measurements confirmed Joly's measurements showing high ^{226}Ra concentration in deep sea sediments.

Urry (1941) presented a method for direct determination of uranium concentration by chemical separation, drying the uranium fraction to a thin film on a brass plate, and measuring the activity of the plate. He could measure the uranium concentration to a precision of ±20% (2 sigma) using a sample size of several micrograms (10^{16} atoms) of uranium. Using this method, it was demonstrated that the $^{226}Ra/^{238}U$ activity ratio in deep sea sediments was much greater than unity (Urry, 1941; Piggot and Urry, 1941), confirming the supposition of Joly (1908). Piggot and Urry (1942) measured ^{226}Ra and ^{238}U concentrations as a function of depth in deep sea sediments. The shape of the ^{226}Ra profiles indicated that, if post-depositional

remobilization had not occurred, the $^{230}Th/^{238}U$ activity ratio in surficial deep sea sediments must be greater than unity and suggested that the cause of the high ^{226}Ra concentrations was the separation of ^{230}Th from ^{238}U in seawater, not separation of ^{226}Ra from ^{230}Th. Direct confirmation of this was only possible when techniques were developed to measure ionium abundances.

The measurement of ionium activity could not be accomplished in the same straightforward manner as the uranium measurements. If it is assumed that ^{234}U and ^{238}U are in equilibrium, then the three naturally occurring isotopes of uranium are present in constant proportions. Therefore, the measurement of total activity in a uranium separate is proportional to the ^{238}U activity and the proportionality constant is known. The proportions of the six naturally occurring isotopes of thorium can vary by large amounts in natural samples, so the activity of ^{230}Th cannot be calculated from the measured total activity of a thorium separate. The major sources of alpha-activity (besides ^{230}Th) in a thorium separate are ^{228}Th and ^{232}Th. Isaac and Picciotto (1953) developed a method to correct for ^{228}Th and ^{232}Th activity. They coated a photographic plate with the thorium fraction and counted the resultant alpha-tracks. The tracks for ^{228}Th decay were "stars" with five branches because ^{228}Th is the parent of four very short-lived alpha-emitting daughters. Both ^{230}Th and ^{232}Th produce single alpha-tracks. ^{232}Th was assumed to be in equilibrium with ^{228}Th allowing the calculation of ^{232}Th activity and ^{230}Th activity by difference. Using this method, they could measure ^{230}Th abundance to a precision of ±20% (2 sigma) using several hundred

picograms of ionium (10^{12} atoms). They showed that ionium activities in deep sea sediments were comparable to ^{226}Ra activities, confirming the idea that high ^{226}Ra concentrations in sediments were due to separation of ^{230}Th from uranium in seawater.

2.4 ^{230}Th, ^{234}U, and ^{238}U measurements by alpha-spectrometry

Barnes et al. (1956) measured ionium and ^{238}U as a function of depth in corals from drill core at Elugelab Island. Ionium was measured by pulse analysis of the thorium fraction. These are the first ionium measurements in natural materials, which used pulse height analysis to resolve the energies of the alpha-particles. The corals near the surface had $^{230}Th/^{238}U$ activity ratios that were indistinguishable from zero. The $^{230}Th/^{238}U$ activity ratio generally increased with depth to a value close to unity in the deepest part of the core. These data clearly demonstrated that initial $^{230}Th/^{238}U$ in corals was low, that this ratio increased with stratigraphic age, and that ionium dating of corals was plausible.

Cherdyntsev (1955) demonstrated that the $^{234}U/^{238}U$ activity ratio in some natural waters was different from unity, a surprising result, since ^{234}U and ^{238}U are separated from each other by only two short lived intermediate daughters. Thurber (1962) demonstrated that the $^{234}U/^{238}U$ activity ratio in seawater was 1.15 ± 0.06 (2 sigma). Since then, measurements have shown that most surface waters have $^{234}U/^{238}U$ activity ratios greater than unity (see Ivanovich and Harmon, 1982). Values as high as 16 have been reported in terrestrial spring water (Szabo, 1982). Soils generally have $^{234}U/^{238}U$ activity ratios less

than unity (Ivanovich and Harmon, 1982), and the separation of ^{234}U from ^{238}U is thought to occur during the weathering process. The separation is thought to be associated with recoil when an alpha-particle is ejected from a ^{238}U atom. Because of the effect of alpha-recoil, the resulting ^{234}Th atom is likely to be located in a damaged site in the crystal lattice. ^{234}Th is short-lived and decays in a matter of days to ^{234}U by giving off two beta particles. The separation of ^{234}U from ^{238}U may be due to (1) recoil ejection of the ^{234}Th out of the crystal lattice into a solution, or (2) preferential leaching of ^{234}U because it occupies a damaged site (see Ivanovich and Harmon, 1982).

Broecker (1963) derived the ^{230}Th age equation for corals subject to the assumption that initial ^{230}Th was zero, taking into account the fact that the $^{234}U/^{238}U$ activity ratio in seawater was different from unity. Thurber et al. (1965) and Broecker and Thurber (1965) measured ^{230}Th, ^{234}U, and ^{238}U in corals by alpha-counting, using pulse height analysis and using ^{232}U and ^{228}Th tracers. This alpha-counting technique and minor variations of this technique would prove to be the standard method for measuring ^{230}Th abundances and uranium isotopic composition in natural materials for the next twenty years. Thurber et al. (1965) analyzed corals from drill core from Eniwetok Island and showed that corals near the surface had $^{230}Th/^{238}U$ close to zero, that $^{230}Th/^{238}U$ increased with depth in the core, that $^{234}U/^{238}U$ and $^{230}Th/^{238}U$ activity ratios in a miocene coral were indistinguishable from unity, and that within analytical error, ^{230}Th ages were the same as ^{14}C ages of corals. Thus, the ionium method of dating corals

appeared to be valid, and over the next decade this method was applied to fossil corals as a means of determining the timing of sea level fluctuations in the late Quaternary (see section 7.1).

In the 1970's and 1980's the approach stagnated because the precision of the alpha-counting methods was not high enough to clearly resolve the ages of successive sea level rises (see section 7.1, figure 7.2). The precision of the measurements also limited the ability to test for diagenetic alteration of corals, which might result in shifts in ^{230}Th ages. Thus, the accuracy of the ^{230}Th ages was open to question.

3. The astronomical theory of Pleistocene climate change

3.1 Milankovitch's formulation

The modern version of the astronomical theory of Pleistocene climate change was formulated by Milankovitch (1941). Using the principles of celestial mechanics, he calculated changes in the geometry of the earth's orbit and rotation axis back through time and hypothesized that the changes in the distribution of solar energy reaching the earth, which resulted from the changing orbital geometry, caused the fluctuations in Pleistocene climate observed in the geologic record. Milankovitch believed that hot summers in the northern hemisphere would favor deglaciation, whereas cool summers in the northern hemisphere would favor glaciation. The rationale was that in order to form a glacier, snow cover had to last throughout the year. Snow cover would best be preserved during a cool summer. The seasonality of the northern hemisphere was thought to be critical because most of the continental area is in the northern hemisphere and because large continental glaciers were located in the northern hemisphere during the Pleistocene.

Milankovitch calculated the position and orientation of the earth relative to the sun over the past 600,000 years. The results of a modern version of this calculation (Berger, 1978) are shown in figures 3.1 and 3.2. The results can be described by three time dependent variables, the obliquity of the ecliptic (figure 3.3), the eccentricity of the earth's orbit (figure 3.4), and the precession parameter (figures 3.3 and 3.4). The obliquity of the ecliptic is the angle between the earth's axis and a normal to the earth's orbital

Figure 3.1. Calculated values of the eccentricity of the earth's orbit (dashed line), the obliquity of the ecliptic (solid line), and the precession index (dash-dot line) for the last 250 ky years (after Berger, 1978). The values for eccentricity are shown on the left side; the values for obliquity are on the extreme right side in degrees; and the values for the precession index (the sine of the angle between perihelion and the vernal equinox minus the present value of this quantity) are on the right side immediately adjacent to the right ordinate.

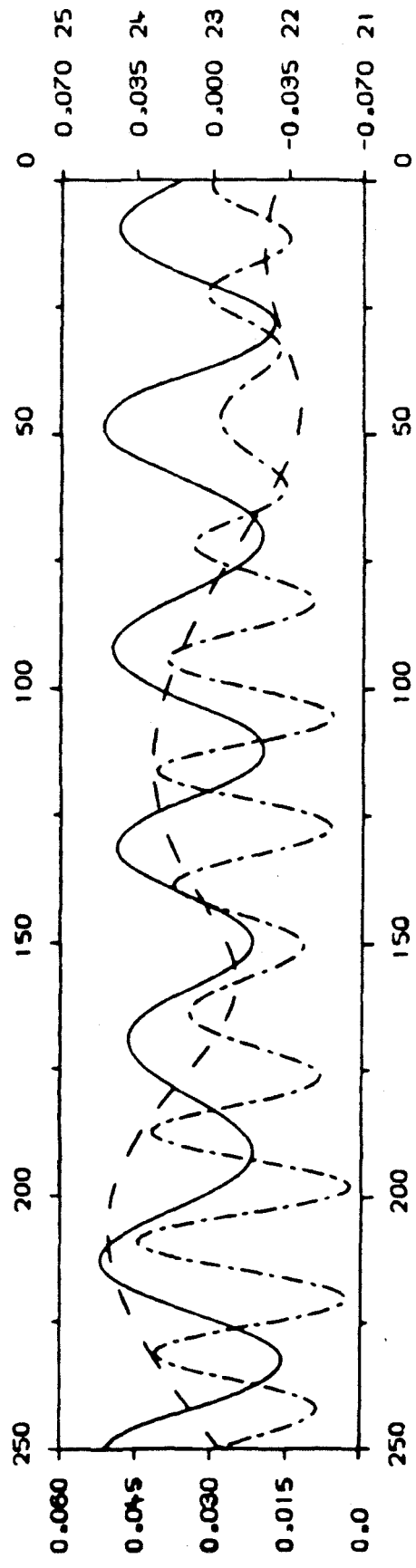
0
0.070 25
0.035 24
0.000 23
-0.035 22
-0.070 21
0
50
100
150
200
250
0.060
0.045
0.030
0.015
0.0
ky before 1950 A.D.

Figure 3.2. Upper diagram: the values for summer solar insolation received at 65°N latitude calculated from the curves in figure 3.1 (after Berger, 1978). The time range is 160 ky ago to present. The units on the vertical axis are percent above the present value of summer solar insolation at 65°N. Milankovitch (1941) hypothesized that this curve has controlled the earth's climate in the Pleistocene. If so, then a plot of sea level height for the same time range should resemble this curve. The times of high sea level as determined in this study will be compared to the times of high insolation (shown in this figure) in chapter 11.

Lower two diagrams: similar to upper diagram but for 45°N and 80°N latitudes. The relative values of the major insolation highs change slightly with latitude, but the timing of the major peaks does not shift significantly.

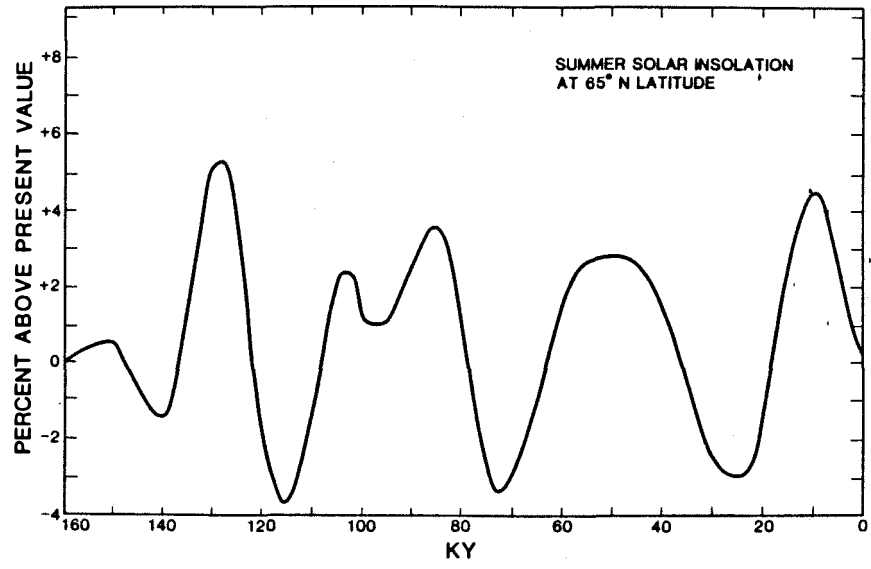
SUMMER SOLAR INSOLATION
AT 65° N LATITUDE
PERCENT ABOVE PRESENT VALUE
+8
+6
+4
+2
0
-2
-4
160
140
120
100
80
60
40
20
0
KY

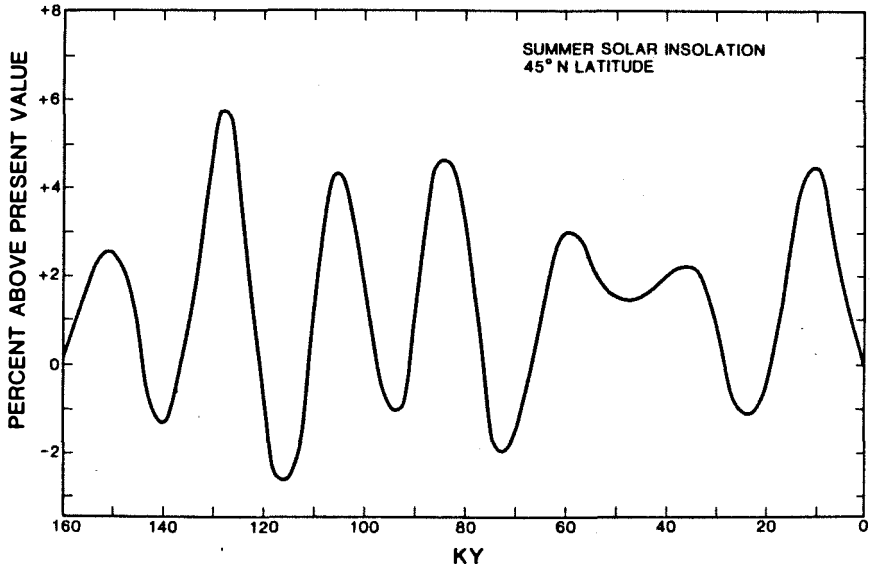
SUMMER SOLAR INSOLATION
45° N LATITUDE
PERCENT ABOVE PRESENT VALUE
+8
+6
+4
+2
0
-2
160
140
120
100
80
60
40
20
0
KY

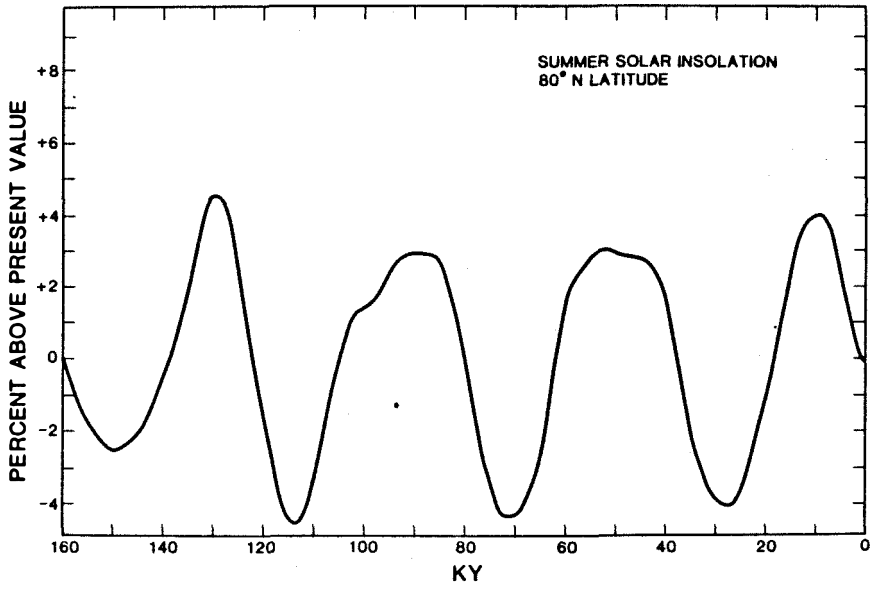
SUMMER SOLAR INSOLATION
80° N LATITUDE
PERCENT ABOVE PRESENT VALUE
+8
+6
+4
+2
0
-2
-4
160
140
120
100
80
60
40
20
0
KY

Figure 3.3. The present value between a normal to the earth's orbital plane and the earth's axis (the obliquity of the ecliptic) is 23.5°. As this value increases, the seasons become more extreme. The arrows denote precession of the axis, which changes the time of year at which the earth reaches perihelion. This also changes the distribution of solar energy received at the earth as shown in figures 3.1 and 3.2. (after Imbrie and Imbrie, 1986).

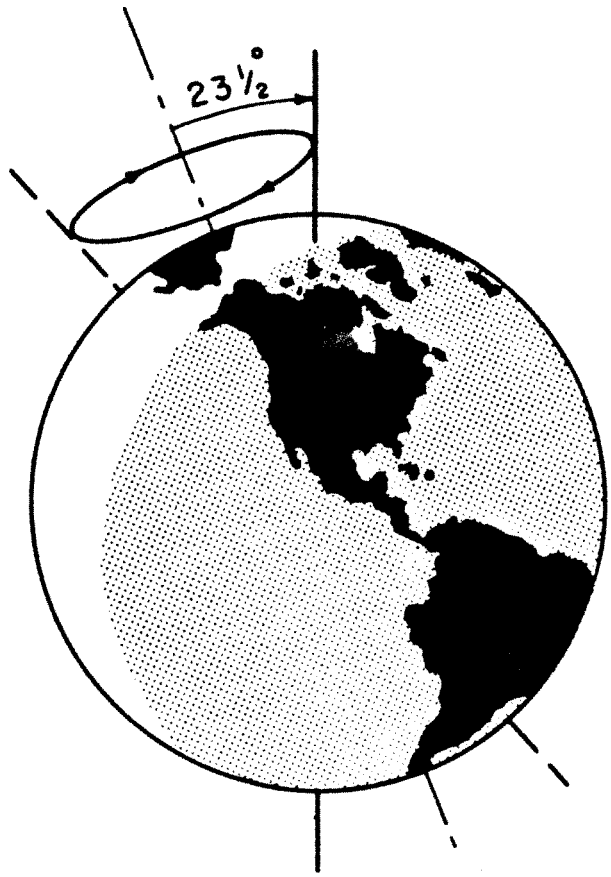
23½°

Figure 3.4. The earth's orbit showing the present relationship between the major axis of the eliptical orbit and the seasons in the northern hemisphere. Precession causes this relationship to change with time. The earth goes through one precession cycle in about 21,000 years. (After Imbrie and Imbrie, 1986).

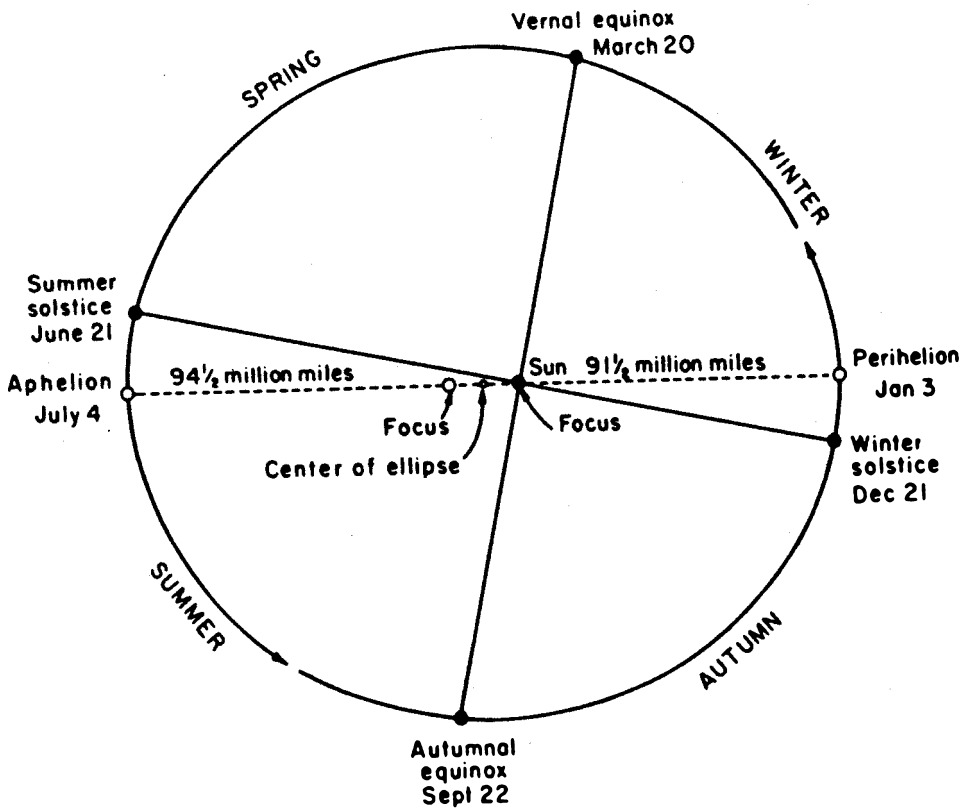
Vernal equinox
March 20
SPRING
WINTER
Summer
solstice
June 21
Aphelion
July 4
94½ million miles
Sun
91½ million miles
Perihelion
Jan 3
Focus
Center of ellipse
Focus
Winter
solstice
Dec 21
SUMMER
AUTUMN
Autumnal
equinox
Sept 22

plane. The present value is 23.5° and it has ranged from about 22° to about 24° during the Pleistocene (figure 3.1). The obliquity is roughly periodic with a period of about 41,000 years. High values of obliquity would result in high summer insolation and low winter insolation. The resulting warm northern hemisphere summers would favor deglaciation according to Milankovitch's hypothesis.

The eccentricity of the earth's orbit has varied from close to zero to about 5% during the Pleistocene and the present value is quite low (figure 3.1). It has a period of roughly 100,000 years. The effect of eccentricity on the distribution of solar energy received by the earth depends on where the earth is in its precession cycle, i.e., on the season during which the earth reaches perihelion. In the present geometry, the earth reaches perihelion during the northern hemisphere's winter and aphelion during summer in the northern hemisphere (figure 3.4). According to Milankovitch's hypothesis, the lower values of insolation in the northern hemisphere during summer and the resulting cool summers would favor glaciation. If all other parameters were held constant at their present values and the eccentricity were increased, the northern hemisphere summers would be even cooler and glaciation would be even more strongly favored.

The earth's axis precesses with a period of about 21,000 years (figures 3.1-3.4). About 11,000 years ago perihelion occurred during the northern hemisphere's summer. Milankovitch would consider this geometry favorable to deglaciation. Thus, precession and eccentricity work in concert; the magnitude of the eccentricity determines the magnitude of the effect and the position in the precession cycle

determines the nature of the effect (whether glaciation or deglaciation is favored). The precession index accounts for both of these effects (figure 3.1) and is defined as the eccentricity times the sine of the angle between perehelion and the the vernal equinox minus the present value of this product. This parameter is a sine wave whose amplitude is modulated by eccentricity. It has a period of 21,000 years. High values would favor deglaciation and low values would favor glaciation. The present value is an intermediate value.

The values of the orbital elements shown at the top of figure 3.1 can be used to calculate the solar insolation received at the top of the atmosphere as a function of latitude and time. The results of such a calculation for average insolation received during the summer half year at 65°N, 45°N, and 80°N are shown in figure 3.2 (Berger, 1978). The average summer solar insolation received during the summer half year at 65°N latitude has a range of approximately 8% of its mean value during the Pleistocene. The highest values are at times when the values of obliquity, eccentricity, and the precession index are all high. Milankovitch viewed the 65°N curve as the critical function that controlled climate. The choice of 65°N as the critical latitude is nominal. The rationale was that this latitude was appropriate for the generation of continental glaciers. The continental glaciers in Eurasia in the Pleistocene were located at about this latitude whereas the Laurentide ice sheet in North America was located between the latitudes of 45° and 80°N. Comparison of the 65°N curve with curves of significantly different latitudes (45°N and 80°N; figure 3.2) shows that the relative values of the major insolation peaks change slightly

with latitude, but the timing of the major peaks does not change significantly. The confirmation of the Milankovitch hypothesis, in the strictest sense, would require extracting evidence from the geologic record that demonstrates that some measure of the state of the earth's climate such as average temperature or ice volume correlates exactly with the 65°N curve.

3.2 Testing the astronomical theory

The Milankovitch theory is unique among the theories of the causes of the Pleistocene glaciations because it predicts the timing of climatic changes and is therefore testable if the appropriate information is preserved in and can be extracted from the geologic record. A rigorous test of the Milankovitch theory would require an accurate calculation of the 65°N curve as well as a method to determine accurately the state of the earth's climate in the past. If one could perform such a test, a positive result would indicate that (1) the earth's climate responds to changes in the geometric relationship between the earth and the sun, (2) of the possible curves that could be calculated from the orbital parameters, the 65°N curve is the one that controls climate, and (3) there is no phase lag between orbital forcing and climatic response. A negative result would indicate that one of the three statements is not true. Thus, if climate does respond to orbital forcing, a negative result might provide insight into the mechanism that causes the earth's climate to respond to changes in orbital geometry.

3.3 The accuracy of the orbital parameters

The calculation of the 65°N curve is an approximation as the analytical solution to the problem is not known. Thus, the difference between the true solution and the approximation is also not known. The accuracy of various calculations is assessed by comparing different solutions. The timing of the inflection points for obliquity and precession are not different by more than 1000 years over the past 400,000 years for the most recent published calculations (Berger, 1978; Vernekar, 1972). On this basis, it is presumed that the calculation of the 65°N curve is accurate to within 1000 years. As the periods of the orbital parameters are $\geq 2 \times 10^4$ years, the accuracy is sufficient to allow a critical evaluation of the astronomical theory.

3.4 A forward calculation

Peltier and Hyde (1986) and Hyde and Peltier (1985) have modeled the response of the earth's climate, in terms of ice volume, to insolation forcing. The model constrains summer solar insolation to change in a harmonic fashion. The model considers the growth and decay of a ring-shaped continental glacier (figure 3.5, see Birchfield et al., 1981), which is bounded poleward by an ocean that limits its expansion in this direction. The glacier changes its volume and geometry by ablation, accumulation, and ice flow. The zone of ablation is separated from the zone of accumulation by a line of constant slope that emanates from the climate point. The model accounts for changes in insolation by moving the climate point. At

Figure 3.5. Schematic diagram of the model used by Birchfield et al. (1981) and Hyde and Peltier (1985) to calculate the response of the earth's climate to orbital forcing (after Hyde and Peltier, 1985). The model considers a polar ice sheet that is bounded to the north by an ocean. This ice sheet grows and shrinks in response to changes in insolation. The climate point is the intersection of the 0°C isotherm and sea level. The climate surface is the line that extends from the climate point and delineates the shift in latitude of the 0°C isotherm with change in elevation. The intersection of this surface with the surface of the ice sheet is the latitude that separates the zone of ablation from the zone of accumulation. Changes in insolation are introduced by displacing the climate point northwards and southwards. This changes the latitude that separates the zone of ablation from the zone of accumulation. The model considers changes in ice volume resulting from glacial dynamics and isostatic readjustments of the crust under the ice sheet. If the crust were subsiding while the position of the climate point and the shape of the ice sheet were held constant, the latitude separating the zone of ablation from the zone of accumulation would move northward. Similarly, if the crust and climate point were held at constant positions and the glacier were allowed to flow, then the latitude separating the zone of ablation from the zone of accumulation would shift because the surface of the ice sheet would intersect the climate surface at a different latitude.

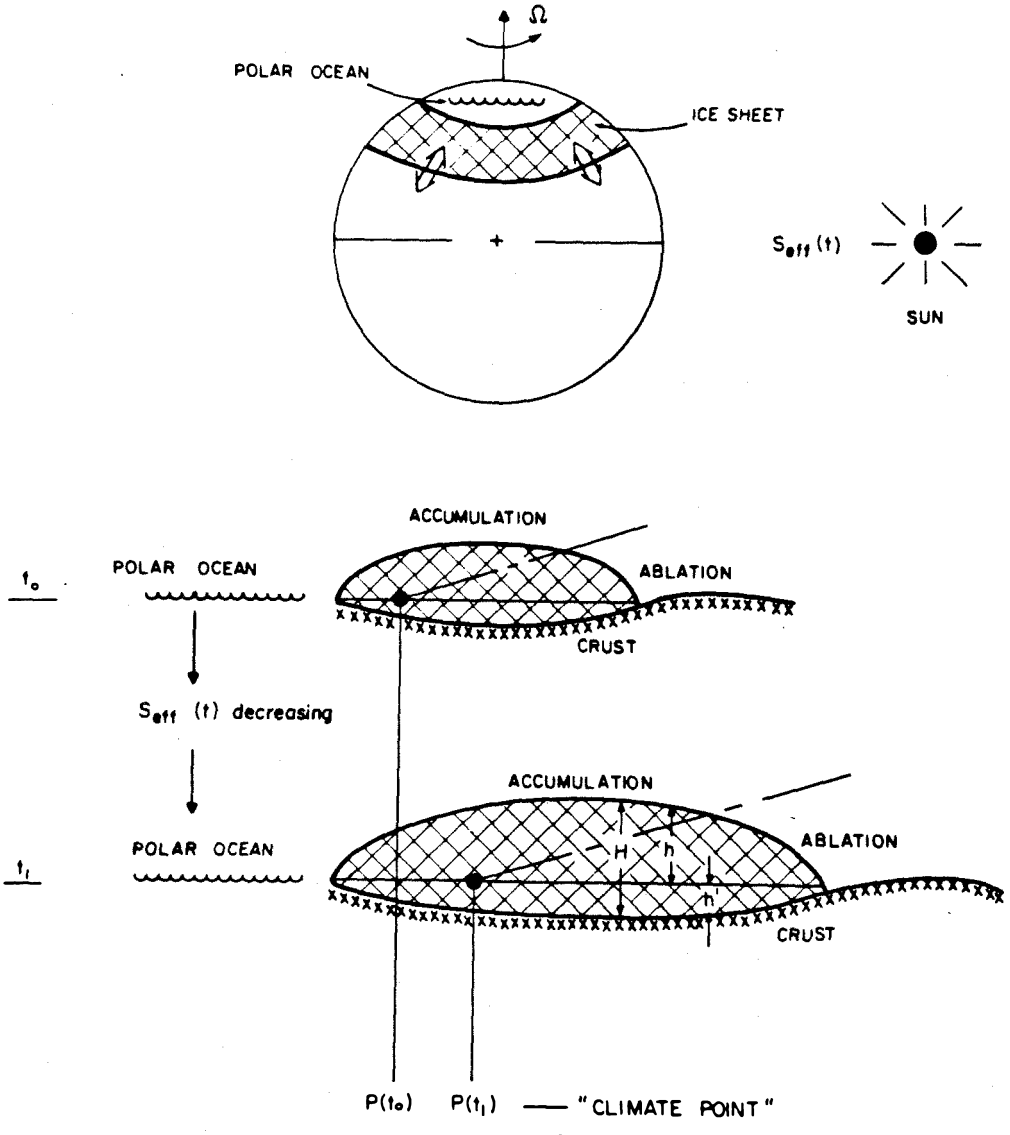
Ω
POLAR OCEAN
ICE SHEET
$S_{eff}(t)$
SUN
ACCUMULATION
t_o
POLAR OCEAN
ABLATION
CRUST
S_{eff} (t) decreasing
ACCUMULATION
POLAR OCEAN
t_1
ABLATION
H
h
h'
CRUST
$P(t_o)$ $P(t_1)$ —— "CLIMATE POINT"

times of high insolation, the climate point is displaced poleward; at times of low insolation, the point is displaced towards the equator. The model also considers subsidence and rebound of the crust due to loading and unloading of the ice sheet. If the crust is subsiding, the line separating the zone of ablation from the zone of accumulation moves to higher latitude and if the crust is rebounding, it moves to lower latitude. If the climate point did not move, the glacier would reach a steady state volume. However, in the model, the climate point changes latitude in a periodic fashion because of insolation forcing. The summer solar insolation is constrained to vary sinusoidally with a period of 20,000 years, approximating the effect of precession on changes in insolation. The results of the Hyde and Peltier (1985) calculation are shown in figure 3.6. In the course of one cycle of ice sheet growth and decay, the glacier generally grows for 80,000 years, then melts rapidly in about 10,000 years. The whole cycle takes about 100,000 years. Superimposed on the main cycle are smaller cycles of growth and decay that have a period of 20,000 years. The phase lag between a minimum in the insolation curve and a local maximum in the ice volume curve is about 5,000 years. Although the results are certainly quite dependent on the values of input parameters, this model shows that the response of the earth's climate to orbital forcing may be quite complicated and that phase lags may be involved. If orbital forcing does control climate, differences between an accurate 65°N curve and an accurate measure of the state of the earth's climate in the past, may shed light on the nature of the forcing function and the earth's response to the forcing function.

Figure 3.6. Ice volume versus time as calculated by Hyde and Peltier (1985) using the model shown in figure 3.5. For this calculation, the changes in insolation were constrained to vary harmonically with a period of 20 ky. The preferred curve is labelled (b). The other curves show how the curve would shift if different values of the ablation rate were used in the calculation. The difference between the curves shows that the model is sensitive to the values of input parameters. The difference between these curves and the harmonic insolation curve shows that the response of climate to insolation forcing may not be simple.

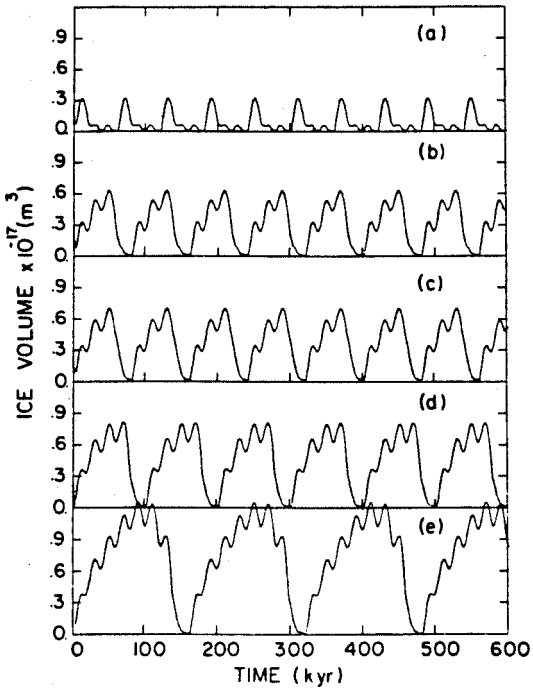
(a)
(b)
(c)
(d)
(e)
.9
.6
.3
0
ICE VOLUME x 10^17 (m^3)
0
100
200
300
400
500
600
TIME (kyr)

4. The state of the earth's climate from the geologic record

4.1 Fluctuations in sea level and the state of the earth's climate

Methods for determining the state of the earth's climate during the Pleistocene have focused on estimating changes in the volume of ocean water as a function of time. At present, 97.6% of the world surface water is contained in oceans, 1.7% in continental glaciers, 0.6% in rivers, lakes, and ground water, and only trace amounts in the atmosphere (Flint, 1971, p.83). During the peak of the Wisconsin glaciation it is estimated that about 5% of the surface water was contained in continental glaciers. If the total volume of surface water and ice has remained constant and the fraction of water contained in rivers, lakes, and ground water has not changed by large amounts, then the volume of water in the sea is directly related to global ice volume.

If the geometry of the ocean basins has not changed, then a measure of sea level height is equivalent to a measure of ocean volume. Of the processes that could change the geometry of the ocean basins, several can be disregarded on the basis of simple calculations. If isostatic compensation did not occur, the ocean floor could be raised by adding sediment. If one takes an average sedimentation rate of 0.5 cm/1000 years, over the course of 100,000 years only 0.5 m of sediment is added to the ocean floor. This is negligible compared to the more than 100 m of sea level rise generally thought to accompany a glacial to interglacial transition.

It is well known that oceanic crust forms at topographic highs and that as the crust ages and cools, it subsides. If the average age

of oceanic crust were to change, then the average depth of the basins would also change. Consider an ocean that is 10,000 km wide, contains one centrally located mid-ocean ridge which has a half-spreading rate of 5 cm/yr, and no subduction zone. Assume that the youngest crust is 2000 m below sea level, the oldest crust is 6000 m below sea level, and the depth increases linearly with age. The average age of the crust is 50 my. In 100,000 years, the average age of the crust will increase by 50,000 years and the average depth by 2 m. This is negligible especially considering that fact that this value must be a maximum since the effect of subduction was not considered.

The slope of the continental shelf is not vertical or constant. Therefore, the change in sea level height is not directly proportional to the change in ocean volume. It can be shown, rather trivially, that for a shift in ocean volume equivalent to a shift in ocean height of about 100 m, the shift in height for the real ocean does not differ by more than 10 cm from the shift in height for a hypothetical vertical sided ocean.

One effect that is important in changing the geometry of the ocean basins on timescales of 10^5 years is the effect of isostatic readjustments associated with the unloading of glaciated areas and the loading of the oceans during a glacial to interglacial transition and the reverse process during an interglacial to glacial transition. For example, marine strandlines that formed during the last deglaciation near Hudson Bay and along the Baltic Sea now stand hundreds of meters above sea level (Flint, 1971), despite the fact that the oceans must have increased in volume by about 3 % during the last deglaciation and

increased in average depth by over 100 m. However, these localities were heavily glaciated and represent extreme examples where the crust has rebounded significantly because of unloading. The apparent changes in sea level along these coastlines are quite different from the average change in sea level over the same time period. Although, in general, apparent changes in sea level along a given coastline are not the same as the average change in sea level, the difference between these quantities (due to isostatic effects) is small for coastlines far from the sites of glaciation (Clark et al., 1978).

In addition to isostatic effects, changes in apparent sea level may be caused by local tectonic effects. Although local tectonic uplift or subsidence may not significantly alter the geometry of an ocean basin, it may shift the height of a fossil marine strandline so that it no longer accurately records an earlier sea level height. Local tectonic effects cannot be isolated, in a rigorous manner, from shifts in sea level that result from changes in ocean volume. It is generally assumed that tectonic effects are small along coastlines far from plate margins, for instance, along certain ocean islands or along passive continental margins. In summary, if local effects are ignored, the difference between the height of sea level today and at some time in the past is directly related to the change in ice volume over that time period and is therefore a measure of the state of the earth's climate at that time.

4.2 A model for determining the timing and height of sea level, rates of sea level rise, and rates of tectonic uplift

If it could be established (1) that a given coastline was tectonically stable, (2) that a material had been continuously deposited right at the sea surface on this coastline, (3) that this material has not been eroded and (4) that one could date this material infinitely precisely, then the ages and heights of this material would provide a continuous record of sea level change (figure 4.1). If a similar material had been continuously deposited on a tectonically active coastline, then the difference between the sea level curve from the stable coastline and the apparent sea level curve from the tectonically active region would provide a continuous record of tectonic movement at the tectonically active site (figure 4.1).

This ideal cannot be realized. Not only are the four stipulations not, in general, strictly true, but also there are sampling problems imposed by the present state of the earth's climate. We are now in an interglacial period; sea level is high. Therefore, virtually all of the record of Pleistocene sea level fluctuations on tectonically stable coastlines is below sea level and not easily accessible (see figure 4.1). There is some controversy concerning the exact number, timing, and height of sea level maxima in the last 200,000 years. However, in this period, there is only one generally agreed upon case (the last interglacial period) when sea level was above present sea level. Therefore, if one works above water in stable regions, one is constrained to determining the height and timing of one sea level maximum.

Figure 4.1. Schematic diagram showing how one could determine the history of sea level fluctuation and vertical tectonic movement by dating a hypothetical material that was deposited continuously right at the sea surface. If this material was deposited on a tectonically stable shoreline, then the present ages and heights of this material would provide an accurate record of past sea level changes (upper diagram). This record could be subtracted from a similar record obtained from a tectonically active region (middle diagram) to yield a record of vertical tectonic movement (lower diagram) for the tectonically active region. One of the problems with this approach is that virtually all of the record from tectonically stable areas is presently under water and relatively inaccessible. At tectonically rising localities, more of the record is preserved subaerially. Because the record from stable localities is fragmentary, the tectonic component of uplift must be interpolated through time in order to extract information about sea level height from the more complete record at the tectonically rising locality.

The diagram is drawn assuming a constant uplift rate. This need not be the case. For the periods of time over which a continuous record can be obtained from both a stable locality and a tectonically active locality, the potential exists to determine the fine details of the tectonic component. This may allow the determination of the times and amounts of coseismic uplift as will be shown in chapter 10.

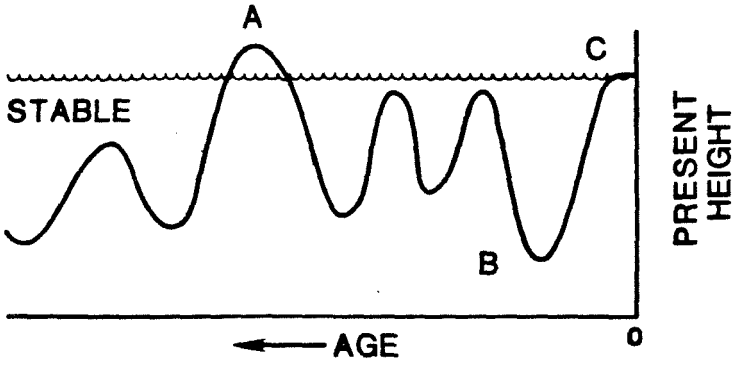
A
C
STABLE
B
PRESENT HEIGHT
AGE
0

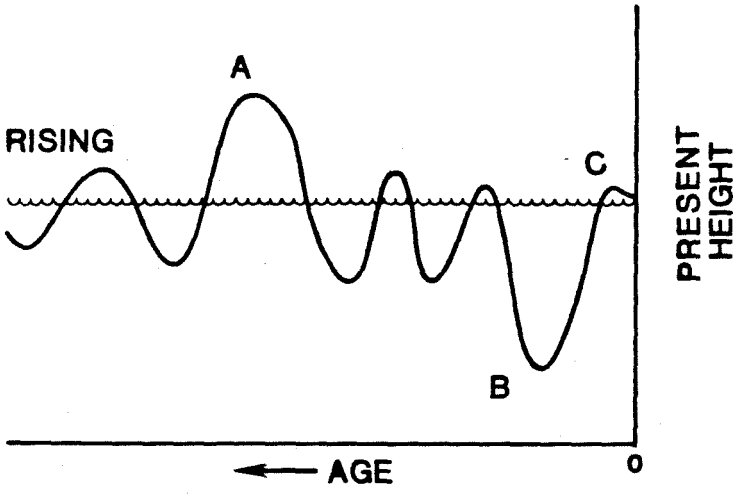
A
RISING
C
B
PRESENT HEIGHT
AGE
0

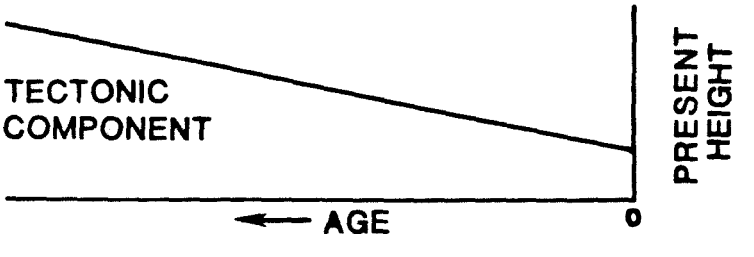
TECTONIC COMPONENT
PRESENT HEIGHT
AGE
0

If one works on coastlines that are being actively uplifted, then some of the record that is below sea level in stable regions may be subaerially exposed (see figure 4.1). In order to extract a valid sea level curve from the apparent changes in sea level recorded on a tectonically active coastline, the tectonic component of movement must be subtracted off. This is possible (1) if it can be shown that a deposit on the tectonically active shoreline formed right at sea level at the same time as a similar deposit on a stable shoreline and (2) if it is assumed that the uplift rate at the tectonically active site has been constant. In this case, one can determine the average uplift rate at the tectonically active site and a sea level curve for the accessible portion of the record at the tectonically active site.

The above approach depends on the ability to identify material on the tectonically active coastline, which was deposited at exactly the same time as material on a stable coastline. However, one does not know, a priori, what piece of material on an active coastline might correlate in time with material on a stable coastline. Indeed, because of the discontinuous nature of such records and the inaccessibility of much of the record, it may not always be possible to find time correlative material. The most accessible portion of the record is the higher portion of the record, which is more likely to be above present sea level. If one considers a single rise and fall of sea level, a portion of the record that is likely to be accessible and recognizable in the field, is the material that was deposited when sea level reached its maximum height relative to a given land mass.

In a stable area, the height of a material with such

characteristics marks the maximum height reached by the sea during the transgression. The age of such a material is equivalent to the time of the sea level maximum. As will be shown below, the age of such a material from a tectonically active coastline is not, in general, the same as the time of the sea level maximum, and the height of the material corrected for tectonic uplift is not the same as the height of the sea level maximum. Although such material from a stable area and similar material from a tectonically active area are not time correlative, I will demonstrate that if one makes an additional assumption about the shape of the sea level curve, then one can place constraints on both the uplift rate at the tectonically active site and the height of sea level at the time the material was deposited at the tectonically active site.

Consider the following model (figure 4.2). Assume again that (1) uplift rate at a given locality is constant and make the additional assumption that (2) the change in the height of sea level with time has negative curvature over an appropriate time range. The ordinate in figure 4.2 is absolute height and the abscissa, time. The curve labeled "Sea level" represents a single rise and fall of sea level. The slopes of the lines labeled "High uplift," "Low uplift," and "Stable" represent uplift rates of different land masses. The lines are drawn tangent to the "Sea level" curve because this is the highest position on each land mass that is covered by seawater. For the "Stable" locality, seawater reaches this vertical position on the land mass at the same time (T_3) that sea level reaches its maximum height (H_3). However, for a locality undergoing uplift, seawater reaches its

Figure 4.2. A model showing how the ages and heights of material deposited during a single rise and fall of sea level are related. The model assumes that the sea level height versus time curve has negative curvature over an appropriate time period and that the tectonic uplift rate at a given locality is constant with time. The model considers material from localities with different uplift rates. At each locality, the material under consideration was deposited when sea level reached its highest level on that land mass. This material is deposited at times when the uplift lines are tangent to the sea level curve. The material therefore records the times at which sea level was rising at the same rate as the land mass, and may be used to determine the rate of sea level rise as a function of time. Because this set of materials did not form at the same time, the true tectonic uplift rate and the true initial height of the material from the tectonically active localities cannot be calculated; however, bounds can be placed on these quantities as shown in the next figure. The model is testable because it predicts that the material with the oldest ages should have the highest present heights.

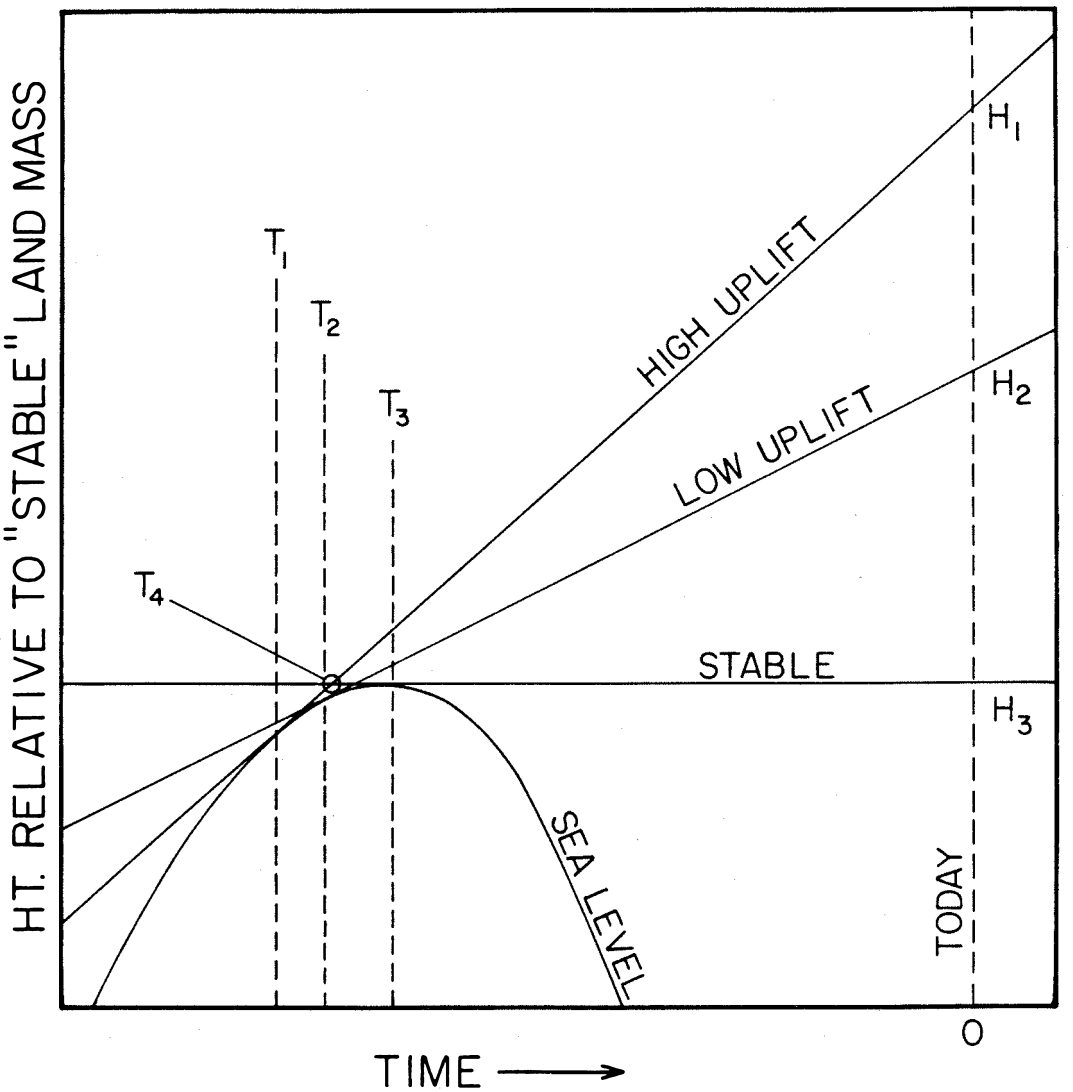
HT. RELATIVE TO "STABLE" LAND MASS
TIME
T1
T2
T3
T4
HIGH UPLIFT
LOW UPLIFT
STABLE
SEA LEVEL
H1
H2
H3
TODAY
0

highest position on the land mass before sea level reaches its maximum height. The higher the uplift rate, the earlier sea level reaches its highest position on the land mass. Seawater reaches its highest position on a land mass at the time that sea level is rising at the same rate as the land mass.

The assumptions of the model are, to some extent, testable because the model predicts that the deposits with the higher present heights should have the older ages (for $H_1>H_2>H_3$, $T_3>T_2>T_1$). The uplift rate of the land mass can be estimated as follows. The true uplift rate at the "High uplift" locality is the present height of the deposit (H_1) minus the height of the deposit from the "Stable" locality (H_3) divided by the time that the "High uplift" deposit was at height, H_3; i.e. $(H_1-H_3)/T_4$. The time, T_4 is not known but it must lie between T_1 and T_3. Therefore, the uplift rate must lie between $(H_1-H_3)/T_1$ and $(H_1-H_3)/T_3$ (figure 4.3). As discussed above, the deposit forms at the time that sea level is rising at the same rate as the land mass. Therefore, the bounds on uplift rate are equivalent to bounds on the rate of sea level rise at the time the material was deposited. Using the bounds on uplift rate, the age (T_1), and the present height (H_1), bounds can be placed on the initial height ($H_1-[H_1-H_3][T_1/T_3] <$ initial height $< H_3$; see figure 4.3) of the deposit, which is equivalent to the height of sea level at the time the material was deposited. Thus, if one can determine the ages and heights of such deposits and establish that one of the localities is stable, one can, subject to the assumptions of the model, constrain the height of sea level and rate of sea level rise at discrete times, constrain the rates of tectonic uplift at different

Figure 4.3. Calculating bounds on uplift rate and initial height using the model shown in figure 4.2. If the assumptions of the model are correct, the true uplift rate must be bounded by the slopes $(H_1-H_3)/T_1$ and $(H_1-H_3)/T_3$. Because the true age of the material is known, bounds can be placed on the initial position of sea level at this time. This approach is used in chapter 11 to estimate sea level heights from the record on Barbados.

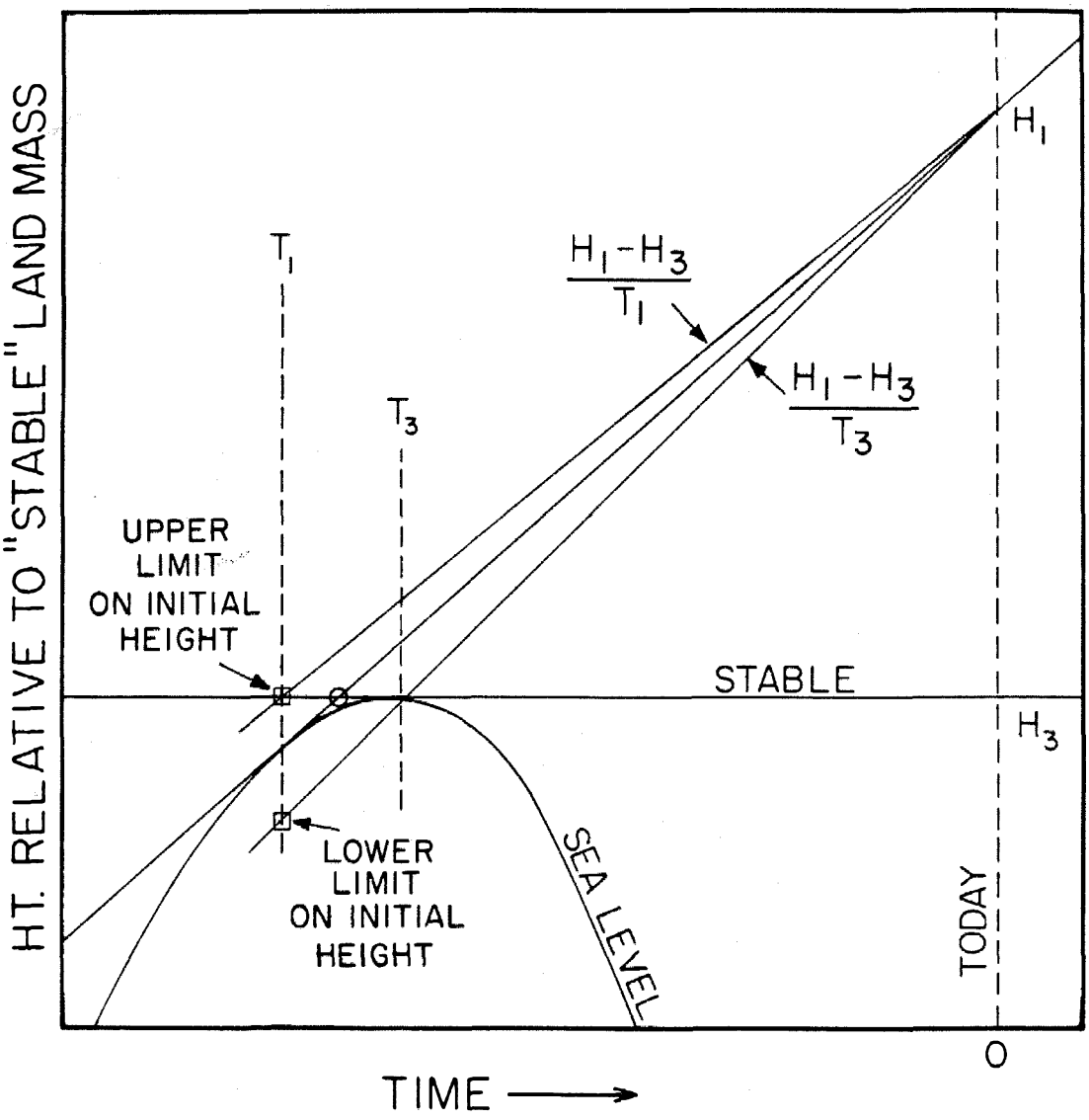
HT. RELATIVE TO "STABLE" LAND MASS
H_1
T_1
$\frac{H_1-H_3}{T_1}$
T_3
$\frac{H_1-H_3}{T_3}$
UPPER LIMIT ON INITIAL HEIGHT
STABLE
H_3
LOWER LIMIT ON INITIAL HEIGHT
SEA LEVEL
TODAY
0
TIME ⟶

localities, and determine the timing and height of the sea level maximum.

Maximum rates of sea level rise are typically much larger than rates of tectonic uplift. If sea level rise curves have negative curvature, as assumed, then the approach described above is limited, in practice, to portions of the curve near the maximum when the rate of sea level rise is much smaller than the maximum rate and is similar to rates of tectonic uplift. Thus, the ages of the described deposits, for the localities that are being uplifted, would in practice represent times prior to the time of the sea level maximum when sea level was close to, but just below its maximum height.

4.3 Conditions of coral growth

The conclusions of the above discussion depend on the supposition that there exist marine deposits that form at the sea surface, and can be dated. The extent to which coral skeletons meet these stipulations will be discussed below.

Stony corals are animals that belong to the phylum coelenterata, class anthozoa, order scleractinia (Barnes, 1974, pp.122 - 136). They are closely related to sea anenomes, which belong to the same class. Many species of stony corals and all hermatypic (reef-building) corals contain symbiotic yellow-brown algae (zooxanthellae) within their cells. Because the algae require light to live, hermatypic corals do not live below certain depths. Some species of scleractinian corals exist as colonies whereas others exist as solitary organisms. Solitary corals have diameters of up to 25 cm. A single colonial head coral can

grow to be more than 10 m in diameter. All scleractinian corals have aragonitic exoskeletons, which serve as a point of attachment for the rather fragile organic living portion of the animal. The bulk of the volume of a coral colony is taken up by the skeleton. The living portion of a colony is a thin organic layer, which covers the upper surface of the skeleton. As the colony grows, the surface, living portion, of the colony deposits layers of aragonite underneath it, increasing the volume of the skeleton and the surface area covered by the organic portion. The living portion of the colony is made up of many polyps (individual organisms), which are connected by organic tissue. The number of polyps in a colony increases by asexual budding. Corals also reproduce sexually and release free-swimming larvae which settle and start new colonies.

Hermatypic corals grow under a rather narrow range of conditions. Although stony corals grow at depths of over 6000 m and at all latitudes (Goreau et al., 1979), hermatypic corals are generally restricted to depths of less than 100 m (Goreau and Wells, 1967) and tropical and subtropical waters (figure 4.4). In waters with mean annual temperatures below about 18°C, hermatypic corals generally do not grow fast enough to generate coral reefs although isolated colonies may exist in slightly colder water (Wells, 1957). The number of hermatypic species that grow in water below 18°C is much smaller than the number that grow in warmer water (Wells, 1957). Corals generally do not grow in waters with salinity less than 30 $^{o}/_{oo}$ or greater than 40 $^{o}/_{oo}$ (Hopley, 1982, p.83), although the species Porites lobata can grow in water as saline as 43 $^{o}/_{oo}$ (Hopley, 1982, p.97).

Figure 4.4. The world distribution of coral reefs (black patches, after Goreau et al., 1979) showing that coral reefs are generally restricted to the tropics.

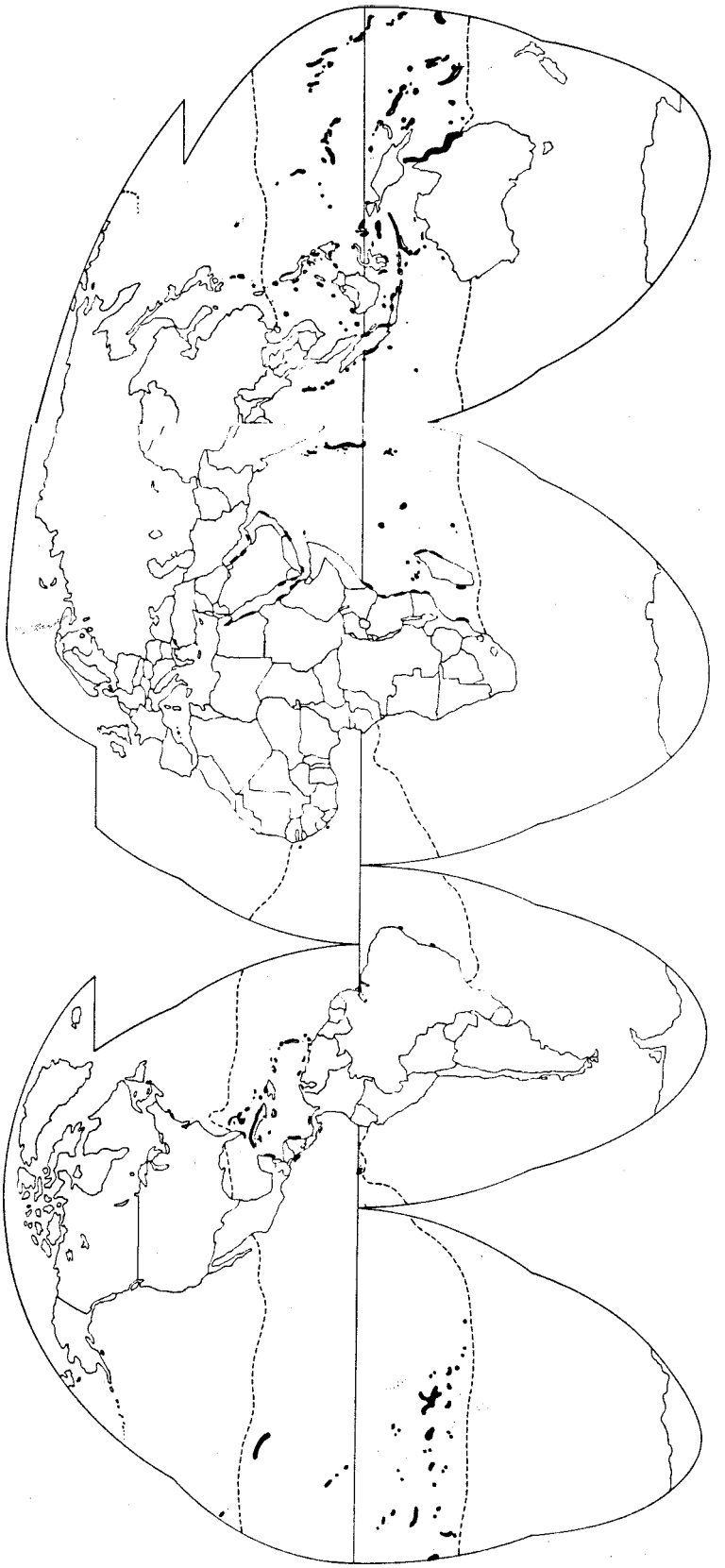

4.4 Zonation of coral species

Different species of hermatypic corals thrive in different environments. This results in a characteristic zonation of species in a reef environment. Species are zoned with respect to depth and distance from the reef crest. An understanding of this zonation is absolutely critical in determining past sea level heights. The zonation is reflected in the number of species that grow at different depths. This number drops sharply between 0 and 15 m (figure 4.5, Wells, 1957). The number of species is correlated with the amount of solar energy reaching a given depth, and it is thought that the species diversity is largely controlled by this parameter. The shape of individual coral colonies may also change as a function of depth. Barnes (1973) has shown that colonies of Montastria annularis growing off Jamaica are shaped like hemispheres above a depth of 5 m, have a columnar form below 5 m, and can have irrregular or platelike forms at depths of greater than 25 m. Numerous studies of living and fossil reefs have established a characteristic zonation of species for a Caribean fringing reef (Goreau, 1959; Goreau and Wells, 1967; Mesolella, 1967; Taylor et al., 1985b; figures 4.6 to 4.8). A reef can be divided into four zones (figures 4.6 to 4.8). The deepest is the coral head zone which is located on the fore-reef slope below about 15 m. This is dominated by the head coral, Montastria annularis and head corals of the genus Siderastria. Higher up the slope, at depths between 5 and 15 m, is a zone that is made up almost solely of the branching coral Acropora cervicornis. The crest of the reef, from 0 to 5 m, is composed dominantly of colonies of the branching coral,

Figure 4.5. Number of coral species versus depth and Bikini Atoll showing that species diversity decreases rapidly with depth (after Wells, 1957).

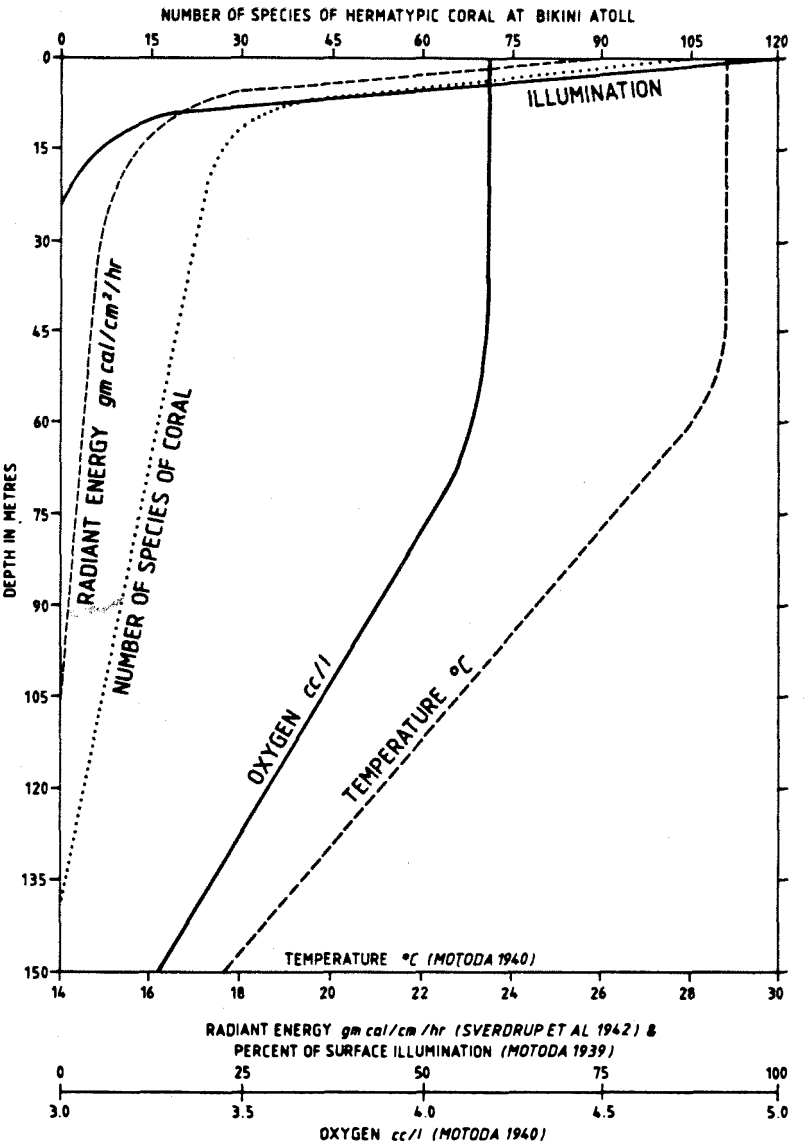
NUMBER OF SPECIES OF HERMATYPIC CORAL AT BIKINI ATOLL
0
15
30
45
60
75
90
105
120
ILLUMINATION
RADIANT ENERGY gm cal/cm²/hr
NUMBER OF SPECIES OF CORAL
OXYGEN cc/l
TEMPERATURE °C
DEPTH IN METRES
0
15
30
45
60
75
90
105
120
135
150
TEMPERATURE °C (MOTODA 1940)
14
16
18
20
22
24
26
28
30
RADIANT ENERGY gm cal/cm /hr (SVERDRUP ET AL 1942) &
PERCENT OF SURFACE ILLUMINATION (MOTODA 1939)
0
25
50
75
100
3.0
3.5
4.0
4.5
5.0
OXYGEN cc/l (MOTODA 1940)

Figure 4.6. Schematic diagram of a Caribbean coral terrace showing the characteristic species zonation (after Mesollela, 1967). The coral head zone is dominantly head corals; the Acropora cervicornis zone is made up almost solely of this species of branching coral; the Acropora palmata zone occurs at the reef crest and implies a shallow water environment; the rear zone is dominantly head corals, many of which also grow in the coral head zone. Photographs of these zones are shown in figures 4.7 and 4.8.

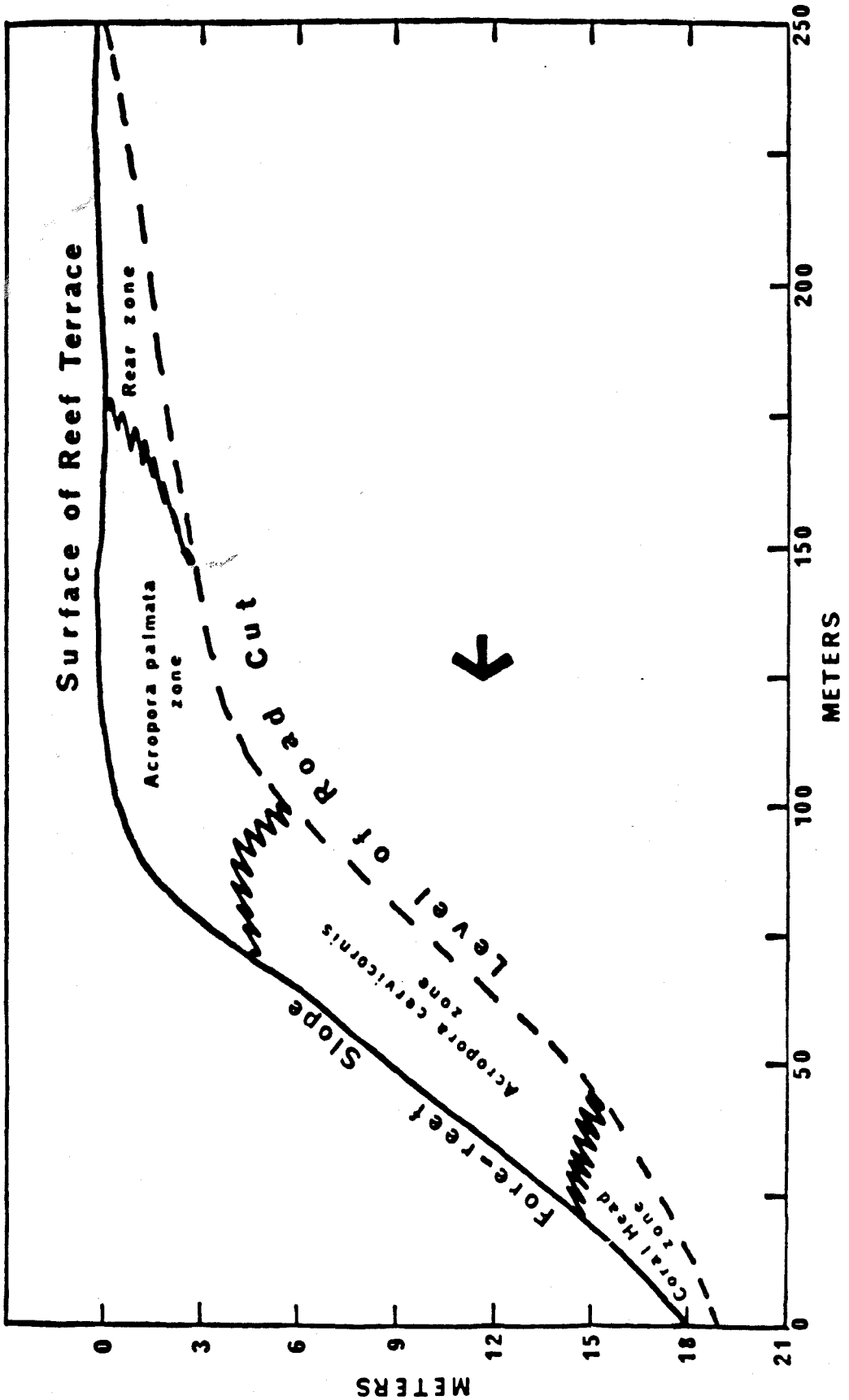
Surface of Reef Terrace
Rear zone
Acropora palmata zone
Level of Road Cut
Acropora cervicornis zone
Fore-reef Slope
Coral Head zone
METERS
0
3
6
9
12
15
18
21
0
50
100
150
200
250
METERS

Figure 4.7. Upper photograph: taken underwater looking up toward the sea surface. The coral is all Acropora palmata. The distance across the bottom of the photograph is about 0.5 m. This shows Acropora palmata living in very shallow water. (Photograph by David C. Smith, Virgin Is.)

Lower photograph: fossil Holocene coral reef from Canada Honda, Enriquillo Valley, Dominican Republic showing the Acropora cervicornis zone. All of the coral in the photograph is Acropora cervicornis. The wasp nests provide scale.

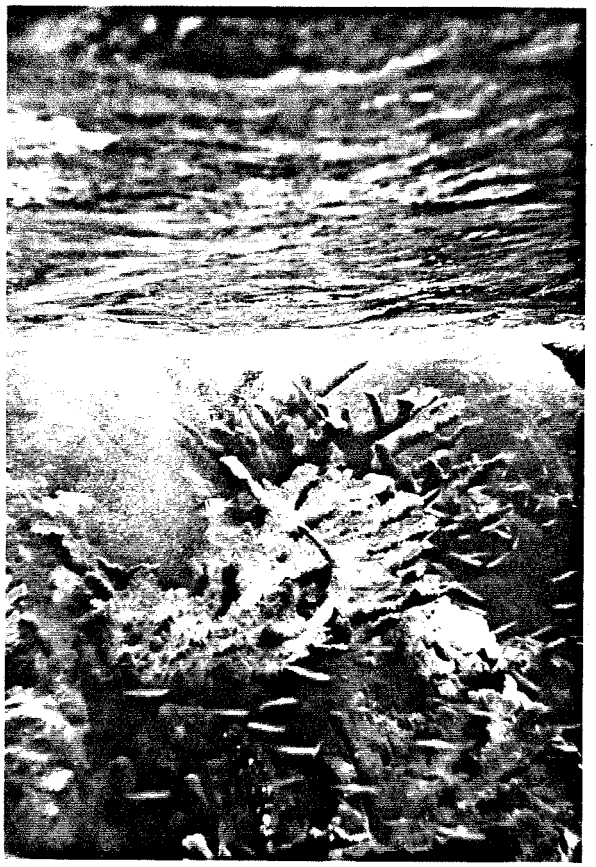

Figure 4.8. Upper photograph: coral terraces on the west coast of Barbados. The most prominent terrace is the Rendezvous Hill Terrace; the two less prominent terraces shoreward from the Rendezvous Hill Terrace are the Ventnor and Worthing Terrace. The distance across the photograph from the shore inland is about 2 km. (Photo courtesy of F.W. Taylor.)

Lower photograph: the coral head zone of the fossil Holocene reef at Canada Honda, Enriquillo Valley, Dominican Republic. All of the coral skeletons in the photograph are head corals mainly of the genus Siderastria. F.W. Taylor is collecting sample CH-19-2.

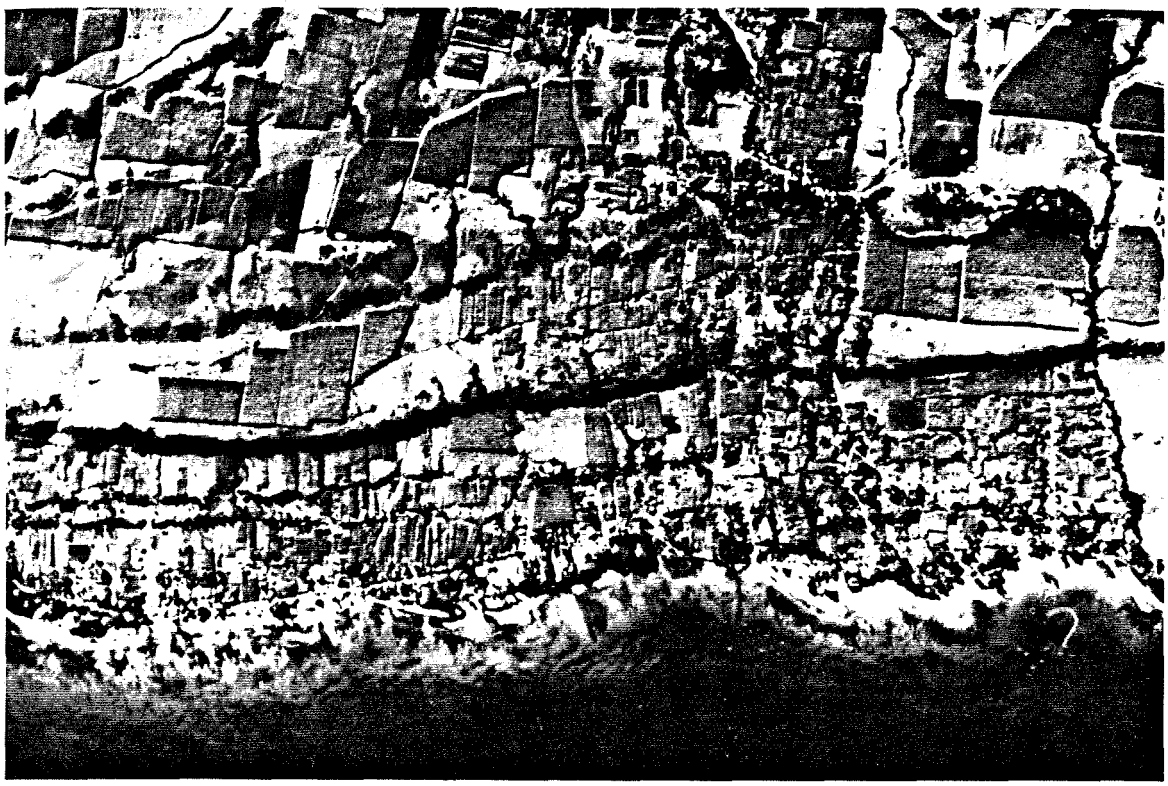

Acropora palmata. Moving back from the crest, the proportion of A. palmata colonies gradually decreases, and head corals such as M. annularis and Siderastria sp. reappear along with Porites sp. This is termed the rear zone (Goreau, 1959). A. palmata is the best indicator of past sea level height because it grows at the reef crest. Although isolated colonies of A. palmata are known to grow at depths as large as 17 m (Goreau and Wells, 1967), the zone that is dominated by A. palmata typically does not extend below 6 m. Some workers have inferred that paleo-sea level was within 2 m of outcrops of fossil A. palmata presumably based on the height of the outcrop above the A. cervicornis - A. palmata transition (Bender et al., 1979). Although somewhat more complicated because of the larger number of species, zonation of reefs in the Indo-Pacific region is fundamentally similar to that of the Caribbean reefs (see Wells, 1957). It is clear that an understanding of species zonation in an outcrop of fossil corals is critical in understanding the former height(s) of sea level relative to the outcrop, and that under favorable circumstances, one should be able to establish this height difference to within a few meters.

4.5 Mechanisms of skeletal growth in corals

Scleractinian coral skeletons are made up dominantly of fibrous aragonite crystals that have diameters of 0.05 to 0.7 microns and are elongated along the c-axis. Each species grows fibers with a characteristic diameter (see Constantz, 1986). These fibers radiate from a linear array of submicron sized crystals called centers of calcification (Ogilvie, 1896). The geometry of the skeleton is not

unlike a series of test tube brushes held together with their axes aligned subparallel to each other. The centers of calcification are represented by the axes of the brushes and the aragonite fibers by the bristles. Newly deposited centers of calcification in the species Mussa angulosa have recently been shown to be made up of calcite (Constantz and Meike, in prep.). These calcite crystals may be of intracellular origin (Constantz, personal communication).

The geometry of the skeleton suggests that the calcite crystals are the sites of nucleation for the aragonite fibers. The mechanism that causes the fibers to crystallize is not well understood. The fibers are similar in shape to inorganically precipitated marine aragonite. U/Ca ratios in coral skeletons are also similar to U/Ca ratios in inorganically precipitated aragonitic oolites (Tatsumoto and Goldberg, 1959). This has led to the idea that the crystallization process is similar to inorganic precipitation and that the organism simply provides nucleation sites (centers of calcification) and a supersaturated solution from which the aragonite precipitates (see Constantz, 1986). Although this provides a general notion of how the skeleton is produced, questions about how the supersaturated solution is produced, how each species produces aragonite crystals of characteristic diameter, and how such a simple process could result in skeletons that have such a regular and species specific geometry remain unanswered.

4.6 Growth rates of coral skeletons and growth band dating

Some hermatypic coral skeletons have regular variations in bulk density that show up as bands parallel to the growth surface in x-radiographs of slabs of the skeleton (figure 4.9). Each band is composed of a high density and a low density layer. Knutson et al.(1972) examined slabs of coral skeleton collected from living corals at Bikini Atoll. Comparison of x-radiographs and auto-radiographs of the same slabs demonstrated that the bands were annual. The ages (determined by counting of growth bands back from the living surface of the coral) that corresponded to the dark portions of the auto-radiographs were identical to the times of extensive bomb testing.

Dating corals by counting annual growth bands has been important in a wide variety of studies including studies of coral growth rate (e.g. Baker and Weber, 1975), studies of initial ^{14}C abundance and the timing of El Nino events (Druffel, 1981), and the ages of corals killed by coseismic uplift (Taylor et al., 1980, 1985a, 1987). The method, however, has the following limitations. Many corals have irregular or indistinct growth bands and cannot be dated by this technique. The surface of the coral must be alive. Corals may live to be over 600 years old, but colonies older than 200 years old are uncommon. Dating by growth bands is therefore, in general, limited to the past two centuries.

From growth band studies, hermatypic coral colonies have been shown to deposit skeletons at rates of 0.3 to 20 cm/y (Hopley, 1982, pp.74-75). Head corals have growth rates of about 1 cm/y, whereas the branching Acropora species have growth rates of about 10 cm/y.

Figure 4.9. X-radiograph of a portion of sample CWS-A which was drilled from a living Goniastria retiformis coral head in 1981. The annual growth bands are clearly visible. The assigned years of growth are shown in F.W. Taylor's handwriting on the left. Fragments selected from the portions of the sample labelled "A" and "B" yielded a ^{230}Th growth date of A.D. 1969 ± 3 (2 sigma, see section 8.3 and figure 8.2).

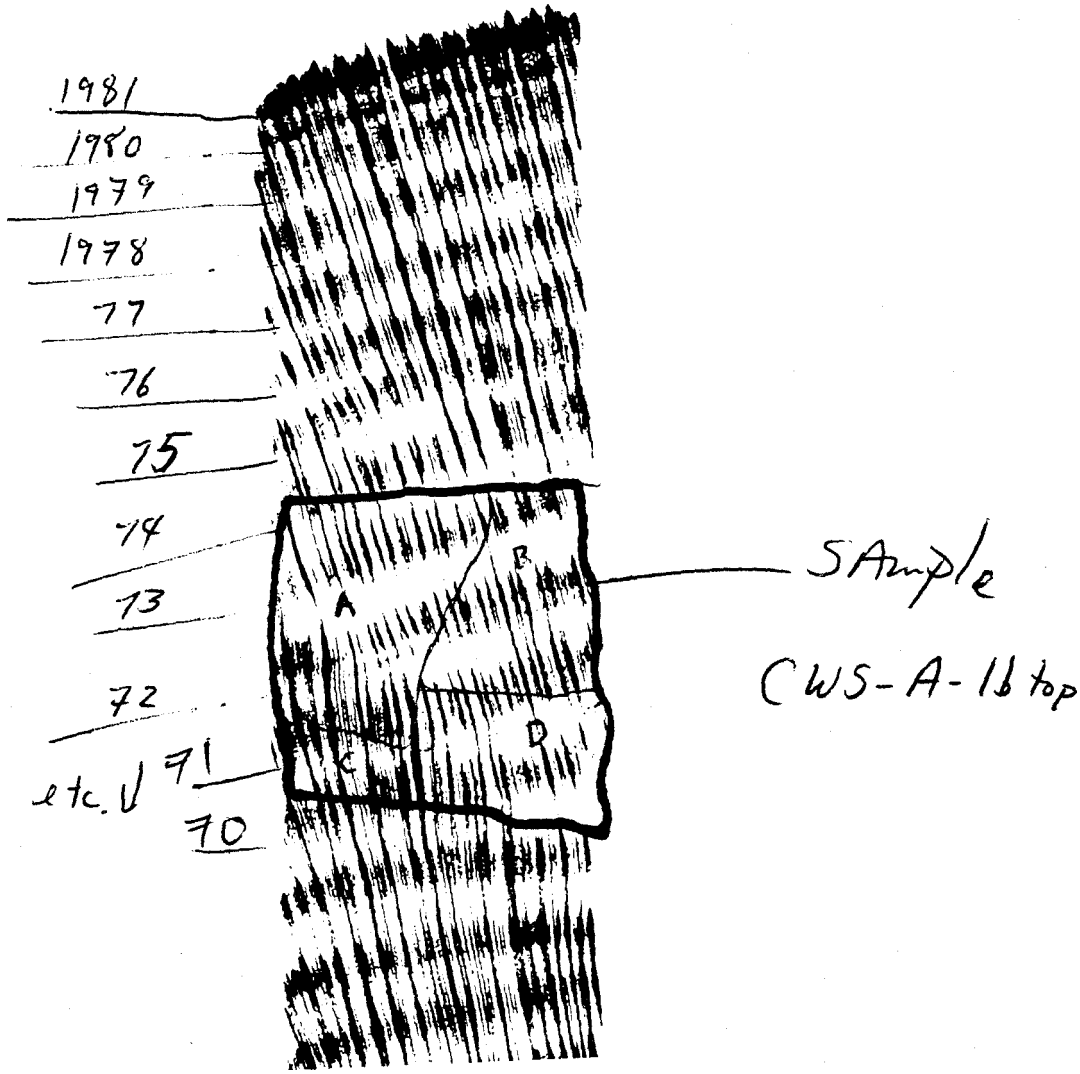
1981
1980
1979
1978
77
76
75
74
73
72
etc. 71
70
A
B
C
D
Sample
CWS-A-1b top

Vertical rates of reef accretion have been estimated by coring of Holocene reefs and dating the coral skeletons by the ^{14}C method. The rates range from 0.02 to 2.1 cm/y (Hopley, 1982, p.224).

4.7 Coral terraces and sea level fluctuations

Terraces composed largely of coral skeletons are distinctive features along the shorelines of many tropical islands. The terraces may be submerged or subaerially exposed. On some islands, flights of several tens of terraces may be exposed (figures 4.8 and 4.10 to 4.12). Most coral terraces can be demonstrated to be constructional features based on the relationship between species zonation and topography (see figure 4.6; Mesollela et al., 1969).

Based on the rates of reef accretion (section 4.6), one would surmise that it would take several thousand years to generate the rather large planar upper surface of a terrace (figures 4.6 and 4.11) from an initially irregular surface, and that in order to do this, sea level must be relatively stable over this time period. Sea level is stable on a given land mass when the rate of tectonic uplift is equal to the rate of sea level rise (tangent points on figure 4.2). Coral terraces are therefore likely to develop at these times. If this is the case and no erosion has occurred, the highest surface on a coral terrace marks the highest position on that land mass reached by seawater. Coral collected from this position has the characteristics of the material discussed in section 4.2, and is therefore subject to the analysis presented there. As noted at the end of that section, rates of tectonic uplift tend to be much smaller than maximum rates of

Figure 4.10. Upper photograph: terrace sequence from the Huon Peninsula on New Guinea. The highest terrace grew during the last interglacial period and is about 300 m above sea level. Tectonic uplift rates on the Huon Peninsula exceed 3 m/ky. (Photograph by A.L. Bloom.)

Lower photograph: single coral terrace from the south shore of Hispaniola. The top of the terrace is 7 m above sea level. This terrace formed during the last interglacial period. This shoreline has not undergone significant uplift in the past 10^5 y.

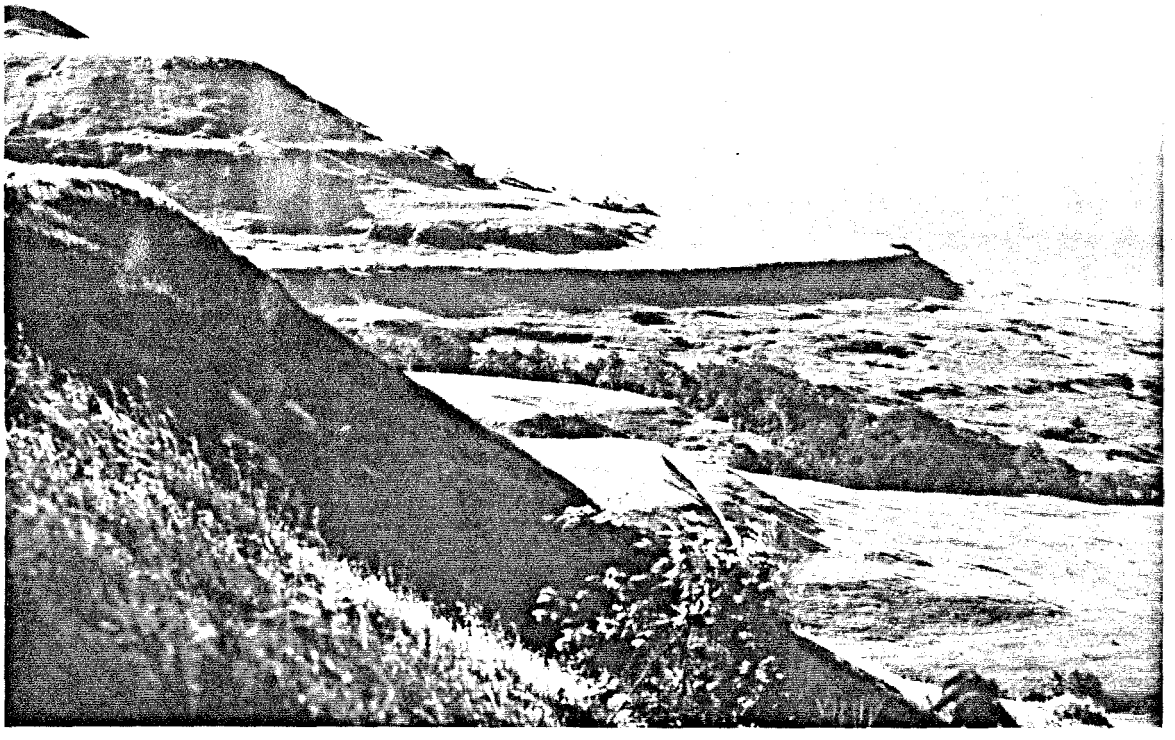

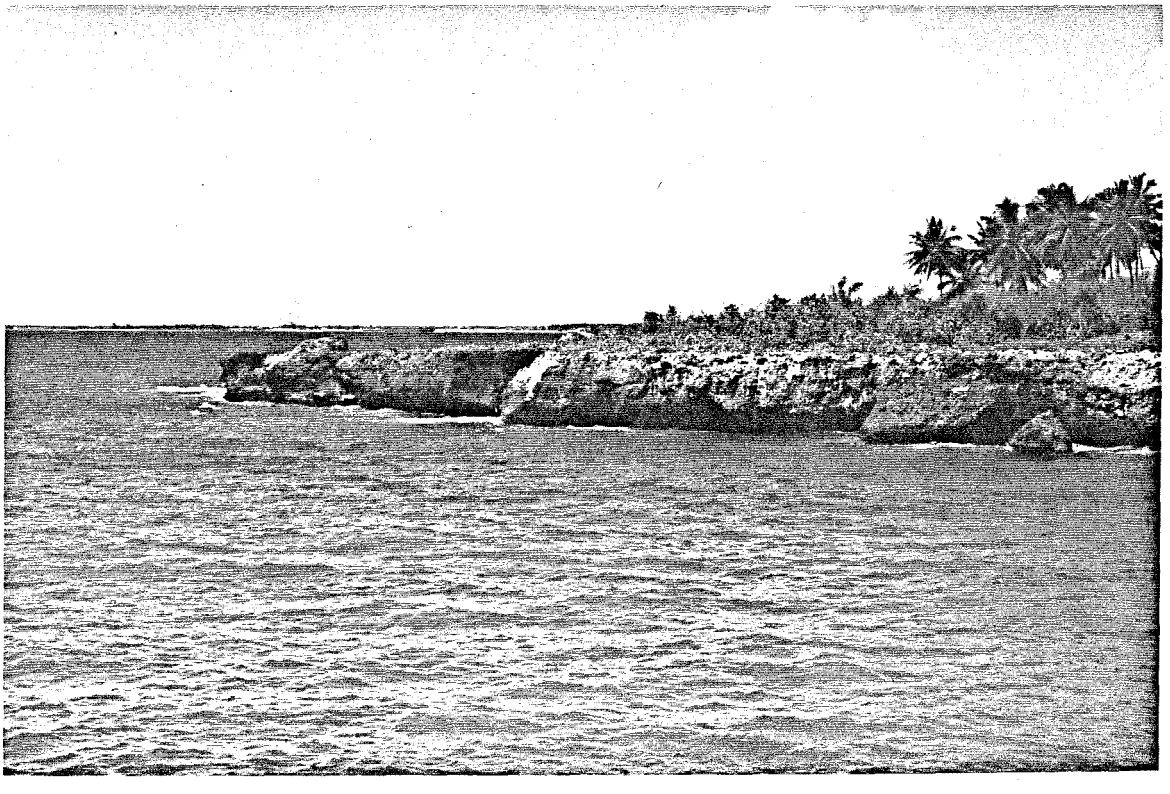

Figure 4.11. Terrace sequence from the west coast of Barbados. The most prominent terrace is the Rendezvous Hill Terrace, which formed during the last interglacial period. The distance across the bottom of the photograph is about 2 km. (Photo courtesy of F.W. Taylor.)

Rendezvous Hill

Terrace

↓

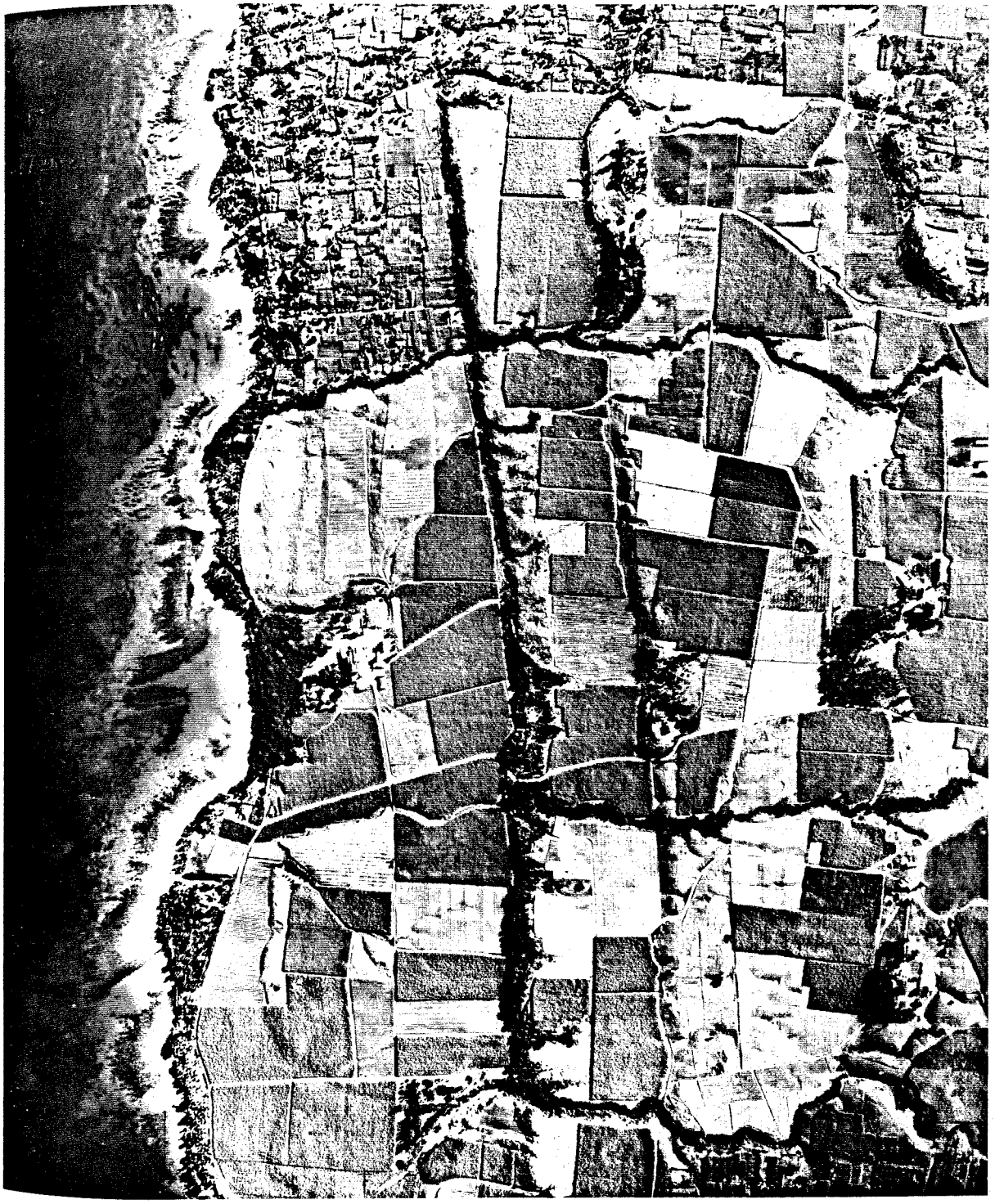

↑

Figure 4.12. Schematic diagram showing that one would not expect material that was formed continuously at the sea surface to be deposited in uniform amounts at all elevations on a shoreline. These diagrams were constructed from the "stable" and "rising" curves in figure 4.1 based on the assumption that material was deposited at a constant rate right at the sea surface. The width of the dark band represents the amount of material deposited on a shoreline at that elevation (normalized to an arbitrary value). Comparison of 'A', 'B', and 'C' in figure 4.1 and this figure shows that large amounts of material are deposited at a particular elevation on a shoreline when the rate of change in sea level with time is equal to the rate of tectonic uplift (i.e., the tangent points in figures 4.2 and 4.3). Comparison of the upper and lower diagrams shows that the record tends to be better resolved on the tectonically rising coast and that more of the record is above present sea level on the tectonically rising coast. On a real coastline, when large amounts of material are deposited at a given elevation on a shoreline, this material takes the form of a terrace.

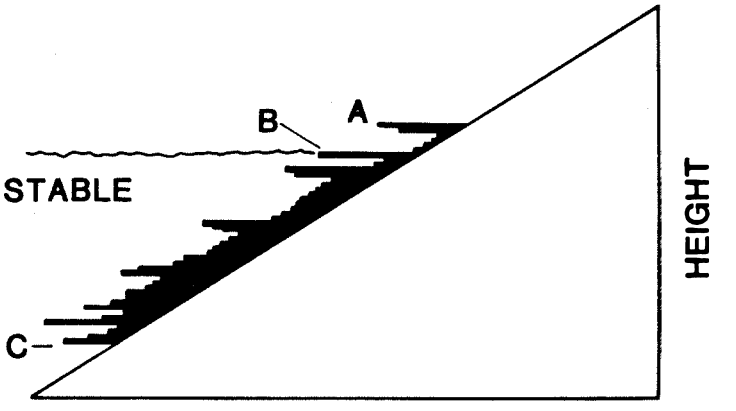
B
A
STABLE
C
HEIGHT

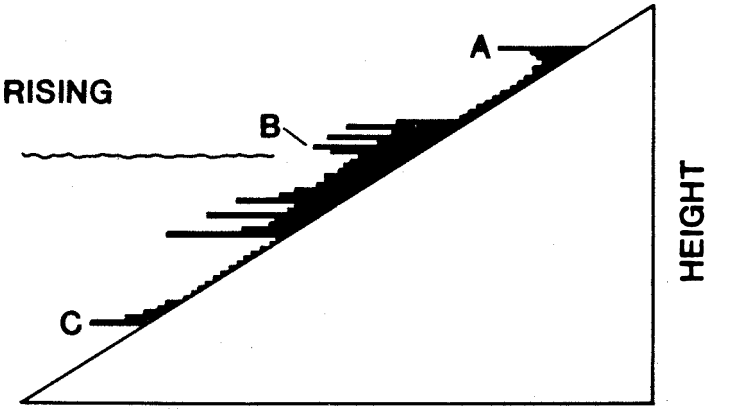
A
RISING
B
C
HEIGHT

sea level rise. Therefore, in practice, tangent points on rising coastlines occur prior to the time of a sea level maximum when sea level is just below its maximum height. The tangent point on a stable coastline occurs at the time and height of a sea level maximum. If the upper surfaces of coral terraces are deposited at tangent points, then terraces deposited on rising and stable coastlines must form at the time of a sea level maximum or prior to it and at the height of a sea level maximum or just below it.

Coral terraces should form under analogous situations during sea level minima (figure 4.12). However, there are reasons why these terraces are unlikely to be sampled. Because present sea level is relatively high, terraces formed during sea level minima on stable coastlines are currently submerged. Terraces formed during sea level minima could be raised above present sea level by tectonic movement. However, sea level minimum terraces would tend to be covered by sea level maximum terraces during the course of tectonic uplift.

4.8 The oxygen isotope record in deep sea sediments

In addition to determining the Quaternary sea level curve using the coral record, attempts have been made to determine changes in the volume of water contained in the oceans using oxygen isotope stratigraphy of deep sea sediments. Emiliani (1955) showed that the $^{18}O/^{16}O$ ratio of foraminifera recovered from deep sea cores changes with depth and, for a particular core, has a range of about 1.6 $^{o}/_{oo}$. He attributed this shift to changes in seawater temperature, which resulted in changes in the degree of fractionation of the oxygen

isotopes between calcite and water. It was later demonstrated (Shackleton, 1967; Shackleton and Opdyke, 1973) that, for the latter part of the Quaternary, the shift was largely due to changes in the isotopic composition of ocean water. This is presumably due to changes in the fraction of water contained in glaciers. Glacial ice is depleted in ^{18}O relative to ^{16}O and extraction of progressively more water to form continental glaciers would result in ocean water that was progressively more enriched in ^{18}O. Thus, changes in the isotopic composition of foraminifera with depth in deep sea cores have been interpreted to represent changes in ice volume with time. The main problems with this approach are (1) bioturbation of the upper ten centimeters or so of sediment, resulting in homogenization of sediments that have age differences of thousands of years (even for locations with extremely high sedimentation rate), and (2) problems with assigning an absolute age to a specific depth in a core.

The latter represents a particularly serious problem because if one wishes to test the astronomical theory, one needs a climatic record with accurate ages. Several depths in a core may have ages that are fairly well known. If the top of the core has not been disturbed during the coring process, then the top has an age of zero. The youngest portion of a core can be dated by the ^{14}C method. The depth of the first magnetic reversal in the core can be assigned an age of $(0.73 \pm 0.02) \times 10^6$ y (Mankinen and Dalrymple, 1979). The depth of the first $^{18}O/^{16}O$ minimum that has a value less than the present value is assumed to have the same age as the last corals that grew above present sea level. Assuming that the correlation is correct, the validity of

this age assignment depends on the accuracy and precision of the coral age. This will be discussed in detail in the following chapters. It is often assumed that sedimentation rates are constant between the depths that have been assigned ages (see Hays et al., 1976).

Important insights into the relationship between orbital geometry and climate have been gained by analysis of the $^{18}O/^{16}O$ record in deep sea sediments. The validity of these insights is of course dependent on the accuracy of the assigned timescale. Spectral analysis of the record from a number of cores shows that a large fraction of the variance in the record occurs at frequencies corresponding to periods of about 100,000, 40,000, and 20,000 years (Hays et al., 1976; Imbrie et al., 1984; figure 4.13). The agreement between these periods and the periods for eccentricity, obliquity, and precession (figure 4.13) suggests that some of the variability in Pleistocene climate is due to orbital forcing. A closer look at the spectrum shows that by far the greatest variance occurs at a period of about 100,000 years. Although eccentricity has a period of about 100,000 years, it is not clear why changes in eccentricity should cause changes in climate. Changes in eccentricity only cause changes in the distribution of insolation when modulated by precession which has a much shorter period. Thus, it is possible that the agreement between the dominant period in the oxygen isotope record and the quasi-period of eccentricity is fortuitous. The cause of the 100,000 year period is enigmatic.

In summary, spectral analysis of the oxygen isotope record shows significant variance at periods of about 20,000 years and 40,000 years. These are similar to the periods of precession and obliquity and

Figure 4.13. Upper diagram: the oxygen isotope record recovered from benthic foramenifera in deep sea core RC11-120 (Hays et al., 1976). The highest peak is oxygen isotope stage 5e, which is thought to represent the last interglacial period.

Middle diagram: power spectrum for the summer solar insolation received at 60°N latitude (Hays et al., 1976).

Lower diagram: power spectrum for the curve in the upper diagram after ages were assigned to some of the depths of the core, and constant sedimentation rates were assumed between these points. Comparison with the middle diagram shows that there are peaks that correspond to the period of obliquity (41 ky) and the precession period (23 ky and 19 ky). However, most of the variance is at lower frequency. This frequency corresponds roughly to the period of eccentricity. However, there is no obvious reason why climate should respond specifically to changes in eccentricity because the percent variance in the insolation curve at the period of eccentricity is negligible (Hays et al., 1976).

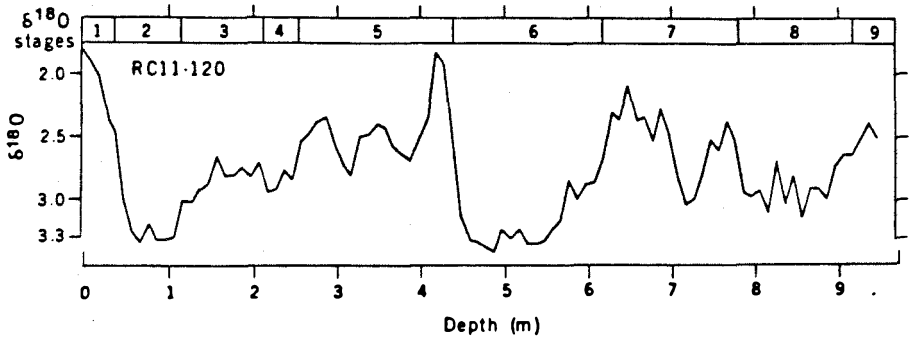
δ18O stages
1
2
3
4
5
6
7
8
9
RC11-120
δ18O
2.0
2.5
3.0
3.3
0
1
2
3
4
5
6
7
8
9
Depth (m)

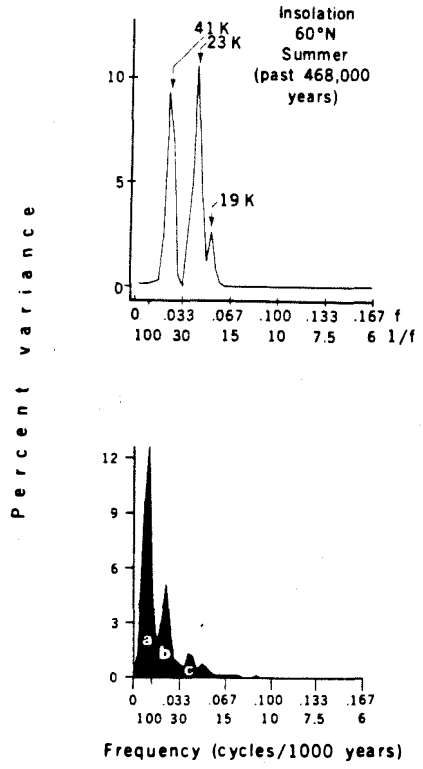
Insolation
60°N
Summer
(past 468,000
years)
41 K
23 K
19 K
10
5
0
0 .033 .067 .100 .133 .167 f
100 30 15 10 7.5 6 1/f
Percent variance
12
9
6
3
0
a
b
c
0 .033 .067 .100 .133 .167
100 30 15 10 7.5 6
Frequency (cycles/1000 years)

indicate that some of the variability in Pleistocene climate is due to orbital forcing. The dominant peak occurs at 100,000 years and is not clearly related to orbital forcing. There is also a continuum underneath the three peaks, which is of unknown origin.

It is hoped that the determination of an accurate and precise sea level curve from coral dating will complement and extend the insights gained from the oxygen isotope record. In particular, an accurate sea level curve would provide information about phase lags between orbital forcing and climatic change and indicate whether major climatic changes, not obviously related to orbital forcing, have occurred. The key characteristic of such a sea level curve would be an accurate knowledge of the timing of climatic change. The key characteristic of the oxygen isotope record is its continuous nature. Ultimately, one would wish to construct a combined climatic curve that takes advantage of both characteristics. This would require correlation of points on the oxygen isotope curve with dated coral terraces.

5. ^{238}U-^{234}U-^{230}Th-^{232}Th systematics

5.1 Solutions to the radioactive decay equations

The ^{238}U decay series with only the nuclides pertinent to this discussion is shown below:

$$^{238}U \xrightarrow{6.446 \times 10^9\ y} {}^{234}U \xrightarrow{352.7 \times 10^3\ y} {}^{230}Th \xrightarrow{108.8 \times 10^3\ y} {}^{206}Pb$$

The times below the arrows are mean lives. The time scale for ionium dating is dependent on and similar to the mean lives of the pertinent intermediate daughters. The mean life of ^{238}U is several orders of magnitude longer than any of the intermediate daughters. Therefore, over time scales appropriate for ionium dating, we can assume that the number of atoms of ^{238}U in a sample does not change due to radioactive decay. If it is also assumed that (1) the number of atoms of either ^{238}U, ^{234}U, or ^{230}Th does not change due to chemical processes, and that (2) the initial $^{230}Th/^{238}U$ ratio in corals is zero, then the equations of radioactive production and decay can be solved to yield two equations that can be used to calculate the initial $^{234}U/^{238}U$ ratio and the age of a coral as a function of the measured $^{234}U/^{238}U$ and $^{230}Th/^{238}U$ ratios. Let ^{230}Th, ^{234}U, and ^{238}U refer to the number of atoms of each nuclide; λ_i = the decay constant for nuclide i; T = time; $f_{230} = (^{230}Th/^{238}U)(\lambda_{230}/\lambda_{238}) - 1$; $f_{234} = (^{234}U/^{238}U)(\lambda_{234}/\lambda_{238}) - 1$; the superscript ° refers to the initial state (at T = 0). The activity ratio $[^{230}Th/^{238}U]_{act} = (^{230}Th/^{238}U)(\lambda_{230}/\lambda_{238})$, and $\delta^{234}U = \{(^{234}U/^{238}U)(\lambda_{234}/\lambda_{238}) - 1\}\{1000\}$. The initial state (assumption (2)

above) is:

$$\text{at } T = 0,\ f^{\circ}_{230} = -1 \tag{5.1}$$

The equations for radioactive production and decay are:

$$(d^{230}Th/dT) = \lambda_{234}{}^{234}U - \lambda_{230}{}^{230}Th \tag{5.2}$$

and

$$(d^{234}U/dT) = \lambda_{238}{}^{238}U - \lambda_{234}{}^{234}U. \tag{5.3}$$

Using the assumption that ^{238}U is constant with time, substituting, and rearranging, I calculate the following analogous equations:

$$df_{230}/dT = \lambda_{230}(f_{234} - f_{230}) \tag{5.4}$$

and

$$df_{234}/dT = -\lambda_{234}(f_{234}). \tag{5.5}$$

Equation 5.5 can be integrated directly and yields:

$$f_{234} = [f^{\circ}_{234}][\exp(-\lambda_{234}T)]. \tag{5.6}$$

Substituting equation 5.6 into 5.4 and rearranging yields:

$$df_{230}/dT + \lambda_{230}f_{230} = \lambda_{230}f^{\circ}_{234}\ [\exp(-\lambda_{234}T)] \tag{5.7}$$

which is a first order linear differential equation whose solution is:

$$f_{230} = f^{\circ}_{234}[\lambda_{230}/(\lambda_{230}-\lambda_{234})][\exp(-\lambda_{234}T)] + C[\exp(-\lambda_{230}T)] \quad (5.8)$$

where C is a constant of integration. Solving for C using equations 5.1 and 5.8 and substituting into 5.8 results in:

$$f_{230}=f^{\circ}_{234}[\lambda_{230}/(\lambda_{230}-\lambda_{234})][\exp(-\lambda_{234}T)-\exp(-\lambda_{230}T)]-\exp(-\lambda_{230}T) \quad (5.9)$$

Substituting for f°_{234} using equation 5.6 yields:

$$f_{230}=f_{234}[\lambda_{230}/(\lambda_{230}-\lambda_{234})][1-\exp(-(\lambda_{230}-\lambda_{234})]-\exp(-\lambda_{230}). \quad (5.10)$$

Substituting for f_{230}, f_{234}, and f°_{234} in equations 5.6 and 5.10, I obtain:

$$[^{230}Th/^{238}U]_{act}-1 = -\exp(-\lambda_{230}T) + [\delta^{234}U(0)/1000][\lambda_{230}/(\lambda_{230}-\lambda_{234})][1-\exp(-(\lambda_{230}-\lambda_{234})T) \quad (5.11)$$

and

$$\delta^{234}U(T) = [\delta^{234}U(0)][\exp(\lambda_{234}T)]. \quad (5.12)$$

Equation 5.11 (originally derived by Broecker, 1963) gives the age as a function of the decay constants and the measured $^{234}U/^{238}U$ and $^{230}Th/^{238}U$ ratios and is plotted in figure 5.1. Equation 5.12 gives the initial $^{234}U/^{238}U$ ratio when the coral grew as a function of the measured $^{234}U/^{238}U$ ratio and T. It is plotted in figure 5.2. For convenience, the $^{234}U/^{238}U$ ratio has been reformulated into δ-notation. The present $\delta^{234}U$ value is:

Figure 5.1. Graphical representation of equation 5.11. The initial $^{230}Th/^{238}U$ ratio at T=0 is assumed to be zero. For $\delta^{234}U(T)=0$, the $[^{230}Th/^{238}U]_{act}$ ratio approaches unity asymtotically with increasing time. For a system that initially has the isotopic composition of seawater ($\delta^{234}U(T)=150$), the position of the curve is slightly different.

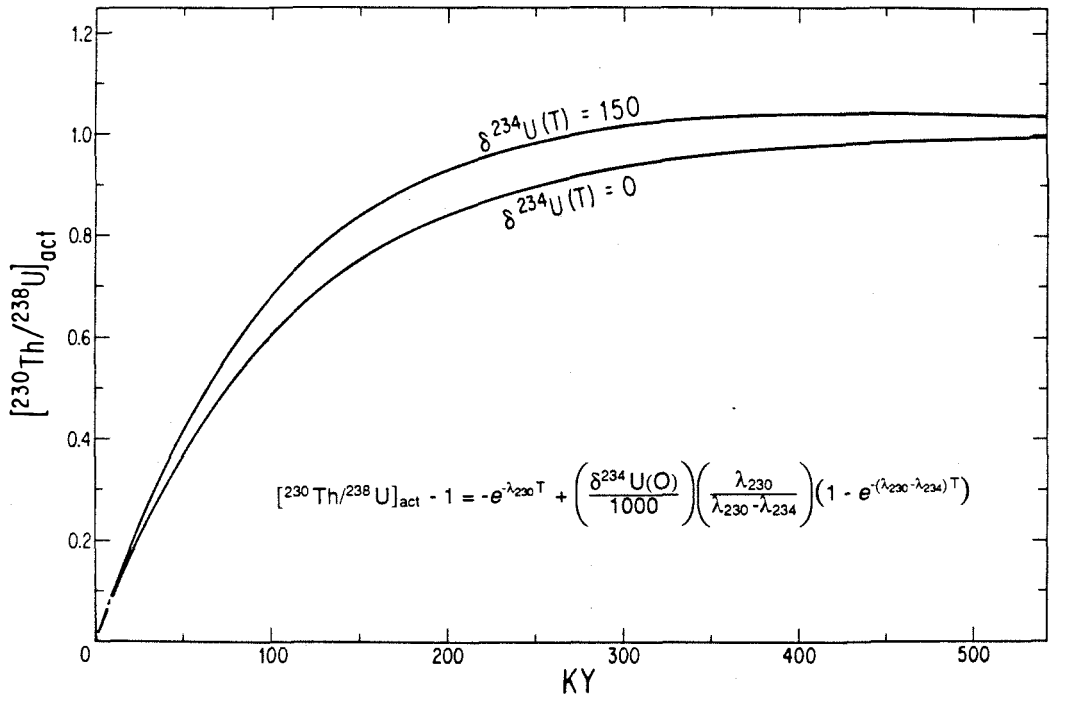
1.2
1.0
0.8
0.6
0.4
0.2
0
100
200
300
400
500
KY
$[^{230}Th/^{238}U]_{act}$
$\delta^{234}U(T) = 150$
$\delta^{234}U(T) = 0$
$[^{230}Th/^{238}U]_{act} - 1 = -e^{-\lambda_{230}T} + \left(\frac{\delta^{234}U(O)}{1000}\right)\left(\frac{\lambda_{230}}{\lambda_{230}-\lambda_{234}}\right)\left(1 - e^{-(\lambda_{230}-\lambda_{234})T}\right)$

Figure 5.2. Graphical representation of equation 5.12. Using T determined with equation 5.11, the measured uranium isotopic composition ($\delta^{234}U(0)$), and the curve defined by equation 5.12, the initial uranium isotopic composition ($\delta^{234}U(T)$) can be determined. $\delta^{234}U$ approaches zero asymtotically with increasing time.

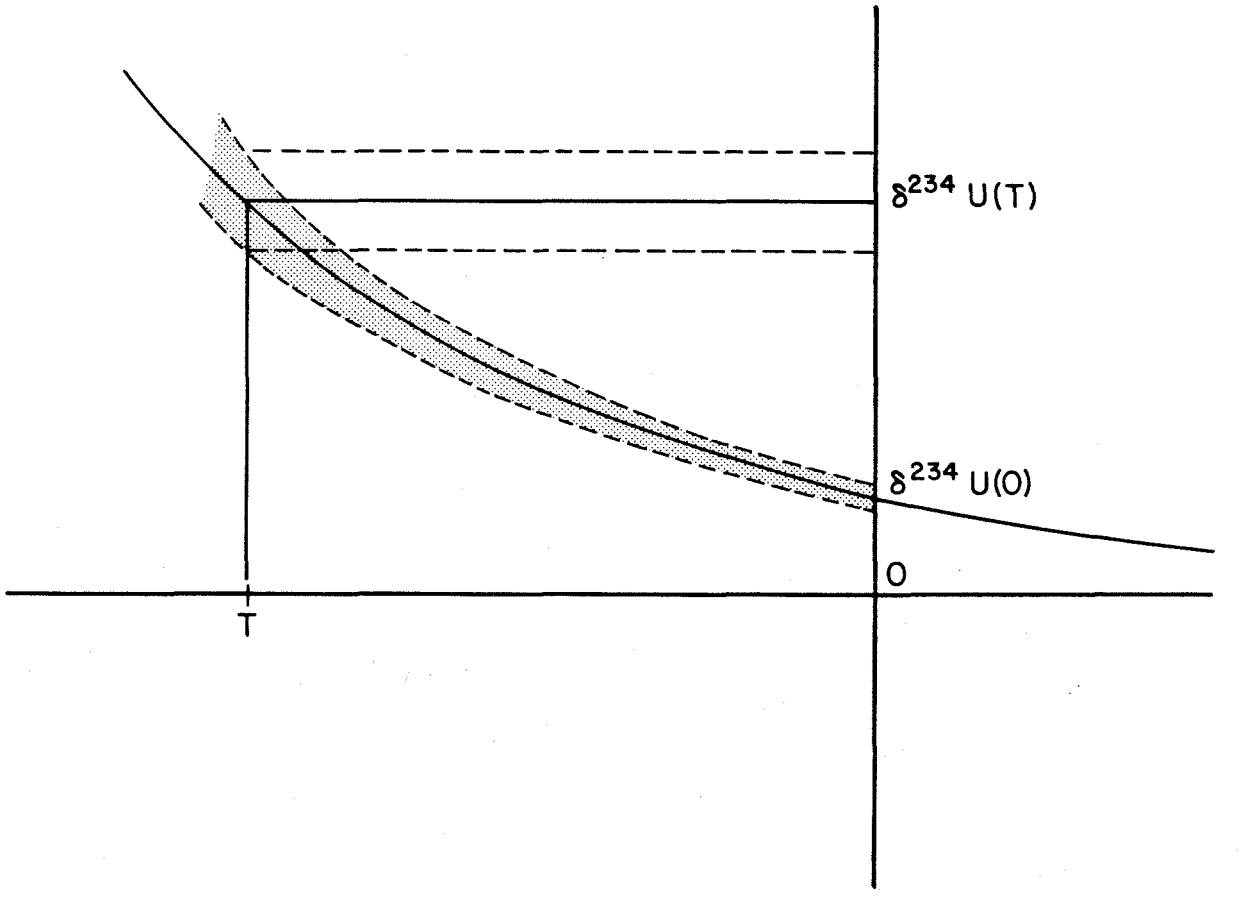
δ^{234} U(T)
δ^{234} U(0)
0
T

$$\delta^{234}U(0) = \{[(^{234}U/^{238}U)/(^{234}U/^{238}U)_{eq}] - 1\} \times 1000 \qquad (5.13)$$

This represents the fractional deviation of the measured $^{234}U/^{238}U$ ratio from the $^{234}U/^{238}U$ value at secular equilibrium $[(^{234}U/^{238}U)_{eq}]$ in parts per thousand. The initial $\delta^{234}U$ value when the system was isolated from seawater is given by $\delta^{234}U(T)$. The measured $^{230}Th/^{238}U$ atomic ratio has been represented as an activity ratio $([^{230}Th/^{238}U]_{act})$ by multiplying the $^{230}Th/^{238}U$ atomic ratio by the ratio of the decay constants $(\lambda_{230}/\lambda_{238})$.

If $\delta^{234}U(T)$ is known, equations 5.11 and 5.12 represent two independent chronometers. I have chosen to use equation 5.12 not as a chronometer but as a means of calculating $\delta^{234}U(T)$ with the value of T determined from equation 5.11 (figure 5.2). If it is assumed that the uranium isotopic composition of seawater is constant with time, a difference between the calculated $\delta^{234}U(T)$ and the present seawater value would indicate that the uranium in the coral was not derived via closed system evolution from normal seawater. The calculated $\delta^{234}U(T)$ therefore provides an independent check of whether the coral has behaved as a closed system.

^{232}Th is not a nuclide in the decay chain shown above and does not appear in equations 5.11 ar 5.12. It has an extremely long mean life (2.0212×10^{10} years (Le Roux and Glendenin, 1963)) and can be considered stable over the time range considered here. Comparison of the $^{232}Th/^{238}U$ ratio in an old coral with the $^{232}Th/^{238}U$ ratio in modern corals would indicate whether substantial differential addition or leaching of ^{238}U or ^{232}Th had occurred subsequent to coral growth.

Since the chemical properties of ^{230}Th and ^{232}Th are the same, knowledge of the $^{232}Th/^{238}U$ ratio provides another check of the closed system assumption used in deriving equation 5.11. Detailed discussion of the validity of the closed system assumption and the assumption that initial $^{230}Th/^{238}U$ is zero will follow in later sections.

5.2 The $\delta^{234}U(0)$ vs. $[^{230}Th/^{238}U]_{act}$ plane

A convenient way to examine uranium and thorium isotopic data is in plots of measured uranium isotopic composition vs. measured $^{230}Th/^{238}U$ ratio (figure 5.3). The abcissa and ordinate in this plot represent measured quantities and therefore the depiction of analytical errors is rather straight forward. If time contours and contours of equal initial uranium isotopic composition are drawn, the plot includes information contained in both eqs. 5.11 and 5.12.

The ordinate and abscissa in figure 5.3 along with time, T, are the variables in eq. 5.11. The derivative of $\delta^{234}U(0)$ with respect to $[^{230}Th/^{238}U]_{act}$ at constant T is a function only of T and therefore contours of equal time in the $\delta^{234}U(0)$-$[^{230}Th/^{238}U]_{act}$ plane are lines. For T=0, the line is coincident with the ordinate as is required by the initial condition $[^{230}Th/^{238}U]_{act}=0$. As T increases, the slopes of the lines of equal T decrease to a minimum value of $(1-\lambda_{234}/\lambda_{230})10^3$ for very large T. Lines of equal T are shown in figure 5.3.

By combining equations 5.11 and 5.12, one can calculate the positions of contours of equal initial $\delta^{234}U$. These contours are not lines as can be seen in figure 5.3. I refer to these contours as closed system trajectories. Each of these contours describes how the

Figure 5.3. A plot of $\delta^{234}U(0)$ versus $[^{230}Th/^{238}U]_{act}$. Both of these variables are measured quantities. The diagram is constructed from equations 5.11 and 5.12, which were derived assuming that at T=0, $^{230}Th/^{238}U=0$ and that the system is closed to chemical exchange. Contours of equal time are lines that decrease in slope with increasing time. Time trajectories start on the y-axis at T=0 and end at the point (0,1) at T=∞. All trajectories asymtotically approach the T=LARGE line. The specific trajectory is dependent on the initial uranium isotopic composition. Present seawater has a $\delta^{234}U$ value of 150 (see section 8.1). Therefore, as time passes, corals that are growing now will have isotopic compositions that are defined by the trajectory labelled "150." If a fossil coral does not plot on this trajectory, this indicates that the sample has been altered, that the isotopic composition of uranium has changed with time, or that the coral did not grow in normal seawater. None of the closed system trajectories plot in the stippled region. If a fossil coral plots in this region, it has been altered.

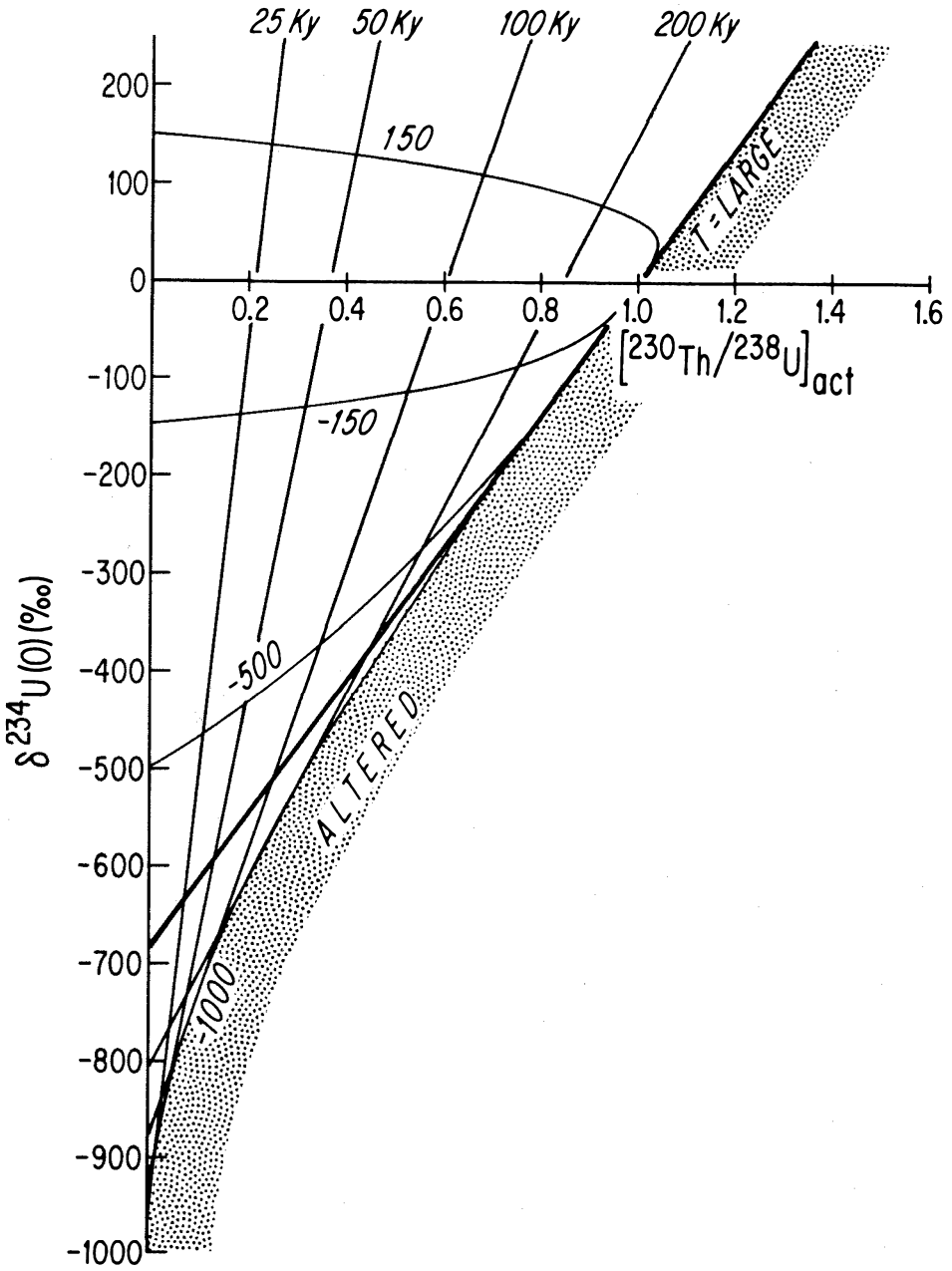
25 Ky
50 Ky
100 Ky
200 Ky
150
-150
-500
-1000
T = LARGE
ALTERED
200
100
0
-100
-200
-300
-400
-500
-600
-700
-800
-900
-1000
0.2
0.4
0.6
0.8
1.0
1.2
1.4
1.6
$\delta^{234}U(0)$ (‰)
$[^{230}Th/^{238}U]_{act}$

isotopic composition of a material with no initial ^{230}Th and a given initial $\delta^{234}U$ changes with time if the system is closed to chemical exchange. As required by the initial conditions, each trajectory starts on the ordinate at T=0. The trajectories all end at the point (0,1) at T=∞. All systems that have reached secular equilibrium lie on this point.

The plot with both sets of contours has several important characteristics. If one plots the isotopic composition of a material on this graph, one can immediately read off (1) the age of the material using the time lines and (2) the initial $\delta^{234}U$, by following the trajectory back to the y-axis. The veracity of the age and initial uranium isotopic composition are, of course, subject to the validity of the assumption that the system has remained closed to chemical exchange. In some instances, the plot may be used to test this assumption. Note, for example, that there are no closed system trajectories in the region labeled "altered" in figure 5.3. A material that plots in this region either was chemically altered or started with an isotopic composition that would have plotted in the "altered" region. In some cases one may know what the initial uranium isotopic composition was. In such cases, if the material does not plot on a trajectory that intersects the y-axis at the known value of initial $\delta^{234}U$, then either the material has been altered or the material did not start out with $^{230}Th/^{238}U$ equal to zero. For instance, as I will discuss in subsequent sections, the $\delta^{234}U$ of present seawater is known and the $\delta^{234}U$ of corals that grew during the last two centuries is the same as the seawater value. Therefore, if the isotopic composition of

uranium in seawater has remained constant with time, then all corals that grew in normal seawater and have not been altered must lie on the trajectory that intersects the y-axis at the $\delta^{234}U$ value of present seawater. If a coral lies off this trajectory, then it has been altered, the isotopic composition of uranium in seawater has changed with time, or it did not grow in normal seawater. These possibilities will be discussed further in other sections.

6. Samples: Geologic setting, collection and preparation

6.1 Goals

Samples were collected and obtained with the following goals in mind: (1) to determine the precision with which corals with different ages could be dated, (2) to compare mass spectrometrically determined ^{230}Th ages with ages determined by other methods (^{14}C, counting of coral growth bands, ^{230}Th by alpha-spectrometry) as a means of understanding the extent to which the assumptions used in obtaining dates are valid, (3) to determine the isotopic characteristics of very young corals and seawater as a means of assessing the validity of the initial condition used in solving equation 5.11 and establishing a value for the present isotopic composition of uranium in seawater, (4) to examine samples of the same age but different states of alteration as a means of establishing the effect of alteration on ^{230}Th ages, (5) to examine the possibility of determining seismic recurrence intervals by dating emerged corals which may have been killed by co-seismic uplift, (6) to determine the timing of sea level rise in the Holocene, and (7) to establish the ages of coral terraces that formed during the last interglacial period and subsequent interstadial periods and compare these ages to the 65°N insolation curve as a means of testing the astronomical theory.

6.2 Sample preparation

All samples except those discussed in section 6.6 were prepared by breaking the sample into fragments several millimeters in diameter with a stainless steel chisel. The fragments were examined under a

binocular microscope. Fragments that had calcite cleavage planes, had chalky surfaces, or were discolored were discarded. The remaining fragments were rinsed twice with distilled water in an ultrasonic cleaner, dried, weighed, dissolved, and the uranium and thorium separated using the procedure discussed in section 7.3.7.

6.3 Holocene corals from Santo and Malekula Islands, Vanuatu

Vanuatu is an island arc that extends some 1000 km roughly north-south just east of the Hebrides trench (figure 6.1) and is the result of the subduction of the Indian Plate under the Pacific Plate at a rate of 10 cm/y. Santo and Malekula Islands, two of the islands in the central portion of the archipelago are about 100 km long and are tectonically active. In some localities, Holocene uplift of tens of meters has occurred. For each of these islands the last large earthquake is documented in the historical record (M_S = 7.5 on Malekula in 1965 and M_S = 7.5 on Santo in 1977). Taylor et al. (1980, 1985a, 1987) examined partially emerged corals from both of the islands. The lower portions of the coral heads were below sea level and were still alive. The upper portions of the heads were above sea level and had died. Because the lower portion of each head was still alive, the authors were able to determine the time of death of the upper portion of each head by counting annual growth bands. They demonstrated, for each island, that the time of death (and presumably emergence) was the same as the time of the last major earthquake and documented the amount of emergence associated with each event.

At each locality, there were also completely emerged coral heads

Figure 6.1. Map of Vanuatu. Holocene samples in this study were collected from the islands of Santo, Malekula, and Tangoa, which is the small island between Santo and Malekula. Pleistocene samples in this study were collected from Efate Island. (After Taylor et al., 1987.)

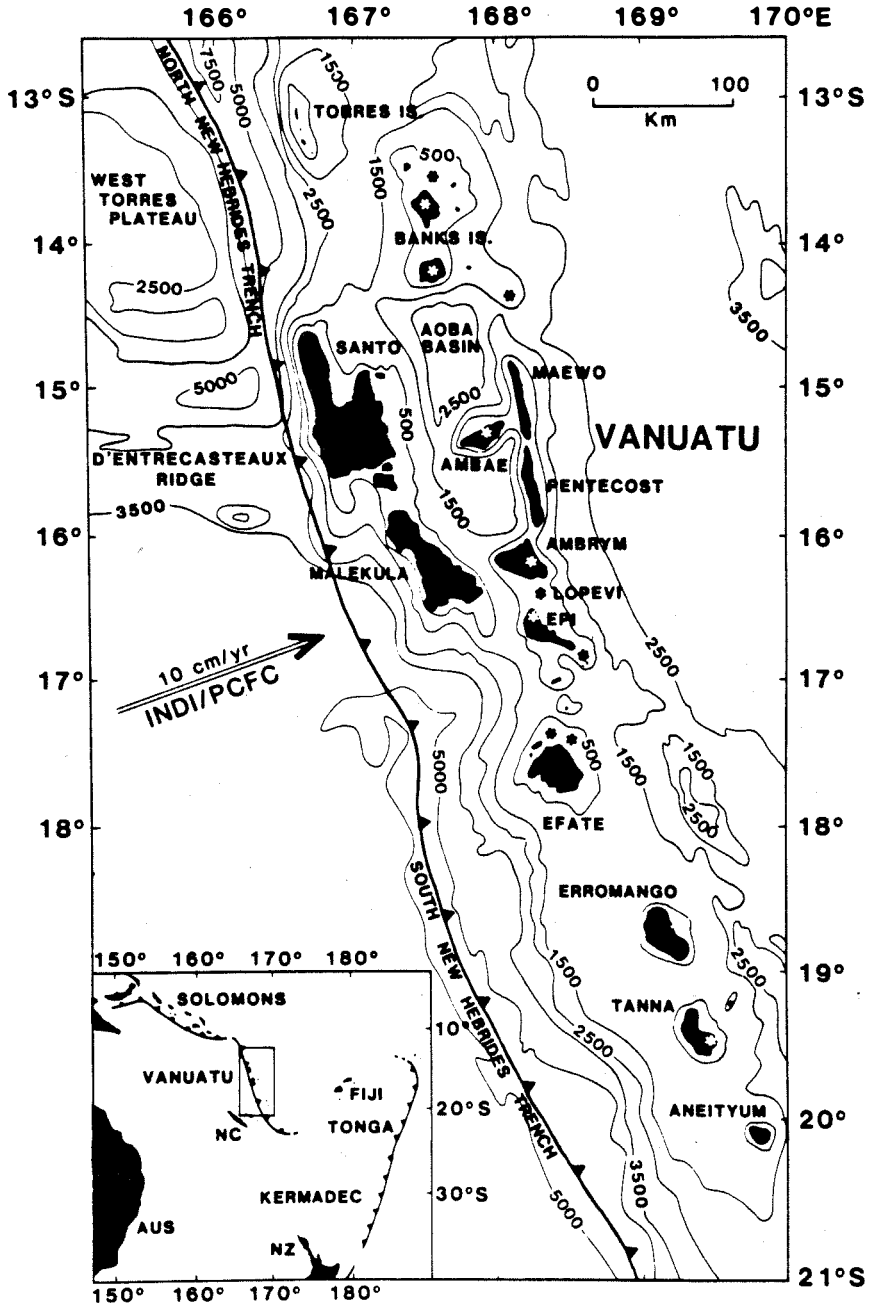
166°
167°
168°
169°
170°E
13°S
14°
15°
16°
17°
18°
19°
20°
21°S
0
100
Km
NORTH NEW HEBRIDES TRENCH
TORRES IS.
WEST TORRES PLATEAU
BANKS IS.
AOBA BASIN
SANTO
MAEWO
VANUATU
D'ENTRECASTEAUX RIDGE
AMBAE
PENTECOST
AMBRYM
MALEKULA
LOPEVI
EPI
10 cm/yr
INDI/PCFC
EFATE
ERROMANGO
TANNA
ANEITYUM
SOUTH NEW HEBRIDES TRENCH
7500
5000
2500
1500
500
3500
150°
160°
170°
180°
10°
20°S
30°S
SOLOMONS
VANUATU
NC
FIJI
TONGA
KERMADEC
AUS
NZ

that were slightly higher than the partially emerged heads. They could not be dated by growth band dating because the coral colonies had died. By analogy to the partially emerged heads, it was thought that these heads were killed by earlier co-seismic uplift events at each locality. If this is the case, then emerged coral heads of the same height and locality must have died at the same time. If no erosion of the surface of the coral heads has occurred, then the present age of the surface of coral heads at the same locality and height must be the same.

In order to address this issue, establish limits on the amount of ^{230}Th initially incorporated in corals, and determine the initial isotopic composition of uranium in corals, a series of corals were obtained from this area from F.W. Taylor (see table A1(I)). The samples are from three different localities. The samples labelled "CWS" are from the "OLP" locality (Taylor et al., 1987) on northwest Santo Island (figure 6.1). TAN-E-1g is from Tangoa Island, a small island just south of Santo Island. Samples MAF and MAG are from the "M-A" locality (Taylor et al., 1980) on northern Malekula Island, and MY2 is from the nearby "MY" locality (Taylor et al., 1980). The present heights of the samples are given in Table A1(I).

CWS-A-1b, CWS-A-1d, and TAN-E-1g had been dated previously by counting of growth bands and grew between 1806 and 1973 (Taylor et al., personal communication; see figures 4.9 and 8.2). These samples were obtained by drilling into living coral heads. The cylindrical core was sawn lengthwise into two half-round cylinders. X-radiographs of the half-round cores were then made. A xerox of a radiograph showing the portion of the core that was analyzed (CWS-A-1b, portions labelled A

and B) is shown in figure 4.6. The head was drilled in 1981. Sample CWS-A-1d is from deeper in the same core. TAN-E-1g is from a coral head from a different locality. Samples TAN-E-1g and CWS-F-1 have been dated previously by the ^{14}C analysis (see Table 9.1).

Samples CWS-C and CWS-D are completely emerged corals that have the same height (1.8 m above the highest living corals at that locality) and that were collected at the same locality as partially emerged corals that died during co-seismic uplift in 1977. MAF and MAG are an analogous pair of corals (1.3 m above the highest living corals) from a different locality. These were collected at a locality on north Malekula Is. where partially emerged corals were killed by co-seismic uplift in 1965. MY2 was collected near the MAF-MAG locality. It was collected from near the top of an emerged Holocene reef (15.3 m above the highest living corals) and was analyzed in order to determine the average Holocene uplift rate at this locality.

6.4 Holocene corals from the Enriquillo Valley, Hispaniola and from Barbados

Outcropping along the shore of Lake Enriquillo on the island of Hispaniola is a subaerially exposed Holocene coral reef (figure 6.2, Taylor et al., 1985b). Exposures of this reef extend for tens of kilometers along the shore of Lake Enriquillo. The width of the reef is about 400 m. Exposures at the reef can be seen between the elevations of 36 m below sea level and 2 m below sea level. The present level of the lake is -41.5 m below sea level. The lake water is hypersaline (49 $^{o}/_{oo}$ salinity) and corals do not currently grow in

Figure 6.2. Map of the Enriquillo Valley. The Holocene reef is denoted by the line of diamonds. Alluvial fans are represented by the bold stippled pattern. The major bodies of water are labelled "Lago Enriquillo" and "Bahia de Neiba". The latter is connected to the ocean. The sill area between Lake Enriquillo and Bahia de Neiba is composed of river and lake sediments and is just above sea level. Samples were collected from Canada Honda, which is labelled "CH". (After Taylor et al., 1985b.)

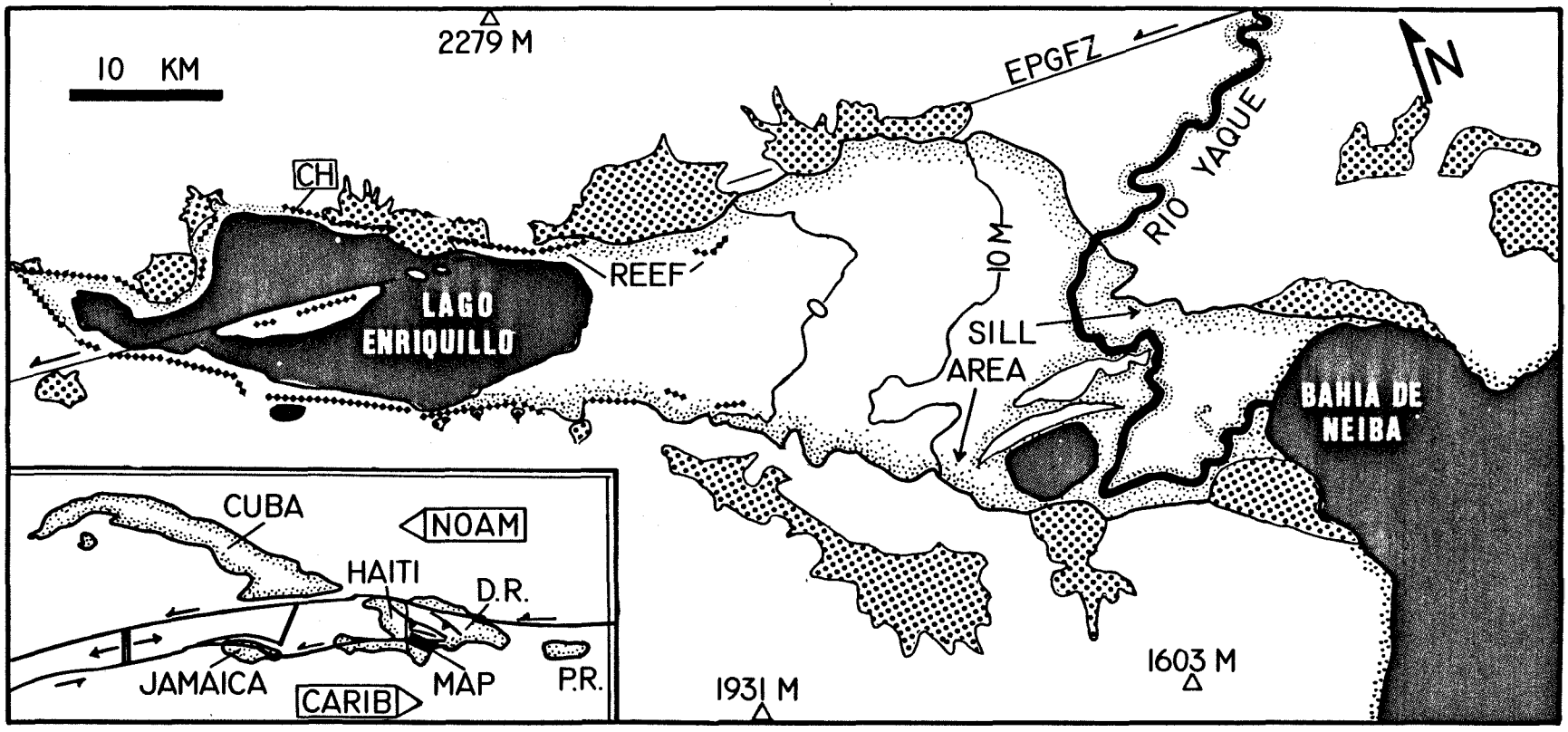
2279 M
10 KM
EPGFZ
N
CH
RIO YAQUE
10 M
REEF
LAGO ENRIQUILLO
SILL AREA
BAHIA DE NEIBA
CUBA
NOAM
HAITI
D.R.
JAMAICA
CARIB
MAP
P.R.
1931 M
1603 M

it. Because corals grew in the Enriquillo Valley in the Holocene, conditions must have been sufficiently "marine" at that time for these organisms to thrive. On this basis, it has been argued that, at that time, the lake was connected to the ocean via the north of the valley to the east (Mann et al., 1984; Taylor et al., 1985b, figure 6.2). The valley was subsequently isolated from the sea by accumulating deltaic sediments from the Rio Yaque del Sur, and the lake evaporated down to its present level because of extremely arid conditions. If the lake had been connected to the ocean, the corals must record fluctuations in Holocene sea level. This record is unique because it is presently subaerially exposed and can be observed in detail. Analogous records at other localities are below present sea level and are relatively inaccessible. If the water in the Enriquillo Valley was connected to the ocean, the initial $\delta^{234}U$ of the corals should be similar to the seawater value.

In order to test this and determine the timing of the sea level rise in the Holocene, I collected corals from different elevations across this reef in February of 1987 with F.W. Taylor and P. Mann. In several places the reef is cut by gullies that have locally eroded completely through the reef to the underlying unconformity. These gullies offer an excellent view of the reef in a third dimension. The samples which I collected are from or near two such gullies that are adjacent to each other. The location of one of the gullies (Canada Honda) is shown in figure 6.2. The second gully is parallel to Canada Honda and about 1 km to the east. The "CH" samples are from Canada Honda; the "PR" samples are from or near the gully just east of Canada

Honda. The elevation of each of the samples was determined by leveling from bench marks of known elevation using a theodolite. These elevations are accurate to better than ±10 cm and are reported in Table A1(II). The elevations of the samples range from 34 m to 7 m below sea level. All of these samples were in growth position when they were collected. CH-8 had been collected earlier by F.W. Taylor and was dated by ^{14}C methods (Taylor et al., 1985b; Table 9.1). Samples CH-8 and PR-H-1 were collected at localities where the underlying unconformity was exposed. Both of these corals grew directly on top of the unconformity and are the lowest corals exposed at each locality. PR-H-1 and PR-H-2 are from the same locality. PR-H-1 is the lowest exposed coral, and PR-H-2 is the highest exposed coral at that locality. The difference in height is 4.9 m. These samples were analyzed, in part, to determine the vertical rate of reef accretion. All the samples are head corals (Siderastria sideria, Siderastria radians, and Montastria annularis). The species Acropora palmata, which would perhaps be a better indicator of sea level height, is not found in the valley.

One Holocene sample from Barbados (D.W., Table A1(III)) was analyzed in order to determine the uranium isotopic composition and height of a coral that grew at about the same time as the Enriquillo Valley corals but at an open ocean site. D.W. is a sample of Acropora palmata collected at a depth of about 4 m in Deep Water Harbor by B.R. Constantz.

6.5 Pleistocene corals from Barbados and Vanuatu

Barbados is a small island (about 10 km across), located in the fore arc region of the Windward Island Arc (figure 6.3). It is composed of Tertiary sediments from the accretionary wedge and a terraced Quaternary coral cap. The coral cap and the ages of the terraces have been quite extensively studied (see, for example, Mesollela et al., 1969; Broecker et al., 1968; Fairbanks and Matthews, 1978; Bender et al., 1979). This work has established that Barbados has been undergoing tectonic uplift at rates of tenths of a meter per thousand years over the last 10^5 years. Because the island is underlying uplift, portions of the sea level record that would currently be submerged in a stable area are subaerially exposed on Barbados. The ^{230}Th ages of the terraces have been critical in establishing an absolute time scale for the late Pleistocene. However, the precision obtainable by alpha-counting techniques is inadequate for evaluating the Milankovitch hypothesis (see section 7.1) and there are apparent discrepancies between the ages of the Barbados terraces and terrace sequences for other localities (see section 7.1). In order to establish the precise ages of these terraces and their relation to the 65°N curve, I analyzed samples from three of the Barbados terraces.

Samples were obtained directly from R.K. Matthews except for AFS-12A and AFS-12B, which were obtained from T.L. Ku, who had obtained them from R.K. Matthews. Sample localities are described in detail by Bender et al. (1979) and are shown in figures 6.4 and 6.5. All samples are of the species Acropora palmata. All samples have been shown by x-ray diffraction methods to contain less than 1 % calcite (Matthews,

Figure 6.3. Map of the Caribbean Sea showing the location of Barbados in the fore arc region of the arc defined by the Windward Islands. (After Mesollela et al., 1969.)

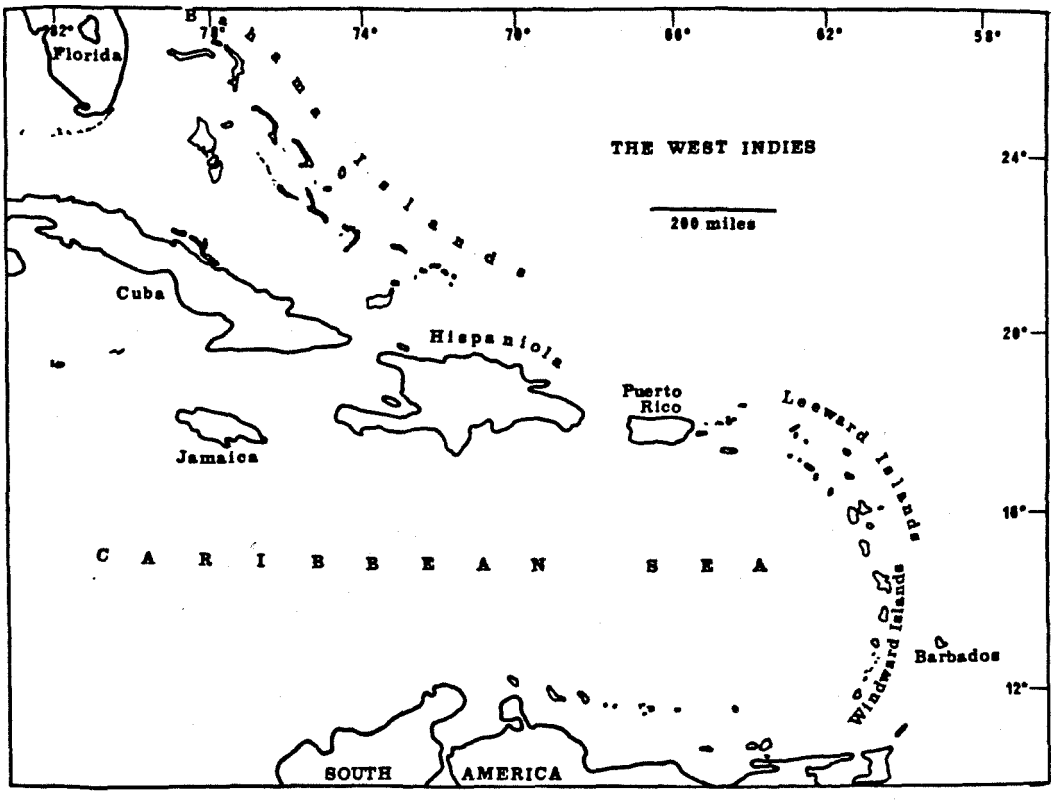
82°
Florida
78°
74°
70°
66°
62°
58°
THE WEST INDIES
200 miles
24°
Bahama Islands
Cuba
Hispaniola
Puerto Rico
Leeward Islands
Jamaica
20°
16°
C A R I B B E A N S E A
Windward Islands
Barbados
12°
SOUTH AMERICA

Figure 6.4. Upper diagram: map of Barbados. The dashed line separates the Scotland District, which is made up of Tertiary accretionary wedge sediments, from the terraced Quaternary coral cap. The Rendezvous Hill Terrace is on top of the "first high cliff." The locations of the Christ Church Ridge and Clermont Nose study areas of Bender et al.(1979) are indicated.

Lower diagram: Topographic map of the Christ Church Ridge study area. The sample localities for R-52, AFS-10, AFS-11, and AFS-12 are indicated. The dark lines show the location of the reef crest facies for each terrace. (After Bender et al., 1979.)

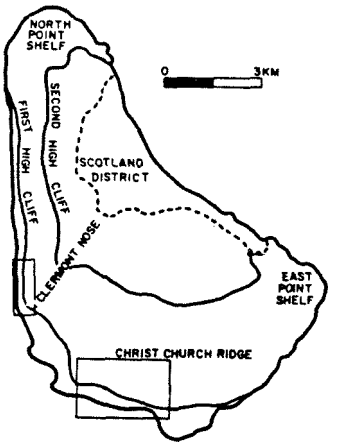
NORTH POINT SHELF
0 3KM
SECOND HIGH CLIFF
FIRST HIGH CLIFF
SCOTLAND DISTRICT
CLERMONT NOSE
EAST POINT SHELF
CHRIST CHURCH RIDGE

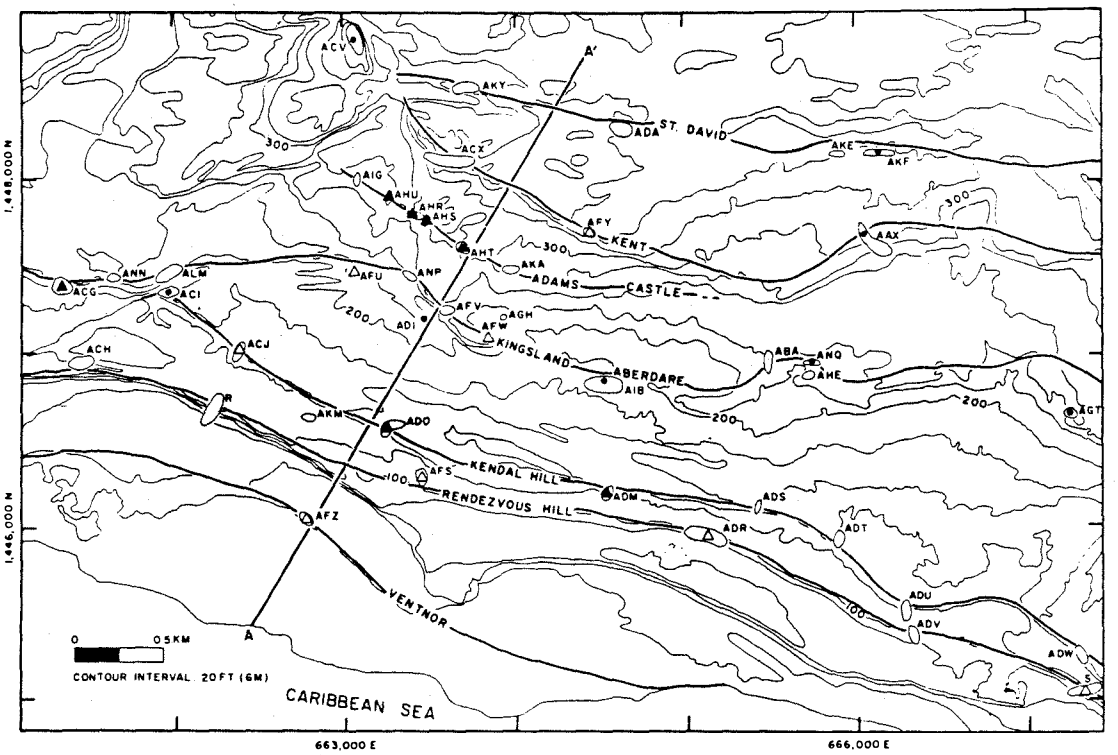
A
A'
ACV
AKY
ADA
ST. DAVID
AKE
AKF
ACX
AIG
AHU
AHR
AHS
AFY
KENT
AAX
AHT
AKA
ADAMS
CASTLE
ANN
ALM
ACG
ACI
AFU
ANP
AFV
AGH
AFW
KINGSLAND
ADI
ACH
ACJ
ABERDARE
AIB
ABA
ANQ
AHE
AGT
AKM
ADO
AFS
KENDAL HILL
RENDEZVOUS HILL
ADM
ADS
AFZ
ADR
ADT
ADU
ADV
ADW
VENTNOR
300
200
100
0 0.5KM
CONTOUR INTERVAL 20FT (6M)
CARIBBEAN SEA
1,448,000 N
1,446,000 N
663,000 E
666,000 E

Figure 6.5. Topographic map of the Clermont Nose study area showing the sample localities for OC-51, FT-50, and AFM-20. (After Bender et al., 1979.)

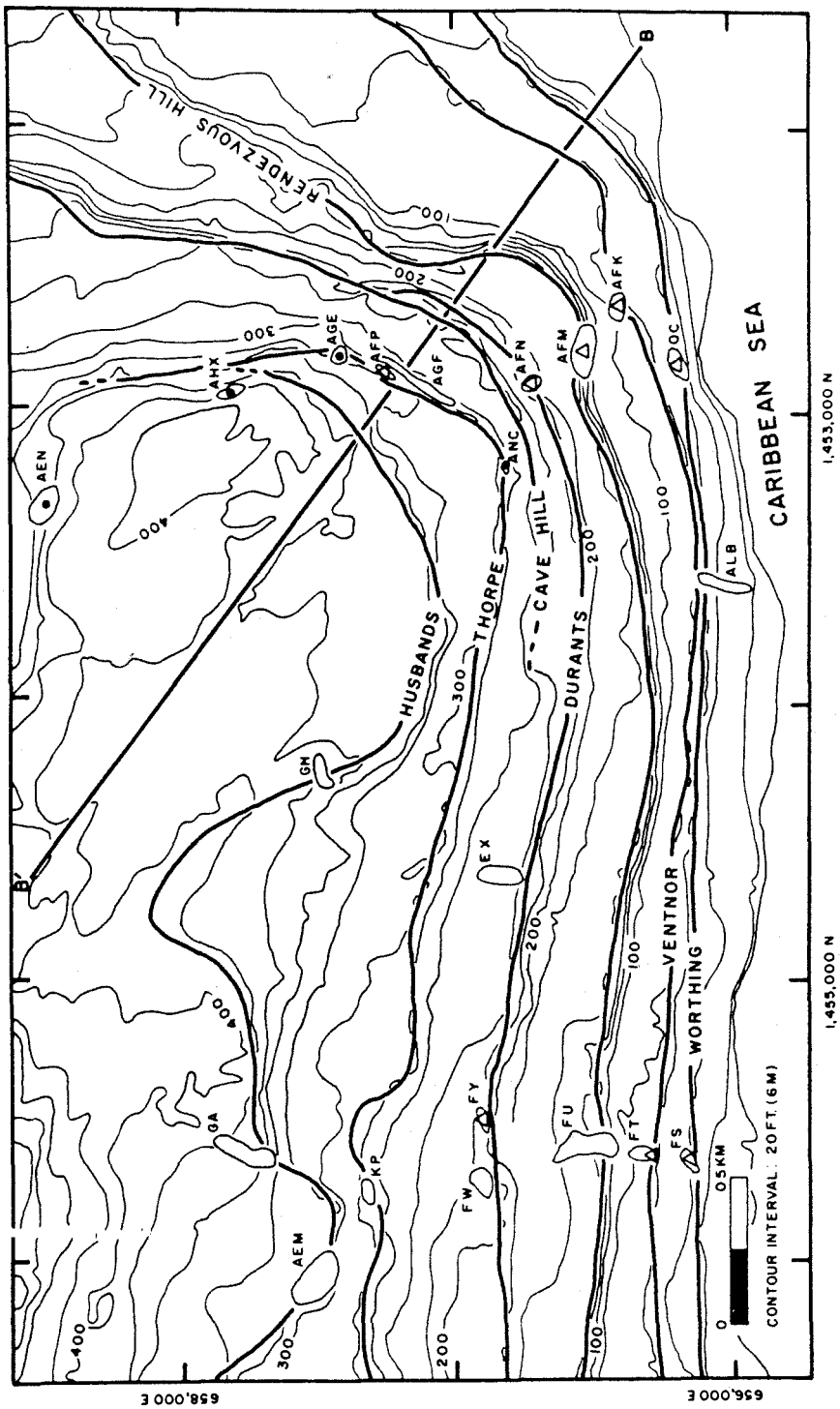
RENDEZVOUS HILL
CARIBBEAN SEA
HUSBANDS
THORPE
CAVE HILL
DURANTS
VENTNOR
WORTHING
B
B'
AEN
AHX
AGE
AFP
AGF
ANC
AFN
AFM
AFK
OC
ALB
GH
EX
FY
FW
FU
FT
FS
GA
KP
AEM
100
200
300
400
CONTOUR INTERVAL: 20FT.(6M)
0
0.5KM
658,000 E
656,000 E
1,455,000 N
1,453,000 N

personal communication). The present heights of the samples are given in Table A1(IV). These heights were read off topographic maps that have contour intervals of 20 feet (figures 6.4 and 6.5). Sample OC-51 is from the Worthing Terrace, and FT-50 is from the Ventnor Terrace. Samples AFS-10, AFS-11, AFS-12, AFM-20, and R-52 are from the Rendezvous Hill Terrace. The AFS samples are from the same outcrop. All samples were prepared as described in section 6.2 except for AFS-12A and AFS-12B, which are different fractions of a powdered sample provided by T.L. Ku. All of these samples have previously been dated by alpha-counting techniques by T.L. Ku (see Table 7.2). Sample VA-1 was collected from the Hill View Terrace. It has a much higher present elevation than the other samples and has been dated by U-He methods at 520 ky (Bender et al., 1979). VA-1 was analyzed in order to determine the isotopic characteristics of a relatively old coral.

A similar sequence of terraces cover portions of Efate Island (just south of Malekula Is., Vanuatu, figure 6.1). A terrace doublet on Efate formed at about the same time (based on ^{230}Th ages by alpha-counting) as the Rendezvous Hill terrace on Barbados. Similar terrace doublets on New Guinea have led to the idea that there may have been two sea level highs during the last interglacial period (see figure 7.1 and Moore, 1982). The ^{230}Th ages (by alpha-counting) of the Rendezvous Hill terrace on Barbados (about 125 ky) have generally been taken as evidence in support of the astronomical theory because a high sea level stand at that time would coincide with a time of high summer insolation at 65°. However, the ^{230}Th ages (by alpha-counting) of the older of the terrace doublets on New Guinea (about 140 ky, figure 7.1) would

imply that a high sea level stand occurred prior to the insolation high and after a prolonged period of low summer insolation in the northern hemisphere (see figure 3.2). A high sea stand at this time cannot be the direct result of orbital forcing. In order to examine the apparent discrepancy between the New Guinea-Vanuatu ages and the Barbados Rendezvous Hill ages, samples from the terrace doublet on Efate Is. were obtained from A.L. Bloom. E-T-2 is from the higher terrance of the terrace doublet, E-L-3 is from the lower terrace. Both have previously been dated by alpha-counting methods at 141±16 ky (2 sigma, (Bloom et al., 1978)). Both have been shown by x-ray diffraction methods to contain less than 1% calcite (A.L. Bloom, personal communication). The present heights of the samples are given in Table A1(V).

6.6 "Altered" - "Unaltered" paris from Barbados and Hispaniola

In order to examine how alteration might shift uranium and thorium isotopic composition and calculated ^{230}Th ages, corals that had been altered to different degrees were analyzed. Four corals of the species Acropora Palmata were obtained from B.R. Constantz (PB-2, PB-4, PB-5, and PB-9). These corals were collected from the wall of the Cement Mill Quarry 0.5 km northwest of the town of Checker Hall on the island of Barbados at an elevation of about 30 m above sea level (Table A1(VI), from the area labelled "North Point Shelf" in the upper part of figure 6.4). Each of these corals had a portion much less porous than the rest of the hand specimen. This portion had abundant calcite cleavage planes that were visible to the naked eye. A sample of the

calcite-rich portion of the coral was separated from a sample at the aragonite-rich portion of each coral as follows. A 1 cm slab of each coral was cut using a Felker Bay State saw with an eight inch diameter diamond blade, lubricated with deionized water. A block of the calcite-rich portion and a block of the aragonite-rich portion were then cut out of each slab using a low speed Isomet saw with a four inch diameter diamond blade lubricated with ethanol. Each of the blocks was then cleaned in an ultrasonic bath with acetone and then twice with distilled water, dried, weighed, and dissolved in nitric acid. Each of the solutions was then aliquoted. The largest aliquot was processed as described in section 7.3.7 in order to obtain uranium and thorium separates. The smaller aliquot was set aside for analysis of Mg and Sr abundance by atomic absorption spectroscopy. Polished sections were made from adjacent blocks of each sample. These sections were etched with a 2% formic acid solution for one minute. The etched sections were examined by scanning electron microscopy. For the "PB" samples, the letter "A" at the end of the sample number refers to the aragonite-rich portion and the letter "B" refers to the calcite-rich portion.

A pair of samples (BCE-A-3A and BCE-A-3B) from a single piece of Acropora palmata that I collected from a terrace along the southeast coast of Hispaniola was also processed in a similar manner. This sample was collected 6.5 km east of the town of Boca Chica, 50 m south of the main road connecting Santo Domingo and La Romana at an elevation of 7.2 m above sea level. Neither sample showed macroscopic evidence of calcite recrystallization. BCE-A-3A is from a portion of the coral that had a chalky surface; BCE-A-3B is from a portion of the coral that

did not have a chalky surface.

In a separate experiment, a block of PB-2A weighing about 1 g was leached in dilute HCl as a means of determining the isotopic characteristics of a more mobile fraction and a more refractory fraction. After being cleaned in the acetone and distilled water baths, the block was dried, weighed, then placed in about 15 ml of distilled water. Several drops of concentrated HCl were added to the solution over the course of several hours. The solution effervesced mildly upon the addition of each drop. After about 10% of the block had been dissolved, the block was taken out of the solution with tweezers, and rinsed with distilled water from a squirt bottle while being held over the solution. The block (PB-2A residue) was then placed in another beaker, dried, weighed, dissolved, and processed using the procedures for chemical separation described in section 7.3.7. The solution (PB-2A LEACH) was processed similarly.

The analytical blanks for the sawing and acetone cleaning procedure were checked as follows. A piece of Acropora palmata, collected live off Tobago Cays by B.R. Constantz, was processed as follows. Several fragments were chiseled from the skeleton and processed in the standard manner (M.A. (chiseled)). A 1 cm thick slab of the skeleton was then cut using the Felker Bay State saw. Two blocks were cut out of this slab using the Isomet saw. One (M.A. (cut) A) was then cleaned in an ultrasonic bath of acetone and processed in the standard manner. The other (M.A. (cut) B) was cut numerous times with the Isomet saw until the surface area of the saw cuts was about ten times higher than the typical surface area for a block. These

pieces were then cleaned in an ultrasonic bath of acetone and processed in the standard manner.

6.7 A modern Giant Clam

In order to establish values for the ^{238}U and ^{232}Th abundances in a modern mollusk and assess the suitability of this material for dating using the ^{230}Th method, I obtained a portion of a giant clam (Tridacna gigantus) shell from P. Aharon. He had collected this shell (K-133) off the coast of the Huon Peninsula in New Guinea (Aharon and Chapell, 1986). He provided me with a several millimeter thick slab of this shell. An 8 g fragment of the shell was chiseled out and processed using standard procedures.

6.8 Seawater

In order to establish precise values for the $^{234}U/^{238}U$ ratio, the ^{238}U abundance, and the ^{232}Th abundance in seawater, samples of seawater from various depths in the Atlantic and Pacific were analyzed. Samples were collected on the following cruises: Alcyone V (R/V Melville, 31°N 159°W, Pacific, 10/85, collected by myself), OCE 173-IV (R/V Oceanus, 32°N 64°W, Atlantic, 12/85, collected by D.J. Piepgras), TTO/TAS Leg 2 (R/V Knorr, Station 63, 8°N 41°W, Atlantic, collected by D.J. Piepgras and M.A. Stordal, 1/83), and Marine Chemistry 80 (R/V Thompson 14°N 160°W, Pacific, collected by K. Bruland, 10/80). Samples were collected in Niskin and GO-FLO bottles, then transferred to acid cleaned, high density linear polyethylene and polypropylene bottles. On the Alcyone V cruise, samples bottles were rinsed with seawater from

the Niskin before the final sample was added. Samples were not filtered; they were acidified with ~ 2 ml of concentrated HCl or HNO_3 per liter of seawater on shipboard (except for the OCE 173-IV samples, which were acidified several weeks later). Bottles were then tightly capped and stored until laboratory analysis. Reported salinities (Table 8.2) are from CTD measurements made by PACYDORF (Scripps Institution of Oceanography) and in some cases from shipboard salinometer measurements (by P.M. Williams for the Alcyone V cruise and by D.J. Piepgras for the OCE 173-IV cruise).

7. Mass spectrometric measurements of ^{230}Th and ^{234}U

7.1 ^{230}Th ages determined by alpha-spectrometry and the need for high precision measurements

After the development of techniques to measure ^{230}Th, ^{234}U, and ^{238}U abundances by alpha-spectrometry in the late 1950's and 1960's (section 2.4) and the demonstration that ^{230}Th dating of corals was plausible (Barnes et al., 1956; Thurber et al., 1965), these techniques were immediately applied to fossil corals as a means of determining the timing of Pleistocene sea level fluctuations. Coral terraces just above present sea level in tectonically stable areas yielded ages of about 125 ky (1 ky = 1000 years) and led to the idea that the last time sea level was above present sea level (the last interglacial period) was at this time (Veeh, 1966). Coral terraces on Barbados (Broecker et al., 1968; Mesollela et al., 1969) and New Guinea (Veeh and Chappell, 1970) yielded ages of about 80 ky, 105 ky, and 125 ky. The general correspondence of these ages with times of high summer solar insolation (figures 3.1 and 3.2) at 65°N latitude was taken as confirmation of the validity of the Milankovitch hypothesis. More detailed dating of the terrace sequence on the Huon Peninsula in New Guinea, however, yielded ages of about 120 ky and 140 ky on consecutive terraces (Bloom et al., 1974; figure 7.1). Subsequent dating of terraces at other localities yielded similar ages and has led to the idea that there were two sea level highs during the last interglacial period, one about 120 ky ago and another about 140 ky ago (Moore, 1982). A high sea level stand 140 ky ago could not have been the direct result of orbital forcing because it would have occurred at a time of very low summer insolation in the

Figure 7.1. Sea level fluctuations over the last 160 ky as determined from the coral record on the Huon Peninsula, New Guinea using ^{230}Th dating by alpha-spectrometry for age control (Bloom et al., 1974). Note the apparent high position of sea level 140 ky ago. High sea level at this time could not be the direct result of orbital forcing because this is a time of low summer insolation at 65°N, which follows a prolonged period of low insolation (see figure 3.2). (After Bloom, 1980b).

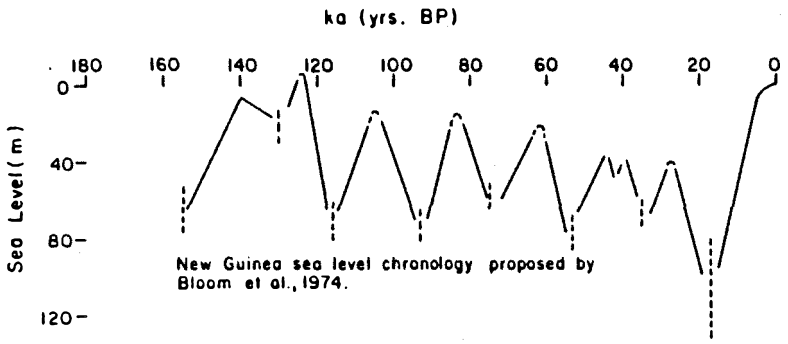

New Guinea sea level chronology proposed by Bloom et al., 1974.

northern hemisphere, after a period of prolonged low summer insolation in the northern hemisphere, and about 10 ky prior to a time of very high summer solar insolation in the northern hemisphere (see figure 3.1). At present, some controversy exists concerning the accuracy and precision of the age determinations (e.g., Moore, 1982; Kaufman, 1986). It is clear that increased analytical precision as well as a better understanding of the process of diagenetic alteration of corals is required in order to establish accurate ages for terraces and resolve this controversy.

Most coral terraces that have been dated by ionium ingrowth and are pertinent to the study of climatic fluctuations in the Pleistocene have ages between 70 and 150 ky. In this age range, a typical alpha-counting analysis gives a 2 sigma error, based on counting statistics, of ±10 ky (Harmon et al., 1979; Table 7.3). Because the time between successive peaks in the 65°N summer insolation curve is about 20 ky (figure 3.2), if sea level highs correspond to insolation highs, then the ages of two successive terraces are barely resolvable at the 2 sigma level just considering analytical uncertainties. The time difference between a high point and an adjacent low point in the 65°N curve is about 10 ky. Therefore, a clear correlation between times of high insolation and ages of coral terraces representing high sea level cannot currently be made using alpha-counting techniques.

The inadequacy of the precision obtainable by alpha-counting methods for determining the timing of sea level changes is clearly shown in figure 7.2 (Bloom, 1980b). This is a plot of probability density vs. time for 60 ^{230}Th ages from seven successive terraces in

Figure 7.2. Probability density versus age for 60 samples from a sequence of eight terraces on Vanuatu (after Bloom, 1980b). Each of the samples was dated by the ^{230}Th method using alpha-spectrometry to measure the abundances of the nuclides. Each of the samples was assigned a mean age and an error in age based on analytical errors. The error in each age was represented as a probability distribution. The curve in this figure is the sum of the 60 distributions and represents the probability that a given age is the true age of one of the samples. If the ages of successive terraces and presumably the ages of successive sea level highs are resolvable by this method, then there should be distinct peaks in the curve. There is a sharp peak at an age of zero to 6 ky, which represents the Holocene terrace. Then there is a period around 20 ky with no ages, hints of peaks at 40, 50, and 60 ky, and a continuum for ages older than 65 ky. This indicates that the ages of the terraces older than 65 ky were not resolvable.

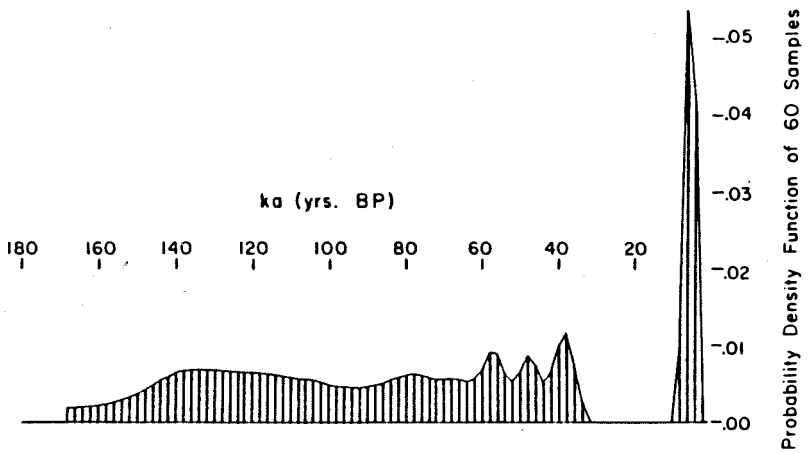
ka (yrs. BP)
180
160
140
120
100
80
60
40
20
.05
.04
.03
.02
.01
.00
Probability Density Function of 60 Samples

Vanuatu. Each age has an error due to counting statistics which can be translated into a plot of probability versus time. Figure 7.2 was constructed by adding the probabilities for all 60 dates. The resulting curve is a measure of the probability that a certain age is represented by one or more of the samples. Each terrace presumably formed during a single rise and fall of sea level and has a finite range of ages that is different from the ages of the other terraces. If the the ages of successive coral terraces and, by inference, successive sea level maxima are resolvable, one would expect peaks in probability at the ages of each of the terraces. There is one sharp peak at about 5 ky, representing the Holocene rise in sea level. There is very low probability between 7 and 35 ky and hints of peaks at about 40, 50, and 60 ky. However, beyond 60 ky there is a continuum and the ages of the terraces in this time period are definitely not resolved, indicating a clear need for higher precision measurements.

7.2 The development of mass spectrometric techniques

The idea that measurements of ^{230}Th and ^{234}U abundances by mass spectrometry could have higher precision than the same measurements by alpha-spectrometry is based on the following rationale. The precision of a measurement is limited by the number of atoms (or alpha-particles) that can be detected during a measurement. By alpha-spectrometry only decaying particles can be detected. ^{230}Th has a mean life of about 10^5 years, so for a laboratory counting time of one week, only one out of 10^7 ^{230}Th atoms in a sample can be detected. In mass spectrometric measurements, ions are detected, and the precision of a measurement is

limited by the fraction of ^{230}Th atoms that one can ionize. If ionization efficiencies of one out of 10^3 could be obtained for thorium, then, for the same size sample, 10^4 times more atoms of ^{230}Th would be detected by mass spectrometric determination than by alpha-counting methods. Based solely on counting statistics, a ^{230}Th measurement by mass spectrometry would be about 100 times more precise than the same measurement on the same size sample by alpha-counting. Similar arguments can be made for ^{234}U which has a longer mean life (about 3×10^5 years) than ^{230}Th, and ^{238}U and ^{232}Th which have much longer mean lives (6×10^9 and 2×10^{10} years) than ^{230}Th. Mass spectrometric measurements of ^{238}U and ^{232}Th abundances in natural materials have, of course, been made previously but not in corals or mollusks. Mass spectrometric measurements of ^{234}U in natural materials had been made previous to the Chen et al.(1986) paper (Appendix B), but did not result in sample sizes or analytical errors which were significantly lower than for alpha-counting measurements (Somayajulu et al., 1966; Rosholt et al., 1966; Szabo and Rosholt, 1969; Rosholt and Tatsumoto, 1970; Barnes et al., 1972). Mass spectrometric measurements of ^{230}Th in natural materials had not been made previous to this study.

Prior to my involvement with uranium and thorium measurements at the Lunatic Asylum, techniques had been developed to measure ^{238}U abundances and $^{238}U/^{235}U$ ratios in very small samples (about 10^9 atoms of ^{235}U; Chen and Wasserburg, 1980, 1981a,b). The key aspects of this technique were (1) the use of a double ^{233}U-^{236}U tracer to monitor instrumental fractionation, (2) the development of a chemical procedure to separate uranium from the rest of the sample with low analytical

blank and high chemical yield, and (3) the use of filament loading techniques, resulting in high ionization efficiencies for uranium (about 1%).

This technique was then used to measure $^{234}U/^{238}U$ ratios in solutions rich in uranium, which had been prepared in the laboratory, in seawater, and in hydrothermal water (Chen et al., 1983; Chen and Wasserburg, 1984). It was demonstrated that the $^{234}U/^{238}U$ ratio could be measured to a precision of ±5 ‰ (2 sigma) using a sample size of 5×10^9 atoms of ^{234}U. At this time, there was some concern about the accuracy of the measurements. The concern centered on the accuracy of the subtraction of the background from the ^{234}U peak. My initial involvement with uranium measurements focussed on establishing that significant inaccuracy was not introduced when the background was subtracted from the ^{234}U peak. I continued by measuring $^{234}U/^{238}U$ ratios in seawater and in solutions prepared in the laboratory. These measurements confirmed the precision of the earlier measurements.

These techniques were then extended to the measurement of ^{230}Th abundances as described in the rest of this chapter. The basic problem with mass spectrometric determinations of both ^{230}Th and ^{234}U is the extremely low abundance of these nuclides in natural materials and possible contributions at masses 230 and 234 from tails of much higher abundance isotopes of thorium and uranium. Consider that ^{238}U, the ultimate parent of ^{230}Th, is typically present in quantities of parts per million (about 10^{16} atoms/g) or parts per billion in most natural materials. At secular equilibrium, the ^{230}Th abundance is lower by a factor of $\lambda_{238}/\lambda_{230}$ or about 10^{-5} (^{230}Th abundances of about 10^{11}

atoms/g). Young corals have $^{230}Th/^{238}U$ ratios below the value at secular equilibrium. One would wish to measure ^{230}Th abundances in corals that have $^{230}Th/^{238}U$ ratios more than 1000 times below the equilibrium value (^{230}Th abundances of about 10^8 atoms/g). Because of the low abundances, the techniques described below are designed to maximize ionization efficiency, maximize chemical yield, and minimize analytical blank. Even with high ionization efficiency and chemical yield, the currents generated by the $^{230}Th^+$ ion beam are very small (10^2 to 10^4 ions/s) and require amplification using an electron multiplier before measurement.

The process of developing techniques to measure ^{230}Th by mass spectrometry required (1) establishing the ionization efficiencies that could be obtained for thorium using the graphite loading technique, (2) calibrating a ^{229}Th tracer, (3) establishing the level of chemical and filament blanks, (4) modifying uranium and thorium chemical separation techniques for corals, (5) evaluating the effect of instrumental fractionation on measured $^{230}Th/^{229}Th$ ratios, (6) determing the source, magnitude, and spectral distribution of background ion currents, (7) establishing that the measurements were reproducible, and (8) demonstrating that small differences in ^{230}Th abundances could be resolved.

Initially thorium samples derived from laboratory standards were run as a means of establishing ionization efficiencies for thorium using the graphite loading technique, which had proven to yield relatively high ionization efficiencies for uranium. Ionization efficiencies of about 1 in 1000 were obtained for samples of less than

about 10^{13} atoms of total thorium. For samples containing 10^{10} atoms of ^{230}Th (the amount of ^{230}Th in about 100 mg of 100 ky old coral), 10^{7} ions of $^{230}Th^{+}$ would be generated. Taking into account the time required to measure backgrounds and other thorium ion beams, one would be able to measure about 10^{6} ions of $^{230}Th^{+}$. Based solely on counting statistics, this number of ions could be measured to a precision of ±2‰ at the 2 sigma level. This precision would be more than 40 times higher than typical precisions obtainable by alpha-counting methods using much larger samples.

The initial measurements also showed that for total thorium loads of more than about 10^{13} atoms, the ionization efficiency dropped substantially. It may be possible to modify loading techniques to improve the ionization efficiency for samples with large numbers of thorium atoms. Without such improvements, however, one obtains higher ionization efficiencies with smaller thorium loads. Therefore, for a fixed number of ^{230}Th atoms loaded on a filament, one obtains higher ionizations efficiencies and higher precision ^{230}Th measurements for samples with low ^{232}Th content.

This reasoning led me to search for natural materials with very low $^{232}Th/^{238}U$ ratios. Since ^{230}Th is the daughter of ^{238}U, such materials would generally have low $^{232}Th/^{230}Th$ ratios, and ^{230}Th abundances in these materials could be measured to a relatively high degree of precision. Values of $^{232}Th/^{238}U$ in the literature indicated that corals had the lowest reported $^{232}Th/^{238}U$ values in natural materials. This is the reason why, initially, I considered analyzing ^{230}Th in corals. Using the reported $^{232}Th/^{238}U$ values, I calculated

that the $^{232}Th/^{230}Th$ ratio at secular equilibrium in a coral would be about 10^3 or about two orders of magnitude lower than the value for igneous rocks. As will be discussed below, when the ^{232}Th concentration in a coral was measured by mass spectrometric techniques, I obtained values 10^2 to 10^3 times lower than the literature values. Some of the corals that I analyzed had $^{232}Th/^{230}Th$ ratios close to unity or about 10^5 times lower than most igneous rocks. This low $^{232}Th/^{230}Th$ ratio resulted in very low total thorium loads. The resulting high ionization efficiency generated high ion yields which reduced the error due to counting statistics and also generated high $^{230}Th^+$ currents that increased the signal to noise ratio, also reducing measurement error. Finally, the extremely low $^{232}Th/^{230}Th$ ratios obviated the issue of whether the tail of a large $^{232}Th^+$ beam would contribute to the measured intensity at mass 230.

In the following section, I will (1) describe the techniques which I have used to measure both ^{230}Th and ^{234}U abundances in corals, (2) establish the precision and accuracy of the measurements and the sample size requirements, and (3) compare the ages determined by mass spectrometric methods to those determined by alpha-counting methods.

7.3 Experimental method

7.3.1 Instrumental procedure

Mass spectrometric procedures used in the Lunatic Asylum for measuring ^{235}U and ^{238}U in small samples have been described by Chen and Wasserburg (1981a). For the $^{234}U/^{238}U$ measurements, a double spike with $^{233}U/^{236}U \sim 1$ is used and the sample is spiked so that $^{235}U/^{236}U \sim$

10. The measurements are carried out on the Lunatic I (LI) mass spectrometer using an electron multiplier with a gain of 4 X 10^3 in the analogue mode and an electrometer (Cary 401) with a 10^9 Ω feedback resistor (Wasserburg et al., 1969). Data are acquired in the sequence ^{236}U-^{235}U-^{234}U-^{234}U-^{233}U. Zeros are measured 0.5 mass units above and below each mass. Integration time for zeros and peaks are one second for all masses except ^{234}U. ^{234}U peaks are measured for four seconds and zeros for two seconds. Data acquisition takes ~ two hours and 100 to 200 ratios (50 to 100 cycles with two ^{234}U measurements/cycle) are measured. Data are acquired at filament temperatures of 1640°C to 1800°C. A mass spectrum of uranium from coral sample AFS-12 from Barbados is shown in figure 7.3). The $^{234}U^+$ current ranges from 1500 to 3000 ions/sec. The total number of ^{234}U ions collected in one run is ~ 2 X 10^6. The ionization efficiency (ions produced/atoms loaded) for this procedure is U^+/U ~ 5 X 10^{-4} because of the large sample size.

All data sets of ten ratios are normalized using the power law (see Wasserburg et al., 1981) and the mean $^{233}U/^{236}U$ ratio for that set of ten ratios. The isotopic ratios and deviations of these ratios are then reduced using the full double spike equations. All quoted errors are 2 sigma of the mean. $^{234}U/^{238}U$ ratios are calculated from normalized $^{234}U/^{235}U$ ratios and ^{238}U concentrations calculated from the normalized $^{235}U/^{236}U$ ratios using $^{238}U/^{235}U$ = 137.88. For a single run 2 sigma of the mean for the $^{234}U/^{238}U$ ratios is typically ±3 to 6°/oo (see Tables A1, A2).

Some experiments were designed specifically to determine the ^{238}U concentration in seawater. For these uranium concentration runs, the

Figure 7.3. Mass spectrum of uranium (5 X 109 atoms) from coral sample AFS-12. A ^{233}U-^{236}U spike is added to the sample so that $^{236}U/^{234}U$ ~ 10. In this spike, the $^{233}U/^{236}U$ ratio is about one, and $^{234}U/^{236}U$ ~ 2 X 10^{-3}. The ^{238}U peak is off scale to the right of the diagram. The small arrows represent positions where the zeros are measured. The arrow marked 'A' denotes where the accelerating voltage was turned off. Details of the background characteristics are discussed in the text. Note the change in scale for ^{235}U, ^{233}U, and ^{236}U.

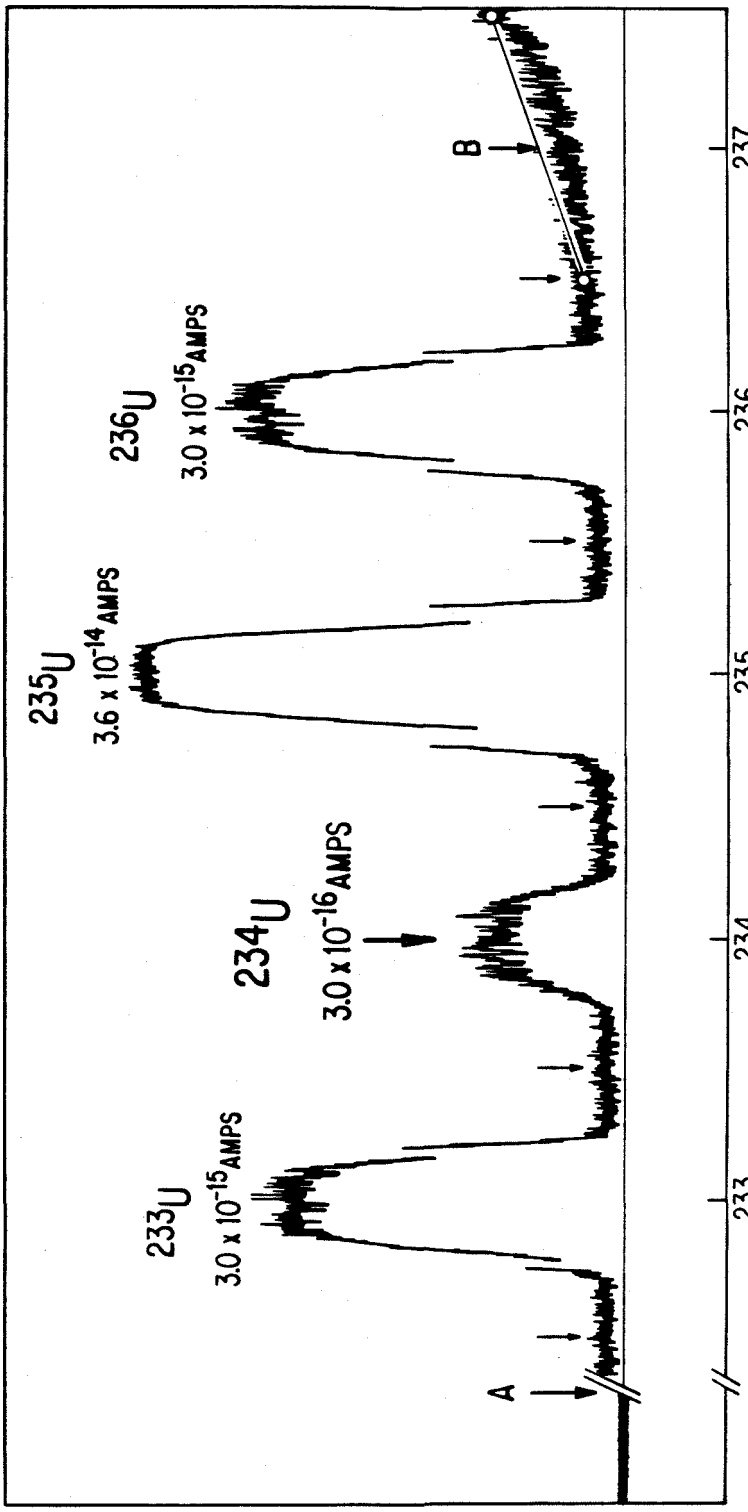
^{233}U
3.0 x 10^{-15} AMPS
^{234}U
3.0 x 10^{-16} AMPS
^{235}U
3.6 x 10^{-14} AMPS
^{236}U
3.0 x 10^{-15} AMPS
A
B
233
234
235
236
237
MASS

sample was spiked so that $^{238}U/^{236}U \sim 10$. Data were acquired in the sequence ^{238}U-^{236}U-^{235}U-^{234}U-^{233}U. Zeros were measured 0.5 mass units above and below each mass. Integration times for zeros and peaks were one second. Instrumental fractionation was corrected for as above using the ^{233}U-^{236}U double spike. Data acquisition takes about two hours. About 100 ratios of $^{236}U/^{238}U$ are measured at filament temperatures of 1600°C-1700°C. The $^{238}U^+$ current is 0.6 X 10^6 to 3 X 10^6 ions/sec. Typically, 6 x 10^{13} atoms of ^{238}U were loaded on the filament and ionization efficiencies are >1 °/oo and ^{238}U concentrations were measured to ±2 °/oo.

Measurement of the thorium isotopes is also carried out on the LI spectromenter using the same detector system. The sample is spiked with a ^{229}Th tracer so that each run contains ~ 2 X 10^{11} atoms of ^{229}Th. The number of ^{230}Th atoms loaded on the filament ranges from 6 X 10^8 for a 180 year old sample to 6 X 10^{10} for a sample of several hundred ky as shown in Table A3. Analogue scans of the thorium spectrum for a young and old sample are shown in figures 7.4 and 7.5. At running conditions, the $^{229}Th^+$ current is ~ 1 X 10^5 ions/s and the $^{230}Th^+$ current ranges from 4 X 10^2 to 4 X 10^4 ions/s. Data are acquired at filament temperatures of 1800 to 1870°C. The isotopes are measured in the sequence ^{229}Th-^{230}Th-^{230}Th-^{232}Th. Zeros are measured 0.5 mass units above and below each mass. Integration time for the ^{230}Th peaks is 4 seconds; for the ^{230}Th zeros and ^{229}Th peak, 2 seconds; and for the remaining peak and zeros, 1 second. Data acquisition takes ~ 40 minutes and 40 to 60 ratios (20 to 30 cycles with two ^{230}Th measurements/cycle) of $^{230}Th/^{229}Th$ are measured. The

Figure 7.4. Analogue scan of the thorium spectrum for CWS-F-1 (845 years old) at a filament temperature of 1840°C. The sample was spiked with ^{229}Th. 4.3 X 10^9 atoms of ^{230}Th which had been extracted from 4.6 g of coral were loaded on the filament. The ionization efficiency was 0.8 °/oo. Arrows show the position where zeros were measured. The background with the accelerating voltage on is slightly higher than the background with the accelerating voltage off because of the reflection of the ^{187}Re and ^{185}Re beams off the flight tube. The ^{230}Th abundance was determined to ±8 °/oo (2 sigma). Note the change in scale for ^{229}Th and ^{232}Th.

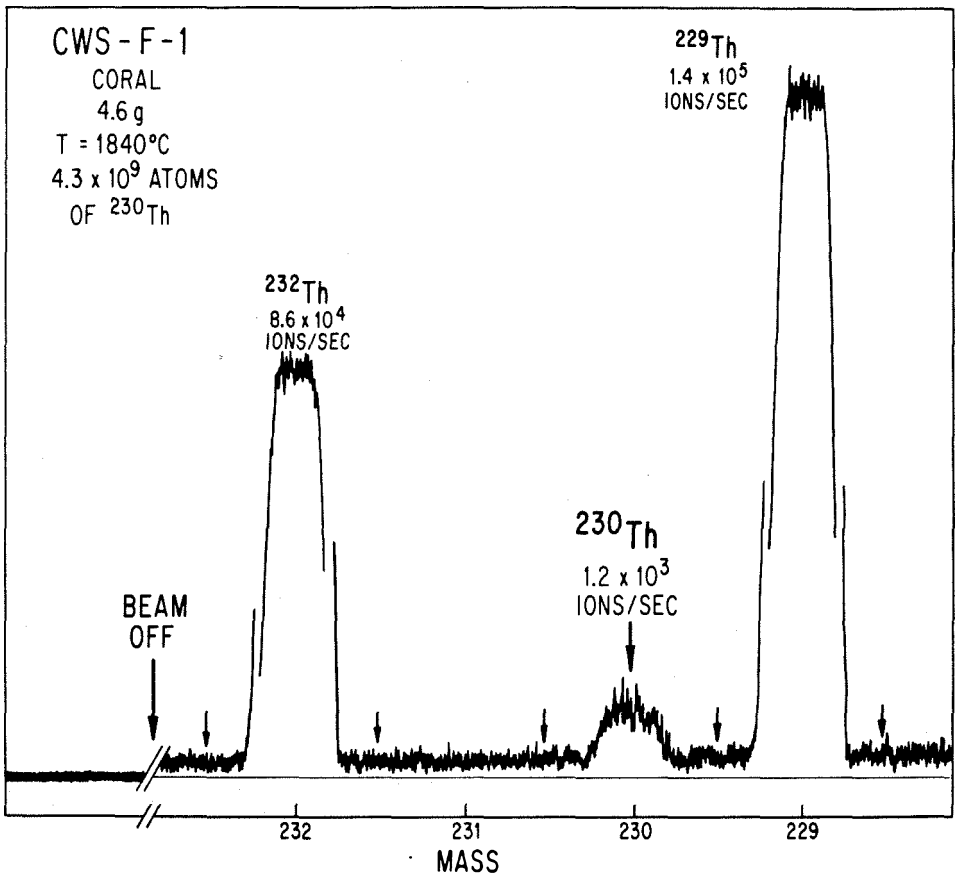
CWS - F - 1
CORAL
4.6 g
T = 1840°C
4.3 x 10^9 ATOMS
OF 230Th
232Th
8.6 x 10^4
IONS/SEC
229Th
1.4 x 10^5
IONS/SEC
230Th
1.2 x 10^3
IONS/SEC
BEAM
OFF
232
231
230
229
MASS

Figure 7.5. Analogue scan of the thorium spectrum similar to figure 7.4, but for a much older sample (E-L-3, 125.5 ky). 2.3 X 10^{10} atoms of ^{230}Th that had been extracted from 255 mg of coral were loaded on the filament. The ionization efficiency was 0.9 °/oo and the ^{230}Th abundance was determined to ±2 °/oo. Note the change in scale for ^{229}Th and the extremely low $^{232}Th/^{230}Th$ ratio. This ratio is 5 orders of magnitude lower than the same ratio in volcanic rocks.

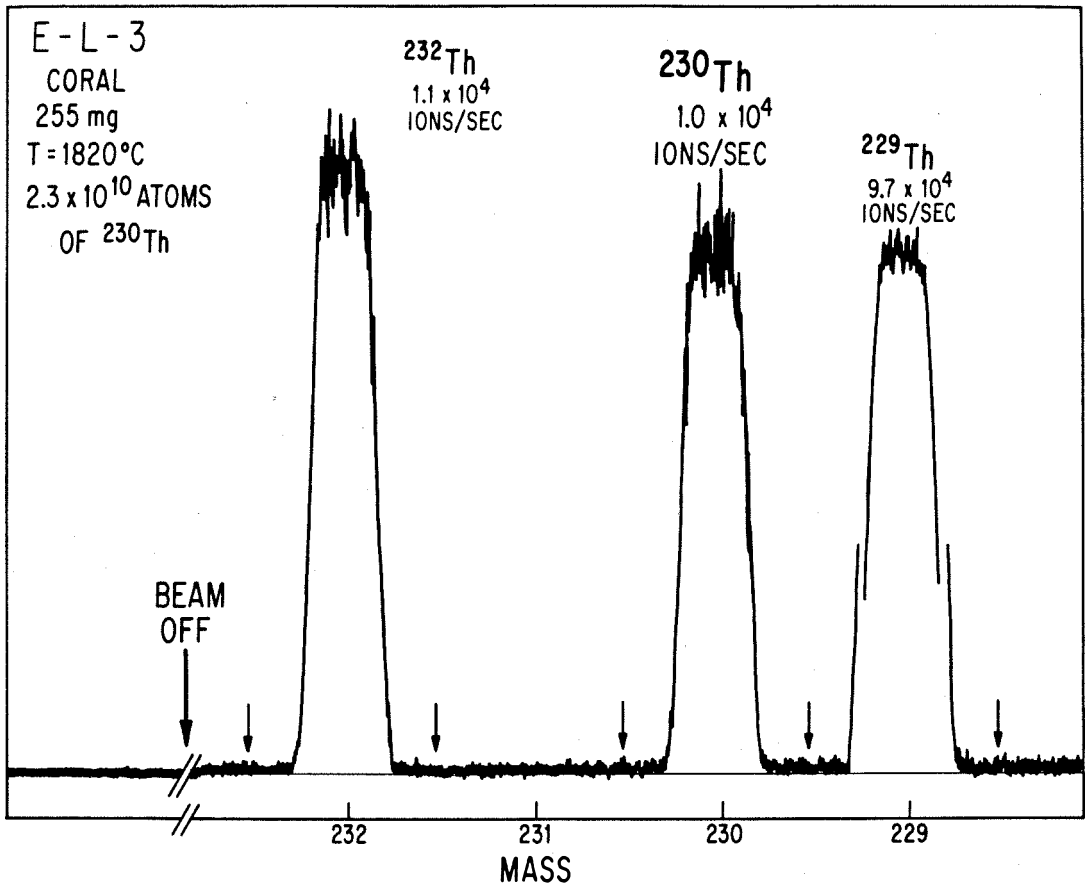
E-L-3
CORAL
255 mg
T = 1820°C
2.3 x 10^10 ATOMS
OF 230Th
232Th
1.1 x 10^4
IONS/SEC
230Th
1.0 x 10^4
IONS/SEC
229Th
9.7 x 10^4
IONS/SEC
BEAM
OFF
232
231
230
229
MASS

total number of $^{230}Th^{+}$ ions collected in a run ranges from 6 X 10^{4} for the 180 year sample to 6 X 10^{6} for the oldest sample. For the $^{230}Th/^{229}Th$ ratio, the value of 2 sigma of the mean for one run ranges from ±132 °/oo for a very young sample (18 years) to ±2 °/oo for samples ~100 ky old (Table A3). These uncertainties are only a factor of 2 to 3 times the error due to counting statistics alone, when the ions making up the background under the ^{230}Th peak and the counting statistics associated with the ^{229}Th peak are included in the calculation.

7.3.2 Multiplier linearity and electrometer noise

It has been shown that the multiplier on the L1 spectrometer is linear to better than ±2°/oo for ratios up to ~100 for ion currents up to 3 X 10^{6} ions/s (Chen and Wasserburg, 1981a). I have checked this in ^{238}U concentration runs by measuring the $^{238}U/^{235}U$ ratio and verifying that it agrees within error with the natural $^{238}U/^{235}U$ ratio (137.88; see figure 7.6, Table 8.2).

For the uranium isotopic composition runs, as $^{235}U/^{234}U$ ~ 100, a potential problem exists if the electrometer is not allowed enough time to settle between the measurement of the ^{235}U signal and the first ^{234}U zero. I measured directly the rate of decay of this signal by putting a beam on the multiplier, turning off the accelerating voltage, and repeatedly measuring the decaying signal using a 125 ms integration time. The signal decays approximately exponentially to a value of ~10^{-4} times the original beam in one second. Since measurement of the ^{234}U zero commences ~5 seconds after measurement of the ^{235}U peak, the

Figure 7.6. Measurements of the $^{238}U/^{235}U$ ratio in seawater using the Lunatic I mass spectrometer. The measurements were made between October 1983 and December 1986. The values are, within error, the same as normal uranium indicating that the multiplier on Lunatic I is linear within the limits of the measurements.

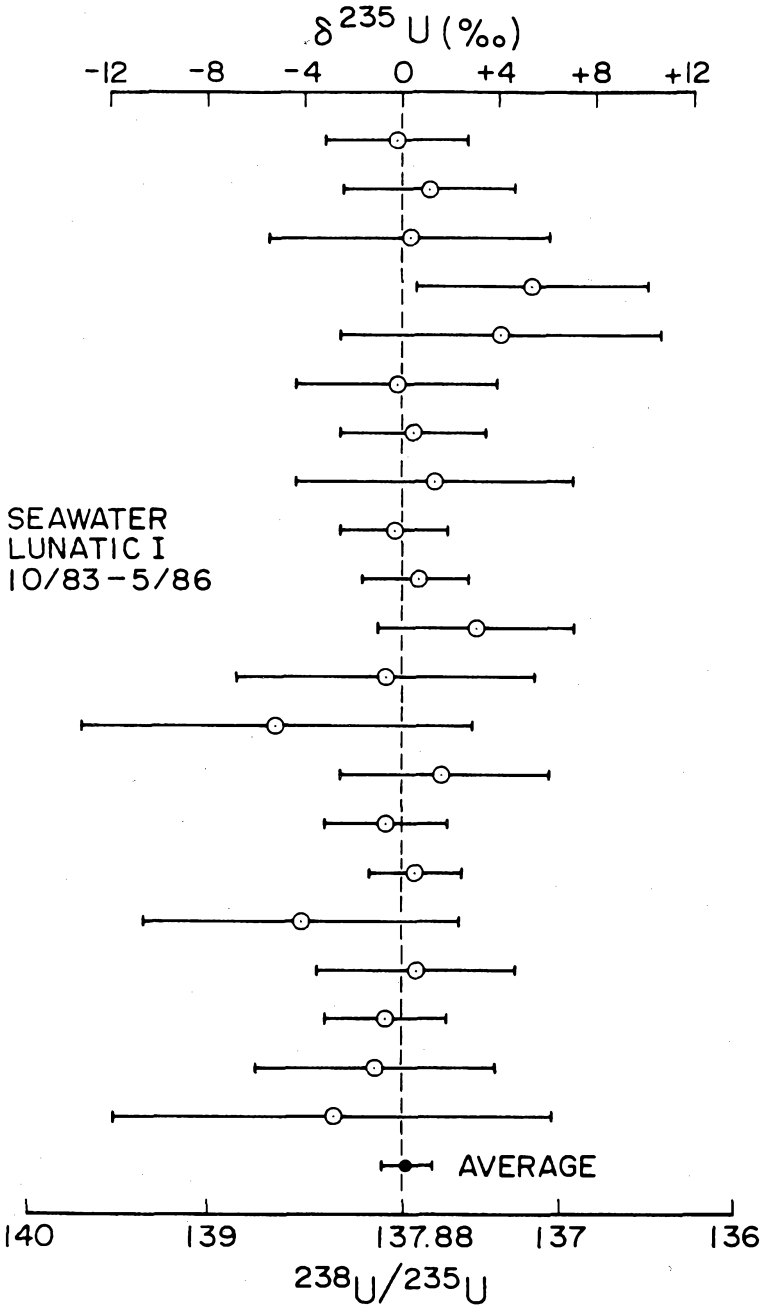
δ 235 U (‰)
-12
-8
-4
0
+4
+8
+12
SEAWATER
LUNATIC I
10/83 - 5/86
AVERAGE
140
139
137.88
137
136
238U/235U

decaying ^{235}U signal does not significantly affect measurement of the ^{234}U zero. In addition, the average of the $^{234}U/^{235}U$ ratios measured in the first ^{234}U channel does not differ significantly from the average of the $^{234}U/^{235}U$ ratios measured in the second ^{234}U channel.

For the thorium measurements, the isotope ratios ($^{229}Th/^{230}Th$ = 5 to 200) and ion currents (up to 1.6 X 10^5 ions/s) are not large enough to cause problems associated with electrometer response time or significant nonlinearity problems. The noise level of the multiplier and amplifier under normal operating conditions is equivalent to ±12 ions/s, where the uncertainty given is 2 sigma of the population for a series of 4-second noise measurements. The 2 sigma error for one ^{230}Th measurement including the background subtraction is ±17 ions/s. Since the ^{230}Th current is measured ~ 40 times in one run, the total error due to electrometer noise is $\pm 17/\sqrt{40} = \pm 3$ ions/sec. For a $^{230}Th^+$ current of 4 X 10^2 ions/sec, this is about a quarter of the ±30 ‰ observed error. For larger samples the error due to noise is smaller.

7.3.3 Background characteristics

For the uranium isotopic composition runs, tailing from the major isotopes could be important because of the low resolution usually used in operating the spectrometer in a high transmission mode. The ^{234}U intensity is determined by subtracting the average of the zeros (measured at mass 234.5 and mass 233.5) from the intensity at mass 234. If the positive curvature of the ^{235}U tail between mass 233.5 and mass 234.5 is significant, the procedure for background correction can result in an underestimate of the intensity of the ^{234}U signal. I

therefore tested the effects of the ^{235}U tail at the center of the spectral line for ^{234}U and at the positions where zeros for ^{234}U were taken. To do this, I measured the tail from ^{238}U at the equivalent mass positions at and near mass 237. This is shown in figure 7.3 under arrow "B." The average of the intensitites at masses 237.5 and 236.5 is slightly higher than the measured intensity at mass 237. I have measured this quantity for different samples at different focusing conditions. For several measurements of the ion beam current (I) at appropriate masses the results are:

$$\{I(237)-[I(237.5)+I(236.5)]/2\}/I(238) = -0.6X10^{-5} \text{ to } -2.0X10^{-5} \quad (7.1)$$

As $^{235}U/^{234}U \sim 10^{2}$, systematic errors introduced by tailing of ^{235}U are < 2 o/oo of the ^{234}U peak and are insignificant. As can be seen in figure 7.3, there is a slight slope to the background across the uranium spectrum. The background is also slightly higher than the background with the accelerating voltage off (arrow "A", figure 7.3) This is due to the reflection of the $^{238}U^{12}C_2^+$ (mass 262) ion beam off the flight tube. The intensity of the reflected peak increases gradually from about mass 228 to a maximum value around mass 244. Typically, $^{238}U^{12}C_2^+/^{238}U^+ \sim 0.015$ and $^{238}U^{12}C_2^+$ reflects to mass 234 with an efficiency of ~ 0.001 contributing ~ 600 ions/s to the background at mass 234 at running conditions. If this reflected peak has significant curvature over the mass range 233.5 to 234.5, the linear background correction might result in inaccurate determination of the ^{234}U intensity. To check whether the background around mass 234

is linear, I scanned over the analogous portion of the ^{238}U reflected peak around mass 212. This scan showed that curvature of the reflected peak does not introduce significant errors.

For the thorium measurements in corals, there is no extremely high abundance isotope, so tailing under mass 230 is not a problem. For similar reasons, there is no large thorium carbide beam, so reflection of a large thorium carbide beam into the thorium metal region is not a problem. However, under normal operating conditions, the background under the thorium spectrum is slightly higher than the background with the accelerating voltage off (see figures 7.4 and 7.5). This difference is typically ~ 100 ions/s and is due to the reflection of the $^{187}Re^{+}$ and $^{185}Re^{+}$ beams off the flight tube. In the vicinity of the ^{230}Th peak, the background, resulting from the reflected peak, is effectively linear. For larger (i.e., older) samples, the background current is only a few per mil of the $^{230}Th^{+}$ current and does not introduce significant errors. For smaller samples, the background current is >10% of the $^{230}Th^{+}$ beam. This has the effect of lowering the precision of the ^{230}Th measurement slightly, since the measurement of the ^{230}Th zero and the ^{230}Th peak are subject to the counting statistics associated with the ~ 100 ions/s. However, the Re beam is reasonably stable and does not change by large amounts during the course of a run. Since a ^{230}Th zero is measured immediately before and immediately after each ^{230}Th peak measurement, I do not believe that significant inaccuracy or imprecision other than that associated with counting statistics is introduced by the background current.

7.3.4 Fractionation

Figure 7.7 shows the change in the measured $^{229}Th/^{232}Th$ during the course of a spike calibration run. This shows that, not including the very end of the run, thorium fractionates by a total range of only 1.5 ‰ per mass unit in the course of a run. This is much less than the ±2‰ error of the highest precision ^{230}Th measurements as shown by the "+2σ" and the "-2σ" lines in figure 7.7. For the data reported here, ratios measured at the end of a run when the beam is decaying by more than 5%/minute are not included. Reproducible results for several spike calibration runs indicate that instrumental fractionation does not introduce errors larger than the ±2 ‰ error of the individual runs even for isotopes different in mass by 3 amu. Fractionation at the multiplier is corrected for by multiplying the measured $^{n}Th/^{m}Th$ ratio by $(n/m)^{1/2}$, where n and m are the mass numbers. It has been shown previously by measuring the same sample with the multiplier and collector, that this relaitonship adequately corrects for multiplier fractionation on the LI system (Chen and Wasserburg, 1983). For the uranium runs, instrumental fractionation is corrected for using the ^{232}U-^{236}U double spike as described in section 7.3.1.

7.3.5 Ionization efficiency

The ionization efficiency for a number of thorium runs on standards and thorium separated from corals is shown plotted as a function of total thorium loaded in figure 7.8. This shows that ionization efficiency decreases with increasing thorium loaded on the filament using this approach. For the corals analyzed, total thorium

Figure 7.7. The measured $^{229}Th/^{232}Th$ ratio versus time for a spike calibration run. $D=\{[(^{229}Th/^{232}Th)_{TEN}/(^{229}Th/^{232}Th)_{GM}]^{1/3}-1\}X10^{3}$ where the subscript TEN refers to the mean of a set of ten ratios and GM refers to the grand mean of all of the ratios in a run. D is a measure of the deviation per mass unit of a given set of ten ratios from the grand mean in parts per thousand. The horizontal axis represents the time of data acquistion (~ 1 hour) and is scaled in cumulative ratios. The error bars for the individual points are 2 sigma of the mean for that set of ten ratios. The vertical dashed line represents the time that the beam began to decay by more than 5% per minute. Data to the right of this line are discarded. 10^{13} atoms of thorium were loaded on the filament for this run. This is somewhat larger than typical filament loads for corals (10^{12} thorium atoms). The horizontal lines labeled '$+2\sigma$' and '-2σ' represent the 2 sigma error in $^{230}Th/^{229}Th$ for high precision coral runs. The total range of fractionation is well within these bounds showing that error due to fractionation is small.

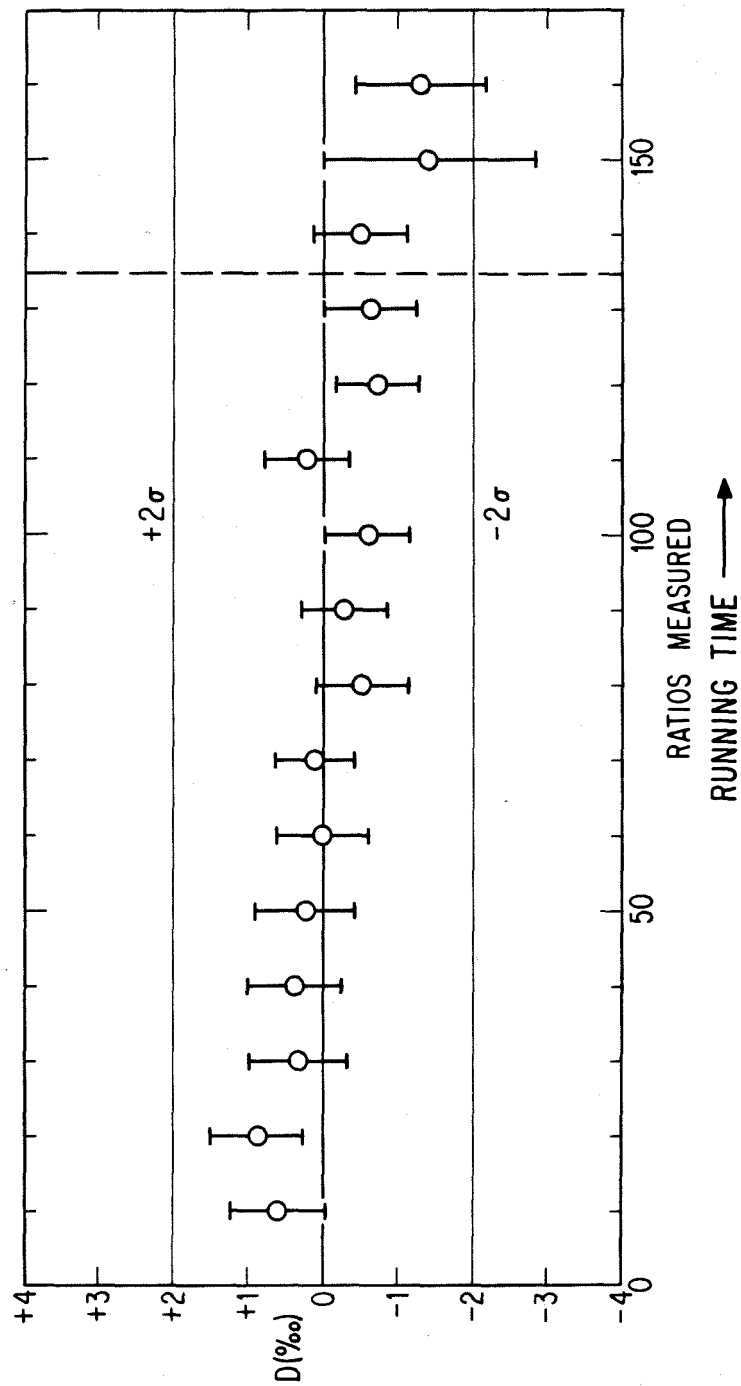
+4
+3
+2
+1
0
-1
-2
-3
-4
D(‰)
+2σ
-2σ
0
50
100
150
RATIOS MEASURED
RUNNING TIME

Figure 7.8. A log-log plot of the ionization efficiency versus the total number of thorium atoms loaded on the filament for corals and for standards. Ionization efficiency decreases with increasing thorium loads. The coral runs all lie to the left of the dashed line marked "corals" and have ionization efficiencies of 0.7 to 1.3 $^{o}/_{oo}$.

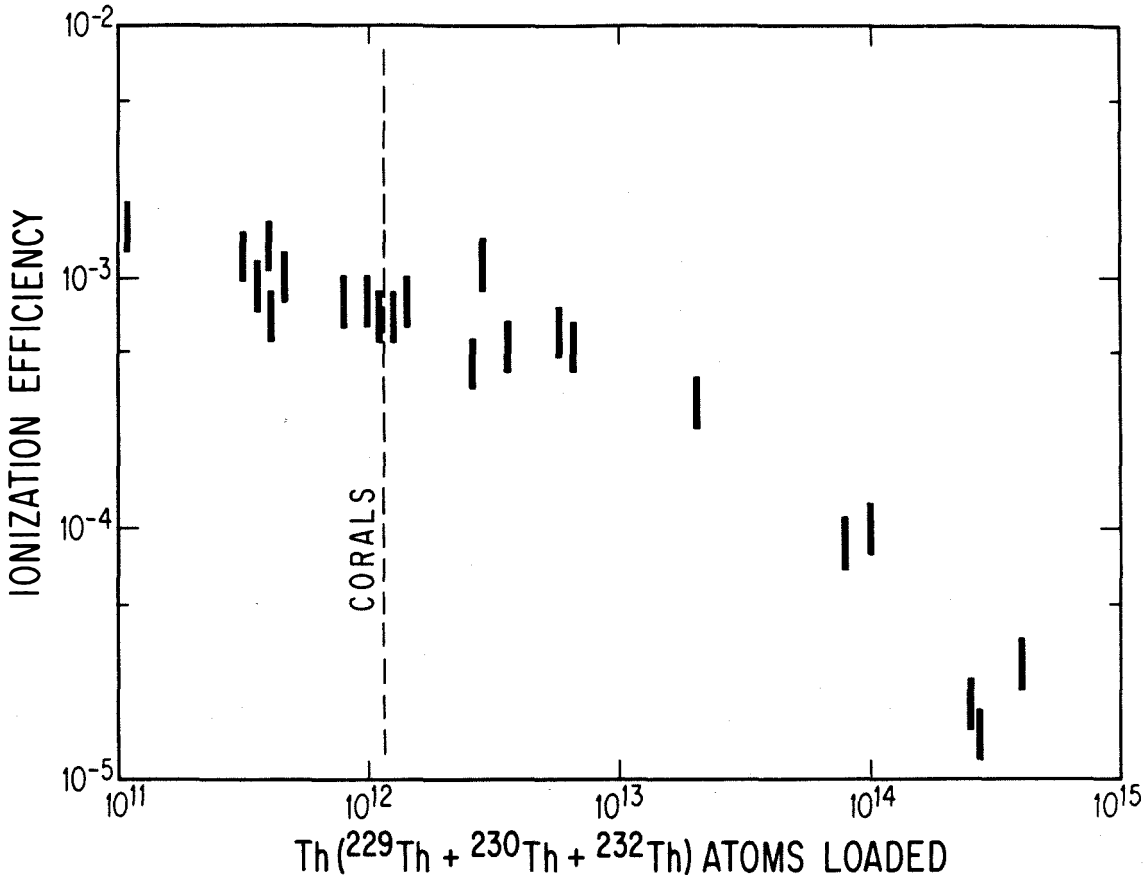
IONIZATION EFFICIENCY
10^{-2}
10^{-3}
10^{-4}
10^{-5}
CORALS
10^{11}
10^{12}
10^{13}
10^{14}
10^{15}
Th (^{229}Th + ^{230}Th + ^{232}Th) ATOMS LOADED

loads were $<10^{12}$ atoms and ionization efficiencies were 0.7 to 1.3 °/oo. As discussed below, corals have relatively high $^{230}Th/^{232}Th$ ratios (see Table A2), so for a fixed amount of ^{230}Th loaded on the filament, very little ^{232}Th is also loaded on the filament. Most natural materials have $^{230}Th/^{232}Th$ ratios that are several orders of magnitude lower than corals, so for the same amount of ^{230}Th loaded, large amounts of ^{232}Th are also loaded. The relationship in figure 7.8 suggests that mass spectrometric ^{230}Th measurements on these materials would have signficantly lower ionization efficiencies and, consequently, larger uncertainties than obtained here. The ionization efficiency for the uranium concentration runs is greater than 1 °/oo. For the uranium isotope composition runs that have much more uranium loaded on the filament, the ionization efficiency is about 0.5 °/oo.

7.3.6 Spikes and standards

The ^{229}Th spike was obtained from Oak Ridge National Laboratory in solution in nitrate form. This was diluted with 1N HNO_3 and stored in a teflon bottle. Mass spectrometer runs to determine the isotopic composition of the spike showed that it was essentially pure ^{229}Th ($^{230}Th/^{229}Th < 2 \times 10^{-5}$ and the amount of ^{232}Th was indistinguishable from the filament loading blank, $^{232}Th/^{229}Th < 7 \times 10^{-4}$). Analogue scans showed that none of the uranium isotopes were present in appreciable amounts. A ^{232}Th standard solution was prepared (T. Wen, Sept. 1976) from 99.998% pure ThO_2 powder (Johnson and Matthey), which was heated to 700°C, weighed, dissolved in a solution of 2.5N HNO_3 and 0.01N HF and stored in a 1-liter teflon bottle. This bottle has been

weighed recently. Comparison with the original weight indicates that evaporative losses could not have increased the ^{232}Th concentration of the solution by more than 0.7 ‰ over the past ten years. The original ^{232}Th solution was diluted twice with ~ 1N HNO_3 in 1985. The dilute solutions had volumes of 1 liter and 500 ml and were stored in tightly capped, nearly full teflon bottles, In isotopic composition, these solutions had $^{230}Th/^{232}Th = 6.8 \pm 0.2 \times 10^{-5}$ and $^{229}Th/^{232}Th < 10^{-5}$. The ^{229}Th spike was calibrated against the most dilute ^{232}Th standard solution. The ^{229}Th abundance of this spike is $(5.508 \pm 0.006) \times 10^{11}$ atoms/g (mean and 2 sigma of the mean for four experiments). The error for each experiment ranged from ±0.9 ‰ to ±2.0 ‰. None of four experiments gave a concentration that differed from the average value by more than 1.5 ‰.

As a further check, another ^{232}Th solution was prepared recently from a thorium metal powder that was significantly less pure than the ThO_2 powder. An aliquot of this solution was mixed with a ^{229}Th tracer and the $^{232}Th/^{229}Th$ ratio was measured. The ^{229}Th concentration determined using the thorium metal standard, agreed to ~ 1% with that determined using the thorium oxide standards and showed that processes such as adsorption of thorium onto the walls of the bottle, or precipitation of thorium salts, which would lower thorium concentration, have not occurred to any significant extent for the thorium oxide standard over the past ten years.

For the uranium measurements, I used a double spike with a ratio of ^{233}U to ^{236}U close to unity as calibrated using the absolute values of the National Bureau of Standards (NBS) U-500 standard ($^{235}U/^{238}U$ =

0.9997 ± 0.001; Garner et al., 1971). The concentration of this spike is calibrated using this U-500 standard, and normal solutions prepared from NBS SRM 960 and NBS SRM 950a. The absolute isotopic composition and concentration of the double spike are given in Chen and Wasserburg (1981a).

7.3.7 Chemical separation of uranium and thorium

The scheme for separating uranium and thorium from corals is shown in figure 7.9. Coral samples (with the exception of some of AFS-12, which was provided to me in powdered form) were prepared by breaking the sample into pieces several millimeters in diameter with a stainless steel chisel. These fragments were examined under a binocular microscope and any pieces that showed signs of secondary alteration were discarded. The remaining pieces were ultrasonically cleaned in distilled water twice. The large pieces were then rinsed individually in distilled waer, dried and weighed. The fine pieces were discarded. Samples of 2.8 to 4.6 grams of young (< 10 ky) coral or ~500 mg of old (> 10 ky) coral were dissolved by first adding several ml of distilled water, then slowly adding concentrated HNO_3 over the course ~ 1 hour. The solution was heated under a heat lamp for ~ 1 hour. This resulted in the oxidation of any remaining organic matter and changed the color of the solution from slightly brown to clear. The sample was then spiked and, in order to insure sample-spike equilibration, dried, fumed with concentrated $HClO_4$, and dried. It was then dissolved in ~ 1N HCl, and ~ 8 mg of Fe in chloride solution were added. The uranium and thorium were then co-precipitated with Fe by the addition of ammonium

Figure 7.9. The chemical separation scheme used for separating uranium and thorium from corals. Yields using this procedure were >95% for uranium and 93% to 98% for thorium.

U–Th SEPARATION FROM CORALS

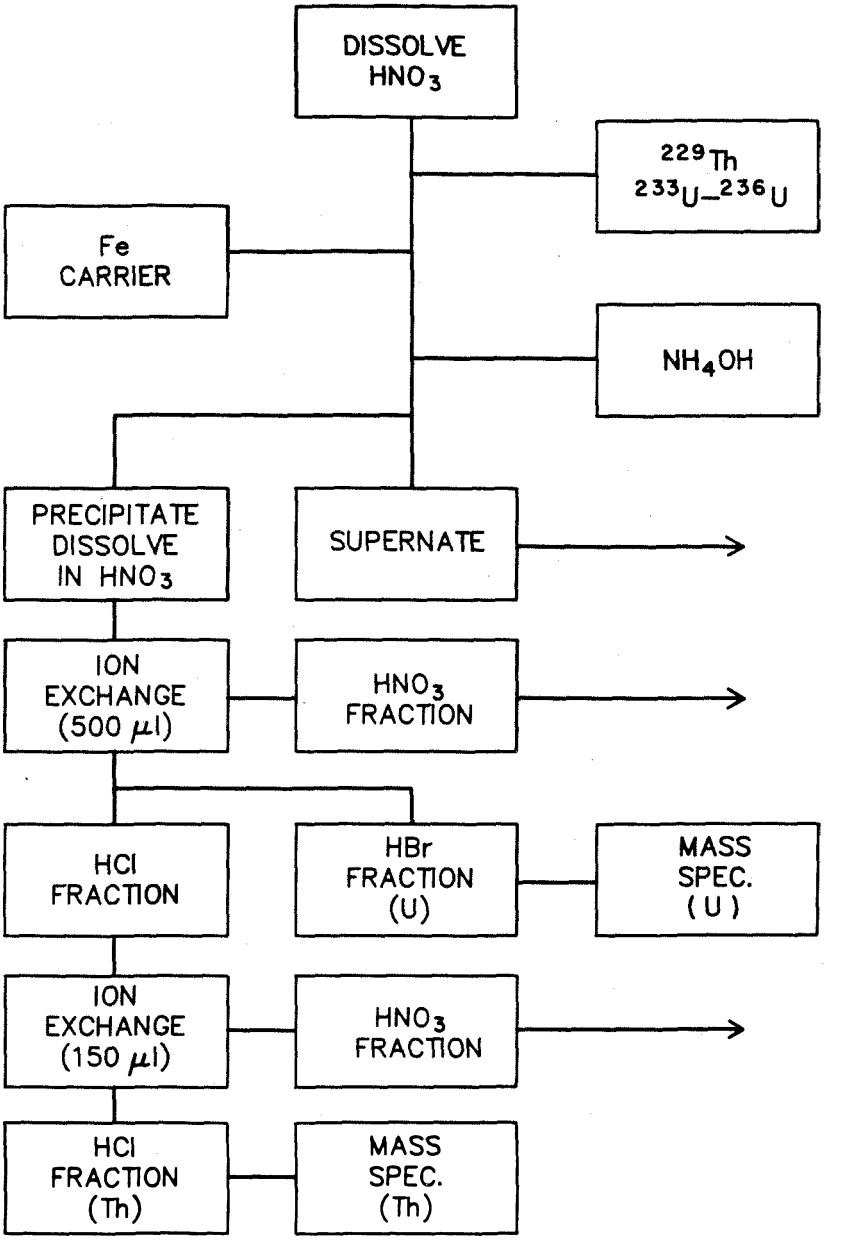

hydroxide until the color of the solution changed from yellow to clear. The mixture was centrifuged and the supernate discarded. The residue was then rinsed twice with distilled water, dissolved in concentrated HNO_3, dried and redissolved in concentrated HNO_3 twice, dried and dissolved in 0.5 ml of 7N HNO_3. This solution was loaded on an anion exchange colun (Dowex AG 1X8 resin) with a volume of 0.5 ml. Fe was eluted using 7N HNO_3. The thorium fraction was then eluted with 6N HCl and the uranium fraction with 1N HBr. The uranium fraction was dried, dissolved with HNO_3, dried and dissolved in 0.1 N HNO_3. An aliquot containing ~ $3x10^{10}$ atoms of ^{234}U (corresponding to ~ 70 mg coral) was loaded on a graphite-coated zone refined Re filament (Chen and Wasserburg, 1981a). The thorium fraction was further purified by drying it down, dissolving it in HNO_3, drying it and dissolving it in 0.15 ml of 7N HNO_3. This solution was loaded on a column similar to the first column but with a volume of 0.15 ml. A similar elution scheme was followed. The subsequent thorium fraction was dried, dissolved in HNO_3, dried and dissolved in 0.1 N HNO_3. For samples younger than 10 ky, the whole thorium fraction was loaded, and for samples older than 10 ky, half the thorium fraction (corresponding to 250 to 390 mg of coral) was loaded on a graphite-coated zone refined Re filament. The loading technique is similar to the uranium loading technique. For the complete procedure, the uranium yield is > 95% and the thorium yield is 93%-98%. The amount of uranium in the thorium fraction is $< 10^{-5}$ times the total uranium processed.

A similar separation scheme was used for seawater analyses. The sample size for the uranium concentration runs was 1 ml of seawater (~

6 X 10^{13} ^{238}U atoms). For the uranium isotopic composition runs, 30 ml of seawater was processed and one third of the uranium fraction (5 X 10^{9} ^{234}U atoms) was loaded on a filament and run in the LI mass spectrometer.

7.3.8 Analytical blank

Zone refined, highly annealed Re filaments (REMBAR Co., Inc.) that had been outgassed at ~ 2000°C for 2 hours were used for both the uranium and thorium runs. Examination of one batch of Re ribbon showed that outgassed filaments coated with graphite following the standard procedure produced $^{232}Th^{+}$ currents of 6 X 10^{2} to 4 X 10^{5} ions/s and $^{238}U^{+}$ currents of < 60 to 3 X 10^{3} ions/s when heated to typical temperatures at which data were acquired. Since typical sample currents are 3 X 10^{7} ions/s for ^{238}U and 8 X 10^{4} ions/s for ^{232}Th, many of the $^{232}Th^{+}$ filament currents were unacceptably high. Outgassing for longer periods of time or at slightly higher temperatures did not lower the currents appreciably. A second batch of Re ribbon from the same supplier gave filament currents of < 60 to 1 X 10^{4} for $^{232}Th^{+}$ and < 60 to 2 X 10^{3} for $^{238}Th^{+}$. Out of 53 filaments, all but three had $^{232}Th^{+}$ currents below 1 X 10^{3} ions/s. Since occasionally, filaments in this batch had high $^{232}Th^{+}$ currents, as standard procedure, I checked every filament in the mass spectrometer before loading a sample on it. Filaments with $^{232}Th^{+}$ currents higher than 10^{3} ions/s were not used.

The total procedural blank including the filament blank is 1.2 X 10^{10} atoms of ^{238}U and 1.0 X 10^{10} atoms of ^{232}Th with upper limits of 9 X 10^{6} atoms of ^{234}U and 6 X 10^{6} atoms of ^{230}Th. The blanks were

determined using standard mass spectrometer runs with digital data acquisition and standard integration times. Blank levels of ^{234}U are presumably ~ 10^{-4} times ^{238}U and levels of ^{230}Th around 10^{-5} times ^{232}Th. In order to avoid introducing ^{230}Th and ^{229}Th contamination from previous samples, all reusable labware, including ion exchange columns, which came in contact with coral solutions were divided into two groups. One group was used for young corals (< 10 ky) that have low ^{230}Th concentrations and, when spiked, have low $^{230}Th/^{229}Th$ ratios, and the other group for old corals (> 10 ky) that have high ^{230}Th concentrations and higher $^{230}Th/^{229}Th$ ratios. The two groups of labware were cleaned and stored separately. Ion exchange resin was discarded after every use. Between samples, ion exchange columns were rinsed with 7N HNO_3 and distilled water, stored (in separate groups) in 7N HNO_3, and rinsed with 7N HNO_3 and distilled water before the next use.

7.3.9 Measurement error and reproducibility

The reported error (Table A2) in the $^{234}U/^{238}U$ ratio is two standard deviations of the mean of 100 to 300 $^{234}U/^{238}U$ ratios measured in the course of a mass spectrometer run. If this is a good estimate of the error in the measurement, then repeated measurements of the same solution should yield identical results within the reported error. A series of measurements of the $^{234}U/^{238}U$ ratio in solutions prepared by dissolving NBS standard reference material 960 and NBS standard reference material 950 are shown in Table 7.1. For each standard, the measurements yield identical values of $^{234}U/^{238}U$ within the roughly

Table 7.1. $^{234}U/^{238}U$ ratios in NBS SRM 960 and NBS SRM 950a.

NBS Standard[a]	$^{234}U/^{238}U(\times 10^5)$[b,c]		$\delta^{234}U$[b,c,d]	
	I	II	I	II
SRM 960[e]	5.260±0.029	5.280±0.024	-39±5	-35±4
	5.267±0.035	5.266±0.019	-37±6	-38±4
	5.245±0.029	5.244±0.024	-41±5	-42±4
	5.280±0.028	5.273±0.029	-35±5	-36±5
	5.280±0.036	--	-35±7	--
	5.267±0.025	--	-37±5	--
average =	5.267±0.011	5.266±0.016	-37±2	-38±3
SRM 950a	5.350±0.033	5.382±0.027	-22±6	-16±5
	5.344±0.032	5.360±0.021	-23±6	-20±4
	5.364±0.018	5.356±0.015	-20±3	-21±3
average =	5.353±0.012	5.366±0.016	-22±2	-19±3

[a] Amount of U analyzed is ~ 30 ng (1 ng = 10^{-9} g).

[b] $\delta^{234}U = \{[(^{234}U/^{238}U)_{sample}/(^{234}U/^{238}U)_{eq}] - 1\}\times 10^3$, where $(^{234}U/^{238}U)_{eq}$ is the atomic ratio at secular equilibrium and is equal to $\lambda^{238}U/\lambda^{234}U = 5.472 \times 10^{-5}$ (De Bievre et al., 1971; Lounsbury and Durham, 1971).

[c] All errors are $2\sigma_{mean}$.

[d] I: Calculated from the measured $^{234}U/^{235}U$ ratio assuming $^{238}U/^{235}U \equiv 137.88$;

II: Calculated from ^{234}U and ^{238}U concentrations.

[e] SRM 950a analyses and most of SRM 960 analyses by J. H. Chen.

±5 °/oo error of each measurement. This shows that the measurements are reproducible and that the error estimates for each individual mass spectrometer runs are reasonable. Measurements of $^{234}U/^{238}U$ in standards (Table 7.1), seawater (Table 8.1), and corals (Table A2) show that $^{234}U/^{238}U$ can be measured to ±3 to ±5 °/oo for samples sizes of 5 X 10^9 to 3 X 10^{10} atoms of ^{234}U.

The reported error in the $^{230}Th/^{238}U$ ratio (Table A2) is calculated from the error in the measured $^{230}Th/^{229}Th$ ratio and the measured $^{235}U/^{236}U$ ratio. The error in each of these quantities is two standard deviations of the mean of 40 to 160 measurements of each ratio. The fractional error in the $^{230}Th/^{238}U$ ratio is taken to be the square root of the sum of the squares of the fractional errors in $^{230}Th/^{229}Th$ and $^{235}U/^{236}U$. The two sigma error in the ^{230}Th abundance for each coral analysis is shown in Table A3 along with the number of ^{230}Th atoms loaded on the filament and the mass of coral used in each experiment. This table shows that 8 X 10^7 ^{230}Th atoms can be measured to ±132 °/oo (2 sigma); 6 X 10^8 atoms to ±29 °/oo, and 3 X 10^{10} atoms to ±2 °/oo. For samples CWS-D, OC-51, FT-50, AFS-12, E-T-2, PB-5B, and PB-9A, I report (Table A2) replicate analyses on either different fragments of the same sample or different aliquots of the same dissolved fragment. For each of these samples, the replicate measurements of the $^{230}Th/^{238}U$ ratio agree within the reported errors. This indicates that the measurements are reproducible and that the reported errors are good estimates of the precision of each measurement. For each of these samples, replicate measurements of the $^{234}U/^{238}U$ ratio (Table A2) also agree within reported errors.

7.3.10 Resolution of small differences in ^{230}Th abundance and time

For one run, the 2 sigma error in $^{234}U/^{238}U$ is ± 3 to 5 °/oo. The error in the ^{238}U abundance is ± 1 to 3 °/oo and the error in the ^{230}Th abundance is ± 29 °/oo for a 180 year old sample (TAN-E-1g) and ± 2 °/oo for a 123.1 ky old sample (AFS-12; see Tables A1, A2, A3). The error in $^{230}Th/^{238}U$, therefore, is ± 30 °/oo for TAN-E-1g and ± 3 °/oo for AFS-12. When the analytical errors in $^{234}U/^{238}U$ and $^{230}Th/^{238U}$ are propagated through the age equation (Equation 5.11), errors in age of ± 5 years for TAN-E-1g and ± 1.1 ky for AFS-12 A are calculated. Based on these errors, one would expect to be able to resolve the ages of two young (~200 year old) corals different in age by ~10 years and two old (~120 ky old) corals different in age by ~2 ky.

In order to confirm this estimate of age resolution, I carried out the following experiment. About 3 g of AFS-12 were dissolved and the solution divided into five aliquots, four aliquots containing ~0.5 g of coral and the remaining aliquot kept in reserve. Known amounts of ^{230}Th from a ^{230}Th standard solution were added to three of the four aliquots. This increased ^{230}Th concentrations in these aliquots by about 8°/oo, 16 °/oo and 32 °/oo. This is equivalent to shifts in age of about 2, 4, and 8 ky. All four aliquots were then spiked, processed, and the thorium isotopes measured as described above. The uranium isotopes were measured in one aliquot. The results are shown in figure 7.10 where the ^{230}Th abundance determined on the mass spectrometer is plotted against the gravimetrically determined ^{230}Th abundance. The ages corresponding to the ^{230}Th concentrations are also shown. These are calculated using equation 5.11 and the results of the

Figure 7.10. The mass spectrometrically determined ^{230}Th abundance (^{230}Th atoms/g) plotted versus the gravimetrically determined ^{230}Th abundance for AFS-12 B and aliquots of AFS-12 B to which known amounts of ^{230}Th had been added. The axes are also scaled in ky using the measured ^{238}U abundance, $^{234}U/^{238}U$ ratio, and equation 5.11. The error bars are 2 sigma of the mean. None of the points deviate by more than 1.2 $^{o}/oo$ or 0.3 ky from a 45° line through the origin. The diagram shows that just considering the error in the ^{230}Th measurement, differences in age of 2 ky are clearly resolvable for a coral that is about 120 ky old.

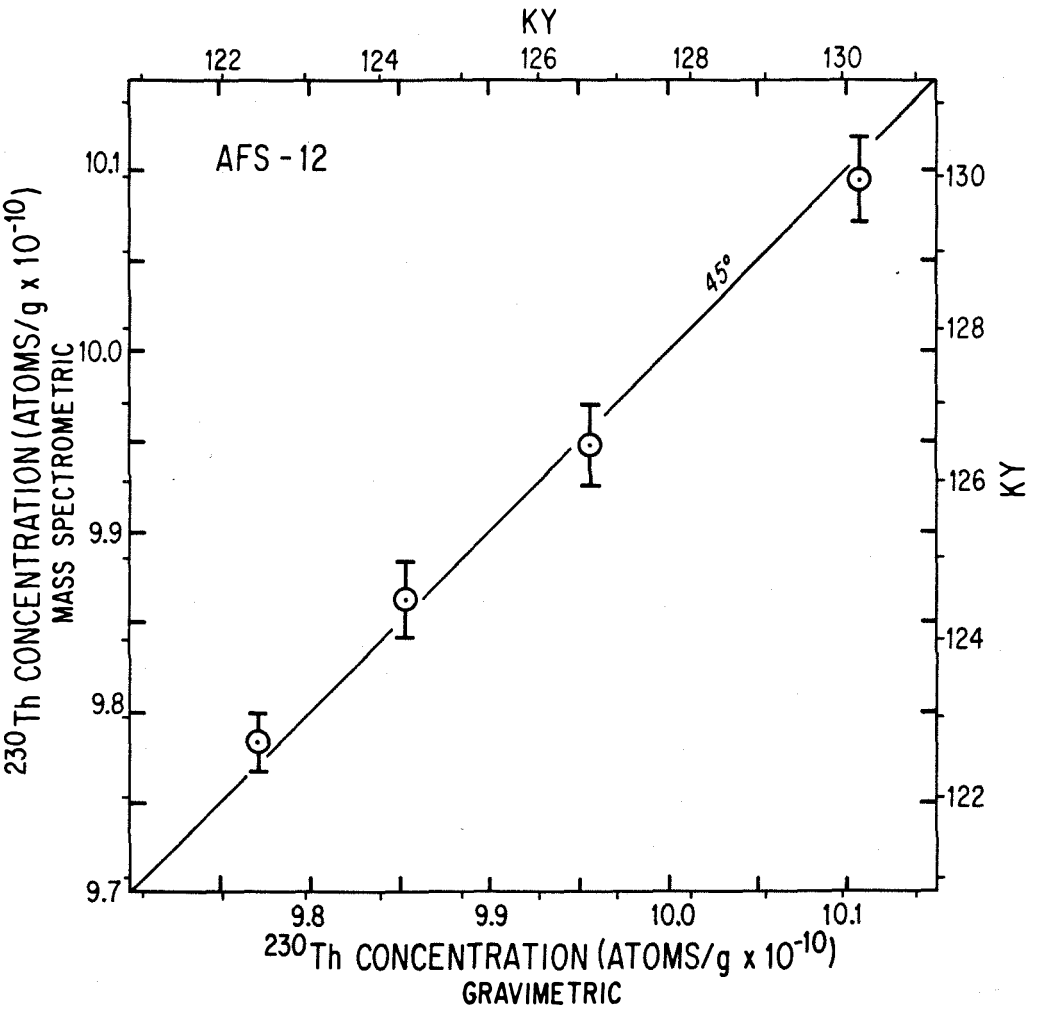
KY
122
124
126
128
130
AFS - 12
45°
10.1
10.0
9.9
9.8
9.7
130
128
126
124
122
KY
^{230}Th CONCENTRATION (ATOMS/g x 10^{-10})
MASS SPECTROMETRIC
9.8
9.9
10.0
10.1
^{230}Th CONCENTRATION (ATOMS/g x 10^{-10})
GRAVIMETRIC

uranium analysis. The ^{230}Th concentration of the initial solution used in the calculation of the gravimetric ^{230}Th concentration is an average of the four ^{230}Th determinations after the known enrichments of ^{230}Th have been subtracted. All four points plot with 1.2 ‰ or 0.3 ky of a 45° line through the origin, indicating agreement between the mass spectrometric and gravimetric determinations well within the error of each individual measurement. Based on this experiment and assuming no error in the uranium analysis, it is clear that, for ~ 120 ky old corals, differences in age of 2 ky are analytically resolvable.

A similar experiment was performed to determine the age resolution for very young corals. About 15 grams of TAN-E-1g were dissolved and the resulting solution divided into four aliquots. Three aliquots contained ~ 3 grams of coral each, and the remainder was kept in reserve. ^{230}Th was added to two of the aliquots in order to increase the ^{230}Th concentration by 90 ‰ and 170 ‰, respectively. The number of ^{230}Th atoms added was 2×10^7 and 4×10^7. This corresponds to shifts in age of 17 to 33 years. The thorium isotopes were measured in all three aliquots and the uranium isotopes in one aliquot. The results of this experiment are shown in figure 7.11. None of the points differ by more than 12 ‰ or 2 years from the 45° line, again well within the error of the individual measurements. This experiment shows that, for corals ~ 200 years old, differences in age of 17 years are clearly resolvable analytically.

7.4 Errors in age due to analytical errors

In the following sections, I discuss errors in age (T) which are

Figure 7.11. A plot similar to figure 7.10 but for a much younger coral (TAN-E-1g, 180 years old). In addition to ^{230}Th atoms/g, the axes are also scaled in years. None of the points deviate from the 45° line by more than 12 °/oo or 2.4 years. The diagram shows that for corals that are about 200 years old, differences in ^{230}Th concentration of about 10^7 atoms/g, corresponding to differences in age of 17 years, are clearly quantitatively resolvable.

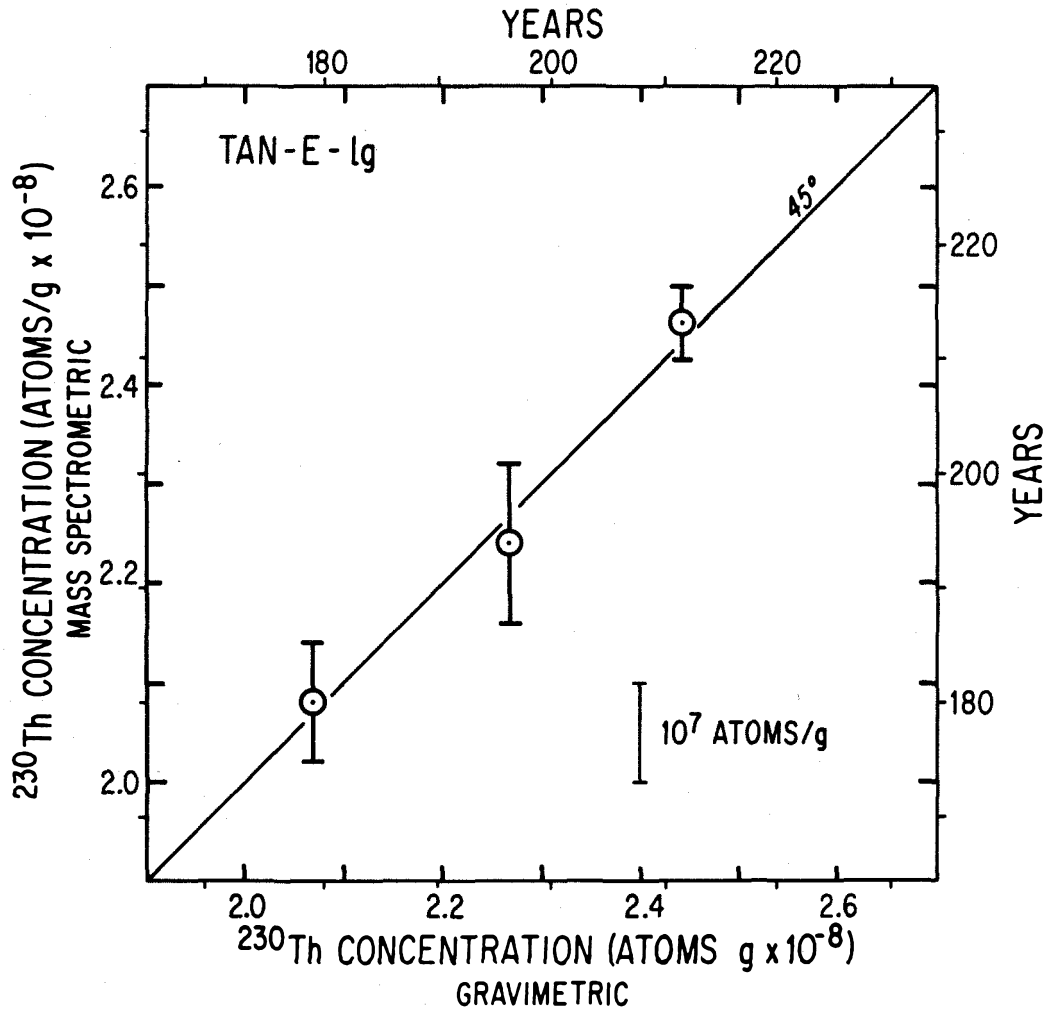
YEARS
180
200
220
TAN-E-lg
45°
2.6
2.4
2.2
2.0
220
200
180
YEARS
^{230}Th CONCENTRATION (ATOMS/g x 10^{-8})
MASS SPECTROMETRIC
10^7 ATOMS/g
2.0
2.2
2.4
2.6
^{230}Th CONCENTRATION (ATOMS g x 10^{-8})
GRAVIMETRIC

generated by propagating error in the decay constants, $[^{230}Th/^{238}U]_{act}$, and $\delta^{234}U(0)$ through the age equations (equation 5.11). In order to determine the error in T generated by error in one particular variable, I hold all variables constant except for one. I will call the mean value of this variable, x. The 2 sigma error in x is Δx. I then calculate three ages T, $T+\Delta T_x^+$, and $T-\Delta T_x^-$ using equation 5.11, x, $x+\Delta x$, and $x-\Delta x$. The error in T due to the error in x is $+T_x^+$ and $-T_x^-$. T_x^+ and T_x^- are not in general equal but are approximately equal if $\Delta x/x$ is small. The total error in T due to uncorrelated error in two dependent variables, x and y, is given by $\Delta T^+ = \{\Delta T_x^{+2} + \Delta T_y^{+2}\}^{1/2}$ and $\Delta T^- = \{\Delta T_x^{-2} + \Delta T_y^{-2}\}^{1/2}$ (Bevington, 1969). This approach can be extended to any number of variables whose errors are uncorrelated.

7.4.1 Errors in decay constants

In order to calculate the age accurately, accurate values for the decay constants must be known. Previous studies have used mean lives of 108,500 yr for ^{230}Th and 357,800 yr for ^{234}U, based on the studies of Attree et al. (1962) and presumably Fleming et al. (1952), respectively. I have chosen to use the more recent determinations of 108,750 ± 850 years (2 sigma, Meadows et al., 1980) for the mean life of ^{230}Th and 352,740 ± 710 years (2 sigma; Lounsbury and Durham (1971); De Bievre et al. (1971)) for the mean life of ^{234}U. Within error, the earlier ^{230}Th value is the same as the more recent value, but the analytical uncertainty of the more recent value is much smaller. The value for ^{234}U is the average of the two 1971 references. These two values are different by 200 years. The 2 sigma error which I quote is

from the latter reference. For ^{238}U, I use (6.4464 ± 0.0069) X 10^9 years (2 sigma, Jaffey et al., 1971).

The fractional errors in the decay constants are as follows: λ_{238}, ± 1 °/oo; λ_{234}, ± 2 °/oo; and λ_{230}, ± 8 °/oo. Errors in the decay constants will yield systematic errors in T. Errors in λ_{238} and λ_{234} are insignificant compared to analytical errors in $[^{230}Th/^{238}U]_{act}$ and $\delta^{234}U(0)$ for all T. For $\lambda_{230}T < 1$, λ_{230} is not an important term and does not introduce significant error in T. As T increases, λ_{230} becomes a more important term and the uncertainty in T increases. For T < 150 ky, the error in T due to error in λ_{230} is less than the error in T due to the analytical uncertainty in $[^{230}Th/^{238}U]_{act}$ and $\delta^{234}U(0)$. For T larger than 150 ky, the error in T due to error in λ_{230} is up to 1.5 times larger than the error due to analytical uncertainty. The total error due to errors in all three decay constants is ± 0.4 years for T = 200 years, ± 2 years for T = 1000 years, ± 22 years for T = 10 ky, ± 0.8 ky for T = 120 ky, and ± 17 ky years for T = 300 ky and is insignificant compared to analytical error except at large T.

7.4.2 Errors in mass spectrometric measurements

Uncertainties in T are also introduced by uncertainties in $\delta^{234}U(0)$ and $[^{230}Th/^{238}U]_{act}$. These uncertainties were the dominant source of error in earlier studies. I showed in section 7.3.10 that, based on the addition of a known quantity of ^{230}Th atoms, the ages of two ~ 200 year old corals different in age by 17 years and the ages to two ~ 120 ky old corals different in age by 2 ky could be resolved. I now examine error in T, ΔT, introduced by analytical error, as a

function of T. I have analyzed a number of corals of different ages. The calculated ages using equation 5.11 and the 2 sigma errors in age based on the propagation of the analytical errors in $\delta^{234}U(0)$ and $[^{230}Th/^{238}U]_{act}$ through equation 5.11 are listed in Table A2. Selected coral data are plotted on a $\Delta T/T$ versus T plot (figure 7.12) and a ΔT versus T plot (figure 7.13). I have drawn an error envelope through these points. This envelope has been extrapolated to larger and smaller T using the following assumptions: For extrapolating to large T, I assumed that the analytical uncertainty for older corals is the same as the analytical uncertainty for ~ 120 ky corals. This assumption is reasonable since the number of atoms/gram of ^{230}Th and ^{234}U for an infinite age coral are both within 50% of the values for a ~ 120 ky coral. For extrapolating to T younger than 18 years, I assumed that the fractional error is inversely proportional to the square root of the number of ^{230}Th atoms per analysis. This error envelope shows that the smallest fractional errors in age of about ± 5 o/oo are obtained for corals several thousand to several tens of thousands of years old. These samples are old enough to have enough ^{230}Th atoms for a high precision analysis (using small amounts of coral) yet are young enough ($\lambda_{230}T < 1$) to fall on the initial linear part of the $[^{230}Th/^{238}U]_{act}$ growth curve (see figure 5.1). The error envelope shows that $\Delta T/T < 0.10$ for corals as young as 15 years old and as old as 500,000 years old. Corals as old as 600 ky have ages distinguishable from infinity at the 2 sigma level. Figure 7.12 is also contoured in absolute error, T. Examination of the $T = 10^4$ years contour shows that, for all T < 300 ky, T < 10 ky. If sea level

Figure 7.12. $\Delta T/T$ plotted versus T, where T is the age and ΔT is the 2 sigma error in age based on the propagation of analytical errors through equation 5.11. T is plotted on a log scale. Between 180 years and 129.9 ky, the error envelope is drawn through the observed values for several corals. The error envelope is extrapolated to younger and older T as described in the text. The lowest values of $\Delta T/T$ are at about 10^4 years and values of $\Delta T/T < 0.10$ can be obtained over the range T=15 years to T=500,000 years. Parts of the diagram are contoured in ΔT. The intersection of the $\Delta T=10^4$ contour with the error envelope shows that $\Delta T<10^4$ years for all $T<3 \times 10^5$ years.

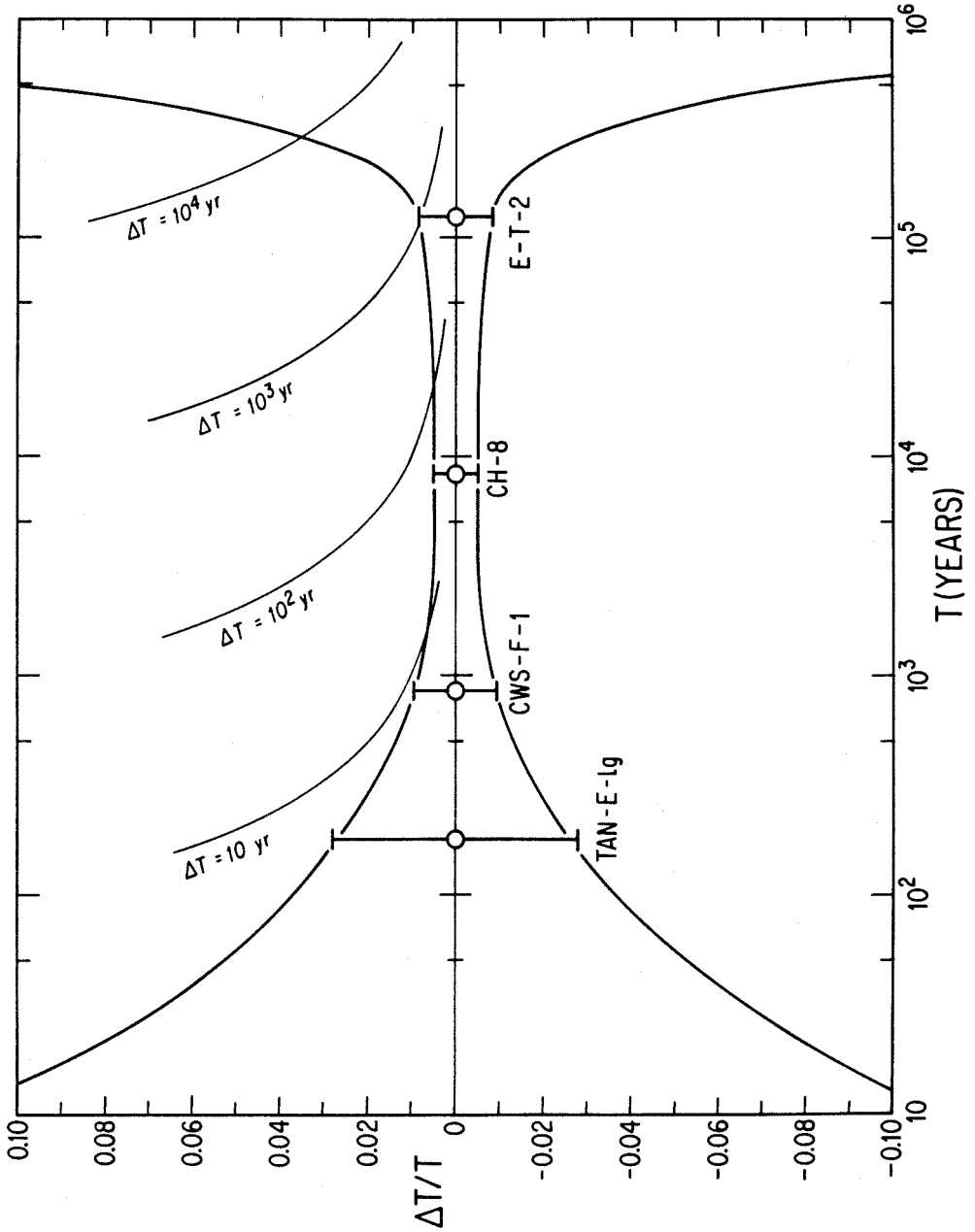
ΔT = 10⁴ yr
ΔT = 10³ yr
ΔT = 10² yr
ΔT = 10 yr
E-T-2
CH-8
CWS-F-1
TAN-E-lg
0.10
0.08
0.06
0.04
0.02
0
-0.02
-0.04
-0.06
-0.08
-0.10
ΔT/T
10
10²
10³
10⁴
10⁵
10⁶
T (YEARS)

Figure 7.13. A diagram similar to figure 7.12 but with ΔT plotted versus T and contoured in $\Delta T/T$. Both of the axes are log scales. The points represent the age determined from equation 5.11 and the error in age determined by propagating analytical error through equation 5.11. A line has been drawn through these points and extrapolated to higher age assuming typical analytical error. The youngest sample analyzed had a ^{230}Th age of 18 years at the time of analysis. The 2 sigma error in age was ±3 years. Corals that grew during the last interglacial period (about 125 ky ago) have errors in age of about ±1 ky. Samples as old as 600 ky have ages that are distinguishable from infinite age and samples as young as 3 years old have ages distinguishable from zero age. Fractional errors in age as small as 0.005 can be obtained for samples that are 10 ky to several tens of ky old as shown by the contours of $\Delta T/T$.

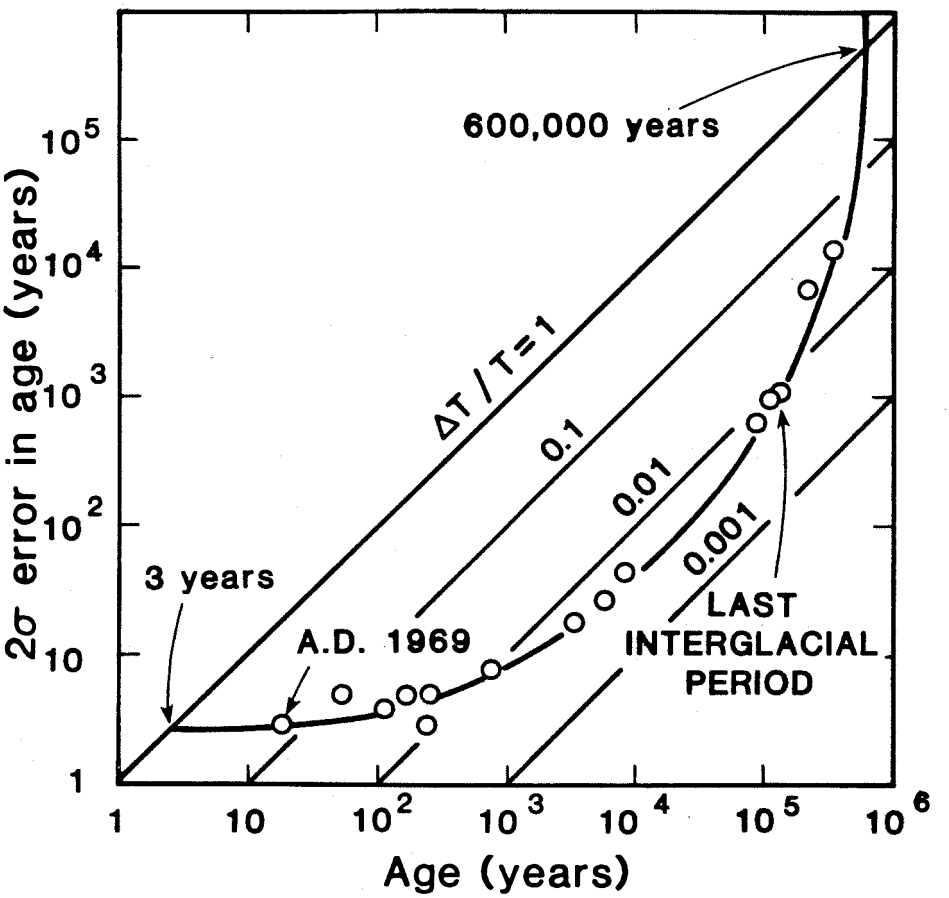
600,000 years
ΔT / T=1
0.1
0.01
0.001
3 years
A.D. 1969
LAST
INTERGLACIAL
PERIOD
2σ error in age (years)
Age (years)
1
10
10^2
10^3
10^4
10^5
10^6

highs are separated by about 20 ky, all coral terraces that represent sea level highs and are younger than 300 ky, have ages that are analytically resolvable at the 2 sigma level.

7.4.3 Analytical errors in ^{230}Th age: a comparison of mass spectrometric and alpha-counting techniques

A number of the samples which I analyzed had previously been analyzed by alpha-counting techniques (see Tables 7.2 and 7.3). The mass spectrometric determinations agree with the earlier results at the 2 sigma level of uncertainty of the quoted errors. However, the uncertainties in the present study are around an order of magnitude smaller. It is clear from Table 7.3 that the main reason behind the improved precision is that more ions can be measured by mass spectrometry than alpha-particles by counting decays. Using mass spectrometric methods about 10^6 ions of $^{230}Th^+$ or $^{234}U^+$ can be measured per run, whereas in a typical alpha-counting run, about 10^3 alpha particles are measured. The sample size (250 mg of coral for 120 ky old samples) is also about 40 times smaller than the typical sample sizes used for alpha-counting. In section 7.1 and figure 7.1, ^{230}Th ages that had been determined by alpha-counting for a series of terraces in Vanuatu (Bloom, 1980b) were discussed. Bloom demonstrated that the ages of successive terraces that were about 100 ky old were not resolvable. Figure 7.14 shows a histogram of mass spectrometrically determined ^{230}Th ages for three distinct terraces on Barbados. Two ages from a terrace doublet in Vanuatu are also plotted. The ages of the Barbados samples fall into three distinct age groups

Table 7.2. Coral ages determined by α-counting and mass spectrometric methods. Reported errors are 2σ. For α-counting, the errors are based on counting statistics. Errors in mass spectrometric ages are based on the standard deviation of the mean of 60 to 300 isotope ratios measured in the course of a mass spectrometric run.

Sample	^{238}U-^{234}U-^{230}Th[a] (α-counting) (ky)	^{238}U-^{234}U-^{230}Th (mass spectrometric)
WORTHING TERRACE		
OC-51 A	85 ± 4	87.5 ± 0.6 ky
B		87.9 ± 0.7 ky
VENTNOR TERRACE		
FT-50 A	107 ± 7	112.0 ± 1.0 ky
B		111.8 ± 1.3 ky
C		112.3 ± 1.1 ky
RENDEZVOUS HILL TERRACE		
AFS-10	123 ± 8	125.7 ± 1.2 ky
AFS-11	127 ± 9	122.6 ± 1.5 ky
AFS-12 A	129 ± 9	122.1 ± 1.1 ky
B		122.7 ± 1.3 ky
C		124.5 ± 1.3 ky
AFM-20 A	117 ± 8	129.2 ± 1.4 ky
B	127 ± 9	
R-52 A	107 ± 6	128.1 ± 1.7 ky
B	120 ± 9	
VANUATU		
E-T-2 A	141 ± 16	129.9 ± 1.1 ky
B		129.2 ± 1.1 ky
E-L-3	141 ± 16	125.5 ± 1.3 ky

[a] α-counting ages from Ku (pers. commun.) except for E-T-2 and E-L-3 which are from Bloom et al. (1978).

Table 7.3. Comparison between mass spectrometric and α-counting methods for measuring ^{230}Th and ^{234}U in a ~ 120 ky old coral.

		# of ions or alpha particles measured/run		2σ uncertainty[a]		
Method	Sample size	^{230}Th	^{234}U	$^{230}Th/^{238}U$	$^{234}U/^{238}U$	Age
Mass spec.	200mg coral	5×10^{6}	2×10^{6}	±2°/₀₀	±5°/₀₀	±1ky
α-counting	10g coral	3×10^{3}	5×10^{3}	±40°/₀₀	±30°/₀₀	±10ky

[a] The α-counting uncertainties are taken from Harmon et al. (1979) and are based on counting statistics.

Figure 7.14. Histogram of ^{230}Th ages by mass spectrometry for corals from the Rendezvous Hill, Ventnor, and Worthing Terraces on Barbados and from a terrace doublet on Efate Island in Vanuatu. The error bar shows the typical 2 sigma uncertainty in age based on analytical error. The ages of the three terraces are clearly resolved. The Vanuatu corals have the same age as the Rendezvous Hill corals. The Rendezvous Hill and Vanuatu corals range in age from 130 to 122 ky suggesting that the last interglacial period lasted from 130 to at least 122 ky ago.

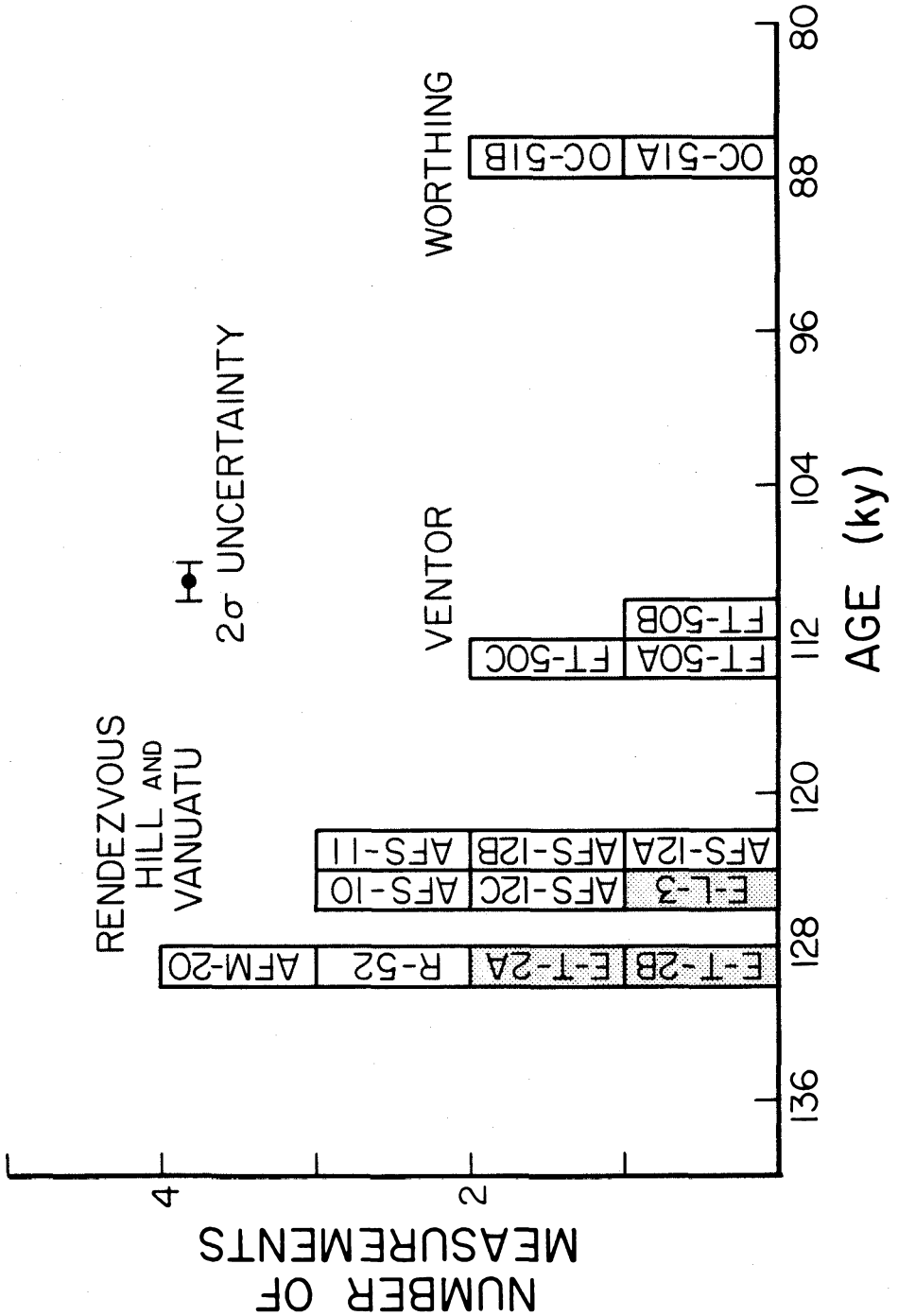
NUMBER OF MEASUREMENTS
4
2
136
128
120
112
104
96
88
80
AGE (ky)
RENDEZVOUS HILL AND VANUATU
E-T-2B
E-T-2A
R-52
AFM-20
E-L-3
AFS-12C
AFS-10
AFS-12A
AFS-12B
AFS-11
VENTOR
FT-50A
FT-50C
FT-50B
WORTHING
OC-51A
OC-51B
2σ UNCERTAINTY

depending on which terrace the coral was collected from. This demonstrates that the ages of successive terraces on Barbados are clearly resolvable. Figure 7.15 shows data for the same samples plotted in a $\delta^{234}U(0)$ versus $[^{230}Th/^{238}U]_{act}$ plot. Each measurement is represented by a 2 sigma error ellipse. (The probability is 95% that the true isotopic composition lies within the boundaries of each ellipse). The data cluster in three different areas depending on which terrace the samples came from. From the time contours, it is clear (as in figure 7.14) that the ages of the terraces are resolvable.

7.4.4 ^{232}Th concentrations and $\delta^{234}U(T)$

The mass spectrometric ^{232}Th determinations in corals are extremely low (0.032 to 2.05 pmoles/g; Table A1). Because of the extremely low values and the long mean life of ^{232}Th, alpha-counting studies have often not reported ^{232}Th. Examination of the reported ^{232}Th concentrations (see for example Thurber et al., 1965, Veeh, 1966; Ku, 1968; Marshall and Thom, 1976; Harmon et al., 1983; Dodge et al., 1983; Somayajulu et al., 1985) shows that the typical detection limit in the alpha-counting studies is about 100 pmoles/g and that values as high as 10^4 pmoles/g have been measured. Thus, the previous values (with the possible exception of Bender et al., 1979) are at least two orders of magnitude higher than the values reported in Table A1. The reliable determination of ^{232}Th may permit use of the ^{232}Th concentration as a geochemical tracer. The range of $^{232}Th/^{238}U$ ratios for corals (Table A1) is 0.35×10^{-5} to 17.2×10^{-5}. The $^{232}Th/^{238}U$ ratio in open ocean water is 3.7×10^{-5} (see chapter 8). From my

Figure 7.15. Plot of $\delta^{234}U(0)$ versus $[^{230}Th/^{238}U]_{act}$ for corals from the Rendezvous Hill, Ventnor, and Worthing Terraces on Barbados and from a terrace doublet on Efate Island on Vanuatu. The elipses represent 2 sigma errors. Analyses of different fragments of the same coral for OC-51, FT-50, AFS-12, and E-T-2 agree within error for each of these hand specimens, demonstrating that if any of the samples were altered, the whole hand specimen had to have been altered in the same manner. The ages of the three terraces are clearly resolved. The ages of the Rendezvous Hill and Vanuatu samples range from 130 to 122 ky, suggesting that the age of the last interglacial period lasted from 130 to at least 122 ky ago. There is a hint that the initial $\delta^{234}U$ values of the corals are slightly above the present sea water value of 150. If this is the case, then the samples may have been slightly altered or the uranium isotopic composition of seawater may have changed slightly. A change in the $\delta^{234}U$ of seawater of 10 or 20 δ-units over 100 ky would not be unrealistic (see section 9.4).

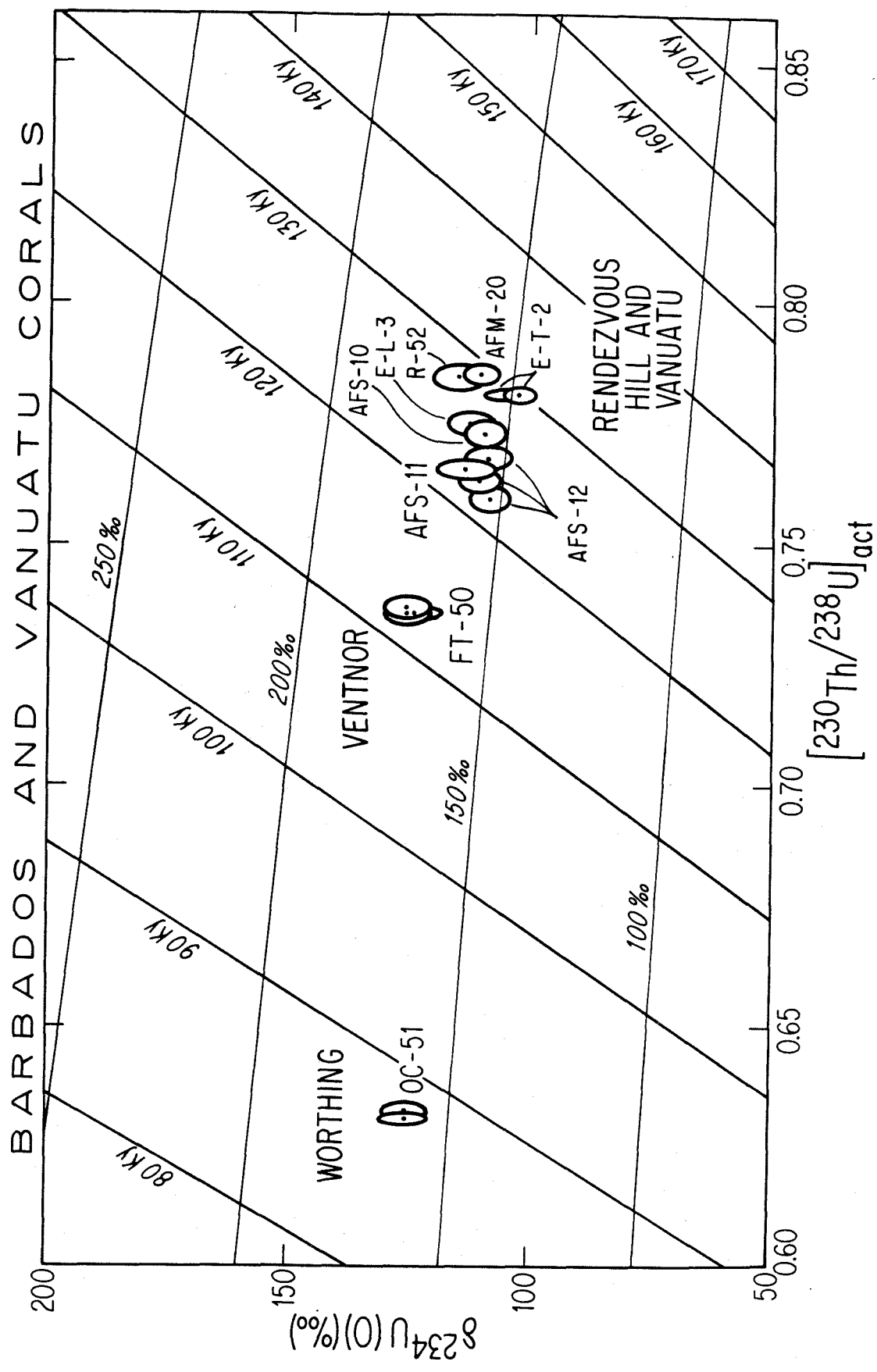
BARBADOS AND VANUATU CORALS
80 KY
90 KY
100 KY
110 KY
120 KY
130 KY
140 KY
150 KY
160 KY
170 KY
250‰
200‰
150‰
100‰
WORTHING
OC-51
VENTNOR
FT-50
AFS-11
AFS-10
E-L-3
R-52
AFM-20
E-T-2
AFS-12
RENDEZVOUS HILL AND VANUATU
200
150
100
50
0.60
0.65
0.70
0.75
0.80
0.85
δ234U (0) (‰)
[230Th/238U]act

results, it appears that $^{232}Th/^{238}U$ ratios in corals are about the same as open ocean surface water, suggesting that these elements do not substantially fractionate during coral growth. Substantial shifts in this ratio can therefore be used to indicate thorium addition to diagenesis (see Bender et al., 1979), metabolic effects, or growth from water with different $^{232}Th/^{238}U$ than open ocean water.

The measurements of $\delta^{234}U(0)$ in standards (Table 7.1), seawater (see Table 8.1), and corals (Table A2) demonstrate that this quantity can be measured to ± 3 to ± 5 ‰ at the 2 sigma level of uncertainty. This precision is 5 to 10 times higher than that obtained by alpha-counting. The precision in the $^{230}Th/^{238}U$ measurement is about 20 times higher than that obtainable by alpha-counting. This results in a subtantial reduction in the error in age calculated using equation 5.11 as discussed in the previous section (Table 7.3). This reduction in error can be seen in figure 7.15. The error ellipses shown here have areas that are almost 100 times smaller than an error ellipse for a typical alpha-counting measurement. The reduction in the area of the error ellipse reduces the error in age as can be seen from the time contours. Furthermore, the reduction in ellipse area results in a reduction of the error in initial $\delta^{234}U$ as can be seen by the relationship between ellipse area and the contours of equal initial $\delta^{234}U$. If the isotopic composition of uranium in seawater has remained constant with time, then the ability to determine $\delta^{234}U(T)$ precisely may allow us to recognize subtle degrees of diagenesis. Values of $\delta^{234}U(T)$ may also indicate whether corals grew in isolated bodies of water not directly connected to the sea.

8. Initial conditions

8.1 ^{238}U and ^{234}U in seawater

One would like to determine $\delta^{234}U$ values in modern corals for comparison with $\delta^{234}U(T)$ values of fossil corals. Differences would indicate that $\delta^{234}U$ of seawater has changed with time, the fossil coral has been altered, or the fossil coral did not grow in normal seawater. A pertinent question is whether or not there is a geographic variation in $\delta^{234}U$ in modern corals. One could answer this by analyzing uranium in many modern corals, and to some extent this approach has been followed. An indirect but more fundamental approach would be to develop some understanding of the uranium cycle in the ocean. Such an understanding might allow one to predict the range of variability of $\delta^{234}U$ in the ocean and might allow one to estimate $\delta^{234}U$ changes in seawater with time. Toward this goal, $^{234}U/^{238}U$ ratios and ^{238}U abundances were determined in water column profiles from both the Atlantic and Pacific Oceans (section 6.8) using the techniques described in chapter 7.

Seawater $^{234}U/^{238}U$ data for a vertical profile in the Atlantic and a vertical profile in the Pacific are presented in Table 8.1. The 2 sigma error for each measurement ranges from $\pm 3^{o}/oo$ to $\pm 7^{o}/oo$. The measured $\delta^{234}U$ values range from 140 to 150. The mean $\delta^{234}U$ for all the measurements is $144 \pm 2^{o}/oo$ where the error is 2 sigma of the mean of all the data. None of the individual measurements differs significantly from this value. The mean values for the Atlantic (143 ± 3) and Pacific (144 ± 4) are identical within error.

The uranium concentration data for Atlantic and Pacific seawater

Table 8.1. U isotope ratios in seawater.[a]

Location	Depth	$^{234}U/^{238}U(\times 10^5)$	$\delta^{234}U$
Pacific	Raft	6.239±0.026	140±5
(14°41'N, 160°01'W)	30	6.292±0.026	150±5
	2000	6.245±0.021	141±4
	4900	6.262±0.032	144±6
Atlantic	10	6.263±0.039	145±7
(7°44'N, 40°43'W)	690	6.240±0.036	140±7
	1640	6.250±0.042	142±8
	2910	6.250±0.037	142±7
	4280	6.283±0.046	148±8
	average =	6.258±0.012	144±2

[a] All errors are $2\sigma_{mean}$; Atlantic analyses are by J. H. Chen.

are presented in Table 8.2. Duplicate analyses were done on several samples and show excellent agreement except in one case (3200 m, Pacific) for which the concentrations are different by about 6°/oo (slightly outside of the ±2°/oo error for each individual measurement). The observed uranium content shows a range of 5.1% (3.156 to 3.317 ng/g) or a range of 3.8% (3.162 to 3.281 ng/g) when normalized to 35°/oo salinity (Table 8.2). The salinity normalized range for the Atlantic samples (3.162 to 3.256 ng/g) overlaps the range for the Pacific samples (3.244 to 3.281 ng/g) but the Pacific samples appear to have slightly higher (by about 1%) uranium concentrations. In the Atlantic, the uranium concentrations at 8°N appear to be about 1% higher than those at 32°N. A small fraction of uranium must reside in particulates. The concentration of particulates in seawater varies but is generally $<10^{-8}$ g/g (Biscaye and Ettriem, 1977) and the concentration of uranium in particulates has been reported as 10^{-6} g/g (Anderson, 1982); therefore, one gram of seawater contains only about 10^{-5} ng of uranium in particulate form. It appears that the observed variation in uranium content cannot be due to variations in particulate uranium. Although the samples have been acidified, the possibility cannot be ruled out that small but measurable amounts of uranium have been lost to the walls of the bottle. Ku et al. (1977) have shown that this was not a problem at the ± 3% level, but this possibility needs to be reevaluated for the higher precision measurements.

In order to provide a framework within which to view the uranium abundance and isotopic data, consider a simple one-dimensional, two box model consisting of a deep water mass (D) and a surface layer (S). The

Table 8.2. U concentrations in seawater.

Location	Depth[a] (m)	Salinity[b]	U (ng/g)[c,e] M	U (ng/g)[c,e] N	$^{238}U/^{235}U$[d,e]
Pacific	10	35.275	3.296±7	3.270	138.61±0.66
(31°4'N,	450	34.140	3.171±8	3.251	138.43±0.91
159°1'W)	900	34.233	3.174±7	3.245	137.86±0.57
	1800A	34.588	3.232±6	3.270	137.93±0.41
	B		3.242±4	3.281	138.06±0.79
	3200A	34.689	3.214±6	3.243	138.29±0.54
	B		3.235±4	3.264	138.11±0.59
	4200	34.687	3.231±5	3.261	137.95±0.57
	5710A	34.695	3.236±7	3.264	137.72±0.67
	B		3.240±6	3.268	137.84±0.80
	5740	34.695	3.230±7	3.258	138.04±0.48
Atlantic[f]	10A	36.080	3.317±7	3.218	137.86±0.40
(7°44'N,	B		3.315±8	3.216	137.84±0.30
40°43'W)	690	34.611	3.207±6	3.243	137.95±0.30
	1640	34.981	3.229±7	3.231	137.78±0.35
	2910	34.938	3.208±6	3.214	137.95±0.26
	4280	34.811	3.238±6	3.256	137.78±0.35
Atlantic	1600	35.035	3.210±6	3.207	137.48±1.24
(31°49'N,	3400A	34.930	3.156±3	3.162	137.31±0.88
64°6'W)	B		3.166±10	3.172	137.78±0.84
	4550	34.897	3.198±9	3.207	137.17±1.10
			average =	3.238 ng/g	137.89±0.15

[a] A and B indicate duplicate analyses.

[b] From PACYDORF (Scripps Institution of Oceanography) and shipboard salinometer measurements by D. J. Piepgras and P. M. Williams.

[c] M = Measured, N = Normalized to 35°/₀₀ salinity.

[d] The $^{238}U/^{235}U$ ratio for natural U is 137.88.

[e] All errors are $2\sigma_{mean}$.

[f] 7°44'N, 40°43'W analyses by J. H. Chen.

model is based on the assumptions that: (1) the system is at steady state; (2) all uranium is injected into surface water and all uranium is removed from deep water; (3) the mean life of ^{238}U with respect to radioactive decay is much longer than water mixing times; (4) the uranium removed from deep water has the isotopic composition of deep water; and (5) ^{238}U and ^{234}U are transported by mixing of water between the deep layer and the surface layer. The model can be easily generalized to include scavenging of uranium from surface water and addition of uranium from sediment pore fluids, but, for simplicity, these terms have not been included. The variables are defined as follows: τ_{234} and τ_{238} are the mean lives of ^{234}U and ^{238}U with respect to radioactive decay; τ_S and τ_D are the mean lives of water in the surface and deep reservoirs; τ_U is the mean life of uranium relative to removal from the deep reservoir (N^D_{238}/rate of removal of ^{238}U atoms from deep water); N^S_{238}, N^D_{238}, N^S_{234}, and N^D_{234} are the number of atoms of ^{238}U and ^{234}U in the surface and deep reservoirs; C^S_{238} and C^D_{238} are the ^{238}U concentrations; W_D and W_S are the masses of water in the two reservoirs; and $C^S_{238}=N^S_{238}/W_S$ and $C^D_{238}=N^D_{238}/W_D$. At steady state, the number of ^{234}U atoms in the deep reservoir is constant with time yielding:

$$dN^D_{234}/dT=0=-N^D_{234}/\tau_{234}+N^D_{238}/\tau_{238}-N^D_{234}/\tau_D+N^S_{234}/\tau_S-N^D_{234}/\tau_U, \quad (8.1)$$

where the first two terms account for radioactive decay and production of ^{234}U, the next two terms account for ^{234}U transport to and from the surface reservoir, and the last term is the rate of removal of ^{234}U

from deep water. Similarly for ^{238}U in deep water:

$$dN^D_{238}/dT=0=-N^D_{238}/\tau_{238}+N^S_{238}/\tau_S-N^D_{238}/\tau_D-N^D_{238}/\tau_U, \qquad (8.2)$$

where the radioactive decay term is assumed to be negligable (assumption 3), there is no radioactive production term, and the other terms are analogous to terms in equation 8.1. The mass of water in the deep reservoir is constant with time yielding:

$$dW_D/dT=0=W_S/\tau_S-W_D/\tau_D. \qquad (8.3)$$

Combining equations 8.1 and 8.2 and using the equation defining $\delta^{234}U$ (equation 5.13) yields:

$$\delta^{234}U_S/\delta^{234}U_D=(\tau_S N^D_{238}/\tau_{234}N^S_{238})+1. \qquad (8.4)$$

Combining equations 8.3 and 8.4 yields:

$$\delta^{234}U_S/\delta^{234}U_D=(\tau_D/\tau_{234})(C^D_{238}/C^S_{238})+1, \qquad (8.5)$$

which relates the ratio of $\delta^{234}U$ in the two reservoirs to the mean life of water in the deep layer. Combining equations 8.2 and 8.3 gives:

$$(C^S_{238}-C^D_{238})/C^D_{238}=\tau_D/\tau_U, \qquad (8.6)$$

which relates the difference in ^{238}U concentration in surface and deep

water to the mean life of uranium relative to removal from deep water. Equations 8.5 and 8.6 predict that both $\delta^{234}U$ values and uranium concentrations in seawater should be extremely constant. For $C^S_{238} \sim C^D_{238}$ (see Table 8.2), $\tau_D = 10^3$ years (from ^{14}C, see Arnold and Anderson, 1957; Craig, 1957; Revelle and Suess, 1957; Broecker and Li, 1970), and $\delta^{234}U_D = 144$ (Table 8.1), equation 8.5 gives an essentially identical value for $\delta^{234}U_S$ (=144.4). Using equation 8.6 and taking $\tau_D = 10^3$ years and $\tau_U = 3 \times 10^5$ years (Ku et al., 1977), the predicted surface water concentration is only 3‰ higher than the deep water concentration.

The data indicate that $^{234}U/^{238}U$ in the open ocean is constant to ±5‰. The observed constancy in $\delta^{234}U$ is consistent with the small range of $\delta^{234}U$ predicted by equation 8.5 and therefore consistent with the value of τ_D determined from ^{14}C.

The most striking feature of the observed salinity normalized uranium concentrations is the rather narrow range of values (Table 8.2), in rough agreement with the model prediction. The salinity normalized data show a spread of 3.8%. The oceanic profiles have ranges of 1.2% (Pacific), 1.4% (32°N, Atlantic), and 1.3% (8°N, Atlantic). The total range is about an order of magnitude larger than the range predicted by the model. It can be shown that, even if a scavenging term is added to the model and the maximum value for the observed flux of uranium from the surface is used (3.4 $\mu g/cm^2/10^3$ years; Anderson, 1982), the predicted $(C^S_{238} - C^D_{238})/C^D_{238}$ does not change substantially. This suggests that if uranium loss to the walls of the bottles is not a problem, either present estimates of the residence

time of uranium in the oceans are too large and/or uranium is redistributed within the ocean at higher rates than have previously been documented.

Despite some discrepancy, both the seawater data and the simple model indicate that ^{238}U abundance in open ocean water is rather constant and that $\delta^{234}U$ is constant within analytical error. One would therefore expect that if local effects are not important, all modern corals would have $\delta^{234}U$ values that are identical to the seawater value (140-150). If all corals fractionate uranium from calcium in a similar fashion, then modern corals should also have similar ^{238}U abundances.

8.2 ^{238}U and ^{234}U in modern corals

The results of measurements of $\delta^{234}U$ values and ^{238}U abundances in corals that grew in the last few centuries in Vanuatu are shown in Tables A1(I) and A2(I) and figure 8.1. The measured $\delta^{234}U$ values range from 144 to 153 with 2 sigma errors of ± 3 to ± 6 δ-units for each analysis. The ^{238}U abundances range from 9.13 to 11.30 nmol/g with 2 sigma errors of ±1 to ±4 $^{o}/_{oo}$ for each analysis. The variation in ^{238}U is clearly larger than analytical error and has a range of about 20%.

Because the corals are very young, the $\delta^{234}U(T)$ values are essentially identical to the $\delta^{234}U(0)$ values. This can be seen in figure 8.1 which shows the analyses plotted in a $\delta^{234}U(0)$ versus $[^{230}Th/^{238}U]_{act}$ plot. The lines of equal initial $\delta^{234}U$ are essentially horizontal over the range of $[^{230}Th/^{238}U]_{act}$ for these samples. For each analysis, the error ellipse overlaps the range that was established for modern seawater in the previous section. The initial

Figure 8.1. Plot of $\delta^{234}U(0)$ versus $[^{230}Th/^{238}U]_{act}$ for analyses of eighteenth, ninteenth and twentieth century corals from Santo, Malekula, and Tangoa Islands in Vanuatu. Note the extremely low values of $[^{230}Th/^{238}U]_{act}$ on the x-axis. The error elipses represent 2 sigma errors. The error in age ranges from ±3 to ±5 years. All of the samples have $\delta^{234}U(T)$ values that are identical, within error, to the present seawater value as indicated by the intersection of each of the ellipses with the stippled band. CWS-C and CWS-D, which were hypothesized to have been killed by the same co-seismic uplift event on northwest Santo Island, have ages identical within error. MAF and MAG, which were hypothesized to have been killed by a different co-seismic uplift event on north Malekula Island, have ages that are similar but analytically distinguishable. The slight difference in age may be due to erosion of the outer, younger part of the MAG coral head.

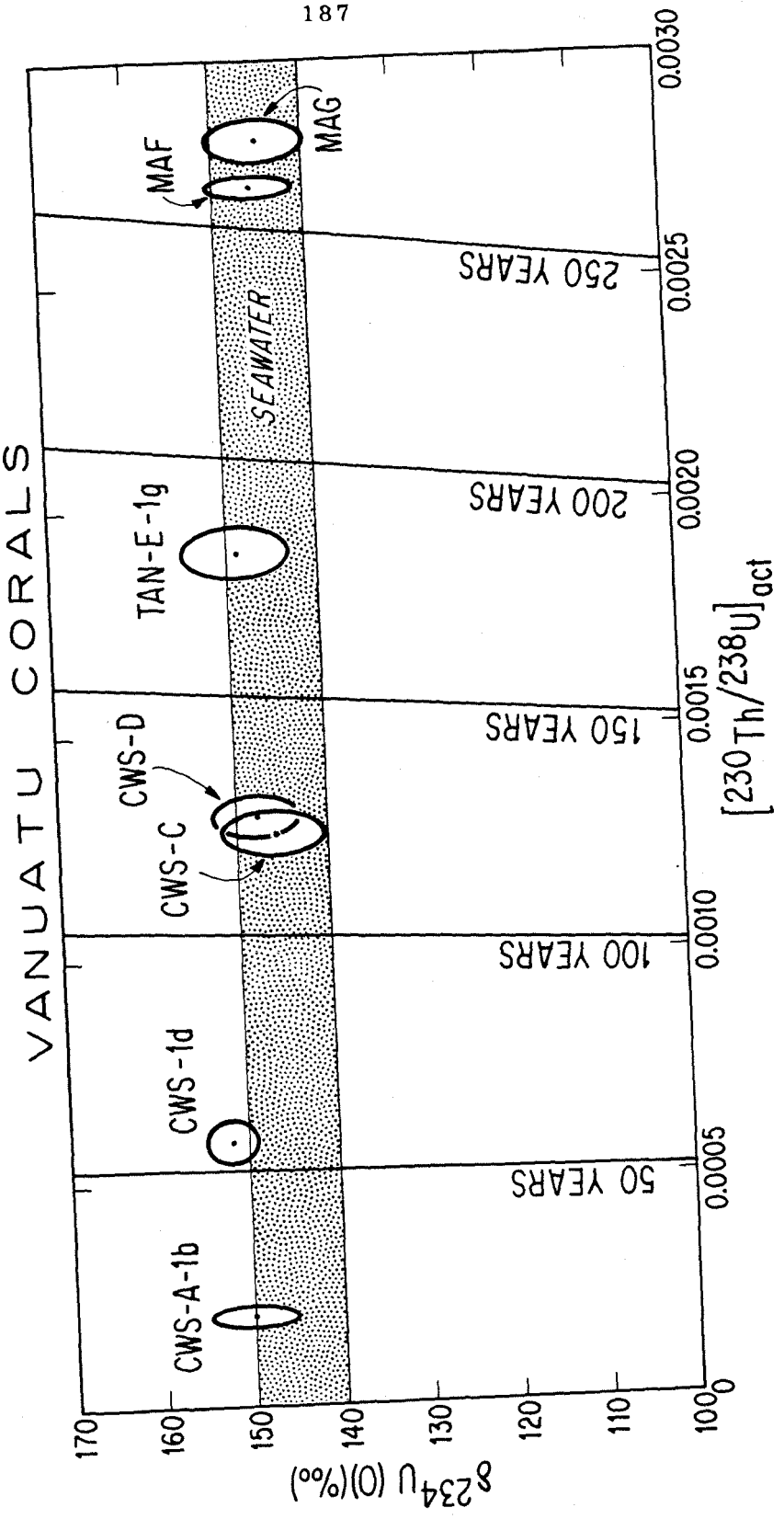
VANUATU CORALS
SEAWATER
MAF
MAG
TAN-E-1g
CWS-D
CWS-C
CWS-1d
CWS-A-1b
250 YEARS
200 YEARS
150 YEARS
100 YEARS
50 YEARS
0.0030
0.0025
0.0020
0.0015
0.0010
0.0005
0
[230Th/238U]act
δ234U (0)(‰)
170
160
150
140
130
120
110
100

$\delta^{234}U$ values for this set of corals are, within analytical error, identical to each other and identical to the $\delta^{234}U$ value of seawater. Therefore, one has some basis for believing that aside from local effects, corals that grew at the same time in the past should have had identical $\delta^{234}U(T)$ values. If the seawater value has not changed with time then the initial value must be between 140 and 150.

8.3 Initial ^{230}Th abundance in corals

A critical issue is the amount of ^{230}Th initially incorporated in a coral skeleton during growth. In solving equation 5.11, it is assumed that initial ^{230}Th is zero. If appreciable amounts of ^{230}Th are incorporated during skeletal growth, this would result in calculation of ages that are greater than the true age. Limits on initial ^{230}Th can be established (1) by direct measurement of very young skeletal material or (2) by measuring $^{230}Th/^{232}Th$ in seawater, the ^{232}Th abundance in corals, and taking the product of these quantities.

^{232}Th abundances for the Vanuatu corals that grew in the last few centuries are presented in Table A1(I). They range from 0.032 to 0.340 pmol/g. These values are extremely low. Because of the extremely low values and the long mean life of ^{232}Th, alpha-counting studies have often not reported ^{232}Th concentrations. Examination of reported concentrations (see Thurber et al., 1965; Veeh, 1966; Ku, 1968; Marshall and Thom, 1976; Harmon et al., 1983; Dodge et al., 1983; Somayajulu et al., 1985) shows that the detection limit in the alpha-counting studies is about 100 pmol/g and that values as high as 10^4

pmol/g have been measured. The lowest previous values are more than two orders of magnitude higher than the mass spectrometrically determined values. As discussed in section 7.2, the low ^{232}Th abundances obviate a number of analytical problems associated with the measurement of ^{230}Th.

Measurements of ^{232}Th abundances determined by isotope dilution mass spectrometry (by J.H. Chen) in water samples from various depths at 8°N 41°W in the Atlantic Ocean are shown in Table 8.3. The ^{232}Th abundances range from 0.40 to 0.62 fmol/g. Nozaki et al. (1981) have reported ^{230}Th abundances in open ocean surface water of 4×10^{-6} to 1×10^{-5} fmol/g. Taking the average of the highest and lowest value in each range: $(^{230}Th/^{232}Th)_{seawater} \times {}^{232}Th_{coral} = 0.003$ fmol/g of initial ^{230}Th. Dividing by the average ^{238}U abundance in Table A1(I) (10.34 nmol/g) gives an initial $^{230}Th/^{238}U$ atomic ratio of 3×10^{-10}. Plugging this ratio into equation 5.11 and taking $\delta^{234}U(0)$ to be 150, yields an "initial age" of one and a half years. This is small compared to analytical error, as even the most precise ^{230}Th ages in Table A2 have 2 sigma errors of ±3 years.

The initial ^{230}Th abundance can also be measured directly if the age of the sample is known independently. Samples CWS-A-1b, CWS-A-1d, and TAN-E-1g were collected live and the range of ages of the portion of the sample that was analyzed are known from growth band dating (F.W. Taylor, personal communication). For CWS-A-1b, the portion of the skeleton from which fragments were chosen for analysis is labelled "A" and "B" in figure 4.9. Most of this portion of the skeleton grew in the years 1971, 1972, and 1973. CWS-A-1d grew in the years 1935, 1936,

Table 8.3. Th concentrations in seawater.[a]

Location	Depth[b]	Wt(g)	^{232}Th	
			Total(pg)[c]	Conc.(pg/g)[d]
Atlantic (7°44'N, 40°43'W)	10	258	33.5	0.118±0.008
	690	509	77	0.145±0.004
	1640	251	26.1	0.092±0.008
	2910A	958	112	0.114±0.002
	B	987	143	0.142±0.002
	C	518	67.1	0.124±0.004
	4280A	969	109	0.110±0.002
	B	983	113	0.112±0.002

[a] Analyses by J. H. Chen.

[b] A, B and C indicate replicate analyses.

[c] pg = 10^{-12} gram; total Th = dissolved + particulate + analytical blank.

[d] Subtracting 3 ± 2 pg Th blank.

and 1937. TAN-E-1g grew in the years 1804 to 1810. ^{230}Th ages and growth dates for these samples are shown in figure 8.1 and Tables 9.1 and A2(I). The ^{230}Th growth date for CWS-A-1b is A.D. 1969 ± 3, A.D. 1932 ± 5 for CWS-A-1d, and A.D. 1806 ± 5 for TAN-E-1g.

Figure 8.2 shows ^{230}Th age plotted versus growth band age for these three samples. Each sample is represented by a box. The height of the box represents the 2 sigma error in ^{230}Th age; the width of the box represents the range of ages (as determined by growth band dating) for the portion of the sample that was analyzed. For this plot, the ages are calculated relative to July, 1987. If the ^{230}Th age is the same as the growth band age, then the samples should plot on the line labelled 45°. If significant ^{230}Th was incorporated into the skeletons during growth, then the samples would plot above the 45° line. Within error, all three samples plot on the 45° line, indicating that the ^{230}Th ages are indistinguishable from the growth band ages.

An upper limit can be placed on the amount of initial ^{230}Th incorporated in a coral skeleton using any of the three points in figure 8.2. Because the absolute analytical error is smallest for sample CWS-A-1b, this sample places the tightest constraints on initial ^{230}Th abundance. The ^{230}Th age of this sample is 3 years older than the mean growth band age; the 2 sigma error for the ^{230}Th age is ±3 years. Therefore, the maximum amount of initial ^{230}Th that could have been incorporated during growth is equivalent to the amount of ^{230}Th produced by radioactive decay in 6 years. This upper limit agrees with the value calculated using the thorium isotopic composition of seawater. These lines of reasoning indicate that, within present

Figure 8.2. Plot of ^{230}Th age versus age determined by counting of coral growth bands for three samples from Santo and Tangoa Islands, Vanuatu. Boxes indicate the error limits of the age determinations. The error in ^{230}Th age is 2 sigma and is based on analytical errors. The error in the growth band age is the range of ages in the portion of the sample that was analyzed. All of the boxes intersect the 45° line, indicating that the ^{230}Th ages are identical to the growth band ages within error. The error in the ^{230}Th age of CWS-A is ±3 years and the mean value of the ^{230}Th age is 3 years older than the mean growth band age. This places an upper limit on the amount of initial ^{230}Th that could have been incorporated into the coral during growth. The upper limit (6 X 10^6 atoms of ^{230}Th/g coral) is an amount equivalent to the amount of ^{230}Th produced by radioactive decay in 6 years.

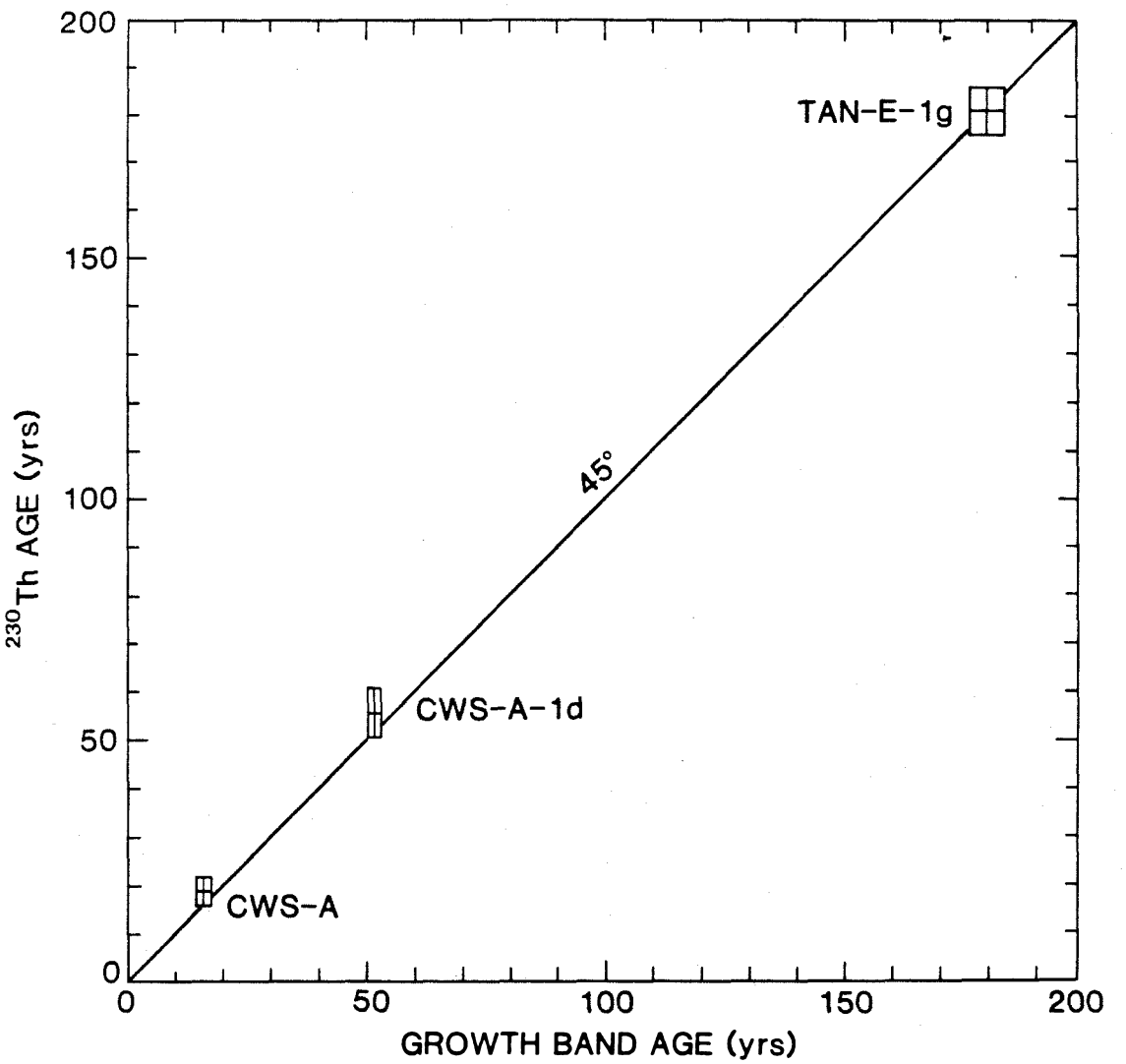
200
150
100
50
0
0
50
100
150
200
^{230}Th AGE (yrs)
GROWTH BAND AGE (yrs)
45°
TAN-E-1g
CWS-A-1d
CWS-A

analytical errors, the assumption that the initial $^{230}Th/^{238}U$ ratio in corals is zero is valid.

8.4 ^{238}U and ^{232}Th abundances in a mollusk

The ^{238}U and ^{232}Th abundances of K-133, the giant clam shell, are presented in Table A1(VII). The ^{232}Th concentration is 0.249 pmol/g which is similar to the value for corals. However, the ^{238}U concentration is 3.08×10^{-4} nmol/g. This is about 10^2 times lower than the lowest previously reported values for a mollusk (Broecker, 1963) and 4×10^4 times (figure 8.3) lower than the coral uranium content. The extremely large difference between giant clam and coral uranium contents indicates that these organisms have different mechanisms (or microenvironments) for incorporating uranium into their skeletons. Because of the low ^{238}U content, ^{230}Th dating of such a material would require a large sample. As giant clams have a mass of about 50 kg, large samples can be found. With the use of mass spectrometric techniques, such an analysis would, in principle, be possible. At secular equilibrium, 200 g of sample would contain 6×10^8 atoms of ^{230}Th. With present analytical capabilities, this number of ^{230}Th atoms could be measured to an accuracy of ±3% (2 sigma; see Table A1). Although dating of such a sample is now technically feasible, it is clear from previous work (Broecker, 1963; Kaufman et al., 1971) that uranium in fossil mollusks is dominantly of diagenetic origin and that the process of uranium uptake must be understood before any serious attempt to date fossil mollusks can be made.

Figure 8.3. Histogram of the U/Ca ratio in corals and a modern giant clam. The horizontal axis has a log scale. Corals do not appreciably fractionate uranium from calcium during skeletal growth. The giant clam has a U/Ca ratio, which is almost 5 orders of magnitude lower than corals, indicating that these organisms have different mechanisms (or microenvironments) for incorporating uranium into their skeletons. Even with these extremely low uranium concentrations, dating giant clam shells would be possible using mass spectrometric techniques and several hundred grams of sample, but only if fossil clams that have not incorporated uranium into their shells during diagenesis can be found.

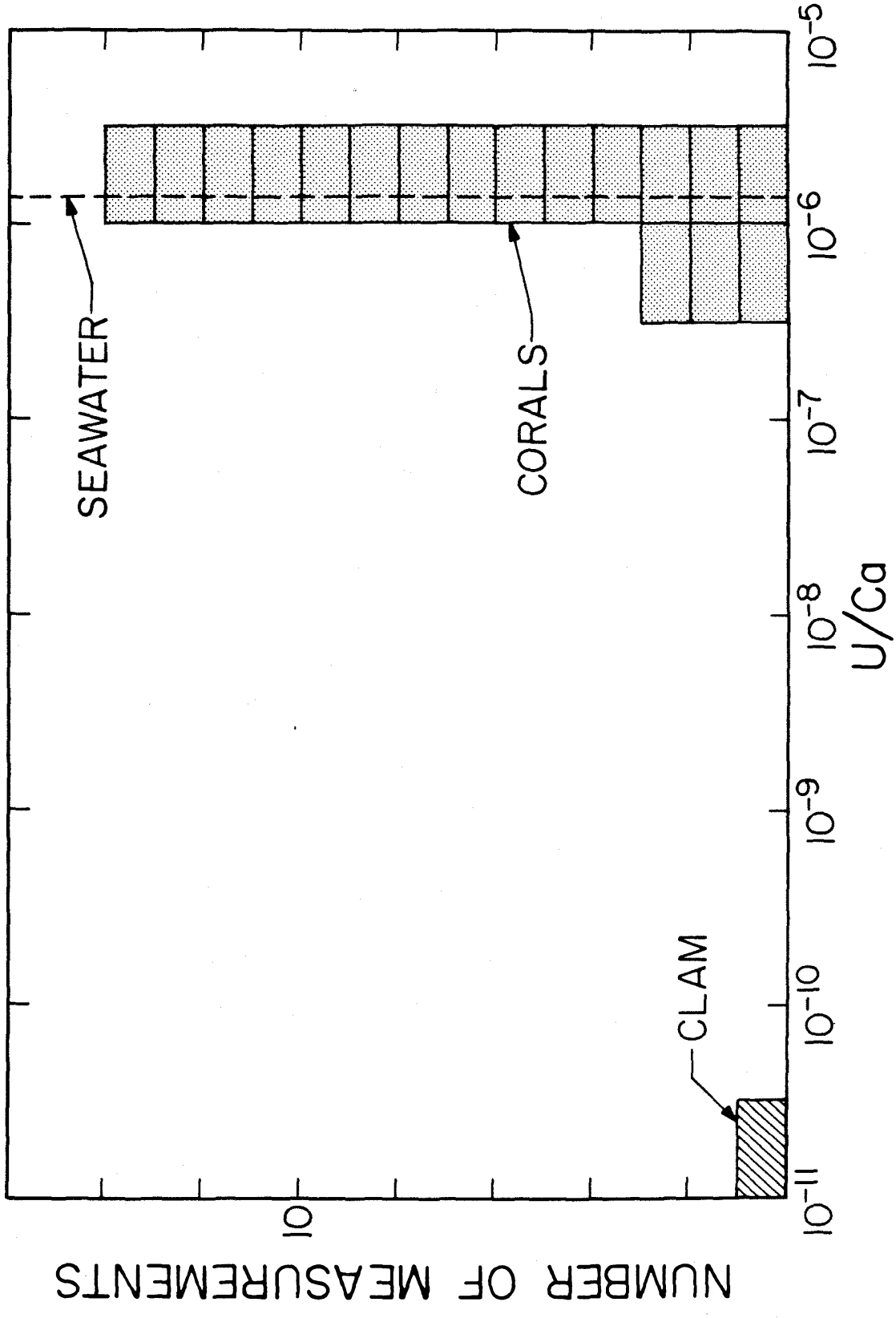
SEAWATER
CORALS
CLAM
U/Ca
10^{-5}
10^{-6}
10^{-7}
10^{-8}
10^{-9}
10^{-10}
10^{-11}
10
NUMBER OF MEASUREMENTS

9. Tests of the closed system assumption

9.1 Comparison of ^{230}Th ages with ages determined by other methods.

A critical assumption used in deriving equation 5.11, which must be tested is the assumption that one can choose fossil corals that have remained closed to diagenetic alteration. One way to test this assumption is to analyze the same sample using different dating schemes and compare the results. Some of the samples that were analyzed had also been dated by the ^{14}C method and by growth band dating. The results of these age determinations are shown in Table 9.1. The data on which the ^{230}Th ages are based are presented in Table A2. The ^{230}Th ages and growth band ages of CWS-A-1b, CWS-A-1d, and TAN-E-1g were discussed in section 8.3. TAN-E-1g has also been dated by the ^{14}C method as have CWS-F-1 and CH-8. The ^{14}C ages have been reported in conventional radiocarbon years (Taylor et al., 1985b; Taylor, personal communication) and as corrected ages (Table 9.1). For TAN-E-1g and CWS-F-1, the corrected ages were determined from the conventional ages with the use of the calibration curve of Stuiver (1982). For CH-8, the corrected age has been given as an approximation, since the precise value of the ratio of ^{14}C to C in the atmosphere at this time is not now known. The corrected ^{14}C ages do not include adjustments for the natural fractionation of carbon isotopes or for the difference between ^{14}C in the atmosphere and surface waters. For TAN-E-1g, the corrected age is given by three time intervals since the conventional radiocarbon age intersects the calibration curve three times.

For TAN-E-1g, the corrected radiocarbon age is between 30 and 70 years, 180 and 270 years, or 300 to 500 years; the ^{230}Th age is 180±5

Table 9.1. Coral ages in years using different methods.[a]

Sample	^{14}C[b] (conventional)	^{14}C[c] (corrected)	Growth band Counting	^{230}Th age (this study)
CWS-A-1b	-	-	15-17 (1)	19 ± 3
CWS-A-1d	-	-	51-53 (1)	56 ± 5
TAN-E-1g	270 ± 120 (1)	30-70, 180-270, or 300-500	176-182 (1)	180 ± 5
CWS-F-1	980 ± 120 (1)	780-1010	-	845 ± 8
CH-8	8990 ± 120 (2)	~ 10,000	-	8294 ± 44

[a] All errors are 2σ. Ages refer to the ages at the time of analysis (A.D. 1986 and 1987). Numbers in parentheses refer to the following sources: (1) F. W. Taylor (written comm.), (2) Taylor et al. (1985).

[b] ^{14}C ages are as reported by the sources in radiocarbon years using the 8033 year mean life; no corrections have been made for natural fractionation of carbon isotopes, the difference between $^{14}C/C$ in surface water and the atmosphere, or differences in initial $^{14}C/C$.

[c] ^{14}C ages have been corrected by us to dendroyears using the curves of Stuiver (1982) for TAN-E-1g and CWS-F-1 and assuming a $^{14}C/C$ initial ratio from Klein et al. (1982) for tree rings ~ 8,000 years old. No corrections have been made for natural fractionation of carbon isotopes or the difference between $^{14}C/C$ in the surface water and the atmosphere.

years. For CWS-F-1, the corrected radiocarbon age is between 780 and 1010 years; the ^{230}Th age is 845±8 years. For CH-8, the corrected radiocarbon age is about 10000 years; the ^{230}Th age is 8294±44 years.

For TAN-E-1g and CWS-F-1, the ^{230}Th and ^{14}C ages agree within analytical error. The error for the radiocarbon ages is, however, much larger than the error for the ^{230}Th ages. For CH-8, There is a substantial difference between the ^{230}Th age and the corrected ^{14}C age. It will be shown in section 10.1 that the simplest interpretation of the uranium isotopic data for CH-8 is that this coral grew in water that was different from normal seawater. It is therefore possible that the water from which CH-8 grew had a $^{14}C/C$ ratio that was lower than the ^{14}C ratio in the atmosphere at that time and that the age discrepancy is due to this difference. Nevertheless, the reality of this discrepancy demands a more serious comparison of both methods.

The general agreement between radiocarbon ages and ^{230}Th ages suggests that, within the limits of the errors of the measurements, diagenetic shifts did not occur in these samples. Because the errors in growth band ages are much smaller than the ^{14}C ages, these ages place much tighter constraints on possible diagenetic shifts but over a rather limited time scale (the last 200 years). The agreement between the growth band ages and ^{230}Th ages for CWS-A-1b, CWS-A-1d, and TAN-E1g (figure 8.2) indicates that if shifts in the ^{230}Th age due to diagenetic processes had occurred, the shifts were less than the analytical error of ±3 to 5 years.

9.2 ^{230}Th ages of different fragments of the same coral

Beyond the range of growth band dating and beyond the range of ^{14}C dating, there are no obvious chronometers that one could use to check for diagenetic alteration of the ^{238}U-^{234}U-^{230}Th system. Because individual coral colonies grow over periods of time that are small compared to the analytical error in the ^{230}Th age of a 100 ky old coral, one would expect that if diagenetic alteration had not occurred, different fragments of such a coral would yield identical ^{230}Th ages. Based on the conclusions of section 8.2, one would also expect such fragments to have the same initial $\delta^{234}U$ values. If they have not been altered and they have identical ages, they must also have analytically indistinguishable $\delta^{234}U(0)$ values (equation 5.12). If the age and $\delta^{234}U(0)$ of such materials are the same and the sample has not been altered, the $[^{230}Th/^{238}U]_{act}$ ratios must also be the same (equation 5.11).

Analyses of different fragments of the same coral were performed on a number of corals (Tables A1 and A2; figure 7.15; analyses OC-51 A and B; FT-50 A and C; AFS-12 A,B, and C; E-T-2 A and B). As opposed to the samples discussed in section 9.4 where fragments that showed signs of secondary alteration were deliberately chosen for analysis, all of the samples listed above were examined under a binocular microscope and were chosen because they appeared to be primary, based on the criteria discussed in section 6.2. For each of the corals listed above (except for AFS-12), different fragments of the same coral yielded ^{230}Th ages, $\delta^{234}U(0)$ values, and $[^{230}Th/^{238}U]_{act}$ ratios that were analytically indistinguishable (figure 7.15). AFS-12 A, B, and C have, within

error, identical $\delta^{234}U(0)$ values and ^{230}Th ages. The $[^{230}Th/^{238}U]_{act}$ ratio for AFS-12 C is slightly higher than the $[^{230}Th/^{238}U]_{act}$ ratio of AFS-12 A although it is analytically indistinguishable from the ratio for AFS-12 B, and $[^{230}Th/^{238}U]_{act}$ for AFS-12 A is indistinguishable from the ratio for AFS-12 B (figure 7.15). Because the ^{230}Th age, $\delta^{234}U(0)$, and $[^{230}Th/^{238}U]_{act}$ ratio of different fragments of the same sample are the same, if any of these samples had been altered, different fragments of the same hand specimen must have been altered exactly the same way.

9.3 The isotopic characteristics of secondary calcite

9.3.1 Approach

The accuracy of the ^{230}Th age of a coral is dependent on the assumption that the uranium and thorium have not been mobilized since the time of coral growth. The most obvious manifestation of alteration is the presense of calcite in the originally aragonitic skeleton. In order to examine the effect of crystallization of secondary calcite on ^{238}U-^{234}U-^{230}Th systematics, I analyzed four pairs of samples of Acropora palmata (PB-2 to PB-9; Tables A1(VI) and A2(VI)) from the same outcrop on northwest Barbados (see section 6.6). The terrace from which these samples were collected was thought to represent a northward extension of the Rendezvous Hill Terrace and had been assigned an age of about 125 ky based on this correlation (Mesollela, 1968). Each pair is from the same coral and therefore the original aragonite in each pair must have formed at the same time (within several decades). One of each pair (samples labelled "A" in Tables A1(VI) and A2(VI)) is

Figure 9.1. Upper photograph: scanning electron photomicrograph of an etched section of a portion of an Acropora palmata skeleton that was collected live. The scale bar is 100 microns.

Lower photograph: scanning electron photomicrograph the same section but at higher magnification. The scale bar is 10 microns. The aragonite fibers making up the skeleton are visible as are the centers of calcification in the upper right portion of the photograph.

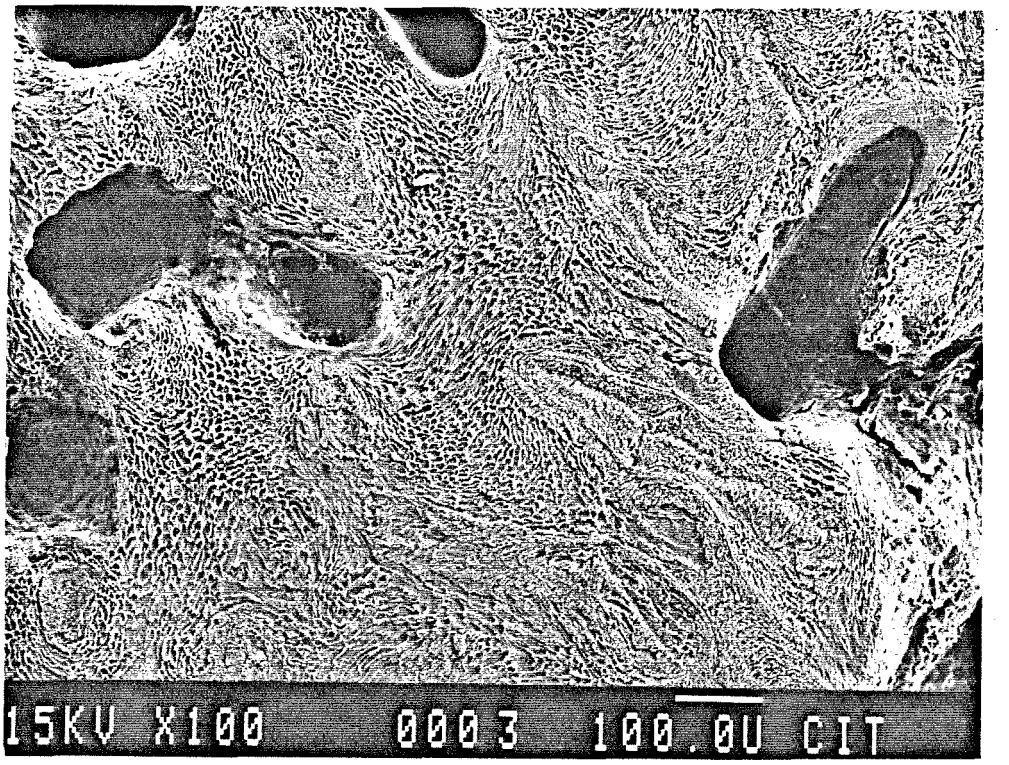
15KV X100 0003 100.0U CIT

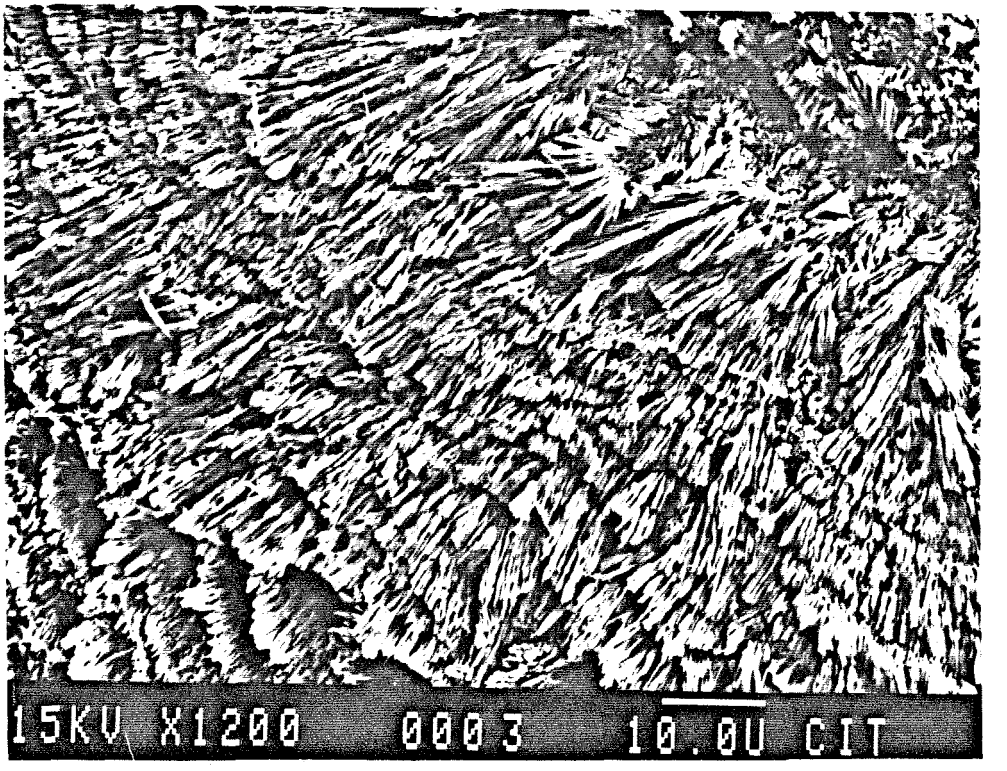
15KV X1200 0003 10.0U CIT

Figure 9.2. Upper photograph: photomicrograph of an etched section of AFS-12, which is a sample of fossil Acropora palmata from the Rendezvous Hill Terrace on Barbados. The scale bar is 10 microns. The fibrous crystals have the same morphology as aragonite fibers that make up the modern Acropora palmata skeleton in figure 9.1.

Lower photograph: photomicrograph of an etched section of PB-5B, which is a sample of fossil Acropora palmata collected from North Point Shelf on Barbados. Some crystals with the morphology of the aragonite crystals that make up the modern skeleton are visible. Also visible is a large secondary calcite crystal (dark area in the upper right portion of the photograph).

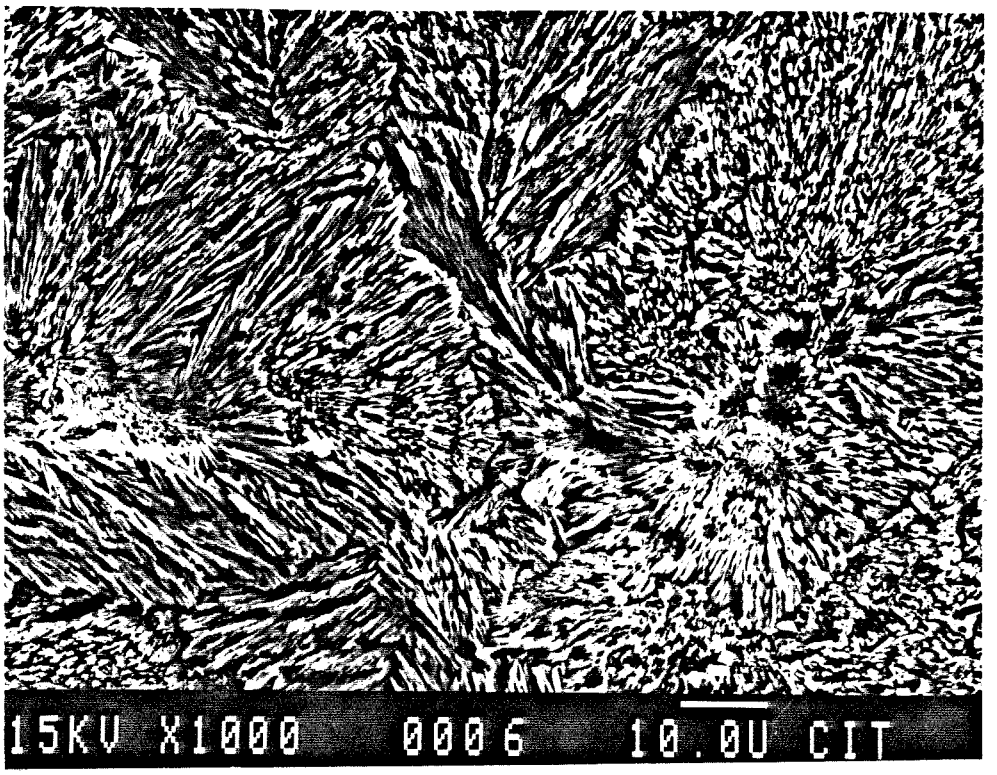
15KV X1000 0006 10.0U CIT

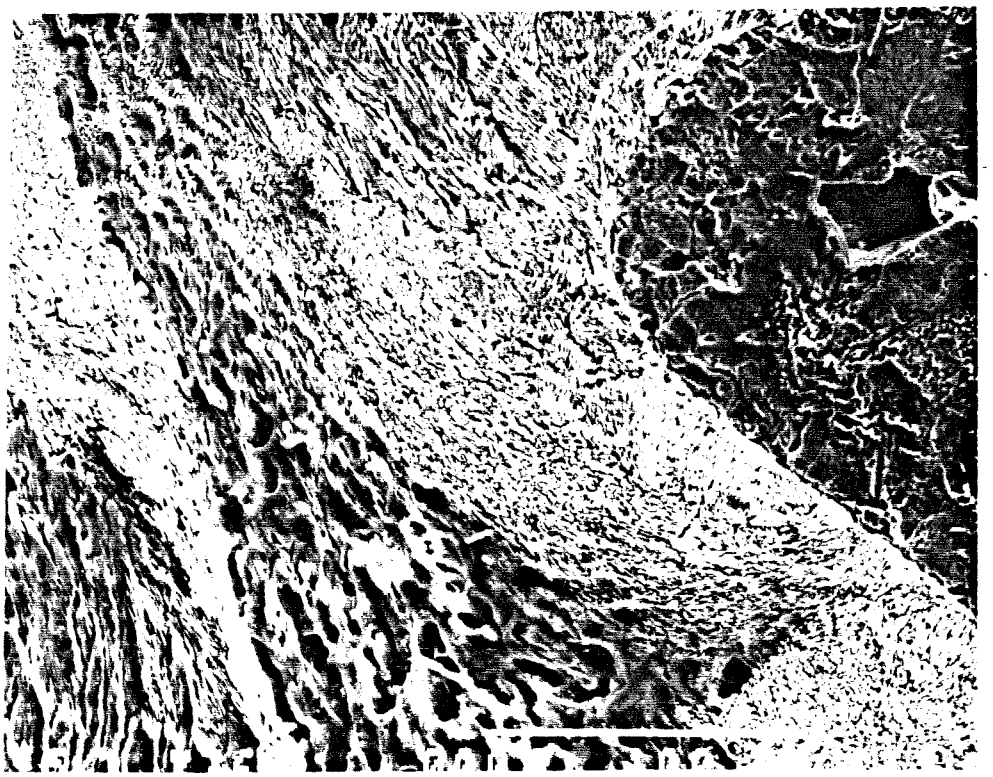

composed dominantly of aragonite crystals that have morphologies similar to crystals deposited by living corals (figures 9.1 and 9.2). The second of each pair (labelled "B" in Tables A1(VI) and A2(VI)) is dominantly calcite.

In addition to analyzing each sample for ^{238}U, ^{234}U, ^{230}Th and ^{232}Th abundances, Mg and Sr abundances were also determined using atomic absorption spectroscopy, and fragments adjacent to each sample were examined using scanning electron microscopy. Shifts in Sr and Mg concentrations away from the values for modern corals have been taken as indicative of the presense of secondary calcite because calcite tends to have much higher Mg and much lower Sr concentrations than coral aragonite (see Bloom et al., 1974).

The calcite-rich and aragonite-rich portions of each coral were identified with the unaided eye using cleavage planes to identify the calcite. Blocks of about 2 g were sawn out of each portion as described in section 6.6. Each block was then sawn in half. One half was dissolved and divided into three aliquots for uranium-thorium, Mg, and Sr analysis. A polished section was made from the other half. The polished sections were etched with dilute formic acid for one and a half minutes in an ultrasonic bath, then examined with a scanning electron microscope.

9.3.2 Sample preparation blank

The saw blades used for cutting the samples were new and used only on this set of samples. The analytical blank for the sawing procedure was checked by analyzing three different fragments of a piece of

Acropora palmata, which had been collected live (Tables A1(VII) and A2(VII)). A modern sample was used because it contains very little ^{230}Th. ^{230}Th added during the sawing procedure would therefore be relatively easy to detect. One of the three samples (M.A. chiseled) was a fragment that was chiseled from the coral with a stainless steel chisel. The second sample (M.A. cut A) was a block which was sawn from the sample in the same fashion as the PB blocks. The third sample (M.A. cut B) was sawn in the same fashion as the PB blocks, then cut several more times so that the surface area of the saw cuts was about ten times the saw cut area of a typical block.

The results of the M.A. analyses are shown in Tables A1(VII) and A2(VII). The uranium isotopic values for the three samples range from 143 to 151 and, considering analytical error, are identical. This indicates that if significant uranium had been added during the sawing process it had to have had the same uranium isotopic composition as the chiseled sample. The ^{238}U abundances range from 13.31 ± 0.02 to 13.62 ± 0.04 nmol/g. The ^{238}U abundances of the sawn samples is actually lower than the chiseled sample, and it is likely that the slight difference in concentration is due to sample heterogeneity. The ^{232}Th abundances range from 0.10 ± 0.01 pmol/g for M.A. chiseled to 0.33 ± 0.01 pmol/g for M.A. cut A. If the coral is homogeneous in ^{232}Th abundance, then as much as 0.35 pmol of ^{232}Th could have been added in the sawing process. The $^{230}Th/^{238}U$ ratios of the three samples are identical within error, indicating that the upper limit on the amount of ^{230}Th added is 4×10^7 atoms and is insignificant. The introduction of small but measurable amounts of ^{232}Th may have occurred during the

sawing process, but measurable shifts in $\delta^{234}U$ and $^{230}Th/^{238}U$ did not occur.

9.3.3 Results

The results of the analyses of the PB pairs are shown in figures 9.3 (Sr and ^{238}U), 9.4 (Mg and ^{238}U), and 9.5 ($\delta^{234}U$ and $^{230}Th/^{238}U$) and Tables A1(VI) and A2(VI). Scanning electron photomicrographs of an etched section of a modern Acropora palmata skeleton are shown in figure 9.1. Photomicrographs of fossil Acropora palmata skeletons are shown in figure 9.2.

The Mg concentrations (figure 9.4) of the calcite-rich samples range from 1500 to 3300 ppm. The Mg concentrations of the aragonite-rich samples are lower and range from 700 to 1400 ppm. These values are similar to values for modern Acropora palmata (1000 to 1100 ppm). For each pair, the Mg concentration of the aragonite-rich sample is lower than the value for the calcite-rich portion, indicating that Mg abundance correlates with calcite content.

The Sr concentrations (figure 9.3) of the calcite-rich samples range from 1800 to 6400 ppm. The Sr concentrations of the aragonite-rich samples are higher and range from 10,000 to 12,000 ppm. These values are similar to the values for modern Acropora palmata (12,000 to 13,000 ppm). For each pair, the calcite-rich portion has a lower Sr concentration than the aragonite-rich portion, indicating that Sr abundance is anticorrelated with calcite content.

The ^{238}U abundance of the calcite-rich samples ranges from 6.75 to 11.79 nmol/g. The ^{238}U abundance of the aragonite-rich samples is

Figure 9.3. Plot of ^{238}U abundance versus Sr abundance for the PB samples. The samples are labelled as in figure 9.3. This shows that ^{238}U abundance is correlated with Sr abundance and anticorrelated with calcite content.

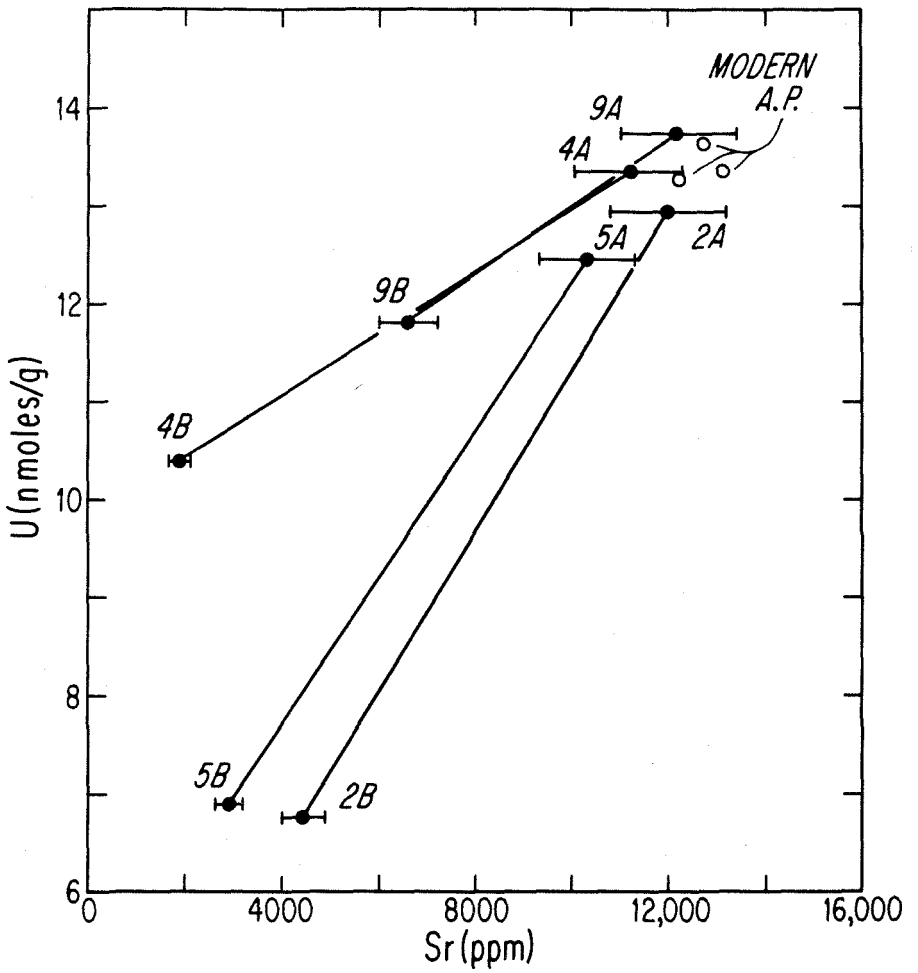
MODERN
A.P.
9A
4A
5A
2A
9B
4B
5B
2B
14
12
10
8
6
0
4000
8000
12,000
16,000
U(nmoles/g)
Sr (ppm)

Figure 9.4. Plot of ^{238}U abundance versus Mg abundance for the PB samples. The lines connect pairs of samples from the same coral. The samples labelled "A" are aragonite-rich and the samples labelled "B" are calcite-rich. Three analyses of a modern Acropora palmata skeleton are represented by open circles. This shows that uranium abundance is anticorrelated with both Mg abundance and calcite content.

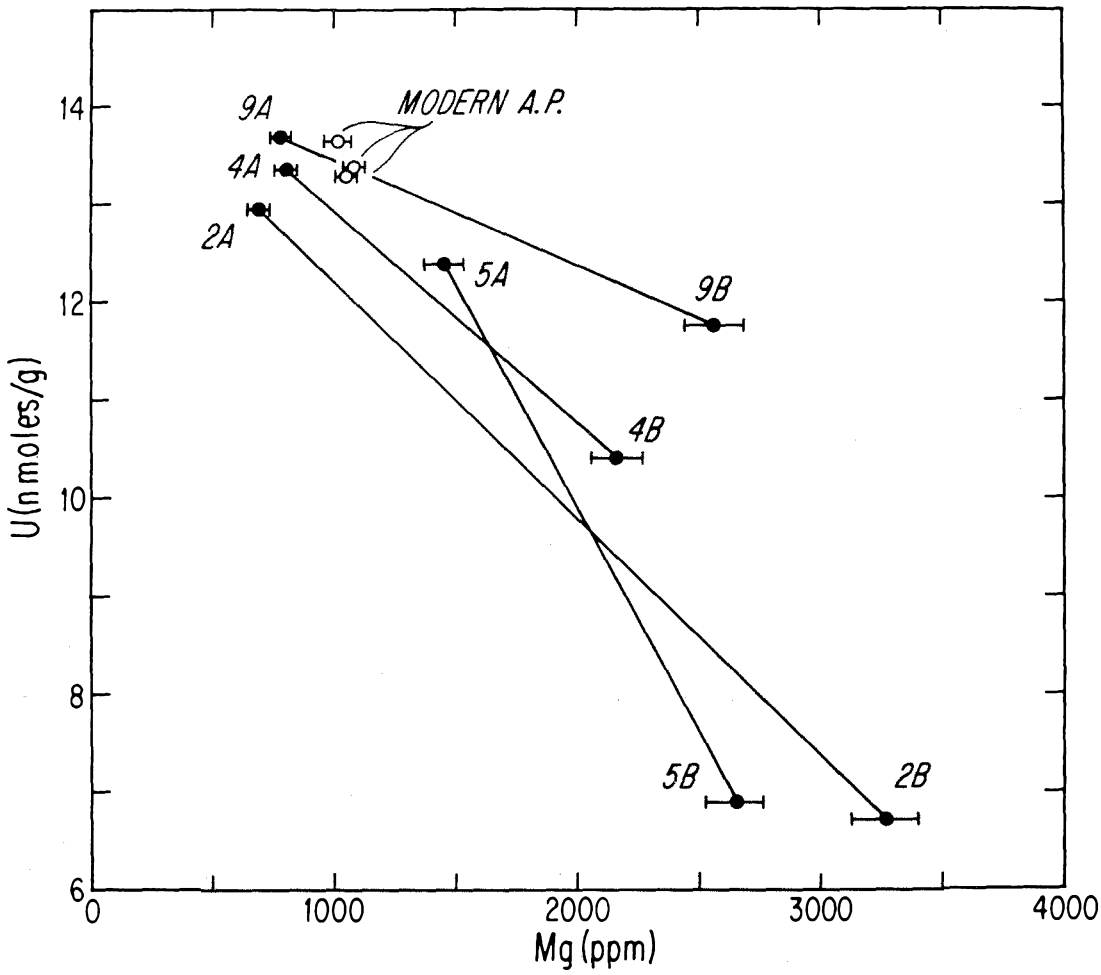
14
12
10
8
6
U(nmoles/g)
0
1000
2000
3000
4000
Mg (ppm)
9A
MODERN A.P.
4A
2A
5A
9B
4B
5B
2B

Figure 9.5. Plot of $\delta^{234}U(0)$ versus $[^{230}Th/^{238}U]_{act}$ for the PB corals. The ellipses represent 2 sigma errors. Each line joins a pair of samples from the same coral. For each pair, the sample labelled 'A' is aragonite-rich and the sample labelled 'B' is calcite-rich. All of the samples lie above the $\delta^{234}U(T)=150$ closed system trajectory indicating that either the samples have been altered or that the isotopic composition of uranium in seawater has changed with time. The aragonite-rich samples are even further from the 150 contour than the calcite-rich samples. If it is assumed that the ^{230}Th ages of the samples are true ages, then secondary calcite must have crystallized relatively soon after coral growth because the apparent age of each of the calcite-rich samples is not much younger than the age of the corresponding aragonite-rich sample.

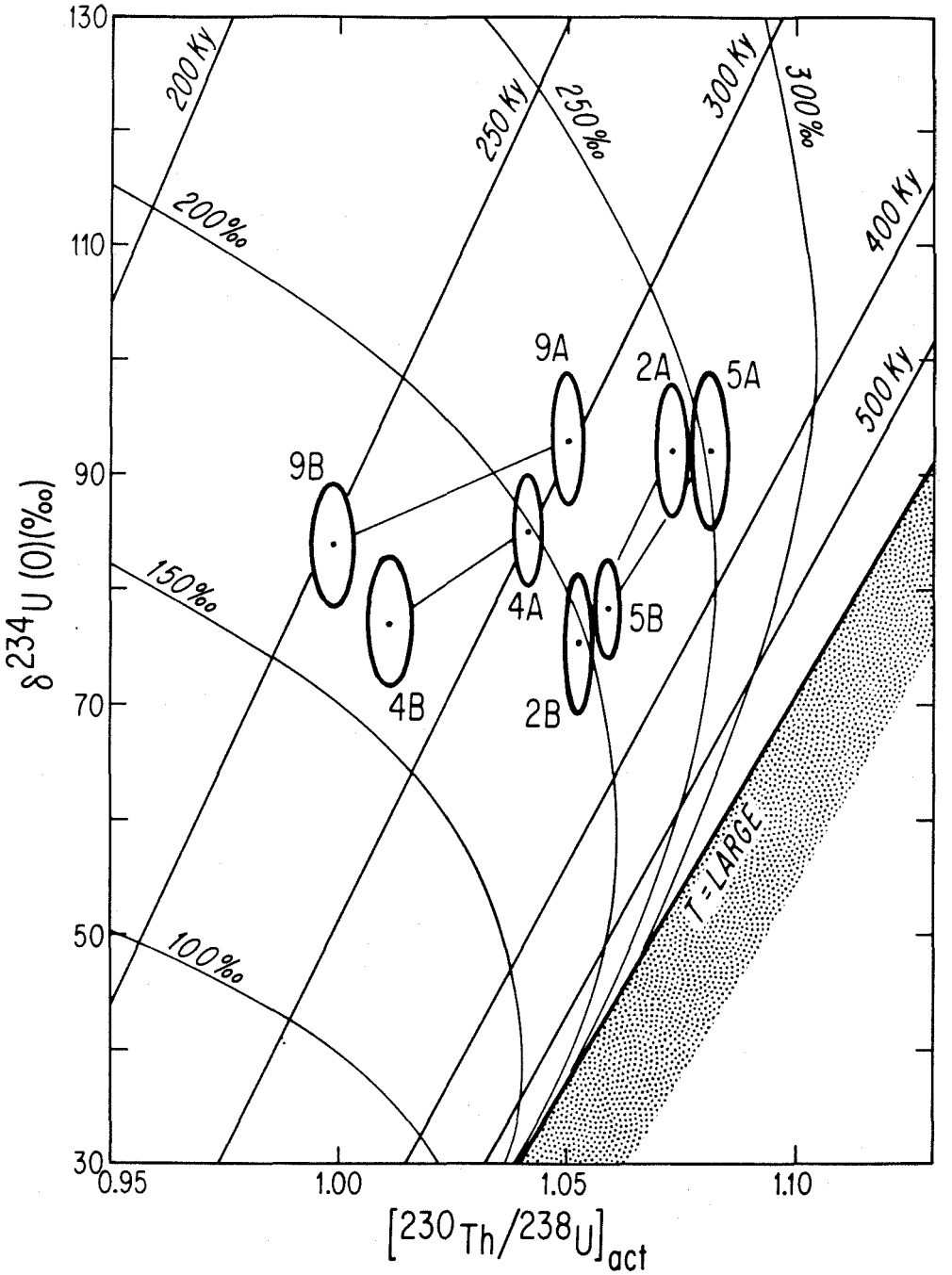
130
110
90
70
50
30
0.95
1.00
1.05
1.10
$\delta^{234}U\ (0)(‰)$
$[^{230}Th/^{238}U]_{act}$
200 KY
250 KY
300 KY
400 KY
500 KY
200‰
250‰
300‰
150‰
100‰
9A
2A
5A
9B
4A
5B
4B
2B
T = LARGE

higher and ranges from 12.41 to 13.74 nmol/g. These values are similar to the values of modern Acropora palmata (13.31 to 13.62 nmol/g). For each pair, the calcite-rich portion has a lower ^{238}U abundance than the aragonite-rich portion, indicating that ^{238}U abundance is anti-correlated with calcite content.

The measured $\delta^{234}U$ values (Table A2(VI), figure 9.5) for the aragonite-rich samples range from 85 to 92. For the calcite-rich samples, the range is slightly lower (75 to 84). The aragonitic portions of PB-2 and Pb-5 have $\delta^{234}U(0)$ values that are clearly higher than their calcitic counterparts. The aragonitic portions of PB-4 and PB-9 have $\delta^{234}U(0)$ values that are, within error, the same as the calcitic portions.

$[^{230}Th/^{238}U]_{act}$ for each of the aragonitic samples is distinctly higher than the value for each of their calcitic counterparts. The calcitic range is 0.9983 to 1.0520 and the aragonitic range is 1.0408 to 1.0803. The initial $\delta^{234}U$ values are all higher than the present seawater value, indicating that all the samples have been altered or that the isotopic composition of uranium in the oceans has changed with time. The $\delta^{234}U(T)$ values for the calcitic portions range from 163 to 208 and for the aragonitic portions, 198 to 251. The apparent ages of the aragonitic portions are 300 to 354 ky, and 252 to 346 ky for the calcitic portions. The apparent ages for the aragonitic portions of PB-2 and PB-5 are, within error, identical to their calcitic counterparts. PB-4A has an apparent age that is barely older than PB-4B, and PB-9A has an age that is slightly older than PB-9B.

9.3.4 Discussion

The proportions of calcite and aragonite in each sample have not yet been measured. Even before these measurements are made, some idea of the calcite-aragonite ratio in each sample can be gleaned from the ^{238}U-Sr plot (figure 9.3). If it is assumed that there are two components in each coral, an aragonite component with ^{238}U and Sr abundances equal to modern Acropora and a calcitic component with constant values of ^{238}U and Sr abundance, then the lines joining the pairs in figure 9.3 are mixing lines. The 100% aragonite end member is represented by the modern Acropora palmata points. For each coral, the 100% calcite endmember must lie between the point labelled "B" and the intersection of the y-axis on the extension of the line connecting each pair. It cannot lie beyond the y-axis because the calcite end member cannot have a negative Sr concentration. All four points labelled "A" plot close to the modern Acropora palmata points and must be more than about 80% aragonite. The points 2B, 4B, and 5B lie fairly close to the y-axis and must be more than about 70% calcite. The point 9B lies further from the y-axis but must have more than 50% calcite.

Because the calcite end member must lie on the extension of the mixing line between the y-axis and the points labelled "B," bounds can be placed on the ^{238}U abundance of the calcite endmember. For PB-4 the ^{238}U abundance of the calcite endmember is about 10 nmol/g; for PB-9, between 8 and 12 nmol/g; for PB-5, between 4 and 7 nmol/g; and for PB-2, between 2 and 7 nmol/g. PB-4 and PB-9 have calcite ^{238}U abundances that are clearly higher than the values for PB-2 and PB-5. It is clear that the calcite ^{238}U abundance is lower than the value for aragonite

and that this value is not the same for all calcites.

The effect of secondary calcite on the ^{238}U-^{234}U-^{230}Th systematics of each coral is not clear. All of the samples have $\delta^{234}U(T)$ different from the present seawater value (figure 9.5) indicating that the samples have all been altered or the $\delta^{234}U$ of seawater has changed with time. The aragonitic samples have $\delta^{234}U(T)$ even further from the seawater value than the calcitic samples. Finally, the apparent age of the aragonitic samples is very different from the age of the Rendezvous Hill Terrace indicating that either the stratigraphic assignment is incorrect or that the $^{230}Th/^{238}U$ ratio has been shifted 30% with no accompanying change in crystal structure.

The samples could have reached their final isotopic compositions (figure 9.5) in many different ways. If we assume that the aragonitic samples have not been altered, then $\delta^{234}U$ of seawater must have had a value of about 250 350 ky ago and a value of about 210 300 ky ago. If the calcite started out with no initial ^{230}Th, then all of the calcite ^{230}Th is radiogenic. In this case, the calcite must have been added relatively soon after coral growth, because the apparent age of the calcite is the same as that of the aragonite except for PB-9. PB-9B has an apparent age some tens of thousands of years younger than PB-9A. If none of the calcite ^{230}Th is radiogenic, then the calcite must have been added recently and crystallized with about the same $^{230}Th/^{238}U$ ratio as the aragonite. The data do not allow the possibility that the calcite crystallized soon after coral growth with significant initial ^{230}Th, because none of the calcites have apparent ages older than the corresponding aragonites. In all of the above

cases, the calcite must have crystallized from a solution with a $\delta^{234}U$ value, which was lower than the δ^{234} value of its aragonitic counterpart at that time.

The difference between $\delta^{234}U(T)$ in the aragonitic samples and present seawater may be due to alteration and not to a shift in the isotopic composition of seawater. If this is the case, the true age of each the coral is not known. The relationship between the timing of the calcite crystallization event and the aragonite alteration event is also not known. The aragonitic portion of the coral is now very porous and has been accessible to migrating fluids, whereas the calcitic portion is not as porous. The aragonitic portion has been open to alteration over its whole history, but the calcitic portion could not easily have been altered after crystallization. The isotopic composition of the aragonitic portion may have been affected by rather continuous alteration, whereas the calcitic portion may not have been chemically altered after crystallization. If the calcite crystallized with an initial $^{230}Th/^{238}U$ ratio of zero, then the ^{230}Th age of the calcite may actually place more accurate constraints on the true age of the coral than the ^{230}Th age of the aragonite. As the calcite must have crystallized after the coral, the true age of the coral must be older than the age of the calcite. If the ^{230}Th age of the calcite is the same as the true age of the calcite, then all of the PB samples must be older than 250 ky.

In summary, as calcite content increases, Mg content increases from the value for modern corals, Sr content decreases from the modern coral value, and ^{238}U content decreases from the modern coral value.

The $\delta^{234}U(T)$ for the aragonite samples is clearly above the present seawater value, indicating that the samples have been altered or that the seawater $\delta^{234}U$ has changed. The possibility that fossil coral can retain its original aragonite but exchange uranium and thorium must be investigated. If it is assumed that the ^{230}Th ages of all the samples represent true ages, than the crystallization of the calcite occurred fairly soon after coral growth for all four samples. If only the ^{230}Th age of the calcite samples are regarded as true ages, then the samples still must all be older than 250 ky, which is significantly older than the age of the Rendezvous Hill Terrace (122 to 129 ky, section 11.1).

9.4 How fast can seawater change its $\delta^{234}U$?

The observation that aragonitic fossil corals can have $\delta^{234}U(T)$ different from the present seawater value brings up the issue of the time scale over which one might expect to see changes in the uranium isotopic composition of seawater. This issue is addressed using a simple model. I assume that the ocean consists of one well mixed box with homogeneous ^{238}U abundance and $\delta^{234}U$. ^{238}U is added at a constant rate and is removed at the same constant rate. The uranium that is removed has the $\delta^{234}U$ value of the uranium in the ocean. The uranium that is initially added has a $\delta^{234}U$ value that is equal to δ^{1}_{i}. By time t=0, uranium with this δ-value has been added to the ocean for a long time compared to the residence time of uranium in the ocean, and the $\delta^{234}U$ has reached a steady state value. At time t=0, the $\delta^{234}U$ value of the added uranium is instantaneously changed to a different value and is held constant at this new value.

The following calculation shows how the $\delta^{234}U$ value of the ocean changes in response to the instantaneous change in the $\delta^{234}U$ of the uranium added to the ocean. Using an approach similar to the approach used in section 8.1, it can be shown that the initial steady state δ-value of the ocean is related to the δ-value of the uranium initially added to the ocean by the following relationship:

$$\delta_O^1(ss) = \delta_I^1/(1+\tau_U/\tau_{234}), \tag{9.1}$$

where $\delta_O^1(ss)$ is the initial steady state δ-value of the ocean, δ_I^1 is the initial δ-value of the uranium input into the ocean, τ_U is the residence time of uranium in the ocean, and τ_{234} is the decay constant for ^{234}U. Similarly, long after the δ-value of the uranium added to the ocean has been changed to its new value, the δ-value of the ocean will approach an new steady state:

$$\delta_O^2(ss) = \delta_I^2/(1+\tau_U/\tau_{234}), \tag{9.2}$$

where the superscript 2 refers to the new set of δ-values after t=0. In the time between the initial steady state and the final steady state, the δ-value of the ocean changes as follows:

$$\delta_O = \delta_O^2(ss) + (\delta_O^1(ss)-\delta_O^2(ss))\ \{\exp[-(1/\tau_U+1/\tau_{234})t]\}, \tag{9.3}$$

where t is the time after the shift in the isotopic composition of the uranium added to the ocean. This shows that the isotopic composition

of the ocean changes from its initial steady state value to its final steady state value in an exponential fashion with a time constant of $1/\tau_U+1/\tau_{234}$. For times that are short compared to this time constant, equation 9.3 can be approximated by:

$$\Delta\delta_o = \Delta\delta_i(t/\tau_U), \tag{9.4}$$

where $\Delta\delta_o$ is the shift in the δ-value of the ocean from its initial steady state value and $\Delta\delta_i$ is the instantaneous shift in the δ-value of the input uranium that occurs at t=0.

Although there is a large range in the δ-values of modern rivers, most have values between 100 to 500 (Ivanovich and Harmon, 1982). If the average δ-value of river input were to shift say 20% of the typical range, $\Delta\delta_i$ would be equal to 80. Reported values of τ_U are about 3 X 10^5 y (Ku et al., 1977). If the shift in δ_i were maintained for 50 ky, then after this period of time, $\Delta\delta_o$ would be equal to 12 δ-units. Therefore shifts on the order of ten to perhaps tens of δ-units over time periods of about 10^5 y would appear to be possible. Therefore the hints of $\delta^{234}U(T)$ values higher than the present seawater value for the corals shown in figure 7.15 could be due to a change in the isotopic composition of seawater. The much larger differences between $\delta^{234}U(T)$ of the aragonitic PB corals and present seawater are probably due to diagenetic alteration.

10. The rise of sea level and tectonic movement in the Holocene

10.1 The record of Holocene sea level rise in the Enriquillo Valley, Hispaniola

Results on the corals from the Enriquillo Valley are presented in Tables A1(II) and A2(II), and figures 10.1, 10.2, and 10.3. The ^{238}U concentrations in these corals range from 9.68 to 10.96 nmol/g (Table A1(II). This range is similar to the range for very young corals from Vanuatu (9.13 to 11.30 nmol/g; Table A1(I)). The ^{232}Th abundances range from 0.140 to 0.668 pmol/g (Table A1(II)) and are similar to the values for the young Vanuatu corals.

The ^{230}Th ages (Table A2(II)) range from 8294 to 4951 years and have 2 sigma errors of ±30 to ±456 years. The relatively high errors in age for PR-D-1 (±140 y), PR-H-1 (±94 y), and CH-18 (±456 y) are due to poor thorium yields caused by an error in the chemical separation procedure used for these samples. Samples with high thorium yields, in this time range, generally have errors of ±20 to ±40 years.

The ages are shown plotted versus their present heights in figure 10.1. The oldest coral, CH-8, has a present elevation of 33 m below sea level. The youngest coral has a present elevation of 7 m below sea level. Samples PR-H-1 and CH-8 are the first corals to grow above an unconformity. Below the unconformity are alluvial fan gravels that were deposited subaerially. If the corals grew soon after water submerged the alluvial fan, then CH-8 and PR-H-1 must have grown in relatively shallow water.

The isotopic data are shown in a $\delta^{234}U(0)$ versus $[^{230}Th/^{238}U]_{act}$ plot (figure 10.2). Also shown in figure 10.2 are closed system

Figure 10.1. Present elevation versus date of growth as determined by ^{230}Th dating. The samples are from the subaerially exposed Holocene reef in the Enriquillo Valley except for D.W. which was collected under water off the west coast of Barbados. The tips of the arrows represent the present elevation and ^{230}Th growth date of each sample. The water level in the basin had to have been higher than each coral at the time that coral grew. CH-8 and PR-H-1 grew directly on top of an unconformity, which is underlain by alluvial fan gravels. They were therefore the first corals to grow at each locality above a subaerially deposited unit and must have grown in shallow water. D.W. is of the species Acropora palmata, was collected from a reef crest, and must have also grown in shallow water. The estimated sea level rise curve is drawn close to the tips of the arrows for these three points. The average rate of water level rise between 6306 B.C. and 5863 B.C. is 32 mm/y. PR-H-1 and PR-H-2 are from the same locality, but the latter has an elevation that is 4.9 m higher. The average rate of reef accretion at this locality is 1.7 mm/y.

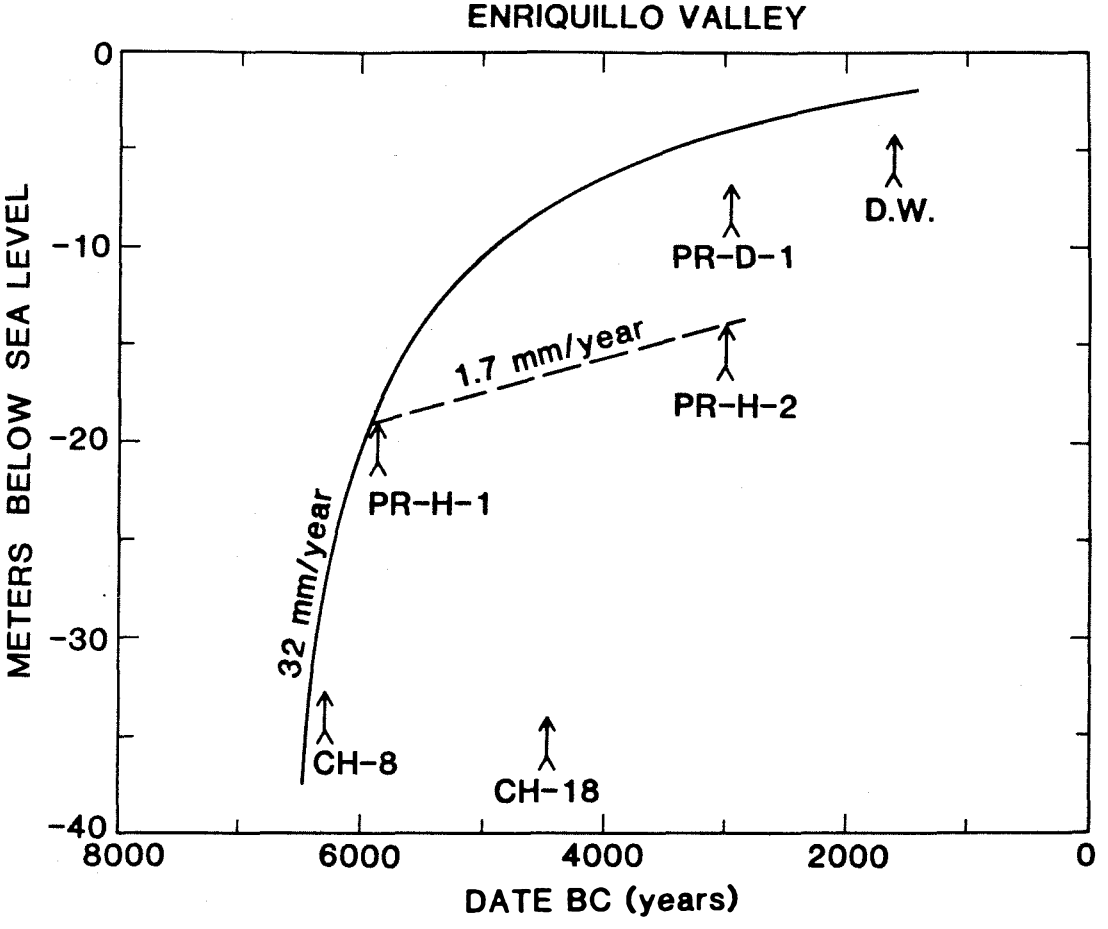
ENRIQUILLO VALLEY
METERS BELOW SEA LEVEL
0
-10
-20
-30
-40
8000
6000
4000
2000
0
DATE BC (years)
D.W.
PR-D-1
1.7 mm/year
PR-H-2
PR-H-1
32 mm/year
CH-8
CH-18

Figure 10.2. Plot of $\delta^{234}U(0)$ versus $[^{230}Th/^{238}U]_{act}$ for the Enriquillo Valley samples and two samples from open ocean sites (D.W. from Barbados and MY2 from Malekula Is., Vanuatu). Some of the samples have relatively large errors in $^{230}Th/^{238}U$ because the wrong normality acid was added to the ion exchange column during the chemical separation procedure and the thorium yields were low. The open ocean corals have $\delta^{234}U(T)$ that is the same as present seawater, but the Enriquillo Valley samples have $\delta^{234}U(T)$ values that are below present seawater, indicating the these corals grew from a body of water that did not have the same uranium isotopic composition as seawater. The trend in $\delta^{234}U(T)$ with time is shown in the next figure.

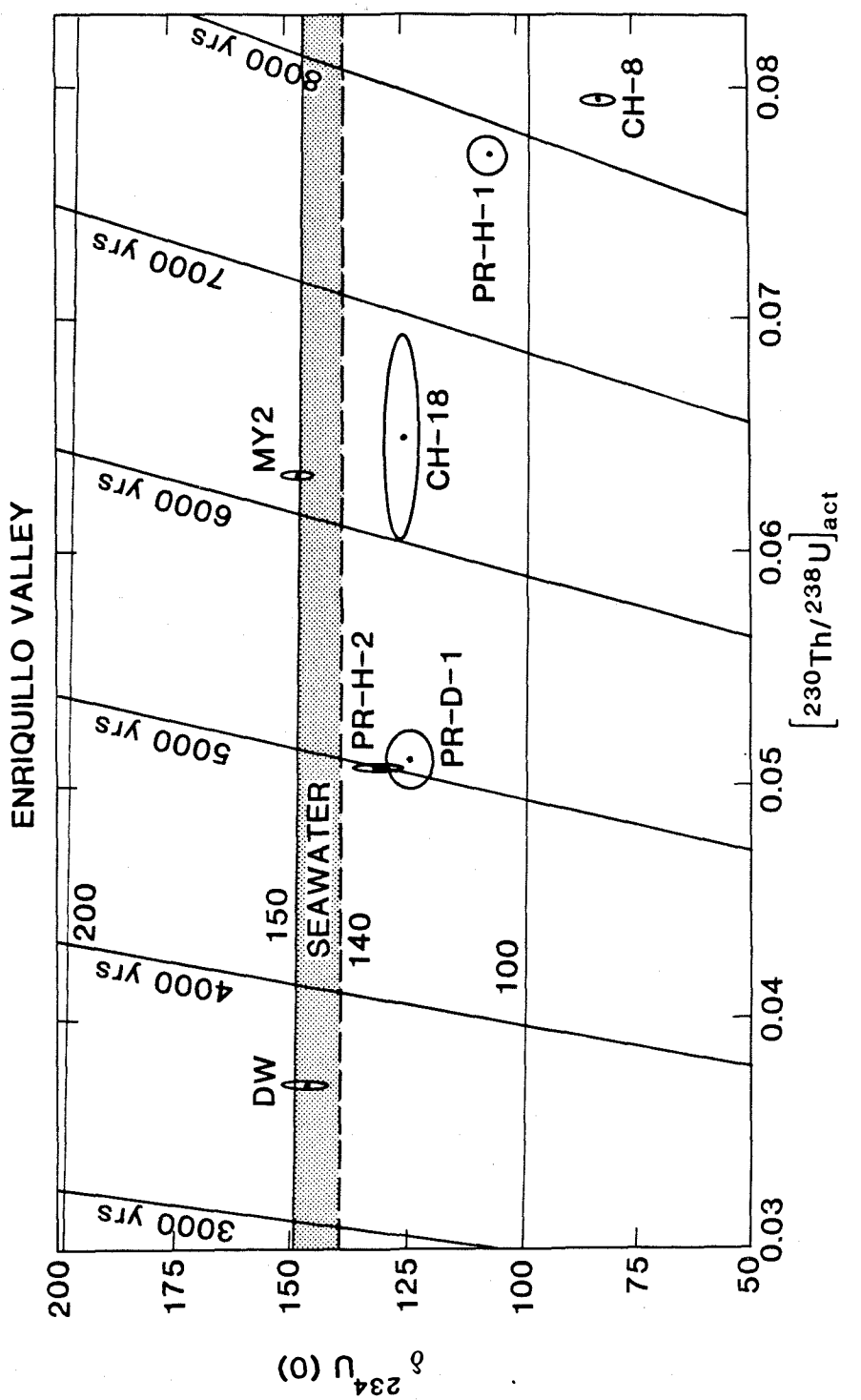
ENRIQUILLO VALLEY
$\delta^{234}U$ (0)
$[^{230}Th/^{238}U]_{act}$
3000 yrs
4000 yrs
5000 yrs
6000 yrs
7000 yrs
8000 yrs
SEAWATER
DW
MY2
PR-H-2
PR-D-1
CH-18
PR-H-1
CH-8
200
150
140
100
200
175
150
125
100
75
50
0.03
0.04
0.05
0.06
0.07
0.08

Figure 10.3. Plot of $\delta^{234}U(T)$ versus time for the Enriquillo Valley corals and two corals from open ocean localities (D.W. and MY2). The open ocean corals have the same isotopic composition as present seawater. The Enriquillo samples have lower $\delta^{234}U(T)$ values. The $\delta^{234}U(T)$ values increase toward the seawater value with time. Over the same period of time, the water level in the basin was rising (figure 10.1). It appears that the change in uranium isotopic composition is due to flooding of the valley with seawater as sea level rose above the level of the sill separating the valley from the ocean.

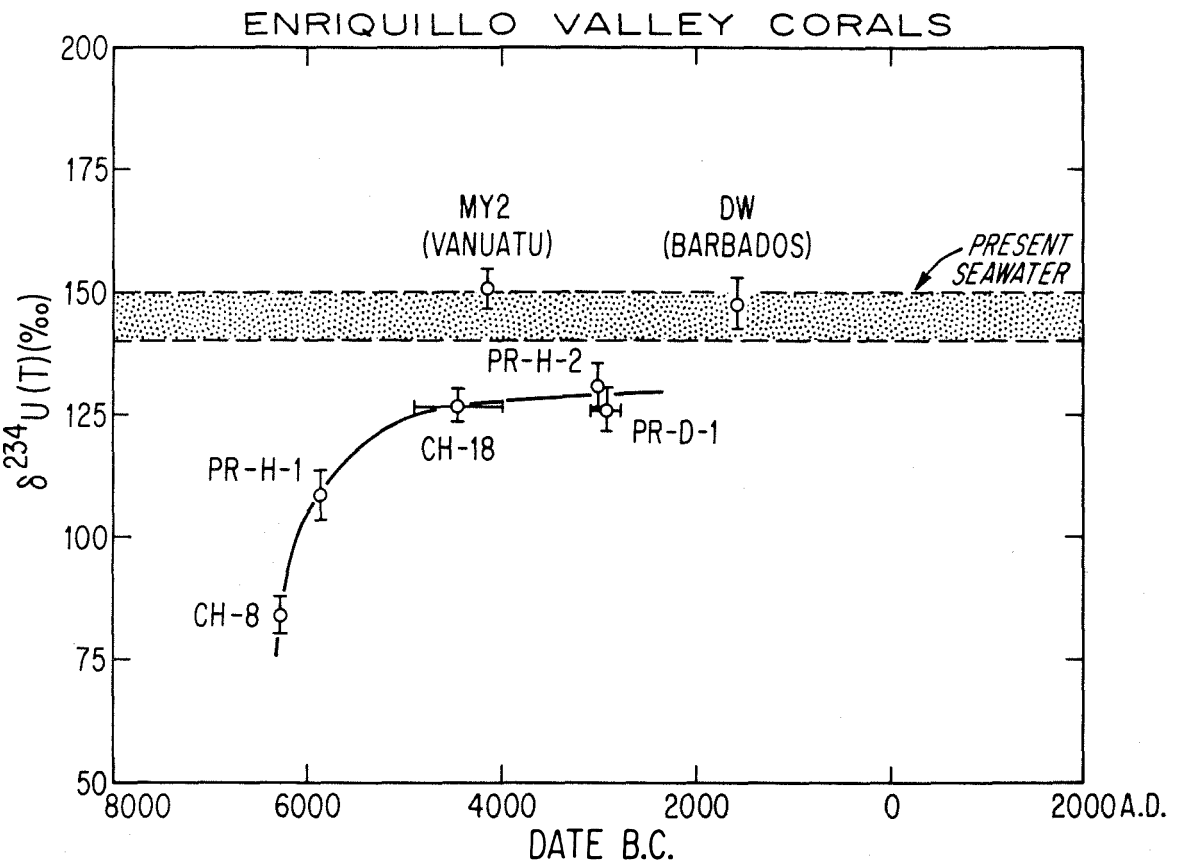
ENRIQUILLO VALLEY CORALS
200
175
150
125
100
75
50
$\delta^{234}U(T)(‰)$
MY2
(VANUATU)
DW
(BARBADOS)
PRESENT
SEAWATER
PR-H-2
PR-D-1
CH-18
PR-H-1
CH-8
8000
6000
4000
2000
0
2000 A.D.
DATE B.C.

trajectories for initial $\delta^{234}U$ equal to 140 and 150 which are the highest and lowest values measured in seawater (Table 8.1). Two samples (DW, Barbados; MY2, Vanuatu) that grew at about the same time as the Enriquillo Valley corals but at open ocean sites are also plotted. Both DW and MY2 plot on the seawater band. The Enriquillo Valley corals all plot distinctly below the "seawater" band and have initial $\delta^{234}U$ values ranging from 84 to 130.

As discussed in section 5.3, samples that plot off the closed system trajectory for seawater indicate that seawater had a different uranium isotopic composition at the time the samples grew, the samples were altered, or the samples grew in a restricted or isolated body of water that had a different uranium isotopic composition than seawater. Corals that grew outside of the valley in open ocean sites (DW and MY2) at about the same time that the Enriquillo Valley corals grew have initial $\delta^{234}U$ values which are identical to present seawater. Therefore, the possibility that the uranium isotopic composition of seawater was different from today's value can be excluded. The possibility that the Enriquillo samples have been altered cannot definitely be ruled out; however, there is no reason to believe that the valley corals would be more susceptible to alteration than corals growing outside the valley. Also, the, the present configuration of the Enriquillo Basin suggests that it could have been isolated from the ocean at the time the corals grew and therefore could have had a different uranium isotopic composition than seawater.

The configuration of the basin is shown in figure 6.2. Lake Enriquillo is not now connected to the ocean. The basin is separated

from the sea by a sill that is slightly higher than present sea level. Because sea level has not been appreciably above present sea level in the last several tens of thousands of years, one wonders if the valley was connected to the ocean at any time in the recent past (figure 6.2).

The evidence that the valley was connected to the ocean is the presence of the corals themselves. Corals can only live in water with salinities between 30 and 43 °/oo (see section 4.3). Therefore, if the water in which the corals grew was not seawater, it must have had salinities that which were fortuitously close to seawater salinities.

Assuming that the valley corals have not been altered, the initial uranium isotopic composition of the corals provides critical information concerning the extent to which the water in the valley was connected with seawater at the time the corals grew. Figure 10.3 is a plot of $\delta^{234}U(T)$ versus ^{230}Th growth date. As in figure 10.2, the open ocean corals plot on the seawater band, whereas the Enriquillo Valley corals plot below the band. This shows that the water in the Enriquillo Valley was at least partially isolated from the ocean at the time the corals grew. With increasing time, $\delta^{234}U(T)$ of the corals increases from a value of 84 at the time CH-8 grew to a value of 130 some 3000 years later at the time PR-H-2 grew. The $\delta^{234}U(T)$ value approaches the seawater value but does not reach it. The increasing $\delta^{234}U$ value could be explained by addition of seawater to water that initially had a $\delta^{234}U$ value that was lower than 84.

Over the same period of time that $\delta^{234}U$ was increasing, it appears that the water level in the basin was rising. In figure 10.1,

I have drawn in an estimated water level rise curve. Because corals grow under water, water level is constrained to lie above the height of each coral at the time that each coral grew. As discussed above, CH-8 and PR-H-1 are likely to have grown in shallow water. Therefore, the curve is drawn just above the heights of these corals. The average rate of water rise between these two points is 32 m/ky, an extremely high rate. The total increase in water level between 6306 B.C. (when CH-8 grew) and 2963 B.C. (when PR-D-1 grew), a period of about 3300 years, is more than 26 m.

Because the water level in the basin was rising at the same time that the uranium isotopic composition of the water in the basin was shifting toward the isotopic composition of seawater, it is likely that the rise in water level and the shift in isotopic composition were due to the addition of seawater to the basin. Seawater has essentially uniform $\delta^{234}U$ values and ^{238}U abundances (section 8.1). Because these values are uniform and known, if the rise in water level in the Enriquillo Valley was due to seawater addition, then the ^{238}U abundance in valley water at the time each coral grew can be calculated from their isotopic compositions and mass balance considerations. The isotopic composition and uranium abundance of the basin water at some water level must be related to the isotopic composition and uranium abundance at a higher water level (after the addition of a known amount of seawater) by the following relationship:

$$X^\circ\delta^\circ U^\circ + X_{sw}\delta_{sw}U_{sw} = \delta_f U_f, \qquad (10.1)$$

where ° refers to the characteristics of the water in the initial lower water level state, sw refers to seawater, f refers to the characteristics of the water in the final higher water level state. U refers to the ^{238}U concentration, δ refers to the $\delta^{234}U$ value, and X° is the mass of water in the basin at the lower water level divided by the mass of water in the basin at the higher water level; $X_{sw} = 1 - X°$. The ^{238}U concentrations of the water at the two different water levels are related by the relationship:

$$U°X° + U_{sw}X_{sw} = U_fX_f. \qquad (10.2)$$

Combining equations 10.1 and 10.2 yields:

$$U°/U_{sw} = \{(1-X°)(\delta_f-\delta_{sw})\}/\{X°(\delta°-\delta_f)\}. \qquad (10.3)$$

All of the variables in equation 10.3 are known except U°. Therefore equation 10.3 can be used to calculate, for instance, the uranium concentration in the water at the time that CH-8 grew. Taking δ_{sw}=145 (Table 8.1), δ_f=126 (value for PR-D-1), $\delta°$=84 (value for CH-8), X°=0.31 (calculated from the known heights of CH-8 and PR-D-1 and the geometry of the Enriquillo Basin from Taylor et al., 1985b), a value of $U°/U_{sw}$ of 1.0 is calculated. Considering the errors in the isotopic analyses, $U°/U_{sw}$ may have values between 0.7 and 1.4. Thus the concentration of uranium in the water in which CH-8 grew was similar to the concentration of uranium in seawater.

This calculation is shown in figure 10.4, which is a plot of

Figure 10.4. Plot of $\delta^{234}U$ versus the ratio of ^{238}U abundance in seawater to the calculated ^{238}U abundance in the basin water. The ^{238}U abundance in the water from which PR-D-1 and CH-8 grew can be calculated if it is assumed that the volume of water that was added to the basin between the times that the samples grew was all seawater with the isotopic composition of present seawater. This calculation is represented by the mixing line that extends from the point labelled "seawater." Considering the error in the calculation, the basin water at the time PR-D-1 grew could have had the characteristics represented by the stippled band labelled PR-D-1. The characteristics of CH-8 water are also represented by a stippled band. If the water at the time CH-8 grew was also a mixture of seawater and some earlier basin water, then this water must have had characteristics defined by the extension of the mixing line below the CH-8 stippled band (labelled "lake water"). Considering the errors in the calculation, the true mixing line could have slopes as shallow and as steep as the slopes of the dashed lines. It appears that the basin water had ^{238}U abundances similar to seawater but $\delta^{234}U$ values which were lower.

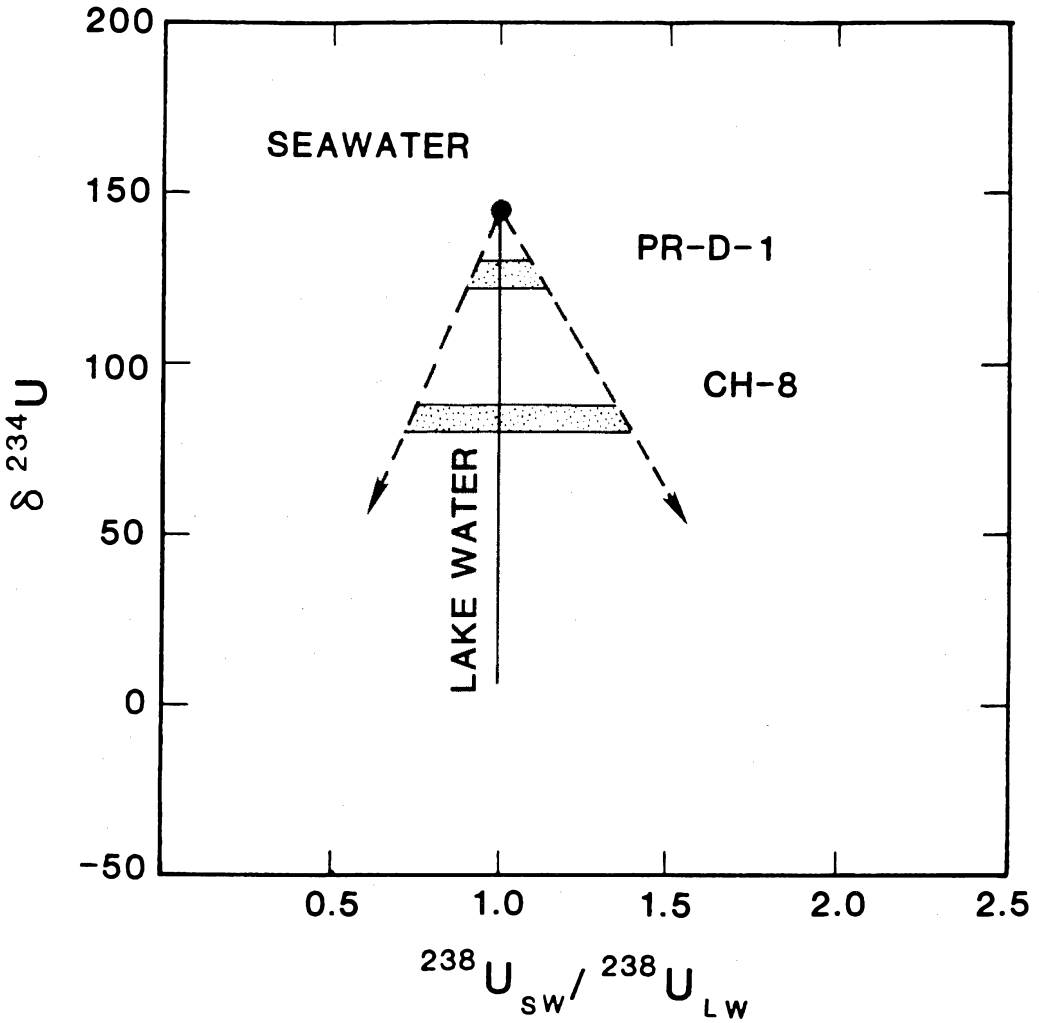
200
150
100
50
0
-50
SEAWATER
PR-D-1
CH-8
LAKE WATER
δ 234U
0.5
1.0
1.5
2.0
2.5
238Usw/ 238ULw

$\delta^{234}U$ versus the seawater ^{238}U concentration divided by the ^{238}U concentration in the water of the Enriquillo Basin. Two-component mixing lines in this diagram are represented by lines. The calculation described above is represented by the solid line extending from the point labelled "seawater." The error in the calculation due to errors in the δ-values substituted into equation 10.3 is represented by the two dashed lines that are the maximum and minimum allowable slopes for the mixing line. The stippled regions represent the range of possible ^{238}U abundances and δ-values for Enriquillo Basin Water at the times that PR-D-1 and CH-8 grew. The ^{238}U abundances of the basin water at these times are similar to seawater ^{238}U abundances.

CH-8 is the oldest Enriquillo Valley coral that has been analyzed. The isotopic composition and uranium abundances of the basin water at the time the younger samples grew can be explained by addition of seawater to basin water at the time CH-8 grew. If it is assumed that the basin water at the time CH-8 grew is itself a mixture of seawater and pre-existing basin water, then constraints can be placed on the isotopic composition and uranium abundance of the pre-existing basin water. Using equation 10.3, it can be shown that the pre-existing basin water must have $\delta^{234}U$ values and ^{238}U abundances that lie along the extension of the solid line (figure 10.4, line labelled "lake water") below the stippled band for CH-8. Considering errors in measured δ-values, the slope of this line must lie between the two dashed lines in figure 10.4. Therefore the pre-existing basin water had a $\delta^{234}U$ value that was less than 84 and a ^{238}U abundance

that was not very different from the seawater abundance.

Other information about the composition of the basin water at the time CH-8 grew can be derived from the ^{14}C data. The ^{14}C age of CH-8 is about 1700 years older than its ^{230}Th age (Table 9.1). If this difference is not due to alteration affecting one or both of the systems, then it may be due to a difference in the $^{14}C/C$ ratio between the basin water and the atmosphere at the time CH-8 grew. As the exposed rock around the basin is composed partly of Tertiary limestone, this could be a source of "dead" carbon. A shift in the ^{14}C age of 1700 years is equivalent to a shift in $^{14}C/C$ ratio of 23%. A shift of 23% in the $^{14}C/C$ ratio could be accomplished by increasing the total carbon concentration in the basin water by 23% with the addition of 'dead' carbon. If it is assumed that the basin had a carbon concentration similar to the seawater value (2 mol/m^3; Broecker and Peng, 1982), then the amount of old limestone that one would need to dissolve to generate the apparent old ^{14}C age can be calculated. If it is assumed that the area of the limestone terrane that drains into the basin is 10 times the surface area of the body of water at the time that CH-8 grew, then an average thickness of only 30μm of limestone would need to be dissolved and transported into the basin to generate the observed shift in apparent age.

Consider the effect of adding the amount of uranium contained in the 30μm thick layer of limestone to a volume of seawater equal to the volume of the basin below the height of CH-8. If it is assumed that the limestone has a ^{238}U abundance of 1 ppm, then the added uranium would increase the the ^{238}U abundance of the seawater by only 1.0%.

If the added uranium has a $\delta^{234}U$ value of zero, this would not shift the $\delta^{234}U$ significantly down from the seawater value. Therefore the addition of carbonate from old limestone could explain the shift in ^{14}C age; however, the same amount of limestone does not contain enough uranium to shift the uranium isotopic composition appreciably.

The source of the low δ-values is particularly enigmatic. The water at the time that CH-8 grew appears to have had salinities similar to seawater salinities and ^{238}U abundances that are similar to seawater ^{238}U abundances but a uranium isotopic composition that is very different from seawater uranium isotopic composition. Although the ^{14}C age of the water is slightly old, the shift in carbon isotopic composition does not appear to be related to the shift in uranium isotopic composition. One possibility is that the uranium in CH-8 water is largely derived from old seawater. The δ-value of seawater that was isolated from the ocean would decrease with time because of radioactive decay (equation 5.11). If the δ-value of the water was 145 when it was isolated from the ocean, it would take 190 ky for $\delta^{234}U$ to drop to a value of 84 (equation 5.12). Over this period of time the water may have evaporated and new fresh water may have been added, but as long as significant amounts of additional uranium are not added to the uranium that was initially isolated from the ocean, the δ-value of the uranium will continue to fall as prescribed by equation 5.12.

In summary, it appears that the water in the Enriquillo Valley between 6306 B.C. and 2963 B.C. was partially isolated from the ocean. Over this period of time, seawater was added to the basin and caused

the water level to rise by more than 26 m. It is known from ^{14}C dating at open ocean localities that sea level was rising at about this time (see, for example, Neumann, 1971; Lighty et al., 1978; Scholl et al.,1969; Macintyre et al., 1977). It is likely that the flooding of the Enriquillo Valley was the result of this rise in sea level. Therefore, the ages and heights of the corals shown in figure 10.1 not only constrain the changes in water level within the basin, but also reflect changes in sea level. Figure 10.1 shows that between the years 6306 and 5863 B.C., sea level rose by about 14 m, an average rate of 32 m/ky. This confirms earlier work that showed that sea level has risen at extremely large rates in the Holocene (Neumann, 1971; Lighty et al., 1978).

10.2 Co-seismic uplift and the ages of emerged eighteen and nineteenth century corals in Vanuatu

Taylor et al.(1980, 1985a, 1987) examined partially emerged coral heads from Santo and Malekula Islands. The upper portions of these heads were above sea level and dead. At the time of these studies, the lower portions of these heads were below sea level and were still alive. Because the lower portions of these heads were still alive, the different portions of the coral heads could be dated by the growth band method. Using this method, it was demonstrated that the time of coral emergence on northwest Santo Island was the same as the time of the last major earthquake (M_S = 7.5, 1973). It was also demonstrated that the time of coral emergence on Malekula Island was the same as the time of the last major earthquake on that island (M_S = 7.5, 1965).

The amount of emergence at each of these localities (0.6 m at northwest Santo and 0.8 m at north Malekula) was determined by measuring the difference in elevation between the highest portion of each head and the highest living portion of each head. The average long term uplift rate (over the past ~6000 years) at each locality was also determined by dating (^{14}C) fossil corals that have present elevations of about 20 m. At each of the localities, there were also coral heads that were at a slightly higher elevation than the partially emerged corals. They were completely emerged and were dead. By analogy to the partially emerged corals, it was thought that these heads were killed by earlier co-seismic uplift events. If this is true, emerged heads from the same locality must have died at the same time. Because these heads were completely dead, they could not be dated by the growth band method.

I analyzed samples from north Malekula and northwest Santo Islands in order (1) to examine the possibility of dating corals that grew in the past few decades and centuries by the ^{230}Th method, (2) to test the hypothesis that the completely emerged corals from each locality died at the same time and therefore could have been killed by co-seismic uplift, (3) to estimate earthquake recurrence intervals for these two islands, and (4) to compare tectonic emergence rates over the past few centuries with emergence rates averaged over ~6000 years.

Results of the analyses on very young corals from Santo and Malekula Islands in Vanuatu are shown in figures 8.1 and 8.2 and Tables A1(I) and A2(I). As discussed in section 8.2 and shown in

figure 8.1, all of these corals have initial $\delta 234_U$ values that are, within error, identical to the present δ-value of seawater. As discussed in section 8.3 and shown in figure 8.2, the ^{230}Th ages of the three samples (CWS-A-1b, CWS-A-1d, and TAN-E-1g) that had previously been dated by counting of growth bands are, within the 2 sigma errors of ±3 to 5 years, identical to the growth band ages. There is, therefore, no reason to suspect that the ^{230}Th ages are different from the true ages of these corals.

The ^{230}Th growth dates of the emerged corals that could not be dated by the growth band method are shown in Table 10.1 along with the present heights of these samples. The two samples from the northwest Santo locality (see section 6.3 and figure 6.1), CWS-C and CWS-D-1, have the same present elevation (1.8 m above the highest living corals at this locality). These corals have ^{230}Th growth dates of 1866 ± 4 A.D. and 1864 ± 4 A.D. Within analytical error, the dates are the same. CWS-D-1 and CWS-D-2 are replicate analyses of different fragments of the same coral. The growth date for CWS-D-2 (1868 ± 8 A.D.) is, within error, the same as the growth date for CWS-D-1.

The two samples from the north Malekula locality (section 6.3, figure 6.1), MAG and MAF, also have the same present elevation (1.3 m above the highest living corals at this locality). MAF has a ^{230}Th growth date of 1729 ± 3 A.D.; MAG has a ^{230}Th growth date of 1718 ± 5 A.D. These dates are similar, but analytically distinguishable. Sample MY2 was collected near the locality where MAF and MAG were collected, but has a much higher elevation (15.3 m, Table A1(I)). The ^{230}Th growth date of MY2 is 4174 ± 25 B.C. (Table A2(I)).

Table 10.1. ^{230}Th ages of emerged corals.

Sample	Island	Height (m)	Date of growth (from ^{230}Th) (yrs A.D.)
CWS-C	N.W. Santo	1.8	1866 ± 4
CWS-D-1[c]	N.W. Santo	1.8	1864 ± 4
CWS-D-2[c]	N.W. Santo	1.8	1868 ± 9
MAF	N. Malekula	1.3	1729 ± 3
MAG	N. Malekula	1.3	1718 ± 5

[a] Above the highest living corals at the same locality (F. W. Taylor, pers. commun.).

[b] Determined by subtracting the ^{230}Th age from the date of analysis; dates are rounded to January 1 of the indicated year; reported errors are 2σ of the mean.

[c] CWS-D-1 and CWS-D-2 are replicate analyses of the same coral.

Figure 10.5 is a plot of the present heights and ages of the north Malekula corals. The highest corals that are currently alive have an elevation of zero. At the top of the first step (0.8 m, A.D. 1965) is the height and age of the top of the partially emerged coral heads that were dated by growth band methods (Taylor et al., 1980, 1985a, 1987). At the top of the second step (1.3 m, A.D. 1729), are the height and ^{230}Th age of the top of the MAF and MAG coral heads. MY2 plots off the diagram at 16.0 m and 4174 B.C. Because corals live below sea level, if sea level has not changed elevation over this period of time, then north Malekula Island has been uplifted at least 16 m since 4174 B.C, at least 1.3 m since A.D. 1729, and at least 0.8 m since A.D. 1965. If it is further assumed that the three groups of corals grew right at sea level, then the values stated above would represent the true amounts of uplift as opposed to minima.

One would like to establish a continuous curve through the points in figure 10.5. Based on the growth band data, the uplift that has occurred since 1965 occurred in one event in 1965, hence, the first step in figure 10.5. The similarity between the ^{230}Th growth dates of MAF and MAG suggest that these corals were killed at the same time. This is consistent with the idea that they, too, were killed by co-seismic emergence. If so, then there must be a discontinuity in figure 10.5 at A.D. 1729. If there was no tectonic uplift between 1729 and 1965, then the length of the discontinuity must be equal to the difference in height between the partially emerged 1965 corals and the completely emerged 1729 corals as shown in figure 10.5.

If, indeed, the scenario described above and depicted in figure

Figure 10.5. Plot of present elevation versus coral growth date for corals from north Malekula Is., Vanuatu. The portion of the curve from 1987 to the top of the first step was determined by growth band dating (Taylor et al., 1987) of partially emerged corals. The age of the top of the second step was determined by ^{230}Th dating of completely emerged corals (MAG and MAF). The portion of the curve between the top of the first step and the top of the second step is inferred to have that form by analogy to the shape of the curve between 1965 and 1987. By analogy to the first step, which occurred at the time of a major earthquake, MAF and MAG are also inferred to have been killed by co-seismic uplift. From the ages of the two events a recurrence interval of 236 y is calculated. The amount of uplift for the two events is not the same indicating that the seismicity is not periodic. The long term average uplift rate (2.3 mm/y; average Holocene) was determined by dating MY2 which has a present height of 16 m and yielded a ^{230}Th growth date of 4174 B.C. The uplift rate determined from the two events using a slip predictable or a time predictable model is similar to the long term uplift rate, indicating that the total Holocene uplift can be accounted for by events similar to the 1965 and 1729 events.

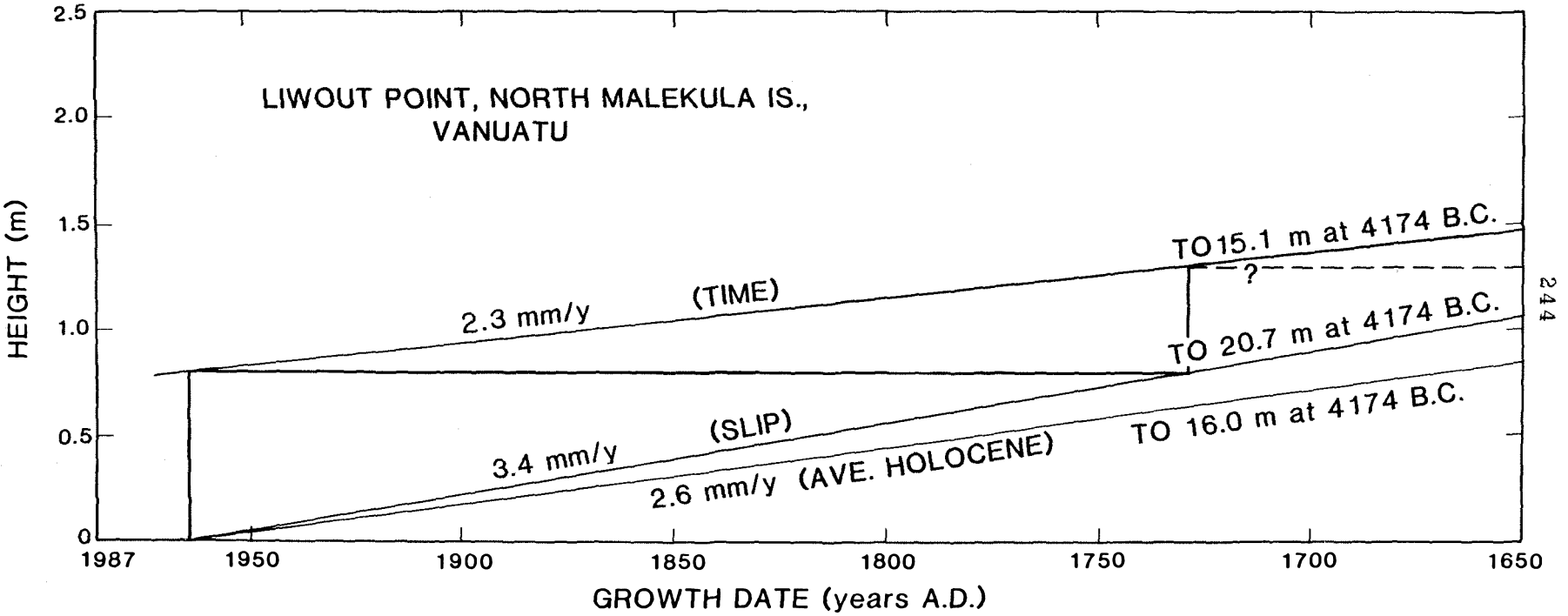
LIWOUT POINT, NORTH MALEKULA IS.,
VANUATU
HEIGHT (m)
2.5
2.0
1.5
1.0
0.5
0
1987
1950
1900
1850
1800
1750
1700
1650
GROWTH DATE (years A.D.)
TO15.1 m at 4174 B.C.
?
2.3 mm/y
(TIME)
TO 20.7 m at 4174 B.C.
3.4 mm/y
(SLIP)
2.6 mm/y (AVE. HOLOCENE)
TO 16.0 m at 4174 B.C.

10.5 is valid, then the seismic recurrence interval for north Malekula Island is 236 years. The amount of uplift for the 1965 and 1729 events is not the same. Therefore, the seismicity is not periodic (equal amounts of displacement at equally spaced intervals, see Shimazaki and Nakata, 1980). If the seismicity is time predictable (the amount of time before the next earthquake depends on the amount of displacement associated with the previous earthquake), then the uplift rate calculated from the two events is 2.3 mm/y (figure 10.5). If the seismicity is slip predictable (the amount of displacement associated with an earthquake is dependent on the interval of time since the last earthquake), then the uplift rate calculated from the two events is 3.4 mm/y. The uplift rate averaged over the past 6128 years (calculated from the present elevation and ^{230}Th age of MY2) is 2.6 mm/y. Thus, both the slip and time predictable models yield short term uplift rates that are quite similar to the long term uplift rate on north Malekula.

Figure 10.6 is analogous to figure 10.5 and depicts a series of events for northwest Santo Island, which are analogous to the events on north Malekula Island. Growth band dating showed that there was 0.6 m of uplift in 1973. The ^{230}Th ages of CWS-C and CWS-D are, within error, identical (average A.D. 1865), indicating that they were killed at the same time and could have been killed by co-seismic uplift. The present heights of these heads is 1.8 m. The calculated recurrence interval is 108 y. The amount of uplift associated with the 1973 event (0.6 m) is only half of the uplift associated with the 1865 event (1.2 m), indicating that the seismicity on northwest Santo

Figure 10.6. Analogous plot to figure 10.5 but for northwest Santo Is., Vanuatu. The age of the top of the second step was determined by dating CWS-C and CWS-D by the ^{230}Th method. The recurrence interval from the two events for this locality is 108 y. The amount of uplift is not the same for the two events, indicating that seismicity is not periodic. Using a time predictable model, the uplift rate from the two events is much higher than the average rate over the past 6000 years; using a slip predictable model, the uplift rate from the two events is similar to the average rate over the past 6000 years.

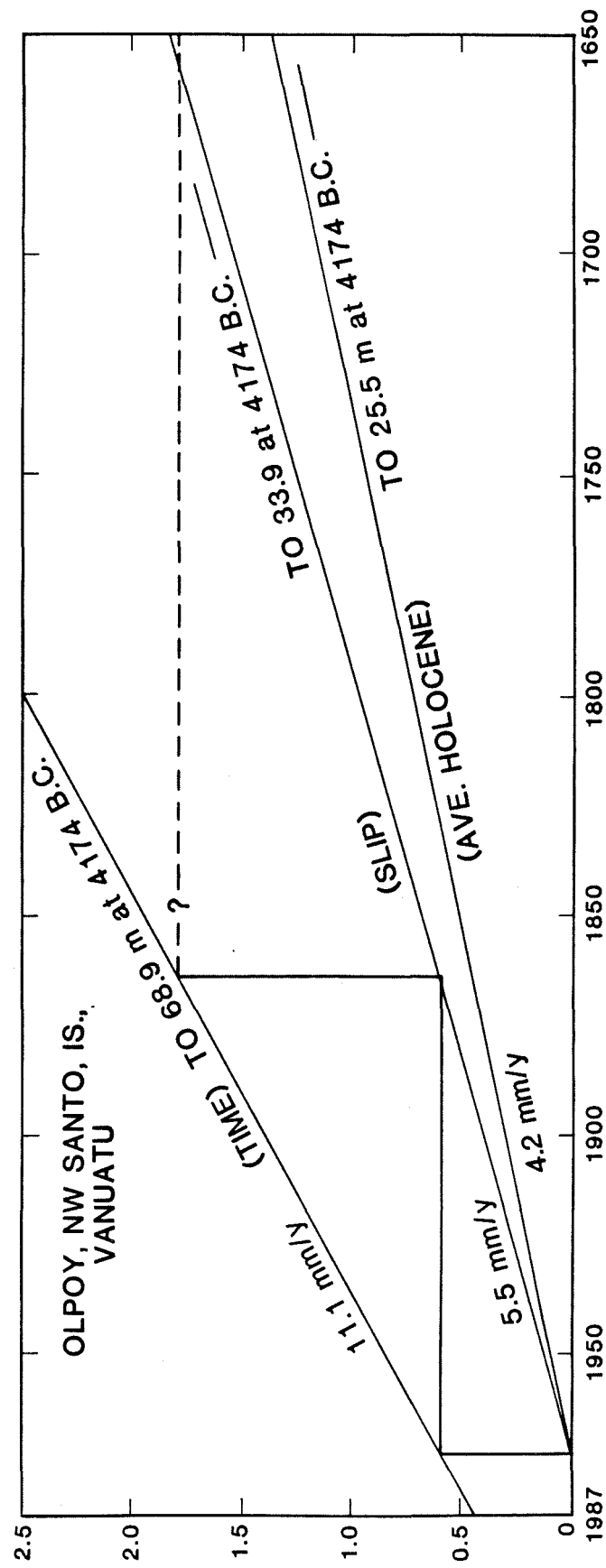
OLPOY, NW SANTO, IS.,
VANUATU
(TIME)
TO 68.9 m at 4174 B.C.
11.1 mm/y
?
(SLIP)
TO 33.9 at 4174 B.C.
5.5 mm/y
(AVE. HOLOCENE)
TO 25.5 m at 4174 B.C.
4.2 mm/y
HEIGHT (m)
2.5
2.0
1.5
1.0
0.5
0
1987
1950
1900
1850
1800
1750
1700
1650
GROWTH DATE (years A.D.)

Island is not periodic. The short term uplift rate, assuming a time predictable model is 11.2 mm/y, whereas a slip predictable model yields an uplift rate of 5.5 mm/y. The age of corals from the top of the Holocene terrace have not been determined, but if the age of these corals is the same as the age of MY2, then the uplift rate averaged over the past 6128 years is 4.2 mm/y. Thus, the short term uplift rate calculated using a time predictable model is much larger than the long term uplift rate, whereas the uplift rate calculated using a slip predictable model is similar to the long term uplift rate.

In summary, it appears that corals that grew in the past few centuries can be dated accurately using the ^{230}Th method. The precision of the ages is ± 3 to 5 years (2 sigma). A pair of corals that have the same present elevation from north Malekula Island have similar ^{230}Th ages and a pair of corals that have the same present elevation from northwest Santo Island have analytically indistinguishable ^{230}Th ages. This shows that each pair of corals died at the same time and could have been killed by co-seismic uplift. The estimated seismic recurrence interval for north Malekula Island is 236 years and for northwest Santo Island, 108 years. Short term uplift rates calculated using a slip predictable model are similar to the uplift rate averaged over the past 6128 years. Therefore the total Holocene uplift at both the Santo and Malekula localities can be accounted for by events similar to the 1973 and 1865 events on Santo and the 1965 and 1729 events on Malekula.

11. The timing of the last interglacial and two interstadial periods

11.1 The record of tectonic uplift and sea level change on Barbados and Vanuatu

As discussed in section 7.4.3 and shown in figures 7.14 and 7.15 and Table A2(IV and V), the ^{230}Th ages of the corals from the Worthing, Ventnor, and Rendezvous Hill Terraces on Barbados and the 110 to 130 m terrace doublet on Efate Island, Vanuatu fall into three distinct age groups. The bulk of the analyses are on samples from the Rendezvous Hill Terrace, which is thought to have developed during the last interglacial period (see section 6.5). These corals and the Efate Is. corals have ^{230}Th ages that range from 122.1 to 129.9 ky. The 2 sigma error in age due to analytical error is about 1 ky for each analysis. The range of ages for these corals is larger than the analytical error of the analyses. Analyses of two different fragments of FT-50 (A and C), which was collected from the Ventnor Terrace, yield analytically indistinguishable ages of 112.0 and 112.3 ky. FT-50 A and B are replicate analyses on different aliquots of the same solution. FT-50 B yields an age of 111.8 ky which, within analytical error, is identical to the age for FT-50 A. Analyses of two fragments of OC-51 which was collected from the Worthing Terrace give analytically indistinguishable ages of 87.5 and 87.9 ky.

The present heights of the samples from the Rendezvous Hill Terrace range from 30 to 55 m (Table A1(VI and V)). The Efate samples were collected from heights between 110 and 130 m. OC-51 was collected at an elevation of 18 m. FT-50 was collected at an elevation of 23 m. The elevation of the Rendezvous Hill Terrace near the location where

OC-51 was collected is 55 m. Near the locality where FT-50 was collected, the Rendezvous Hill Terrace has an elevation of 37 m. All of the Barbados corals are of the species Acropora palmata.

One would like to establish the initial heights of each of the above samples as a means of establishing the height of sea level at the time each sample grew. One would also like to explain why the samples from the Rendezvous Hill Terrace show a range of ages that are analytically distinct. Listed in Table 11.1 are the ^{230}Th age and present elevation of each of the samples from the Rendezvous Hill Terrace. The samples with the older ages have higher present elevations. This set of samples therefore meets the stipulation of the model discussed in section 4.2 and depicted in figures 4.2 and 4.3. The model may therefore be used to estimate the initial height of each sample, the rate of sea level rise at the time each sample grew, and the rate of tectonic uplift at each sample locality.

In order to accomplish this, one needs to know the height and time of the sea level maximum that occurred at about the time the Rendezvous Hill corals grew. Fossil coral reefs of about the same age (as determined from alpha-counting studies) in areas thought to be tectonically stable have present elevations of 6 m above sea level (Ku et al., 1974; Veeh, 1966). This is the value which I will use for the height of the sea level maximum (H_3 = 6 m). The age of such a coral from San Salvador Island, Bahamas has recently been determined using methods identical to those described in chapter 7 (J.H. Chen, personal communication). This age is 121 ky (T_3 = 121 ky).

As depicted in figure 4.3, the lower bound on the uplift rate for

Table 11.1. Elevations and ^{230}Th ages of Barbados corals.

Sample	Present elevation[a] (m above sea level)	^{230}Th age (ky)
RENDEZVOUS HILL TERRACE		
AFS-11	30	122.6
AFS-12	30	123.1
AFS-10	30	125.7
R-52	37	128.1
AFM-20	55	129.2
VENTNOR TERRACE		
FT-50	23	112.0
WORTHING TERRACE		
OC-51	18	87.7

[a] Elevations are read from topographic contours in figures 6.5 and 6.4.

each sample is given by $(H_1-H_3)/T_1$, and the upper bound is given by $(H_1-H_3)/T_3$. The upper bound on initial height for each sample is H_3(=6m), and the lower bound on initial height is $H_1-(H_1-H_3)(T_1/T_3)$. The calculated upper and lower bounds for uplift rate and initial height for each of the Rendezvous Hill samples are shown in Table 11.2. The uplift rates range from 0.19 to 0.38 m/ky. The initial heights have bounds ranging from 3 m to 6 m above sea level. If the model assumptions are correct and the corals grew close to the sea surface (see section 4.4), then the height of the sea surface at the time each coral grew must have been very close to the initial height of each of the corals. The bounds on initial height are all close to the value of the sea level maximum, are all above present sea level and are the same within three meters. This indicates that sea level height was rather constant between 129.2 and 122.6 ky ago and was quite high.

Bounds can be placed on the initial heights of OC-51 (Worthing Terrace), using the bounds on uplift rate calculated for AFM-20, which was collected from the Rendezvous Hill Terrace near the OC locality (Table 11.2). For OC-51, the initial height is between -15 and -17 m. The height of the Rendezvous Hill Terrace near the locality where FT-50 was collected is 37 m. This is the same height as R-52, which was collected from the Rendezvous Hill Terrace at another locality. Using the bounds on uplift rate for R-52, the calculated initial height of FT-50 is between -5 and -4 m. Although these heights are significantly below present sea level, they are much higher than sea level values of less than -100 m, which are thought to be associated with glacial maxima. These samples therefore grew when conditions were closer to

Table 11.2. Bounds on uplift rate and initial height for Barbados corals.

Sample	Bounds on uplift rate (m/ky)	Bounds on initial ht. (m above sea level)
RENDEZVOUS HILL TERRACE		
AFS-11	0.20-0.20	6 to 6
AFS-12	0.20-0.20	6 to 6
AFS-10	0.19-0.20	5 to 6
R-52	0.24-0.25	4 to 6
AFM-20	0.38-0.40	3 to 6
VENTNOR TERRACE		
FT-50	0.24-0.25[a]	-5 to -4
WORTHING TERRACE		
OC-51	0.38-0.40[b]	-17 to -15

[a] from R-52.
b from AFM-20.

interglacial conditions than to glacial conditions.

11.2 The relationship between sea level highs and the 65°N curve.

The three age ranges (section 11.1, figure 7.14, figure 7.15) all represent times when the earth's climate was close to interglacial conditions; the Rendezvous Hill samples represent the least glaciated conditions. These three age ranges have been superimposed on a graph of the summer solar insolation received at 65°N latitude as a function of time (Berger, 1978; figures 3.1, 3.2, 11.1, and 11.2). This curve has low values between 166 and 140 ky, rises to a very high value at 128 ky and drops to a very low value at 116 ky. It has maxima at 103 ky and 85 ky, then drops to a low value at 73 ky. The insolation value at 128 ky is the highest value in the past 200,000 years. The oldest range of coral ages represents a time when sea level was very high and probably the only time that sea level was above present sea level in the past 200,000 years. This range occurs almost exactly at the time of the insolation maximum at 128 ky. The oldest corals in this range may have grown as much as 2 ky before the insolation high; the youngest in this range grew as much as 6 ky after the insolation high.

Previous data (alpha-counting ages) had suggested the possibility that sea level was high about 140 ky ago (see sections 6.5 and 7.1). This would predate the 128 ky insolation high by more than 10 ky and could not be the direct result of orbital forcing. I have found no evidence for high sea level 140 ky ago. The relationship between the oldest range of ages and the highest insolation maximum suggests that this sea level high is the direct result of orbital forcing. The

Figure 11.1. The vertical axis represents the percent difference between the average summer solar insolation received at the top of the atmosphere at 65°N latitude at some time in the past and the present value of this quantity. The curve is drawn for the period of time between 160 ky ago and 70 ky ago (from Berger, 1978). Superimposed on this graph are the ranges of ages of the corals from the three terraces on Barbados and from Efate Is., Vanuatu (figures 7.14 and 7.15). The error bar denotes the typical 2 sigma error in each age determination. The oldest range of ages is from the most prominent terrace (figures 4.8, 4.11, 6.4, and 6.5) and represents the highest position of sea level (3 to 6 m above present sea level, Table 11.2) in the last 200 ky. Terraces of about this age are prominent features along shorelines around the world. The range of ages for this terrace corresponds almost exactly to the time of the highest value of summer solar insolation in the past 200 ky. This indicates that this sea level high (the last interglacial period) may be the direct result of orbital forcing. The range of ages suggests that the last interglacial period lasted from 130 ky ago to at least 122 ky ago, a period of at least 8 ky. The range of ages is offset slightly to the young side of the insolation high. The youngest terrace, represented by the ages in this figure, formed when sea level was 16 m below its present value (Table 11.2). This age slightly predates an insolation high and might be the result of orbital forcing. The other age range (112 ky) represents a terrace that formed when sea level was 5 m below present sea level (Table 11.2). Its age does not correspond to an insolation high and does not appear to be the direct result of orbital forcing.

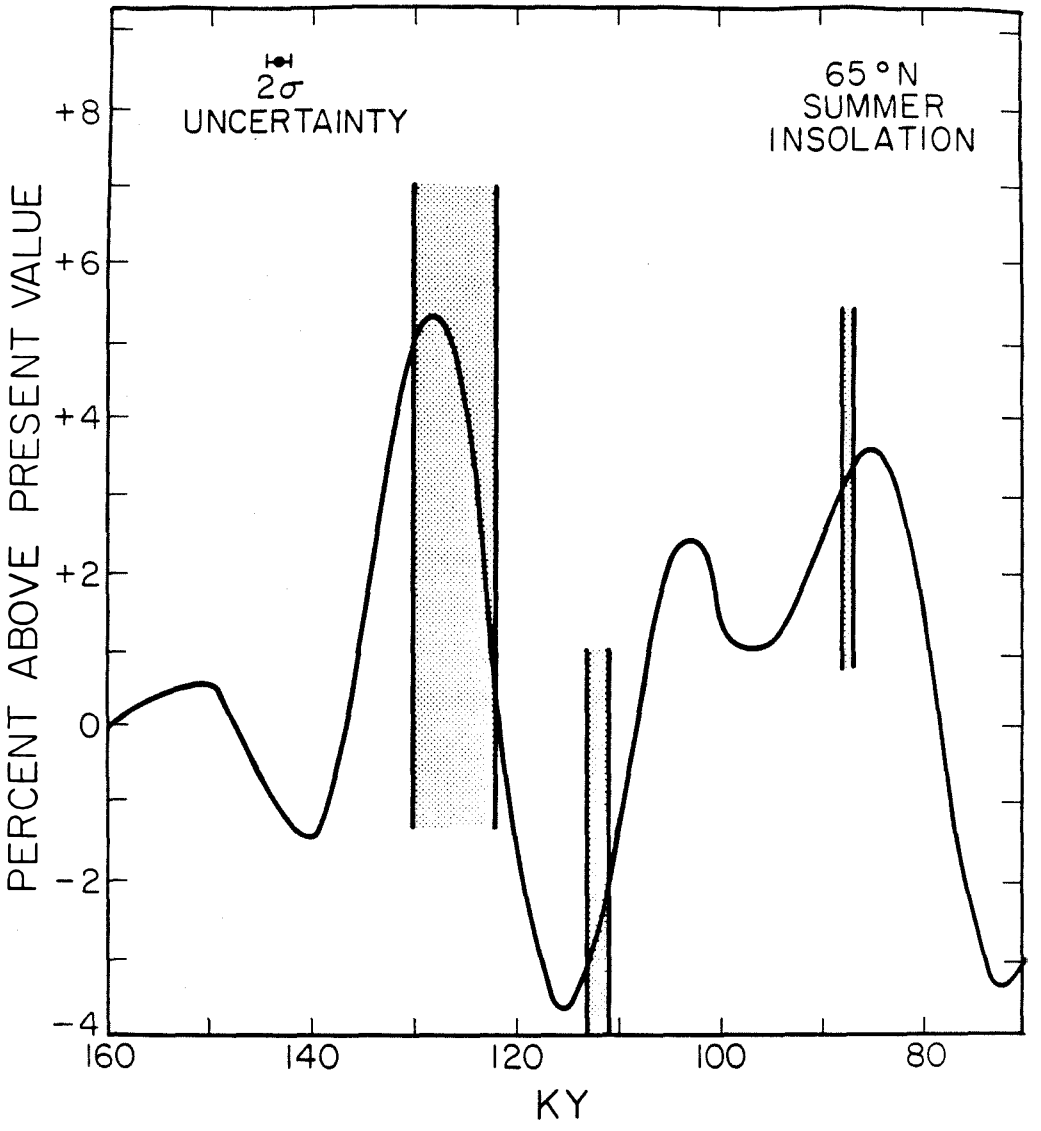
2σ
UNCERTAINTY
65°N
SUMMER
INSOLATION
PERCENT ABOVE PRESENT VALUE
+8
+6
+4
+2
0
-2
-4
160
140
120
100
80
KY

Figure 11.2. A diagram similar to figure 11.1, but the time range has been extended to include the period of time between 70 ky ago and the present. An additional stippled band that represents the period of time over which sea level has been within a few meters of its present value (see figure 10.1, Scholl et al., 1969; Neumann, 1971; Lighty et al., 1978) in the Holocene has been added. This represents the second highest (after the 130 to 122 ky event, last interglacial period) prolonged period of high sea level in the last 200 ky. It occurs just after the second highest insolation peak in the last 200 ky. It appears that prolonged periods of very high sea level (interglacial periods, 130 to 122 ky and 6 to 0 ky) may be the direct result of orbital forcing, but shorter periods when sea level is not quite as high (interstadial periods, 88 ky and 112 ky) may be indirectly related to orbital forcing or may not be related to orbital forcing at all.

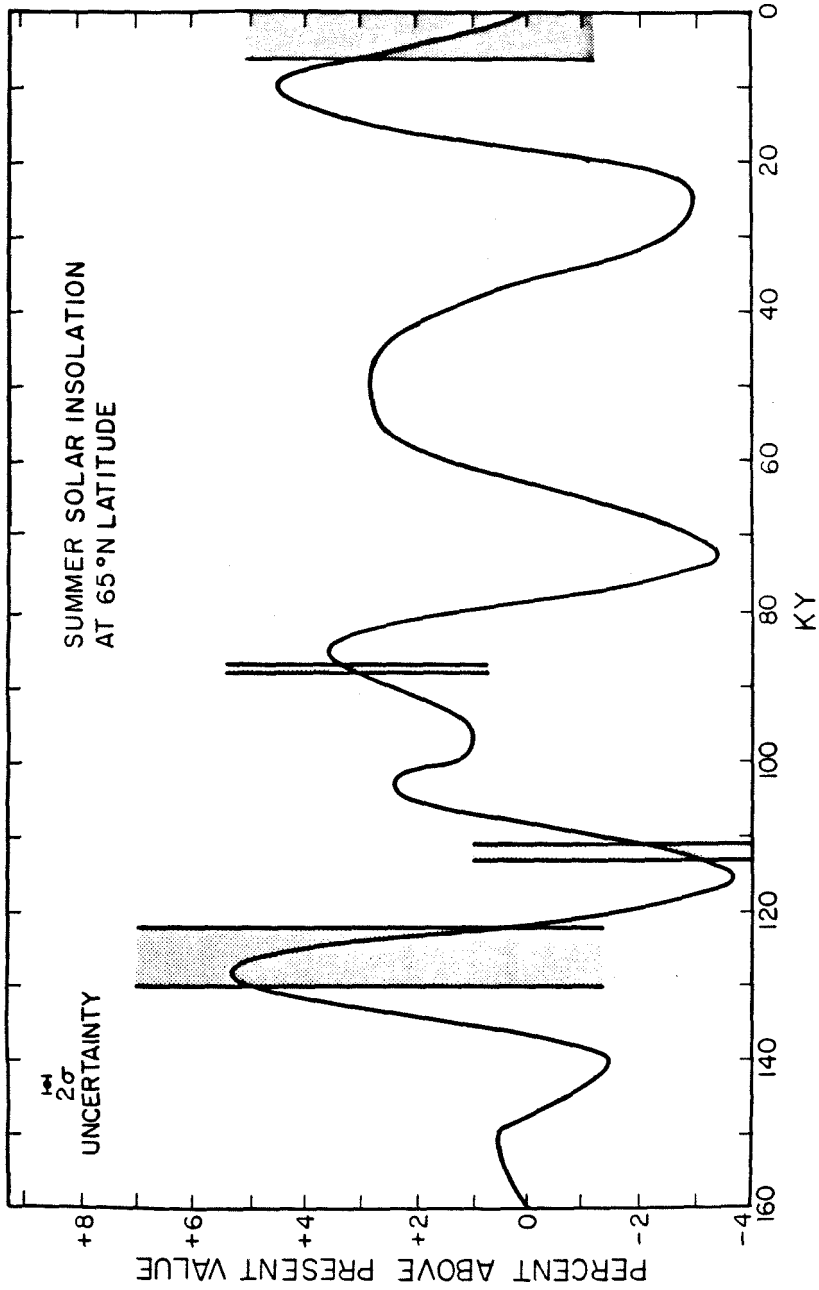
SUMMER SOLAR INSOLATION
AT 65°N LATITUDE
2σ
UNCERTAINTY
PERCENT ABOVE PRESENT VALUE
+8
+6
+4
+2
0
-2
-4
0
20
40
60
80
100
120
140
160
KY

apparent high position (6 m above present) of sea level 130 ky ago requires that, as the insolation curve increases, the phase lag between the insolation and sea level curves is small. The high position of sea level, 6 ky after the insolation peak, suggests that as the insolation curve decreases, the phase lag is significantly larger. From the range of ages, it appears that sea level was high for at least 8 ky during the last interglacial period.

The youngest coral (87.7 ky) grew about 2 ky before the insolation high at 85 ky. The apparent high position (16 m below present) of sea level at this time could be the result of orbital forcing. However, the 112 ky old coral grew 9 ky before the 103 ky insolation high at a time of relatively low insolation. The relatively high position of sea level (5 m below present) at this time does not appear to coincide with an insolation high and does not appear to be the direct result of orbital forcing. Even if an insolation curve for a somewhat higher or lower latitude than 65°N is chosen, the insolation high - sea level high relationships are similar to those described above (see figure 3.2).

In addition to the three Pleistocene sea level highs that were dated in this study and depicted in figure 11.1, the sea level curve for the latter part of the Holocene is well known (see Scholl et al., 1969; Neumann, 1971; Bloom, 1980a; Lighty et al., 1978). The Enriquillo Valley data (section 10.1, figure 10.1) are generally consistent with the earlier curves. Figure 10.1 shows that sea level was within several meters of its present value 6000 years ago and has remained close to present sea level since then. Figure 11.2 contains

the same information as figure 11.1, but the time axis has been extended and a stippled band representing Holocene high sea level added. The rise in Holocene sea level occurred just after a large insolation peak.

The relationship between sea level highs and insolation highs does not appear to be the same for each of the four sea level highs (figure 11.2). Consider the heights of each sea level high and the value of the insolation maxima. The highest value of 65°N summer solar insolation in the last 200 ky is the value at 128 ky. The most prominent coral terrace on Barbados that is younger than 200 ky is the Rendezvous Hill Terrace (122 to 129 ky). There are prominent terraces and reefs from around the world that have ages that are similar to the age of this terrace. The height of sea level when the Rendezvous Hill Terrace formed (about 6 m) is the highest sea level height in the past 200 ky. Therefore, the time of the highest sea level in the past 200 ky corresponds to the time of the highest insolation value and may be the direct result of orbital forcing. The next highest insolation value in the past 200 ky occurred 10 ky ago. The next highest (0 m) prolonged period of high sea level (present interglacial period) occurred just after this insolation high and therefore appears to be related to it with some phase lag. The other two coral terraces that I have dated are less prominent and probably represent shorter events. The estimated sea level heights at these times (-5 m and -16 m) are also significantly lower than the heights of the 122 to 129 ky and the 6 ky to present events. The time of the -16 m event may correspond to the time of an insolation high, but the time of the -5 m event does not

correspond to the time of an insolation high.

At times of very high insolation, the earth's climate appears to respond directly to orbital forcing; however, at times of slightly lower insolation, fluctuations in climate may be indirectly related to orbital forcing (e.g., Peltier and Hyde, 1985; see section 3.4) or not related to orbital forcing at all. The cause of this kind of response is not clear. However, if this is the response, a component of climatic variability at the period of eccentricity would be expected because extremes in the 65°N curve generally occur at times of high eccentricity. The results of this work suggest a component of climatic variability at the approximate period of eccentricity (100 ky, as observed in the oxygen isotope record; Hays et al., 1976) should be present and that the origin of this component may be related to the nature of the earth's response to orbital forcing.

REFERENCES

Agassiz, L. 1840. Etudes sur les glaciers. Neuchatel: privately published.

Aharon, P., and Chappell, J.M.A. 1986. Oxygen isotopes, sea level changes, and the temperature history of a coral reef environment in New Guinea over the last 105 years. Paleogeogr. Paleoclim. Paleoecol. 56: 337-374.

Anderson, R.F. 1982. Concentration, vertical flux and remineralization of particulate uranium in seawater. Geochim. Cosmochim. Acta 46: 1293-1299.

Arnold, J.R., and Anderson, E.C. 1957. The distribution of ^{14}C in nature. Tellus 9: 28-32.

Attree, R.W., Cabell, M.J., Cushing, R.L., and Pieron, J.J. 1962. A calorimetric determination of the half life of Th-230 and consequent revision of its neutron capture cross-section. Can. Jour. Phys. 40: 194-201.

Bailey, R.A., Dalrymple, G.B., and Lanphere, M.A. 1976. Volcanism, structure, and geochronology of the Long Valley Caldera, Mono County, California. Jour. Geophys. Res. 81: 725-744.

Baker, P.A., and Weber, J.N. 1975. Coral growth rate: Variation with depth. Earth Planet. Sci. Lett. 27: 57-61.

Barnes, D.J. 1973. Growth in colonial scleractinians. Bull. Mar. Sci. 23: 280-298.

Barnes, I.L., Carpenter, B.S., Garner, E.S., Gramlich, J.W., Kuehner, E.C., Machlan, L.A., Maienthal, E.J., Moody, J.R., Moore, L.J. Murphy, T.J., Paulsen P.J., Sappenfield, K.M., and Shields, W.R. 1972. Isotopic abundance ratios and concentrations of selected elements in Apollo 14 samples. Proc. 3rd Lunar Sci. Conf. 2: 1465-1472.

Barnes, J.W., Lang, E.J., and Potratz H.A., 1956. The ratio of ionium to uranium in coral limestone. Science 124: 175-176.

Barnes, R.D. 1974. Invertebrate Zoology. 3rd ed. Philadelphia: W.B. Saunders Co.

Bateman, H. 1910. The solution of a system of differential equations occurring in the theory of radioactive transformations. Proc. Cambridge Phil. Soc. 15: 423-427.

Becquerel, H. 1896a. Sur les radiations emises par phosphorescence. Comptes Rendu 122: 420-421.

_____. 1896b. Sur les radiations invisibles emises par les corps phosphorescents. Comptes Rendu 122: 501-502.

_____. 1896c. Sur quelques proprietes nouvelles des radiations invisibles emises par divers corps phosphorescents. Comptes Rendu 122: 559-564.

_____. 1896d. Sur les radiations invisibles emises par les sels d'uranium. Comptes Rendu 122: 689-694.

_____. 1896e. Sur les proprietes differents des radiations invisibles emises par les sels d'uranium, et du rayonnement de la paroi anticathodique d'un tube de Crookes. Comptes Rendu 122: 762-767.

Bender M.L., Fairbanks, R.G., Taylor, F.W., Matthews, R.K., Goddard, J.G., and Broecker, W.S. 1979. Uranium series dating of the Pleistocene reef tracts of Barbados, West Indies. Geol. Soc. Amer. Bull., part I 90: 577-594.

Berger, A.L. 1978. Long-term variations of caloric insolation resulting from the earth's orbital elements. Quat. Res. 9: 139-167.

Bevington, P.R. 1969. Data Reduction and Error Analysis for the Physical Sciences. New York: Mcgraw-Hill Book Co.

Birchfield, G.E., Weertman, J., and Lunde, A.T. 1981. A paleoclimatic model of Northern Hemisphere ice sheets. Quat. Res. 15: 126-142.

Biscaye, P.E., and Ettriem, S.L. 1977. Suspended particulate loads and transports in the nepheloid layer of the abyssal Atlantic Ocean. Mar. Geol. 23: 155-172.

Bloom, A.L. 1980a. Late Quaternary sea level change on South Pacific Coasts: a study in tectonic diversity. In Earth Rheology, Isostasy, and Eustasy, ed. N.-A. Morner, pp. 505-516. New York: Wiley.

_____. 1980b. The sea level-record of the structure of an ice age. AMQUA abstr. and prog., Orono, Me Meeting: 29-30.

Bloom, A.L., Broecker, W.S., Chappell, J.M.A., Matthews, R.K., and Mesollela, K.J. 1974. Quaternary sea level fluctuations on a tectonic coast: new $^{230}Th/^{234}U$ dates on the Huon Peninsula, New Guinea. Quat. Res. 4: 185-205.

Bloom, A.L., Jouannic, C., and Taylor, F.W. 1978. Preliminary radiometric ages from the uplifted Quaternary coral reefs of Efate. In Geology of Efate and Offshore Islands, R.P. Ash, J.N. Carney, and A. Macfarlane, New Hebrides Geol. Surv. Reg. Rep. pp. 47-49.

Boltwood, B.B. 1907a. Note on a new radio-active element. Amer. Jour. Sci. 24: 370-372.

_____. 1907b. The origin of radium. Nature 76: 544-545.

Broecker, W.S. 1963. A preliminary evaluation of uranium series inequilibrium as a tool for absolute age measurements on marine carbonates. Jour. Geophys. Res. 68: 2817-2834.

Broecker, W.S., and Li, Y.H. 1970. Interchange of water between the major oceans. Jour. Geophys. Res. 75: 3545-3551.

Broecker, W.S., and Peng, T.H. 1982. Tracers in the sea. New York: Eldigio.

Broecker, W.S., and Thurber, D.L. 1965. Uranium series dating of corals and oolites from Bahaman and Florida Key limestones. Science 149: 58-60.

Broecker, W.S., Thurber, D.L., Goddard, J., Ku, T.L., Matthews, R.K., and Mesollela, K.J. 1968. Milankovitch hypothesis supported by precise dating of coral reefs and deep sea sediments. Science 159: 297-300.

Chen, J.H., Edwards, R.L., and Wasserburg, G.J. 1986. ^{238}U, ^{234}U, and ^{232}Th in seawater. Earth Planet. Sci. Lett. 80: 241-251.

Chen, J.H., and Wasserburg, G.J. 1980. A search for isotopic anomalies in uranium. Geophys. Res. Lett. 7: 275-278.

_____, and _____. 1981a. Isotopic determination of uranium in picomole and subpicomole quantities. Anal. Chem. 53: 2060-2067.

_____, and _____. 1981b. The isotopic composition of uranium and lead in Allende inclusions and meteorite phosphates. Earth Planet. Sci. Lett. 52: 1-15.

_____, and _____. 1983. The isotopic composition of silver and lead in the Cape York meteorite. Geochim. Cosmochim. Acta 47: 1725-1737.

_____, and _____. 1984. $^{234}U/^{238}U$ and lead isotopic compositions in hot springs on the East Pacific Rise at 21°N. Geol. Soc. Amer. abstr. prog. 16: 469.

Chen, J.H., Wasserburg, G.J., Von Damm, K.L., and Edmond, J.M. 1983. Pb, U, and Th in hot springs on the East Pacific Rise at 21°N and Guaymas Basin, Gulf of California. Trans. Amer. Geophys. Union 64: 724.

Cherdyntsev, V.V. 1955. Transactions of the third session of the commission for determining the absolute age of geological formations. Izv. Akad. Nauk SSSR, Moscow: 175.

Clark, J.A., Farrell, W.E., and Peltier, W.R. 1978. Global changes in postglacial sea level: a numerical calculation. Quat. Res. 9: 265-287.

Constantz, B.R. 1986. The primary surface area of corals and variations in their susceptibility to diagenesis. In Reef Diagenesis, eds. J.J. Schroeder, and B.H. Purser, pp.53-76, Berlin: Springer-Verlag.

Constantz, B.R., and Meike, A. (in prep.). Calcite centers of calcification in Mussa angulosa.

Craig, H. 1957. The natural distribution of radiocarbon and the exchange time of carbon dioxide between atmosphere and sea. Tellus 9: 1-17.

Curie, P., and Curie, M. 1898. Sur une substance nouvelle radio-active contenue dans la pechblende. Comptes Rendu 127: 175-178.

De Bievre, P., Lauer, K.J., Le Duigon, Y., Moret, H., Muschenborn, G., Spaepen, J., Spernol, A., Vaninbroukx, R., and Verdingh, V. 1971. The half-life of ^{234}U, in Proc. Intl. Conf. Chem. Nucl. Data, Measurement and Applications, Canterbury, ed. M.L. Hurrell, pp. 221-225, London: Inst. Civil Engineers.

Dodge, R.E., Fairbanks, R.G., Benninger, L.K., and Maurrasse, F. 1983. Pleistocene sea levels from raised coral reefs of Haiti. Science 219: 1423-1425.

Druffel, E.M. 1981. Radiocarbon in annual coral rings from the eastern tropical Pacific Ocean. Geophys. Res. Lett. 8: 59-62.

Emiliani, C. 1955. Pleistocene temperatures. Jour. Geol. 63: 538-578.

Fairbanks, R.G., and Matthews, R.K. 1978. The marine oxygen isotope record in Pleistocene coral, Barbados, West Indies. Quat. Res. 10: 181-196.

Fleming, E.H., Ghiorso, A., and Cunningham, B.B. 1952. The specific alpha activities and half-lives of ^{234}U, ^{235}U, and ^{236}U. Phys. Rev. 38: 642-652.

Flint, R.F. 1971. Glacial and Quaternary geology. New York: Wiley.

Friedlander, G., Kennedy, J.W., Macias, E.S., and Miller, J.M. 1981. Nuclear and radiochemistry. 3rd ed. New York: Wiley.

Garner, E.L., Machlan, L.A., and Shields, W.R. 1971. Uranium isotopic reference materials. Nation. Bur. Stand. Spec. Pub. 260-17.

Gillespie, A.R., Huneke, J.C., and Wasserburg, G.J. 1984. Eruption age of Pleistocene basalt from $^{40}Ar/^{39}Ar$ analysis of partially degassed xenoliths. Jour. Geophys. Res. 88: 4997-5008.

Goreau, T.F. 1959. The ecology of Jamaican coral reefs: I. Species composition and zonation. Ecology 40: 67-90.

Goreau, T.F., Goreau, N.I., and Goreau, T.J. 1979. Corals and coral reefs. Sci. Amer. 110-120.

Goreau, T.F., and Wells, J.W. 1967. The shallow-water scleractinia of Jamaica: revised list of species and their vertical distribution range. Bull. Mar. Sci. 17: 442-453.

Harmon, R.S., Ku, T.L., Matthews, R.K., and Smart, P.L. 1979. Limits of U-series analyses: Phase I results of the Uranium-Series Intercomparison Project. Geol. 7: 405-409.

Harmon, R.S., Mitterer, R.M., Kriausakul, N., Land, L.S., Schwarcz, H.P., Garrett, P., Larson, G.J., Vacher, H.L., and Rowe, M. 1983. U-series and amino acid racemization geochronology of Bermuda: implications for eustatic sea level fluctuation over the past 250,000 years. Paleogeogr. Paleoclimatol. Paleoecol. 44: 41-70.

Hays, J.D., Imbrie, J., and Shackelton, N.J. 1976. Variations in the earth's orbit: pacemaker of the ice ages. Science 194: 1121-1132.

Hopley, D. 1982. The geomorphology of the Great Barrier Reef: Quaternary development of coral reefs. New York: Wiley.

Hyde, W.T., and Peltier, W.R. 1985. Sensitivity experiments with a model of the ice age cycle: the response to harmonic forcing. Jour. Atmos. Sci. 42: 2170-2188.

Imbrie, J., Hays, J.D., Martinson, D.G., McIntyre, A., Mix, A.C., Morley, J.J., Pisias, N.G., Prell, W.L., and Shackleton, N.J. 1984. The orbital theory of Pleistocene climate: support from a rivised chronology of the marine $\delta^{18}O$ record. In Milankovitch and Climate, Part I, eds. A.L. Berger, J. Imbrie, J.D. Hays, G. Kukla, and B. Saltzman, pp. 269-305. Boston: D. Reidel.

Imbrie, J., and Imbrie, K.P. 1986. Ice ages: Solving the Mystery. Cambridge: Harvard Univ. Press.

Isaac, N., and Picciotto, E. 1953. Ionium determination in deep-sea sediments. Nature 171: 742-743.

Ivanovich, M., and Harmon, R.S., eds. 1982. Uranium Series Disequilibrium: Applications to Environmental Problems. Oxford: Clarendon.

Jaffey, A.H., Flynn, K.F., Glendenin, L.W., Bentley, W.C., and Essling, A.M. 1971. Precision measurements of half-lives and specific activities of ^{235}U and ^{238}U. Phys. Rev. C 4: 1889-1906.

Joly, J. 1908. On the radium-content of deep-sea sediments. Phil. Mag. 16: 190-197.

Kaufman, A. 1986. The distribution of $^{230}Th/^{234}U$ ages in corals and the number of last interglacial high sea stands. Quat. Res. 25: 55-62.

Kaufman, A., Broecker, W.S., Ku, T.L., and Thurber, D.L. 1971. The status of U-series methods of mollusk dating. Geochim. Cosmochim. Acta 35: 1155-1183.

Klein, J., Lerman, J.C., Damon, P.E., and Ralph, E.K. 1982. Calibration of radiocarbon dates: tables based on the consensus data of the Workshop on Calibrating the Radiocarbon Time Scale. Radiocarbon 24: 103-150.

Knutson, D.W., Buddemeier, R.W., and Smith, S.V. 1972. Coral chronometers: seasonal growth bands in reef corals. Science 177: 270-272.

Ku, T.L. 1968. Protactinium 231 method of dating coral from Barbados Island. Jour. Geophys. Res. 73: 2271-2276.

Ku, T.L., Kimmel, M.A., Easton, W.H., and O'Neil, T.J. 1974. Eustatic sea level 120,000 years ago on Oahu, Hawaii. Science 183: 959-962.

Ku, T.L., Knauss, K.G., and Mathieu, G.G. 1977. Uranium in the open ocean: concentration and isotopic composition. Deep-sea Res. 24: 1005-1017.

Le Roux, L.J., and Glendinen, L.E. 1963. Half-life of ^{232}Th. Proc. Nat. Meet. Nucl. Energy, Pretoria, S. Africa: 83-94.

Lighty, R.G., MacIntyre, I.G., and Stuckenrath, R. 1978. Submerged early Holocene barrier reef south-east Florida shelf. Nature 276: 59-60.

Lounsbury, M., and Durham, R.W. 1971. The alpha half-life of 234-U. In Proc. Intl. Conf. Chem. Nucl. Data, Measurement and Applications, Canterbury, ed. M.L. Hurrell, pp. 215-219. London: Inst. Civil Engineers.

MacIntyre, I.G., Burke, R.B., and Stuckenrath, R. 1977. Thickest recorded Holocene reef section, Isla Perez core hole, Alacran Reef, Mexico. Geol. 5: 749-754.

Mankinen, E.A., and Dalrymple, G.B. 1979. Jour. Geophys. Res. 84: 615-626.

Mann, P., Taylor, F.W., Burke, K., and Kulstad, R. 1984. Subaerially exposed Holocene coral reef, Enriquillo Valley, Dominican Republic. Geol. Soc. Amer. Bull. 95: 1084-1092.

Marshall, J.F., and Thom, B.G. 1976. The sea level in the last interglacial. Nature 263: 120-121.

Meadows, J.W., Armani, R.J., Callis, E.L., and Essling, A.M. 1980. Half-life of ^{230}Th. Phys. Rev. C 22: 750-754.

Mesollela, K.J. 1967. Zonation of uplifted Pleistocene coral reefs on Barbados, West Indies. Science 156: 638-640.

_____. 1968. The uplifted reefs of Barbados: physical stratigraphy, facies relationships, and absolute chronology. Ph.D. dissertation Brown University.

Mesollela, K.J., Matthews, R.K., Broecker, W.S., and Thurber, D.L. 1969. The astronomical theory of climatic change: Barbados data. Jour. Geol. 77: 250-274.

Milankovitch, M.M. 1941. Canon of Insolation and the Ice Age Problem. Beograd: Koniglich Serbische Akademie. (English translation, 1969. Washington D.C.: Israel Program for Scientific Translations.)

Moore, W.S. 1982. Late Pleistocene sea-level history. In, Uranium Series Disequilibrium: Applications to Environmental Problems, eds. M. Ivanovich and R.S. Harmon, pp. 481-495. Oxford: Clarendon.

Neumann, A.C. 1971. Quaternary sea-level data from Bermuda. Quaternaria 14: 41-43.

Nozaki, Y., Horibe, Y., and Tsubota, H. 1981. The water column distributions of thorium isotopes in the western North Pacific. Earth Planet. Sci. Lett. 54: 203-216.

Ogilvie, M. 1896. Microscopic and systematic study of Madreporarian types of corals. Phil. Tran. Roy. Soc. Lon. B 187: 83-345.

Papanastassiou, D.A. 1970. Initial strontium isotopic abundances and the resolution of small time differences in the formation of planetary objects. Ph.D. thesis, California Institute of Technology.

Peltier, W.R., and Hyde, W.T. 1986. Sensitivity experiments with a model of the ice age cycle: the response to Milankovitch forcing. Jour. Atmos. Sci. 44: 1351-1375.

Piggot, C.S. 1933. Radium content of ocean-bottom sediments. Amer. Jour. Sci. 25: 229-238.

Piggot, C.S., and Urry, W.D. 1941. Radioactivity of ocean sediments. III. Radioactive relations in ocean water and bottom sediment. Amer. Jour. Sci. 239: 81-91.

_____, and _____. 1942. Time relations in ocean sediments. Bull. Geol. Soc. Amer. 53: 1187-1210.

Radicati di Brozolo, F., Huneke, J.C., and Papanastassiou, D.A., and Wasserburg, G.J. 1981. ^{39}Ar-^{40}Ar and Rb-Sr age determinations on Quaternary volcanic rocks. Earth Planet. Sci. Lett. 53: 445-456.

Revelle, R., and Suess, H.E. 1957. Carbon dioxide exchange between atmosphere and ocean and the question of an increase of atmospheric CO_2 during the past decades. Tellus 9: 18-27.

Rosholt, J.N., Doe, B.R., and Tatsumoto, M. 1966. Evolution of the isotopic composition of uranium and thorium in soil profiles. Geol. Soc. Amer. Bull. 77: 987-1004.

Rosholt, J.N., and Tatsumoto, M. 1970. Isotopic composition of uranium and thorium in Apollo 11 samples. Proc. Apollo 11 Lunar Sci. Conf. 2: 1499-1502.

Rutherford, E. 1905. Radioactivity. Cambridge: Cambridge University Press.

Rutherford, E., and Soddy, F. 1902. The cause and nature of radioactivity: Part II. Phil. Mag. Series 6 4: 569-585.

Scholl, D.W., Craighead, F.C., and Stuiver, M. 1969. Florida curve revised: its relation to coastal sedimentation rates. Science 163: 562-564.

Shackleton, N.H. 1967. Oxygen isotope analyses and Pleistocene temperatures re-assessed. Nature 215: 15-17.

Shackleton, N.J., and Opdyke, N.D. 1973. Oxygen isotope and paleomagnetic stratigraphy of equatorial Pacific core V28-238: oxygen isotope temperatures and ice volumes on a 10^5 year and 10^6 year scale. Quat. Res. 3: 39-55.

Shimazaki, K., and Nakata, T. 1980. Time-predictable recurrence model for large earthquakes. Geophys. Res. Lett. 7: 279-282.

Somayajulu, B.L.K., Broecker, W.S., and Goddard, J. 1985. Dating Indian corals by U-decay-series methods. Quat. Res. 24: 235-239.

Somayajulu, B.L.K., Tatsumoto, M., Rosholt, J.N., and Knight, R.J. 1966. Disequilibrium of the ^{238}U series in basalt. Earth Planet. Sci. Lett. 1: 387-391.

Stuiver, M. 1982. A high-precision calibration of the AD radiocarbon time scale. Radiocarbon 24: 1-26.

Szabo, B.J. 1982. Extreme fractionation of $^{234}U/^{238}U$ and $^{230}Th/^{238}U$ in spring waters, sediments, and fossils at the Pomme de Terre Valley, southwestern, Missouri. Geochim. Cosmochim. Acta 46: 1675-1679.

Szabo, B.J., and Rosholt, J.N. 1969. Uranium series dating of Pleistocene molluscan shells from S. California: an open system model. Jour. Geophys. Res. 74: 3253-3260.

Tatsumoto, M., and Goldberg, E.D. 1959. Some aspects of the marine geochemistry of uranium. Geochim. Cosmochim. Acta 17: 201-208.

Taylor, F.W., Frohlich, C., Lecolle, J., and Strecker, M. 1987. Analysis of partially emerged corals and reef terraces in the Central Vanuatu Arc: comparison of contemporary coseismic and non-seismic with Quaternary vertical movements. Jour. Geophys. Res. 92: 4905-4933.

Taylor, F.W., Isacks, B.L., Jouannic, C., Bloom, A.L., and Dubois, J. 1980. Coseismic and Quaternary vertical movements, Santo and Malekula Islands, New Hebrides Island Arc. Jour. Geophys. Res. 85: 5367-5381.

Taylor, F.W., Jouannic, C., and Bloom, A.L. 1985a. Quaternary uplift of the Torres Islands, northern New Hebrides frontal arc: comparison with Santo and Malekula Islands, central New Hebrides frontal arc. Jour. Geol. 93: 419-438.

Taylor, F.W., Mann, P., Valastro, S., and Burke, K. 1985b. Stratigraphy and radiocarbon chronology of a subaerially exposed Holocene coral reef, Dominican Republic. Jour. Geol. 93: 311-332.

Thurber, D.L. 1962. Anomalous $^{234}U/^{238}U$ in nature. Jour. Geophys. Res. 67: 4518-4520.

Thurber, D.L., Broecker, W.S., Blanchard, R.L., and Potratz, H.A. 1965. Uranium-series ages of Pacific atoll coral. Science 149: 55-58.

Urry, W.D. 1941. The radioactive determination of small amounts of uranium. Amer. Jour. Sci. 239: 191-203.

Veeh, H.H. 1966. $^{230}Th/^{238}U$ and $^{234}U/^{238}U$ ages of Pleistocene high sea level stand. Jour. Geophys. Res. 71: 3379-3386.

Veeh, H.H., and Chappell, J.M.A. 1970. Astronomical theory of climatic change: support from New Guinea. Science 167: 862-865.

Vernekar, A.D. 1972. Long-period global variations of incoming solar radiation. Meteorological Monographs, vol. 12, no. 34. Lancaster: Lancaster Press.

Wasserburg, G.J., Jacobsen, S.B., DePaolo, D.J., McCulloch, M.T., and Wen, T. 1981. Precise determination of Sm/Nd ratios, Sm and Nd isotopic abundances in standard solutions. Geochim. Cosmochim. Acta 45: 2311-2323.

Wasserburg, G.J., Papanastassiou, D.A., Nenow, E.V., and Bauman, C.A. 1969. A programmable magnetic field mass spectrometer with on-line data processing. Rev. Sci. Instrum. 40: 288-295.

Wells, J.W. 1957. Coral Reefs. Geol. Soc. Amer. Memoir 67. 1: 609-631.

APPENDIX A: DATA TABLES

A1. ^{238}U and ^{232}Th concentrations in corals and a mollusk and information about samples.

Sample[a]	Genus and species	Locality	Present elevation above sea level (m)[b]	^{238}U(nmoles/g)[c,d]	^{232}Th(pmoles/g)[d,e]	($^{232}Th/^{238}U$)(10^5)
I. HOLOCENE, VANUATU						
CWS-A-1b	Goniastria retiformis	NW Santo Is. (OLP, Taylor et al., 1987)	~ 0	9.74 ± 0.02	0.187 ± 0.002	1.92 ± 0.02
CWS-A-1d	Goniastria retiformis	NW Santo Is. (OLP, Taylor et al., 1987)	~ 0	10.51 ± 0.02	0.340 ± 0.003	3.24 ± 0.03
CWS-C	Goniastria retiformis	NW Santo Is. (OLP, Taylor et al., 1987)	1.8	11.30 ± 0.01	0.235 ± 0.002	2.08 ± 0.02
CWS-D-1	Goniastria retiformis	NW Santo Is. (OLP, Taylor et al., 1987)	1.8	10.49 ± 0.03	0.152 ± 0.003	1.45 ± 0.03
-2[rh]	-	-	-	10.75 ± 0.03	0.092 ± 0.003	0.86 ± 0.03
CWS-F-1	Platygyra -	NW Santo Is. (OLP, Taylor et al., 1987)		10.21 ± 0.02	0.147 ± 0.002	1.44 ± 0.02
TAN-E-1g	Platygyra -	Tangoa Is., south of Santo Is. (TAN, Taylor et al., 1980)	~ 0	10.80 ± 0.04	0.083 ± 0.003	0.77 ± 0.03
MAF	Goniastria retiformis	north Malekula Is. (M-A, Taylor et al., 1980)	1.3	9.13 ± 0.02	0.032 ± 0.002	0.35 ± 0.02
MAG	Goniastria retiformis	north Malekula Is. (M-A, Taylor et al., 1980)	1.3	9.98 ± 0.01	0.081 ± 0.002	0.81 ± 0.02
MY2	Favia -	north Malekula Is. (MY, Taylor et al., 1980)	15.3	10.53 ± 0.02	0.047 ± 0.002	0.45 ± 0.02
II. HOLOCENE, ENRIQUILLO VALLEY, HISPANIOLA						
PR-D-1	Montastria annularis	Gully 1 km E of Canada Honda, NW Enriquillo Valley	-7	9.90 ± 0.02	0.144 ± 0.004	1.45 ± 0.04
PR-H-2	Siderastria radians	Gully 1 km E of Canada Honda, NW Enriquillo Valley	-14.1	10.96 ± 0.01	0.247 ± 0.004	2.25 ± 0.04
PR-H-1	Siderastria sideria	Gully 1 km E of Canada Honda, NW Enriquillo Valley	-19.0	10.23 ± 0.02	0.140 ± 0.004	1.37 ± 0.04
CH-8	Siderastria radians	Canada Honda, NW Enriquillo Valley (Taylor et al., 1985)	-33	9.68 ± 0.01	0.279 ± 0.002	2.88 ± 0.02
CH-18	Siderastria sideria	Canada Honda, NW Enriquillo Valley	-34.2	9.70 ± 0.01	0.668 ± 0.004	6.89 ± 0.04
III. HOLOCENE, BARBADOS						
D.W.	Acropora palmata	Off of W. Barbados, submerged terrace in Deep Water Harbor	-4	13.12 ± 0.02	0.09 ± 0.04	0.7 ± 0.3

Sample[a]		Genus and species	Locality	Present elevation above sea level (m)[b]	^{238}U(nmoles/g)[c,d]	^{232}Th(pmoles/g)[d,e]	($^{232}Th/^{238}U$)(10^5)
IV. PLEISTOCENE, BARBADOS							
OC-51	A	Acropora palmata	Worthing Terrace, Clermont Nose (Bender et al., 1979)	18	17.05 ± 0.03	0.17 ± 0.02	1.0 ± 0.1
	B^{rh}	-	-	-	17.36 ± 0.03	0.15 ± 0.03	0.9 ± 0.2
FT-50	A	Acropora palmata	Ventnor Terrace, Clermont Nose (Bender et al., 1979)	23	13.93 ± 0.02	0.92 ± 0.02	6.6 ± 0.1
	B^{ra}	-	-	-	13.95 ± 0.02	0.92 ± 0.05	6.6 ± 0.4
	C^{rh}	-	-	-	13.97 ± 0.03	0.42 ± 0.03	3.0 ± 0.2
AFS-12	A	Acropora palmata	Rendezvous Hill Terrace, Christchurch Ridge (Bender et al., 1979)	30	12.66 ± 0.02	1.40 ± 0.05	11.1 ± 0.4
	B^{rh}	-	-	-	12.62 ± 0.03	1.57 ± 0.03	12.4 ± 0.2
	C^{rh}	-	-	-	12.43 ± 0.03	1.37 ± 0.03	11.1 ± 0.2
AFS-11		Acropora palmata	Rendezvous Hill Terrace, Christchurch Ridge (Bender et al., 1979)	30	13.67 ± 0.02	0.74 ± 0.02	5.4 ± 0.1
AFS-10		Acropora palmata	Rendezvous Hill Terrace, Christchurch Ridge (Bender et al., 1979)	30	12.82 ± 0.02	0.28 ± 0.02	2.2 ± 0.2
AFM-20		Acropora palmata	Rendezvous Hill Terrace, Clermont Nose (Bender et al., 1979)	55	13.46 ± 0.04	1.92 ± 0.04	14.3 ± 0.3
R-52		Acropora palmata	Rendezvous Hill Terrace, Christchurch Ridge (Bender et al., 1979)	37	13.98 ± 0.02	0.08 ± 0.06	0.6 ± 0.4
VA-1		Acropora palmata	Hill View Terrace, St. George's Valley (Bender et al., 1979)	149	13.37 ± 0.02	1.08 ± 0.02	8.1 ± 0.2
V. PLEISTOCENE, VANUATU							
E-L-3		Porites lutea	Port Havannah, Efate Is. (Bloom et al., 1978)	110-130	11.39 ± 0.03	0.12 ± 0.03	1.1 ± 0.3
E-T-2	A	Oulophyllia crispa	Port Havannah, Efate Is. (Bloom et al., 1978)	110-130	9.75 ± 0.01	0.12 ± 0.03	1.2 ± 0.3
	B^{rh}	-	-	-	9.72 ± 0.01	0.10 ± 0.03	1.0 ± 0.3

Sample[a]	Genus and species	Locality	Present elevation above sea level (m)[b]	^{238}U(nmoles/g)[c,d]	^{232}Th(pmoles/g)[d,e]	($^{232}Th/^{238}U$)(10^5)
VI. ALTERED - UNALTERED PAIRS						
PB-2A	Acropora palmata	Barbados, 0.5 km NW of Checker Hall	~ 30	12.97 ± 0.3	1.04 ± 0.03	8.0 ± 0.2
PB-2A LEACH	-	-		12.50 ± 0.02	3.27 ± 0.18	26.2 ± 1.4
PB-2A RESIDUE	-	-		13.23 ± 0.04	1.40 ± 0.03	10.6 ± 0.2
PB-2B	-	-		6.75 ± 0.01	0.27 ± 0.02	4.0 ± 0.3
PB-4A	Acropora palmata	Barbados, 0.5 km NW of Checker Hall	~ 30	13.36 ± 0.04	0.51 ± 0.03	3.8 ± 0.2
PB-4B	-	-		10.43 ± 0.04	0.51 ± 0.02	4.9 ± 0.2
PB-5A	Acropora palmata	Barbados, 0.5 km NW of Checker Hall	~ 30	12.41 ± 0.04	0.86 ± 0.03	6.9 ± 0.2
PB-5B (A)	-	-		6.90 ± 0.01	8.46 ± 0.06	122.6 ± 0.9
(B)[ra]	-	-		6.92 ± 0.02	8.51 ± 0.08	123.0 ± 1.2
PB-9A (A)	Acropora palmata	Barbados, 0.5 km NW of Checker Hall	~ 30	13.74 ± 0.02	0.62 ± 0.04	4.5 ± 0.3
(B)	-	-		13.74 ± 0.02	0.62 ± 0.04	4.5 ± 0.3
PB-9B	-	-		11.79 ± 0.03	0.40 ± 0.03	3.4 ± 0.3
BCE-A-3A	Acropora palmata	Hispaniola, SE coast, 6.5 km E of Boca Chica 50 m S of main road	7.2	11.91 ± 0.03	2.05 ± 0.04	17.2 ± 0.03
BCE-A-3B	-	-		12.96 ± 0.04	0.30 ± 0.03	2.3 ± 0.02
VII. MODERN ACROPORA (different methods of sample preparation)						
M.A. (chiseled)	Acropora palmata	Tobago Cays, Windward Islands	-1	13.62 ± 0.02	0.10 ± 0.01	0.7 ± 0.1
(cut) A	Acropora palmata	Tobago Cays Windward Islands	-1	13.40 ± 0.04	0.33 ± 0.01	2.5 ± 0.1
(cut) B	Acropora palmata	Tobago Cays, Windward Islands	-1	13.31 ± 0.04	0.24 ± 0.01	1.8 ± 0.1
VIII. GIANT CLAM						
K-133	Tridacna gigantus	Huon Peninsula, New Guinea	~ 0	(3.08 ± 0.08) × 10^{-4}	0.249 ± 0.002	(8.08 ± 0.22) × 10^{-4}

[a] Analyses denoted with "rh" and "ra" are replicate analyses of the preceding analysis. "rh" refers to replicate analyses of different fragments of the same hand specimen; "ra" refers to replicate analyses of different aliquots of the same dissolved fragment.

[b] Elevations for the Holocene sample from Vanuatu are relative to the highest living corals at each locality; this is approximately the elevation above low tide. Elevations for the samples from the south coast of Hispaniola are relative to sea level at high tide.

[c] Calculated using $^{238}U/^{235}U = 137.88$.

[d] All errors are $2\sigma_{mean}$. 1 nmole/g = 10^{-9} moles/g; 1 pmole/g = 10^{-12} moles/g.

[e] Corrected for the procedural blank of 0.02 ± 0.01 pmoles ^{232}Th; most of the error is due to the uncertainty in the blank correction.

A2. U and Th isotopic composition of corals and ^{230}Th ages of corals.[a]

Sample[b]	$(^{234}U/^{238}U)10^5$	$\delta^{234}U(0)$[c,d]	$\delta^{234}U(T)$[c,d]	$^{230}Th/^{232}Th$[e]	$(^{230}Th/^{238}U)10^5$	$[^{230}Th/^{238}U]^{f}_{act}$	^{230}Th age[g]	^{230}Th growth date (years A.D. and B.C.)[h]
I. HOLOCENE, VANUATU								
CWS-A-1b	6.295 ± 30	150 ± 5	150 ± 5	0.00017 ± 2	$(3.35\pm0.44)\times10^{-4}$	$(1.99\pm0.26)\times10^{-4}$	19 ± 3 y	1969 ± 3
CWS-A-1d	6.304 ± 15	152 ± 3	152 ± 3	0.00031 ± 3	$(9.96\pm0.86)\times10^{-4}$	$(5.90\pm0.51)\times10^{-4}$	56 ± 5 y	1932 ± 5
CWS-C	6.274 ± 31	146 ± 6	146 ± 6	0.00104 ± 4	0.00215 ± 7	0.00128 ± 5	121 ± 4 y	1866 ± 4
CWS-D-1	6.260 ± 28	144 ± 5	144 ± 5	0.0015 ± 1	0.00212 ± 16	0.00126 ± 10	120 ± 9 y	1864 ± 4
-2[rh]	6.283 ± 30	148 ± 5	148 ± 5	0.0026 ± 1	0.00220 ± 7	0.00131 ± 4	124 ± 4 y	1868 ± 9
CWS-F-1	6.306 ± 22	152 ± 4	153 ± 4	0.0105 ± 2	0.01506 ± 13	0.00893 ± 8	845 ± 8 y	1141 ± 8
TAN-E-1g	6.285 ± 31	149 ± 6	149 ± 6	0.0042 ± 2	0.00320 ± 9	0.00190 ± 5	180 ± 5 y	1806 ± 5
MAF	6.270 ± 27	146 ± 5	146 ± 5	0.131 ± 8	0.00458 ± 5	0.002717 ± 28	258 ± 3 y	1729 ± 3
MAG	6.263 ± 31	145 ± 6	145 ± 6	0.0060 ± 2	0.00476 ± 8	0.002822 ± 48	268 ± 5 y	1718 ± 5
MY2	6.283 ± 22	148 ± 4	151 ± 4	0.24 ± 1	0.10683 ± 28	0.06332 ± 17	6162 ± 28 y	4174 ± 25 B.C.
II. HOLOCENE, ENRIQUILLO VALLEY, HISPANIOLA								
PR-D-1	6.150 ± 25	124 ± 5	126 ± 5	0.058 ± 2	0.0845 ± 23	0.0501 ± 14	4951 ± 140 y	2963 ± 140 B.C.
PR-H-2	6.190 ± 25	131 ± 5	133 ± 5	0.038 ± 6	0.08574 ± 37	0.05082 ± 22	4995 ± 30 y	3007 ± 30 B.C.
PR-H-1	6.053 ± 29	106 ± 5	109 ± 5	0.095 ± 3	0.1301 ± 14	0.07712 ± 81	7851 ± 94 y	5863 ± 94 B.C.
CH-18	6.155 ± 17	125 ± 3	127 ± 3	0.016 ± 1	0.1095 ± 75	0.0649 ± 45	6457 ± 456 y	4469 ± 456 B.C.
CH-8	5.290 ± 20	82 ± 4	84 ± 4	0.0465 ± 4	0.13415 ± 48	0.07951 ± 28	8294 ± 44 y	6306 ± 44 B.C.
III. HOLOCENE, BARBADOS								
D.W.	6.274 ± 28	146 ± 5	148 ± 5	0.090 ± 4	0.6276 ± 15	0.03720 ± 9	3585 ± 19 y	1597 ± 19 B.C.
IV. PLEISTOCENE, BARBADOS								
OC-51 A	6.160 ± 28	126 ± 5	161 ± 6	1.1 ± 0.1	1.0640 ± 20	0.6307 ± 12	87.5 ± 0.6 ky	
B[rh]	6.159 ± 26	126 ± 5	162 ± 6	1.2 ± 0.2	1.0667 ± 28	0.6323 ± 17	87.9 ± 0.7 ky	
FT-50 A	6.163 ± 25	126 ± 5	173 ± 7	0.188 ± 4	1.2412 ± 35	0.7357 ± 21	112.0 ± 1.0 ky	
B[ra]	6.168 ± 23	127 ± 4	174 ± 6	0.188 ± 10	1.2416 ± 63	0.7359 ± 37	111.8 ± 1.3 ky	
C[rh]	6.150 ± 30	124 ± 5	170 ± 7	0.42 ± 3	1.2406 ± 38	0.7353 ± 23	112.3 ± 1.1 ky	
AFS-12 A	6.066 ± 22	109 ± 4	153 ± 6	0.116 ± 4	1.2811 ± 47	0.7593 ± 28	122.1 ± 1.1 ky	
B[rh]	6.080 ± 35	111 ± 5	157 ± 7	0.103 ± 2	1.2874 ± 42	0.7631 ± 25	122.7 ± 1.3 ky	
C[rh]	6.068 ± 25	109 ± 5	155 ± 6	0.117 ± 2	1.2957 ± 47	0.7680 ± 28	124.5 ± 1.3 ky	
AFS-11	6.094 ± 32	114 ± 6	161 ± 8	0.239 ± 8	1.2912 ± 34	0.7653 ± 20	122.6 ± 1.5 ky	
AFS-10	6.071 ± 24	110 ± 4	157 ± 6	0.60 ± 4	1.3038 ± 40	0.7728 ± 24	125.7 ± 1.2 ky	
AFM-20	6.081 ± 24	111 ± 4	160 ± 6	0.093 ± 2	1.3247 ± 43	0.7852 ± 26	129.2 ± 1.4 ky	
R-52	6.104 ± 30	115 ± 6	165 ± 8	2.3 ± 1.7	1.3237 ± 52	0.7846 ± 31	128.1 ± 1.7 ky	
VA-1	6.136 ± 32	121 ± 6	-	0.249 ± 5	2.0144 ± 65	1.1940 ± 39	-	

Sample[b]	$(^{234}U/^{238}U)10^5$	$\delta^{234}U(0)$[c,d]	$\delta^{234}U(T)$[c,d]	$^{230}Th/^{232}Th$[e]	$(^{230}Th/^{238}U)10^5$	$[^{230}Th/^{238}U]^{f}_{act}$	^{230}Th age[g]
V. PLEISTOCENE, VANUATU							
E-L-3	6.093 ± 26	113 ± 5	162 ± 7	1.2 ± 0.3	1.3071 ± 40	0.7748 ± 24	125.5 ± 1.3 ky
E-T-2 A	6.036 ± 22	103 ± 4	149 ± 6	1.1 ± 0.2	1.3179 ± 28	0.7811 ± 17	129.9 ± 1.1 ky
B^{rh}	6.054 ± 24	106 ± 4	153 ± 6	1.3 ± 0.4	1.3179 ± 20	0.7811 ± 12	129.2 ± 1.1 ky
VI. "ALTERED" - "UNALTERED" PAIRS							
PB-2A	5.973 ± 33	92 ± 6	240^{+21}_{-18}	0.226 ± 7	1.8104 ± 55	1.0731 ± 33	340^{+18}_{-15} ky
PB-2A LEACH	5.932 ± 29	84 ± 5	164 ± 11	0.063 ± 3	1.6547 ± 98	0.9808 ± 58	236 ± 7 ky
PB-2A RESIDUE	5.961 ± 49	89 ± 4	265^{+44}_{-34}	0.174 ± 3	1.8368 ± 77	1.0887 ± 46	384^{+44}_{-32} ky
PB-2B	5.883 ± 35	75 ± 6	197^{+20}_{-19}	0.44 ± 3	1.7748 ± 51	1.0520 ± 30	339^{+20}_{-17} ky
PB-4A	5.936 ± 27	85 ± 5	198^{+15}_{-14}	0.46 ± 3	1.7559 ± 52	1.0408 ± 31	300^{+10}_{-9} ky
PB-4B	5.896 ± 30	74 ± 6	163^{+14}_{-13}	0.35 ± 2	1.7051 ± 76	1.0107 ± 45	277^{+10}_{-9} ky
PB-5A	5.973 ± 38	92 ± 7	251^{+24}_{-25}	0.26 ± 1	1.8225 ± 62	1.0803 ± 37	354^{+24}_{-20} ky
PB-5B (A)	5.899 ± 24	78 ± 4	208^{+15}_{-14}	0.0146 ± 1	1.7863 ± 42	1.0588 ± 25	346^{+14}_{-13} ky
$(B)^{ra}$	5.894 ± 22	77 ± 4	202^{+14}_{-13}	0.0145 ± 1	1.7797 ± 85	1.0549 ± 50	340^{+16}_{-14} ky
PB-9A (A)	5.953 ± 30	88 ± 6	210 ± 15	0.39 ± 2	1.7700 ± 44	1.0492 ± 26	306^{+12}_{-11} ky
$(B)^{ra}$	5.981 ± 32	93 ± 6	216 ± 15	0.39 ± 2	1.7706 ± 48	1.0495 ± 28	298^{+11}_{-10} ky
PB-9B	5.930 ± 30	84 ± 5	171 ± 12	0.50 ± 4	1.6843 ± 78	0.9983 ± 46	252^{+8}_{-7} ky
BCE-A-3A	6.097 ± 27	114 ± 5	178 ± 8	0.085 ± 2	1.4571 ± 56	0.8637 ± 33	155.2 ± 2.1 ky
BCE-A-3B	6.155 ± 28	125 ± 5	180 ± 8	0.57 ± 5	1.3450 ± 42	0.7973 ± 25	129.5 ± 1.5 ky
VII. MODERN ACROPORA (different methods of sample preparation)							
M.A. (Chiseled)	6.296 ± 25	151 ± 5	151 ± 5	$(2.0\pm0.9)\times10^{-4}$	$(1.5\pm0.7)\times10^{-4}$	$(0.9\pm0.4)\times10^{-4}$	9 ± 4 y
M.A. (Cut) A	6.274 ± 31	147 ± 6	147 ± 6	$(0.8\pm0.4)\times10^{-4}$	$(1.9\pm0.9)\times10^{-4}$	$(1.1\pm0.6)\times10^{-4}$	10 ± 6 y
M.A. (Cut) B	6.257 ± 26	143 ± 5	143 ± 5	$(2.3\pm0.9)\times10^{-4}$	$(4.2\pm1.6)\times10^{-4}$	$(2.5\pm1.0)\times10^{-4}$	23 ± 9 y

[a] All errors are $2\sigma_{mean}$; all isotope ratios are atomic ratios unless otherwise specified.
[b] Analyses denoted with "rh" and "ra" are replicate analyses of the preceding sample. "rh" refers to replicate analyses of different fragments of the same hand specimen; "ra" refers to replicate analyses of different aliquots of the same dissolved fragment.
[c] $\lambda_{238} = 1.551 \times 10^{-10}$ yr $^{-1}$ (Jaffey et al., 1971); $\lambda_{234} = 2.835 \times 10^{-6}$ yr^{-1} (Lounsbury and Durham, 1971; de Bievre et al., 1971); $\lambda_{230} = 9.195\times10^{-6}$ yr^{-1} (Meadows et al., 1980).

[d] $\delta^{234}U = \{[(^{234}U/^{238}U)/(^{234}U/^{238}U)_{eq}] - 1\} \times 10^3$, where $(^{234}U/^{238}U)_{eq}$ is the atomic ratio at secular equilibrium and is equal to $\lambda_{238}/\lambda_{234} = 5.472 \times 10^{-5}$. $\delta^{234}U(0)$ is the measured value; $\delta^{234}U(T)$ is the initial value calculated using the ^{238}U-^{234}U-^{230}Th age (Eq. 6.11) and Eq. 6.12.

[e] Corrected for ^{232}Th blank of 0.02 ± 0.01 pmoles; most of the error is due to uncertainty in the blank correction.

[f] $[^{230}Th/^{238}U]_{act}$ is the activity ratio calculated by dividing $^{230}Th/^{238}U$ by the $^{230}Th/^{238}U$ atomic ratio at secular equilibrium; $(^{230}Th/^{238}U)_{eq} = \lambda_{238}/\lambda_{230} = 1.6871 \times 10^{-5}$.

[g] Age refers to the age of the sample at the time of analysis (May 1986 - Aug. 1987).

[h] Determined by subtracting the ^{230}Th age from the date of analysis; dates are rounded to Jan. 1 of the indicated year. Dates are A.D. unless specifically noted.

A3. Number of ^{230}Th atoms per analysis, mass of coral analyzed, and 2σ uncertainty in ^{230}Th abundance.

Run[a]	10^{10} atoms of ^{230}Th (No.)	Coral mass (g)	2σ uncertainty (‰)
CWS-A-1b	0.0080	4.1	± 132
CWS-A-1d	0.021	3.4	± 86
CWS-C	0.082	5.6	± 35
CWS-D-1	0.058	4.3	± 76
-2	0.046	3.3	± 33
CWS-F-1	0.43	4.6	± 8
TAN-E-1g	0.058	2.8	± 29
MAF	0.10	4.1	± 10
MAG	0.12	4.3	± 16
MY2	0.68	4.5	± 2
PR-H-2	1.5	2.7	± 4
CH-8	3.2	4.1	± 3
D.W.	1.4	2.8	± 2
OC-51 A	4.4	0.41	± 1
B	3.8	0.34	± 2
FT-50 A	4.2	0.41	± 2
B	2.1	0.20	± 5
C	3.5	0.33	± 2
AFS-12 A	2.4	0.25	± 3
B	3.8	0.39	± 2
C	2.7	0.28	± 2
AFS-11	4.4	0.41	± 2
AFS-10	4.3	0.43	± 3
AFM-20	3.0	0.28	± 2
R-52	1.9	0.17	± 3
VA-1	6.2	0.38	± 3
E-L-3	2.3	0.26	± 2
E-T-2 A	2.2	0.28	± 2
B	2.4	0.31	± 2
PB-2A	4.3	0.30	± 2
PB-2A LEACH	0.70	0.057	± 6
PB-2A RESIDUE	5.8	0.40	± 3
PB-2B	3.0	0.42	± 2
PB-4A	4.8	0.34	± 1
PB-4B	4.7	0.44	± 2
PB-5A	4.5	0.43	± 2
PB-5B (A)	2.8	0.38	± 2
(B)	2.0	0.27	± 4
PB-9A (A)	3.9	0.27	± 2
(B)	3.9	0.27	± 2
PB-9B	3.7	0.31	± 2
BCE-A-3A	2.5	0.24	± 3
BCE-A-3B	3.8	0.36	± 1
M.A. (Chiseled)	0.0019	1.5	± 429
M.A. (Cut) A	0.0024	1.6	± 520
M.A. (Cut) B	0.0048	1.4	± 375

[a] The ^{230}Th analyses for PR-D-1, PR-H-1 and CH-18 are not included because the yields were low and the number of atoms loaded on the filament is unknown.

APPENDIX B: PUBLISHED ARTICLES

Earth and Planetary Science Letters, 80 (1986) 241–251
Elsevier Science Publishers B.V., Amsterdam – Printed in The Netherlands

[6]

^{238}U, ^{234}U and ^{232}Th in seawater

J.H. Chen, R. Lawrence Edwards and G.J. Wasserburg

The Lunatic Asylum of the Charles Arms Laboratory, Division of Geological and Planetary Sciences, California Institute of Technology, Pasadena, CA 91125 (U.S.A.)

Received May 21, 1986; revised version received August 26, 1986

We have developed techniques to determine ^{238}U, ^{234}U and ^{232}Th concentrations in seawater by isotope dilution mass spectrometry. U measurements are made using a ^{233}U-^{236}U double spike to correct for instrumental fractionation. Measurements on uranium standards demonstrate that $^{234}U/^{238}U$ ratios can be measured accurately and reproducibly. $^{234}U/^{238}U$ can be measured routinely to $\pm$ 5‰ (2σ) for a sample of 5×10^9 atoms of ^{234}U (3×10^{-8} g of total U, 10 ml of seawater). Data acquisition time is ~ 1 hour. The small sample size, high precision and short data acquisition time are superior to α-counting techniques. ^{238}U is measured to $\pm$ 2‰ (2σ) for a sample of 8×10^{12} atoms of ^{238}U ($\sim 3 \times 10^{-9}$ g of U, 1 ml of seawater). ^{232}Th is measured to $\pm$ 20‰ with 3×10^{11} ^{232}Th atoms (10^{-10} g ^{232}Th, 1 l of seawater). This small sample size will greatly facilitate investigation of the ^{232}Th concentration in the oceans. Using these techniques, we have measured ^{238}U, ^{234}U and ^{232}Th in vertical profiles of unfiltered, acidified seawater from the Atlantic and ^{238}U and ^{234}U in vertical profiles from the Pacific. Determinations of $^{234}U/^{238}U$ at depths ranging from 0 to 4900 m in the Atlantic (7°44′N, 40°43′W) and the Pacific (14°41′N, 160°01′W) Oceans are the same within experimental error ($\pm$ 5‰, 2σ). The average of these $^{234}U/^{238}U$ measurements is 144 $\pm$ 2‰ (2σ) higher than the equilibrium ratio of 5.472×10^{-5}. U concentrations, normalized to 35‰ salinity, range from 3.162 to 3.281 ng/g, a range of 3.8%. The average concentration of the Pacific samples (31°4′N, 159°1′W) is ~ 1% higher than that of the Atlantic (7°44′N, 40°43′W and 31°49′N, 64°6′W). ^{232}Th concentrations from an Atlantic profile range from 0.092 to 0.145 pg/g. The observed constancy of the $^{234}U/^{238}U$ ratio is consistent with the predicted range of $^{234}U/^{238}U$ using a simple two-box model and the residence time of deep water in the ocean determined from ^{14}C. The variation in salinity-normalized U concentrations suggests that U may be much more reactive in the marine environment than previously thought.

1. Introduction

This work was carried out to establish a method for precise and rapid determination of $^{234}U/^{238}U$ and U and Th concentrations in seawater using mass spectrometric techniques. There have been extensive studies of nuclides in the ^{238}U decay chain as a means of studying the mobility and transport of actinide elements in nature (cf. [1]). Cherdyntsev [2] first showed that changes in the $^{234}U/^{238}U$ ratio occur during weathering. Thurber [3] showed that the $^{234}U/^{238}U$ activity ratio in seawater was greater than unity and reported a value of 1.15. Further studies have examined $^{234}U/^{238}U$ ratios and U concentrations in seawater in order to place constraints on the U budget in the oceans (cf. [4–8]). These measurements also pertain to a wide range of problems involving the origin and age of marine precipitates and sediments.

The $^{234}U/^{238}U$ ratios and U concentrations are usually measured by α-counting techniques (see Table 1) and yield 2σ errors based on counting statistics of $\pm$ 20‰ to 40‰, for counting times of tens of hours. Sample sizes for this procedure are typically ~ 10^{17} atoms of ^{238}U (~ 10 l of seawater; ~ 10^{-5} g of U). Previous studies from this laboratory have shown that, using mass spectrometric techniques, it is possible to routinely measure $^{235}U/^{238}U$ on samples of ~ 10^{-9} g of uranium (containing 2×10^{10} atoms of ^{235}U) to a precision of $\pm$ 2‰ (2σ) and samples containing 3×10^8 ^{235}U atoms to $\pm$ 4% [9–11]. It therefore seemed reasonable to extend these techniques to permit the high precision measurement of ^{234}U on ~ 10^{-8} g of natural uranium. The success of this approach

Division Contribution No. 4338 (496).

0012-821X/86/$03.50

TABLE 1

Comparison between mass spectrometric and α-counting methods for ^{234}U in seawater

Method	Sample size		Time (hours)	Counting rate (cts/s)	2σ error (‰)
	^{234}U (atoms)	seawater (l)			
Mass spect.	5×10^9	10^{-2}	1 [a]	2000	± 5
α-counting	5×10^{12}	10	~ 10	0.4 [b]	± 20–40

[a] Total counting time for data acquisition. Actual time spent counting the ^{234}U peak is ~ 400 seconds.
[b] Assumes 100% chemical yield and 100% counting efficiency; usual counting efficiency is only ~ 25%.

would allow studies of ^{234}U disequilibrium on small samples such as sediment pore fluids or more refined studies which require high precision measurements. Mass spectrometric determination of $^{234}U/^{238}U$ ratios in terrestrial and lunar samples has been done previously [12–16], but these studies used sample sizes comparable to those used in α-counting. The precision of the measurements was also comparable to those obtained by α-counting techniques. We will present a series of analyses on two natural uranium standards which show that $^{234}U/^{238}U$ can be measured to high precision. We will then present analyses of U and Th concentrations and $^{234}U/^{238}U$ ratios for unfiltered seawater from vertical profiles in the Atlantic and Pacific Oceans. We have not attempted to directly measure the fraction of U or Th contained in particulates. The constraints these data place on the uranium chemistry of the oceans will then be discussed.

2. Analytical procedure

The mass spectrometric procedures used in this laboratory for measuring small uranium samples have been described earlier [9,10]. The approach used is the double spike technique. The ^{233}U-^{236}U double spike technique was first used by Dietz et al. [17]. We have used a double spike with a ratio of ^{233}U to ^{236}U close to unity as calibrated using the absolute values of the National Bureau of Standards (NBS) U-500 standard ($^{235}U/^{238}U = 0.9997 \pm 0.001$; [18]). The concentration of this spike is calibrated using this U-500 standard, NBS SRM 960 and NBS SRM 950a. The absolute isotopic composition and concentration of our double spike is given in [10]. The U concentration runs were spiked so that $^{236}U/^{238}U \sim 1/10$. Measurements of $^{234}U/^{235}U$ (isotopic composition run) were done in a separate analysis where $^{236}U/^{235}U \sim 1/10$. All measurements were carried out on the Lunatic I mass spectrometer [19] using an electron multiplier in the analog mode with a gain of $\sim 4 \times 10^3$ and an electrometer (Cary 401) with a feedback resistor of 10^9 Ω. For the isotopic composition runs, data were acquired in the following sequence: ^{236}U-^{235}U-^{234}U-^{234}U-^{233}U. Note that ^{234}U was measured twice (channels 1 and 2). Zeros were measured 0.5 mass units above and below each mass. Integration times for zeros and peaks were one second for all masses except ^{234}U. ^{234}U zeros were each measured for two seconds and the ^{234}U peak for four seconds. A mass spectrum of U from a coral sample (Barbados) containing 5×10^9 ^{234}U atoms is given in Fig. 1. The $^{234}U^+$ ion current was typically 2×10^3 ions/s corresponding to 1.4×10^{-3} volts. The noise level of the multiplier and amplifier under normal operating conditions with the ion beam off was $\pm 8 \times 10^{-6}$ volts (the uncertainty given is 2σ of the distribution for a series of four-second noise measurements). Tailing from the major isotopes is important because of the low resolution usually used in operating the spectrometer in a high transmission mode. The ^{234}U intensity is determined by subtracting the average of the zeros (measured at mass 234.5 and mass 233.5) from the intensity at mass 234. If the positive curvature of the ^{235}U tail between mass 233.5 and mass 234.5 is significant, the procedure for background correction can result in an underestimate of the intensity of the ^{234}U signal. We therefore tested the effects of the ^{235}U tail at the center of the spectral line for ^{234}U and at the positions where zeros for ^{234}U were taken. To do this, we measured the tail from ^{238}U at the equivalent mass positions at and near mass 237. This is shown in Fig. 1 under arrow "*B*". The average of the intensities at masses 237.5 and 236.5 is slightly higher than the measured intensity at mass 237. We have measured this quantity for

different samples at different focusing conditions. For several measurements of the ion beam current (I) at appropriate masses the results are:

$$\frac{I(237) - [I(237.5) + I(236.5)]/2}{I(238) - [I(238.5) + I(237.5)]/2} = -0.6 \times 10^{-5}$$

to -2.0×10^{-5}.

As $^{235}U/^{234}U \sim 10^{2}$, systematic errors introduced by tailing of ^{235}U are < 2‰ of the ^{234}U peak and are insignificant. As can be seen in Fig. 1, there is a slight slope to the background across the U spectrum. The background is also slightly higher than the background with the accelerating voltage off (arrow "A", Fig. 1). This is due to the reflection of the $^{238}U^{12}C_2^+$ (mass 262) ion beam off the flight tube. The intensity of the reflected peak increases gradually from about mass 228 to a maximum value around mass 244. Typically, $^{238}U^{12}C_2^+/^{238}U^+ \sim 0.015$ and $^{238}U^{12}C_2^+$ reflects to mass 234 with an efficiency of ~ 0.001 contributing ~ 600 ions/s to the background at mass 234 at running conditions. If this reflected peak has significant curvature for the mass range 233.5–234.5, the linear background correction might result in inaccurate determination of the ^{234}U intensity. To check whether the background around mass 234 is linear, we scanned over the analogous portion of the ^{238}U reflected peak around mass 212. This scan showed that curvature of the reflected peak does not introduce significant errors.

As $^{235}U/^{234}U \sim 10^{2}$, a potential problem exists if the electrometer is not allowed enough time to settle between the measurement of the ^{235}U signal and the first ^{234}U zero. We directly measured the rate of decay of this signal by putting a beam on the multiplier, turning off the accelerating voltage, and repeatedly measuring the decaying signal using a 125 ms integration time. The signal decays approximately exponentially to a value of $\sim 10^{-4}$ times the original beam in one second. Since measurement of the ^{234}U zero commences ~ 5 seconds after measurement of the ^{235}U peak, the decaying ^{235}U signal does not significantly affect measurement of the ^{234}U zero. In addition, the average of the $^{234}U/^{235}U$ ratios measured in the first ^{234}U channel does not differ significantly from the average of the $^{234}U/^{235}U$ ratios measured in the second ^{234}U channel. Data acquisition takes ~ 1 hour and about 80 ratios (40 cycles with two ^{234}U measurements/cycle) of $^{234}U/^{235}U$ are measured. Data are acquired at filament temperatures of 1700–1800°C. The $^{234}U^+$ current ranges from 1500 to 3000 ions/s ($2.4–3.6 \times 10^{-16}$ amperes). Our standard load is 3×10^{-8} g of natural U ($\sim 5 \times 10^{9}$ ^{234}U atoms). The ionization efficiency is ~ 1‰.

For the concentration runs, data were acquired in the following sequence ^{238}U-^{236}U-^{235}U-^{234}U-^{233}U. Zeros are measured 0.5 mass units above and below each spectral line. Integration time for all peaks and zeros is 1 second. Data acquisition

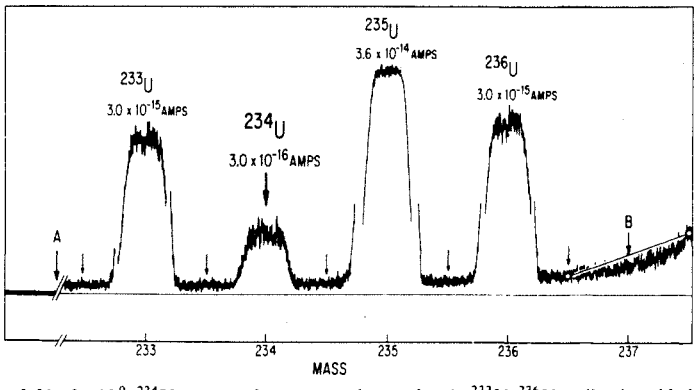

Fig. 1. Mass spectrum of U (5×10^{9} ^{234}U atoms) from a coral sample. A ^{233}U-^{236}U spike is added to the sample so that $^{236}U/^{234}U \approx 10$. In this spike, the $^{233}U/^{236}U$ is ~ 1 and the $^{234}U/^{236}U$ is ~ 2×10^{-3}. The ^{238}U peak is off scale to the right of the diagram. The small arrows represent positions where the zeros are measured. The arrow marked "A" denotes where the accelerating voltage was turned off. Details of the background characteristics are discussed in the text. Note the change in scale for ^{235}U, ^{233}U and ^{236}U.

takes ~ 2 hours. About 100 ratios of $^{236}U/^{238}U$ are measured at filament temperatures ranging from 1600° to 1700°C. The $^{238}U^+$ current is 0.6×10^6 to 3×10^6 ions/s (1×10^{-13} to 5×10^{-13} amperes). Our standard load is 3×10^{-9} g of natural U (~ 10^{13} ^{238}U atoms). Ionization efficiencies are > 1‰. Chen and Wasserburg [10] have shown that the multiplier on the L1 spectrometer is linear to better than ± 2‰ for ratios up to ~ 10^2 for ion currents up to 3×10^6 ions/s (5×10^{-13} amperes). We have checked this in each concentration run by measuring the $^{238}U/^{235}U$ ratio and verifying that it agrees within error with the natural $^{238}U/^{235}U$ ratio (137.88, see Table 4).

For both isotopic and concentration runs, all data sets of ten isotopic ratios were normalized for mass-dependent isotope fractionation using the mean $^{233}U/^{236}U$ ratio for that set of ten ratios. The isotopic ratios and deviations of these ratios were then reduced using the full double spike equations. All errors quoted are 2σ of the mean. For samples for which both concentration and isotopic runs were performed, $^{234}U/^{238}U$ ratios were calculated by two methods. $^{234}U/^{238}U$ was calculated from the $^{234}U/^{235}U$ ratio measured in the isotopic run assuming $^{238}U/^{235}U = 137.88$ (method I). $^{234}U/^{238}U$ was also calculated using the $^{236}U/^{238}U$ ratio from the concentration run and the $^{236}U/^{234}U$ ratio from the isotopic run (method II). The consistency of the $^{234}U/^{238}U$ ratios from these two methods is a good test of the gravimetry and the linearity of the multiplier (see Table 2).

Initially, a ^{230}Th spike was used to determine the ^{232}Th concentration. At a later stage, a ^{229}Th spike was used in some samples so that both ^{230}Th and ^{232}Th could be measured in the same run. The samples were spiked such that $^{230}Th/^{232}Th$ or $^{229}Th/^{232}Th$ ratios were between 0.1 and 10. From 7×10^{10} to 3.8×10^{11} atoms of ^{232}Th were loaded on the filament. Data were acquired for ~ 1 hour at temperatures of 1800–1900°C and a $^{232}Th^+$ current of 1.4×10^4 to 6×10^4 ions/s (2×10^{-15} to 1×10^{-14} amperes). Ionization efficiency was ~ 1‰. Mass-dependent fractionation due to the multiplier was corrected for by multiplying the measured $^{230}Th/^{232}Th$ (or $^{229}Th/^{232}Th$) ratio by $(230/232)^{1/2}$ (or $(^{229}Th/^{232}Th)^{1/2}$).

Uranium and thorium were separated from seawater samples as follows. For the U concentration runs, about 1 ml of seawater was weighed, spiked and slowly dried under a heat lamp. In order to insure sample-spike equilibration and convert the solution to the nitrate form, the resulting salt was dissolved in concentrated HNO_3 and dried twice before being dissolved in 7*N* HNO_3 and loaded on an anion exchange column (Dowex AG 1×8 resin). The majority of cations were eluted using 7*N* HNO_3; uranium was subsequently eluted with 1*N* HBr. The HBr fraction was dried, dissolved in 7*N* HNO_3 and further purified using the same elution scheme and a smaller column. The subsequent HBr fraction was dried, dissolved in one drop of concentrated nitric acid, dried, dissolved in ~ 1 μl of 0.1*N* HNO_3 and loaded on a zone-refined rhenium filament coated with colloidal graphite [10]. The Re filament had previously been outgassed at ~ 2000°C for two hours. The blank for the whole procedure for the concentration run is 4×10^9 to 1×10^{10} ^{238}U atoms. For the U isotopic runs, ~ 3 ml of seawater were spiked and ~ 10 mg of Fe carrier added. This solution was then warmed, partially dried down, and allowed to sit overnight. The U coprecipitated with hydrous ferric oxide upon addition of ammonium hydroxide until the solution reached pH 7–9 [20]. This mixture was centrifuged and the supernate discarded. Distilled water was added to the residue; the mixture was stirred, centrifuged and the supernate discarded. The resulting residue was dissolved in 7*N* HNO_3. This solution was processed through ion exchange columns and ~ 1/3 of the U fraction was loaded on a Re filament as described earlier. The total blank for the full procedure is ~ 1×10^{10} ^{238}U atoms; the typical loading blank is ~ 3×10^9 ^{238}U atoms. The chemical yield for both U procedures is > 95%.

For the determination of Th concentration, 250–1000 ml of seawater was stored in a teflon FEP bottle spiked with ^{230}Th or ^{229}Th, and 10 mg of Fe carrier added. In order to insure complete spike-sample equilibration, the solution was shaken vigorously for several minutes; it appeared homogeneous as indicated by the yellowish color of hexaaquoiron(II) ion. Th was coprecipitated with iron and processed on the ion exchange columns as described above with the exception that Th was eluted with 6*N* HCl instead of HBr. The chemical yield for this full procedure was better

than 95%. The total blank is about 8×10^9 atoms of ^{232}Th and the typical loading blank is ~ 2×10^9 atoms of ^{232}Th.

3. Sample collection

Samples were collected on the following cruises: Alcyone V (R/V "Melville", 31°N, 159°W; Pacific, 10/85, collected by R.L.E.), OCE 173-IV (R/V "Oceanus", 32°N, 64°W; Atlantic, 12/85, collected by D. Piepgras), TTO/TAS Leg 2 (R/V "Knorr", station 63, 8°N, 41°W; Atlantic, collected by D. Piepgras and M. Stordal, 1/83), and Marine Chemistry 80 (R/V "Thompson", 14°N, 160°W; Pacific, collected by K. Bruland, 10/80). Samples were collected in Niskin and Go-Flo bottles, then transferred to acid cleaned, high density linear polyethylene and polypropylene bottles. On the Alcyone V cruise, sample bottles were rinsed with seawater from the Niskin before the final sample was added. Samples were not filtered; they were acidified with ~ 2 ml of concentrated HCl or HNO_3 per liter of seawater on shipboard (except for the OCE 173-IV samples which were acidified several weeks later). Bottles were then tightly capped and stored until laboratory analysis. Reported salinities are from CTD measurements made by PACYDORF (Scripps Institution of Oceanography) and in some cases from shipboard salinometer measurements (by P.M. Williams for the Alcyone V cruise and by D.J. Piepgras for the OCE 173-IV cruise).

4. Results

Measurements of the $^{234}U/^{238}U$ ratio in two standards (NBS SRM 960, NBS SRM 950a) are presented in Table 2. These data have been reformulated into δ-notation where $\delta^{234}U = \{[(^{234}U/^{238}U)_{sample}/(^{234}U/^{238}U)_{eq}] - 1\} \times 10^3$. $(^{234}U/^{238}U)_{eq}$ is the atomic ratio at secular equilibrium and is equal to $\lambda(^{238}U)/\lambda(^{234}U) = (5.472 \pm 0.012) \times 10^{-5}$ (2σ, [21–23]) For each of these measurements, ~ 5×10^9 atoms of ^{234}U (~ 3×10^{-8} g of U) have been loaded on the filament. The 2σ error for each measurement is about ± 5‰. For each of the standards, the measured ratio for a single experiment is the same as the grand mean of all measurements within the errors. Furthermore, within the error of the measurements, the $^{234}U/^{238}U$ ratios calculated using methods I and II agree. The measured $^{234}U/^{238}U$ ratio for NBS SRM 960 differs from the $^{234}U/^{238}U$ for NBS SRM 950a by ~ 16‰, a difference which is larger than either the 2σ error for each individual measurement (± 5‰) or the $2\sigma_{mean}$ calculated from all

TABLE 2

$^{234}U/^{238}U$ ratios in NBS SRM 960 and NBS SRM 950a

NBS standard [a]	$^{234}U/^{238}U$ ($\times 10^5$) [b,c]		$\delta^{234}U$ [b,c,d]	
	I	II	I	II
SRM 960	5.260 ± 0.029	5.280 ± 0.024	−39 ± 5	−35 ± 4
	5.267 ± 0.035	5.266 ± 0.019	−37 ± 6	−38 ± 4
	5.245 ± 0.029	5.244 ± 0.024	−41 ± 5	−42 ± 4
	5.280 ± 0.028	5.273 ± 0.029	−35 ± 5	−36 ± 5
	5.280 ± 0.036	-	−35 ± 7	-
	5.267 ± 0.025	-	−37 ± 5	-
average =	5.267 ± 0.011	5.266 ± 0.016	−37 ± 2	−38 ± 3
SRM 950a	5.350 ± 0.033	5.382 ± 0.027	−22 ± 6	−16 ± 5
	5.344 ± 0.032	5.360 ± 0.021	−23 ± 6	−20 ± 4
	5.364 ± 0.018	5.356 ± 0.015	−20 ± 3	−21 ± 3
average =	5.353 ± 0.012	5.366 ± 0.016	−22 ± 2	−19 ± 3

[a] Amount of U analyzed is ~ 30 ng (1 ng = 10^{-9} g).

[b] $\delta^{234}U = \{[(^{234}U/^{238}U)_{sample}/(^{234}U/^{238}U)_{eq}] - 1\} \times 10^3$, where $(^{234}U/^{238}U)_{eq}$ is the atomic ratio at secular equilibrium and is equal to $\lambda(^{238}U)/\lambda(^{234}U) = 5.472 \times 10^{-5}$ [21–23].

[c] All errors are $2\sigma_{mean}$.

[d] I: calculated from the measured $^{234}U/^{235}U$ ratio assuming $^{238}U/^{235}U \equiv 137.88$; II: calculated from ^{234}U and ^{238}U concentrations.

TABLE 3

U isotope ratios in seawater [a]

Location	Depth (m)	$^{234}U/^{238}U$ ($\times 10^5$)	$\delta^{234}U$
Pacific	raft	6.239 ± 0.026	140 ± 5
(14°41'N,	30	6.292 ± 0.026	150 ± 5
160°01'W)	2000	6.245 ± 0.021	141 ± 4
	4900	6.262 ± 0.032	144 ± 6
Atlantic	10	6.263 ± 0.039	145 ± 7
(7°44'N,	690	6.240 ± 0.036	140 ± 7
40°43'W)	1640	6.250 ± 0.042	142 ± 8
	2910	6.250 ± 0.037	142 ± 7
	4280	6.283 ± 0.046	148 ± 8
	average =	6.258 ± 0.012	144 ± 2

[a] All errors are $2\sigma_{mean}$.

the data for a given standard (±2 to 3‰). It is clear that these two standards cannot both be in secular equilibrium ($\delta^{234}U = 0$). In fact, it appears that both standards may have $^{234}U/^{238}U$ ratios lower than the equilibrium ratio (by 37‰ for NBS SRM 960 and by 21‰ for NBS SRM 950a).

Seawater $^{234}U/^{238}U$ data for a vertical profile in the Atlantic and a vertical profile in the Pacific are presented in Table 3. The 2σ error for each measurement ranges from ± 3‰ to ± 7‰. This is about a factor of two more than the error due to counting statistics for the number of ions collected during the ^{234}U measurements. The mean $\delta^{234}U$ for all the measurements is 144 ± 2‰ where the error is $2\sigma_{mean}$ of all the data. None of the individual measurements differs significantly from this value. The mean values for the Atlantic (143 ± 3) and Pacific (144 ± 4) are identical within error.

The U concentration data for Atlantic and Pacific seawater are presented in Table 4. Duplicate analyses were done on several samples and show excellent agreement except in one case (3200

TABLE 4

U concentrations in seawater

Location	Depth [a] (m)	Salinity [b]	U (ng/g) [c,e]		$^{238}U/^{235}U$ [d,e]
			M	N	
Pacific	10	35.275	3.296 ± 7	3.270	138.61 ± 0.66
(31°4'N,	450	34.140	3.171 ± 8	3.251	138.43 ± 0.91
159°1'W)	900	34.233	3.174 ± 7	3.245	137.86 ± 0.57
	1800A	34.588	3.232 ± 6	3.270	137.93 ± 0.41
	B		3.242 ± 4	3.281	138.06 ± 0.79
	3200A	34.689	3.214 ± 6	3.243	138.29 ± 0.54
	B		3.235 ± 4	3.264	138.11 ± 0.59
	4200	34.687	3.231 ± 5	3.261	137.95 ± 0.57
	5710A	34.695	3.236 ± 7	3.264	137.72 ± 0.67
	B		3.240 ± 6	3.268	137.84 ± 0.80
	5740	34.695	3.230 ± 7	3.258	138.04 ± 0.48
Atlantic	10A	36.080	3.317 ± 7	3.218	137.86 ± 0.40
(7°44'N,	B		3.315 ± 8	3.216	137.84 ± 0.30
40°43'W)	690	34.611	3.207 ± 6	3.243	137.95 ± 0.30
	1640	34.981	3.229 ± 7	3.231	137.78 ± 0.35
	2910	34.938	3.208 ± 6	3.214	137.95 ± 0.26
	4280	34.811	3.238 ± 6	3.256	137.78 ± 0.35
Atlantic	1600	35.035	3.210 ± 6	3.207	137.48 ± 1.24
(31°49'N,	3400A	34.930	3.156 ± 3	3.162	137.31 ± 0.88
64°6'W)	B		3.166 ± 10	3.172	137.78 ± 0.84
	4550	34.897	3.198 ± 9	3.207	137.17 ± 1.10
			average =	3.238 ng/g	137.89 ± 0.15

[a] A and B indicate duplicate analyses.
[b] From PACYDORF (Scripps Institution of Oceanography) and shipboard salinometer measurements by D.J. Piepgras and P.M. Williams.
[c] M = measured, N = normalized to 35‰ salinity.
[d] The $^{238}U/^{235}U$ ratio for natural U is 137.88.
[e] All errors are $2\sigma_{mean}$.

TABLE 5

Th concentrations in seawater

Location	Depth [a] (m)	Wt. (g)	^{232}Th	
			total (pg) [b]	conc. (pg/g) [c]
Atlantic (7°44'N, 40°43'W)	10	258	33.5	0.118 ± 0.008
	690	509	77	0.145 ± 0.004
	1640	251	26.1	0.092 ± 0.008
	2910A	958	112	0.114 ± 0.002
	B	987	143	0.142 ± 0.002
	C	518	67.1	0.124 ± 0.004
	4280A	969	109	0.110 ± 0.002
	B	983	113	0.112 ± 0.002

[a] A, B and C indicate replicate analyses.

[b] pg = 10^{-12} g; total Th = dissolved + particulate + analytical blank.

[c] Subtracting 3 ± 2 pg Th blank.

m, Pacific) for which the concentrations are different by ~ 6‰ (slightly outside of the ± 2‰ error for each individual measurement). The observed U content shows a range of 5.1% (3.156–3.317 ng/g) or a range of ~ 3.8% (3.162–3.281 ng/g) when normalized to 35‰ salinity (Table 4). The salinity-normalized range for the Atlantic samples (3.162–3.256 ng/g) overlaps the range for the Pacific samples (3.244–3.281 ng/g) but the Pacific samples appear to have slightly higher (by ~ 1%) U concentrations. In the Atlantic, the U concentrations at 8°N appear to be ~ 1% higher than those at 32°N. A small fraction of U must reside in particulates. The concentration of particulates in seawater varies but is generally < 10^{-8} g/g [24] and the concentration of U in particulates has been reported as ~ 10^{-6} g/g [25]; therefore, one gram of seawater contains only ~ 10^{-5} ng of U in particulate form. It appears that the observed variation in U content cannot be due to variations in particulate U. Although the samples have been acidified, we cannot rule out the possibility that small but measurable amounts of U have been lost to the walls of the bottle. Ku et al. [6] have shown that this was not a problem at the ± 3% level, but this possibility needs to be reevaluated for our higher precision measurements. The ^{232}Th concentrations measured on Atlantic seawater (Table 5) range from 0.092 to 0.145 pg/g. The total amount of ^{232}Th in each analysis ranges from 26.1 to 143 pg including our analytical blank (3 ± 2 pg). Since the samples were not filtered and were acidified prior to analysis, the ^{232}Th concentrations represent the total ^{232}Th contents which include both dissolved and particulate phases. Two samples were analyzed in duplicate for Th. The data from 4280 m are in very good agreement but at 2910 m, there is ~ 25% spread which is outside the margin of error considering the blank. The cause of this discrepancy is not evident to us.

5. Discussion

Based on standards (Table 2), ^{234}U/^{238}U ratios can be measured to a precision of ± 5‰ (2σ) using ~ 5×10^9 atoms of ^{234}U. Data acquisition time is ~ 1 hour. Individual measurements are the same, within error, as the mean for all the measurements for a given standard. This shows that errors based on within-run statistics are a good estimate of the reproducibility of a given measurement. Checks on the linearity of the multiplier, the effects of the ^{235}U tail and the $^{238}U^{12}C_2^+$ reflected peak on the background around mass 234 and the response time of the electrometer indicate that systematic errors from these sources are insignificant at the ± 5‰ level. The ^{234}U/^{238}U data for seawater show that similar results can be obtained for samples requiring chemical separation. The method presented here has distinct advantages over standard α-counting methods for the measurement of ^{234}U as shown in Table 1. Among these are 4–10 times higher precision, ~ 10^3 times smaller sample size and ~ 10 times shorter data acquisition time.

We have examined ^{238}U-^{234}U in seawater to determine more precise values and to establish the level of variability of ^{234}U/^{238}U and of the U concentrations in seawater. In order to provide a framework within which to view our U concentrations and isotopic data, we present a simple one-dimensional, two box model consisting of a deep water mass (D) and a surface layer (S). The model is based on the assumptions that: (1) the system is at steady state; (2) all U is injected into surface water and all U is removed from deep water; (3) the mean life of ^{238}U with respect to radioactive decay is much longer than water mixing times; (4) the uranium removed from deep water has the isotopic composition of deep water; and (5) ^{238}U and ^{234}U are transported by mixing of water between the deep layer and the surface layer. The

model can easily be generalized to include scavenging of U from surface water and addition of U from sediment pore fluids but for simplicity, these terms have not been included. We define the following: τ_{234} and τ_{238} are the mean lives of ^{234}U and ^{238}U with respect to radioactive decay; τ_S and τ_D are the mean lives of water in the surface and deep reservoirs; τ_U is the mean life of U relative to removal from the deep reservoir (N^D_{238}/rate of removal of ^{238}U atoms from deep water); N^S_{238}, N^D_{238}, N^S_{234} and N^D_{234} are the number of atoms of ^{238}U and ^{234}U in the surface and deep reservoirs; C^S_{238} and C^D_{238} are the ^{238}U concentrations; W_D and W_S are the masses of water in the two reservoirs; and $C^S_{238} = N^S_{238}/W_S$ and $C^D_{238} = N^D_{238}/W_D$. At steady state, the number of ^{234}U atoms in the deep reservoir is constant with time yielding:

$$dN^D_{234}/dt = 0 = -N^D_{234}/\tau_{234} + N^D_{238}/\tau_{238} - N^D_{234}/\tau_D + N^S_{234}/\tau_S - N^D_{234}/\tau_U \quad (1)$$

where the first two terms account for radioactive decay and production of ^{234}U, the next two terms account for ^{234}U transport to and from the surface reservoir, and the last term is the rate of removal of ^{234}U from deep water. Similarly for ^{238}U in deep water:

$$dN^D_{238}/dt = 0 = -N^D_{238}/\tau_{238} + N^S_{238}/\tau_S - N^D_{238}/\tau_D - N^D_{238}/\tau_U \quad (2)$$

where the radioactive decay term is assumed to be negligible (assumption (3)), there is no radioactive production term, and the other terms are analogous to terms in equation (1). The mass of water in the deep reservoir is constant with time yielding:

$$dW_D/dt = 0 = W_S/\tau_S - W_D/\tau_D. \quad (3)$$

Combining equations (1) and (2) and using the equation defining $\delta^{234}U$ (see results section), we calculate:

$$\delta^{234}U_S/\delta^{234}U_D = (\tau_S N^D_{238}/\tau_{234} N^S_{238}) + 1. \quad (4)$$

Combining equations (3) and (4) yields:

$$\delta^{234}U_S/\delta^{234}U_D = (\tau_D/\tau_{234})(C^D_{238}/C^S_{238}) + 1 \quad (5)$$

which relates the ratio of $\delta^{234}U$ in the two reservoirs to the mean life of water in the deep layer. Combining equations (2) and (3) gives:

$$(C^{238}_S - C^{238}_D)/C^{238}_D = \tau_D/\tau_U \quad (6)$$

which relates the difference in ^{238}U concentration in surface and deep water to the mean life of U relative to removal from deep water. Equations (5) and (6) predict that both $\delta^{234}U$ values and U concentrations in seawater should be extremely constant. For $C^{238}_S/C^{238}_D \approx 1$ (see Table 4), $\tau_D \approx 10^3$ years (from ^{14}C, cf. [26–30]), and $\delta^{234}U_D = 144$ (see Table 3), equation (5) gives an essentially identical value for $\delta^{234}U_S$ (= 144.4). Using equation (6), taking $\tau_D \approx 10^3$ years and $\tau_U \approx 3 \times 10^5$ years [6], the predicted surface water concentration is only 3‰ higher than the deep water concentration.

Our observed $\delta^{234}U$ values can be compared to previous values as well as the predicted values from the model. Our data indicate that $^{234}U/^{238}U$ in the open ocean is constant to ± 5‰. This range is about a factor of four smaller than the range determined from earlier, high precision α-counting measurements. For comparison, the higher precision measurements by Ku et al. [6] show a range in $^{234}U/^{238}U$ activity ratio of 1.12–1.16, a range of 40‰. Within analytical uncertainty, the $\delta^{234}U$ values we have determined are the same, consistent with the very small range of $\delta^{234}U$ predicted by equation (5) and therefore consistent with the value of τ_D determined from ^{14}C [26–30].

The most striking feature of the U concentration data is the narrow range of salinity-normalized concentrations (Table 4) in rough agreement with the model prediction. There is an extensive body of U concentration data in the literature (see [6,8]). We compare our data with the results presented by Ku et al. [6] which represent the most recent large body of data on U concentrations. They concluded that salinity normalized U concentrations in the open ocean are the same within analytical error and give a value of 3.3 ± 0.2 μg/l. The range of their higher precision normalized concentrations is 3.17–3.58 μg/l, a spread of 12.9%. Our normalized data show a spread of 3.8%, which is a factor ~ 3 smaller. The oceanic profiles have ranges of 1.2% (Pacific), 1.4% (32° N, Atlantic) and 1.3% (8° N, Atlantic). The total range is about an order of magnitude larger than the range predicted by the model. It can be shown that, even if a scavenging term is added to the model and the maximum value for the observed flux of U from the surface is used (3.4 μg/cm² per 10^3 years, [25]), the predicted $(C^{238}_S - C^{238}_D)/C^{238}_D$

does not change substantially. This suggests that if uranium loss to the walls of the bottles is not a problem, either present estimates of the residence time of U in the oceans are too large and/or U is redistributed within the ocean at higher rates than has previously been documented. Studies of ^{234}U and ^{238}U in marine pore fluids and more extensive high precision measurements of ^{238}U in seawater would be important in distinguishing between these two alternatives.

The determination of ^{232}Th concentrations and their lateral and vertical variability in the ocean is important because ^{232}Th has a different source function than the other isotopes of Th (^{230}Th, ^{228}Th and ^{234}Th) which are intermediate daughters in the ^{238}U and ^{232}Th decay chains (cf. [31,32]). The radiogenic isotopes of Th have been used extensively to study chemical scavenging. In order to apply these studies to other non-radiogenic trace metals for which chemical scavenging is important, ^{232}Th concentration data is required. Substantial and ongoing efforts have been made by many workers to improve the analytical methods and to obtain thorium data. Our results confirm that ^{232}Th concentrations are extremely low. Our ^{232}Th concentrations (0.092–0.145 pg/g; see Table 5) are roughly the same as a number of ^{232}Th determinations in the literature (Table 6). Most previous workers have analyzed ^{232}Th by α-counting which requires extremely large sample sizes ($\sim 10^3$ l of seawater). To overcome the difficulties associated with collection and handling of 10^3 l of seawater, most workers have used ferric hydroxide and manganese oxide impregnated fibers as a means of in-situ scavenging of Th from large volumes of seawater. This requires either mooring of the fibers for long periods of time (~ months) or large amounts of ship time (~ 10 hours/sample) while seawater is pumped through the impregnated fibers. Huh and Bacon [32] have used neutron activation analysis to lower sample sizes to ~ 10 l of seawater. However, even with this quantity of seawater, their reported blanks contribute 25% to 98% of the ^{232}Th signal. The method presented here for mass spectrometric determination of the total ^{232}Th concentration requires ~ 1 l of seawater. The analytical blank for our procedure is ~ 3% of the total amount of ^{232}Th contained in 1 l of seawater. It is known (cf. [32,37]) that a significant fraction of the ^{232}Th resides on particles. Thus, for any investigation of the ^{232}Th concentration in the oceans, studies of filtered and unfiltered water are required. The use of 1–10 l samples for the present procedure should readily permit analysis of both dissolved and particulate loads of ^{232}Th. The small sample size, low blank and rapid analysis required by the method described here should greatly facilitate the collection and processing of seawater samples and allow one to carefully control the degree of contamination.

6. Conclusion

We have developed a procedure to measure $^{234}U/^{238}U$ to a 2σ precision of $\pm$ 5‰ on ~ 5×10^9 atoms of ^{234}U. This method should be applicable to a wide range of geologic problems which are either limited by small sample size or for which higher precision is required. As a first step, this method has been used to more precisely determine the $^{234}U/^{238}U$ ratio in Atlantic and Pacific seawater and put limits on the variability of this

TABLE 6

Summary of ^{232}Th abundances in seawater

Location	^{232}Th [a]		References
	dpm/10^3 kg	pg/g	
Atlantic	0.023–0.035	0.092–0.145	this work
Surface seawater	< 0.024	< 0.10	Kaufman [34]
South Pacific surface water	0.041	0.17	Knauss et al. [35]
Pacific	< 0.01–0.08	< 0.04–0.3	Moore [36]
Panama and Guatemala Basin	0.01–0.09	0.04–0.37	Bacon and Anderson [37]
Northwest Pacific deep water	0.0066–0.033	0.03–0.14	Nozaki and Horibe [31]
Caribbean	0.024	0.10	Huh and Bacon [32]

[a] Using $\lambda(^{232}Th) = 4.9475 \times 10^{-11}$ yr^{-1} [33] and assuming that 1 liter of seawater has a mass of 1 kg in converting dpm/10^3 kg to pg/g.

ratio. U concentrations have been measured as well. The mean $\delta^{234}U$ for nine samples is 144 ± 2 (2σ). U concentrations (normalized to 35‰ salinity) fall in a narrow range between 3.162 ng/g and 3.281 ng/g. Both of these ranges are several times smaller than those determined from earlier measurements. Using a simple two-box model, it has been shown that the narrow range of $^{234}U/^{238}U$ ratios is consistent with what is known about the mixing time of the oceans. The variation in salinity normalized U concentrations (3.8%) is about an order of magnitude larger than the range of concentrations calculated using a simple two-box model and suggests that either estimates of the residence time of U are too long and/or that U is redistributed within the ocean at higher rates than has previously been documented. We also present measurements on ^{232}Th concentrations which confirm that the levels in open ocean water are ~ 0.1 pg/g. The method presented for ^{232}Th determination should be readily applicable to studies of the distribution of ^{232}Th in the oceans both on particulates and in solution since the sample size requirement is small. It should also be evident that many trace elements can be measured to $\pm$ 1‰ using similar methods and can be used to examine transport problems in the ocean.

This approach has potential application to a wide range of problems. The flux of uranium and in particular ^{234}U from marine sediments may have important consequences for the marine U budget. The flux of ^{234}U from deep sea sediments has been estimated from measurements on the sediments themselves [38] but this has never been clearly verified by direct measurements on pore fluids and arguments against a large benthic ^{234}U flux have been presented [39]. The techniques described above should be capable of providing ^{234}U measurements with the required precision on the small quantities of pore fluids from marine sediments collected by presently available in-situ techniques.

Acknowledgements

We appreciate invaluable scientific and technical advice from D.A. Papanastassiou. We would like to thank P.M. Williams, C. Reimers, K.L. Smith, Jr., and the captain and crew of the R/V "Melville" for assistance in collecting and obtaining samples. D. Piepgras, and M. Stordal graciously provided some of the samples. Ship time on the R/V "Melville" was supported in part by NSF grants OCE 8315306 to C. Reimers, OCE 8417913 and OCE 8409075 to K.L. Smith, Jr. and OCE 8417102 to P.M. Williams. We are particularly grateful to K. Turekian and an anonymous reviewer for suggesting different formulations of the box model equations. This work has been supported by NSF grant OCE 8320516. Division Contribution No. 4338 (496).

References

1 M. Ivanovich and R.S. Harmon, Uranium Series Disequilibrium, 571 pp., Clarendon Press, Oxford, 1982.
2 V.V. Cherdyntsev, Trudy Tret'ei Sessii Komissii po opredeleniyu absolyutnogo vozrasta geologicheskikh formatsii (Transactions of the third session of the commission for determining the absolute age of geological formations), Izv. Akad. Nauk SSSR, Moscow, 175, 1955.
3 D. Thurber, Anomalous $^{234}U/^{238}U$ in nature, J. Geophys. Res. 67, 4518, 1962.
4 S.G. Bhat and S. Krishnaswami, Isotopes of uranium and radium in Indian rivers, Proc. Indian Acad. Sci. A 70, 1, 1969.
5 K.K. Turekian and L.H. Chan, The marine geochemistry of the uranium isotopes, ^{230}Th and ^{231}Pa, in: Activation Analysis in Geochemistry and Cosmochemistry, A.O. Brunfelt and E. Stemmes, eds., p. 311, Universitetsforlaget, 1971.
6 T.L. Ku, K.G. Knauss and G.G. Mathieu, Uranium in the open ocean: concentration and isotopic composition, Deep-Sea Res. 24, 1005, 1977.
7 S. Bloch, Some factors controlling the concentration of uranium in the world ocean, Geochim. Cosmochim. Acta 44, 373, 1980.
8 J.K. Cochran, The oceanic chemistry of the U- and Th-series nuclides, in: Uranium Series Disequilibrium, M. Ivanovich and R.S. Harmon, eds., p. 385, Clarendon Press, 1982.
9 J.H. Chen and G.J. Wasserburg, A search for isotopic anomalies in uranium, Geophys. Res. Lett. 7, 275, 1980.
10 J.H. Chen and G.J. Wasserburg, Isotopic determination of uranium in picomole and subpicomole quantities, Anal. Chem. 53, 2060, 1981.
11 J.H. Chen and G.J. Wasserburg, The isotopic composition of uranium and lead in Allende inclusions and meteroritic phosphates, Earth Planet. Sci. Lett. 52, 1, 1981.
12 B.L.K. Somayajulu, M. Tatsumoto, J.N. Rosholt and R.J. Knight, Disequilibrium of the ^{238}U series in basalt, Earth Planet. Sci. Lett. 1, 387, 1966.
13 J.N. Rosholt, B.R. Doe and M. Tatsumoto, Evolution of the isotopic composition of uranium and thorium in soil profiles, Geol. Soc. Am. Bull. 1977, 987, 1966.
14 B.J. Szabo and J.N. Rosholt, Uranium series dating of Pleistocene molluscan shells from S. California—an open system model, J. Geophys. Res. 74, 3253, 1969.
15 J.N. Rosholt and M. Tatsumoto, Isotopic composition of

uranium and thorium in Apollo 11 samples, Proc. Apollo 11 Lunar Sci. Conf. 2, 1499, 1970.

16 I.L. Barnes, B.S. Carpenter, E.L. Garner, J.W. Gramlich, E.C. Kuehner, L.A. Machlan, E.J. Maienthal, J.R. Moody, L.J. Moore, T.J. Murphy, P.J. Paulsen, K.M. Sappenfield and W.R. Shields, Isotopic abundance ratios and concentrations of selected elements in Apollo 14 samples, Proc. 3rd Lunar Sci. Conf. 2, 1465, 1972.

17 L.A. Dietz, C.F. Pachucki and G.A. Land, Internal standard technique for precise isotopic abundance measurements in thermal ionization mass spectrometry, Anal. Chem. 34, 709, 1962.

18 E.L. Garner, L.A. Machlan and W.R. Shields, Uranium isotopic reference materials, NBS Spec. Publ. 260-17, 65, 1971.

19 G.J. Wasserburg, D.A. Papanastassiou, E.V. Nenow and C.A. Bauman, A programmable magnetic field mass spectrometer with on-line data processing, Rev. Sci. Instrum. 40, 288, 1969.

20 E.D. Goldberg, M. Hoide, R.A. Schmitt and J. Smith, Rare earth element distributions in the marine environment, J. Geopnys. Res. 68, 4204, 1963.

21 A.H. Jaffey, K.F. Flynn, L.E. Glendenin, W.C. Bentley and A.M. Essling, Precision measurements of half-lives and specific activities of ^{235}U and ^{238}U, Phys. Rev. C 4, 1889, 1971.

22 M. Lounsbury and R.W. Durham, The alpha half-life of 234-U, in: Proc. Int. Conf. Chem. Nucl. Data, Measurement and Applications, Canterbury, M.L. Hurrell, ed., p. 215, Inst. Civil Engineers, London, 1971.

23 P. De Bievre, K.F. Lauer, Y. Le Duigon, H. Moret, G. Muschenborn, J. Spaepen, A. Spernol, R. Vaninbroukx and V. Verdingh, The half-life of ^{234}U, in: Proc. Int. Conf. Chem. Nucl. Data, Measurement and Applications, Canterbury, M.L. Hurrell, ed., p. 221, Inst. Civil Engineers, London, 1971.

24 P.E. Biscaye and S.L. Ettriem, Suspended particulate loads and transports in the nepheloid layer of the abyssal Atlantic Ocean, Mar. Geol. 23, 155, 1977.

25 R.F. Anderson, Concentration, vertical flux and remineralization of particulate uranium in seawater, Geochim. Cosmochim. Acta 46, 1293, 1982.

26 J.R. Arnold and E.C. Anderson, The distribution of ^{14}C in nature, Tellus 9, 28, 1957.

27 H. Craig, The natural distribution of radiocarbon and the exchange time of carbon dioxide between atmosphere and sea, Tellus 9, 1, 1957.

28 R. Revelle and H.E. Suess, Carbon dioxide exchange between atmosphere and ocean and the question of an increase of atmospheric CO_2 during the past decades, Tellus 9, 18, 1957.

29 W.S. Broecker and Y.H. Li, Interchange of water between the major oceans, J. Geophys. Res. 75, 3545, 1970.

30 W.S. Broecker and T.H. Peng, Carbon cycle: 1985, glacial to interglacial changes in the operation of the global carbon cycle, in preparation.

31 Y. Nozaki and Y. Horibe, Alpha-emitting thorium isotopes in northwest Pacific deep waters, Earth Planet. Sci. Lett. 65, 39, 1983.

32 C.A. Huh and M.P. Bacon, Thorium-232 in the eastern Caribbean Sea, Nature 316, 718, 1985.

33 L.J. Le Roux and L.E. Glendenin, Half-life of ^{232}Th, Proc. Natl. Meet. on Nuclear Energy, Pretoria, S. Africa, 83, 1963.

34 A. Kaufman, The Th-232 concentration of surface ocean water, Geochim. Cosmochim. Acta 33, 717, 1969.

35 K.G. Knauss, T.L. Ku and W.L. Moore, Radium and thorium isotopes in the surface waters of the East Pacific and coastal S. California, Earth Planet. Sci. Lett. 39, 235, 1978.

36 W.S. Moore, The thorium isotope content of ocean water, Earth Planet. Sci. Lett. 53, 419, 1981.

37 M.P. Bacon and R.F. Anderson, Distribution of thorium isotopes between dissolved and particulate forms in the deep sea, J. Geophys. Res. 87, 2045, 1982.

38 T.L. Ku, An evaluation of the $^{234}U/^{238}U$ method as a tool for dating pelagic sediments, J. Geophys. Res. 70, 3457, 1965.

39 D.V. Borale, S. Krishnaswami and B.L.K. Somayajulu, Uranium isotopes in rivers, estuaries and adjacent coastal sediments of western India: their weathering, transport and oceanic budget, Geochim. Cosmochim. Acta 46, 125, 1982.

Earth and Planetary Science Letters, 81 (1986/87) 175–192
Elsevier Science Publishers B.V., Amsterdam – Printed in The Netherlands

[6]

^{238}U-^{234}U-^{230}Th-^{232}Th systematics and the precise measurement of time over the past 500,000 years

R. Lawrence Edwards, J.H. Chen and G.J. Wasserburg

The Lunatic Asylum of the Charles Arms Laboratory, Division of Geological and Planetary Sciences, California Institute of Technology, Pasadena, CA 91125 (U.S.A.)

Received August 11, 1986; revised version received October 22, 1986

We have developed techniques to measure the ^{230}Th abundance in corals by isotope dilution mass spectrometry. This, coupled with our previous development of mass spectrometric techniques for ^{234}U and ^{232}Th measurement, has allowed us to reduce significantly the analytical errors in ^{238}U-^{234}U-^{230}Th dating and greatly reduce the sample size. We show that 6×10^8 atoms of ^{230}Th can be measured to $\pm 30‰$ (2σ) and 2×10^{10} atoms of ^{230}Th to $\pm 2‰$. The time over which useful age data on corals can be obtained ranges from a few years to ~ 500 ky. The uncertainty in age, based on analytical errors, is ± 5 y (2σ) for a 180 year old coral (3 g), ± 44 y at 8294 years and ± 1.1 ky at 123.1 ky (250 mg of coral). We also report ^{232}Th concentrations in corals (0.083–1.57 pmol/g) that are more than two orders of magnitude lower than previous values. Ages with high analytical precision were determined for several corals that grew during high sea level stands ~ 120 ky ago. These ages lie specifically within or slightly postdate the Milankovitch insolation high at 128 ky and support the idea that the dominant cause of Pleistocene climate change is Milankovitch forcing.

1. Introduction

As for most isotopic measurements of radioactive and radiogenic nuclides, studies of ^{238}U-^{234}U-^{230}Th-^{232}Th systematics have two primary aims: to determine the age and/or some aspect of the mechanisms of origin of a geologic material. This system differs from the commonly used isotope systems because ^{234}U and ^{230}Th have relatively short mean lives (~ 10^5 years) and, as intermediate daughters in the ^{238}U decay chain, are both radioactive and radiogenic. Because of the short mean lives, this system is appropriate for the investigation of processes which have occurred in the last ~ 5×10^5 years. Much of this time period is inaccessible by other methods. Conventional ^{14}C dating has a range of up to ~ 4×10^4 years. Measurement of ^{14}C by accelerator mass spectrometry has recently extended this range to ~ 7×10^4 years (see [1]). K-Ar techniques [2–4] (and rarely Rb-Sr [2]) have been used to date K-rich volcanics about 10^5 years old, but the availability of such materials is limited and the analytical uncertainty for these young materials is large.

Because ^{234}U and ^{230}Th are α-emitters and because of their short mean lives, analysis is typically done by isotope dilution α-spectrometry. Over the past several decades, investigators have extensively examined the ^{238}U-^{234}U-^{230}Th-^{232}Th systematics of a variety of geologic materials using these techniques (see [5]). These efforts have focused on two major problems, the study of source region characteristics and fractionation processes during magma generation [6–13], and the dating of marine and lacustrine precipitates [14–20]. The former line of investigation is valuable because in principle ^{238}U-^{234}U-^{230}Th-^{232}Th systematics can be used to determine the U/Th ratio in a young volcanic rock as well as its source region. This provides a test for models of trace element fractionation during magma generation. The latter line of investigation is particularly important because the absolute chronology of the late Pleistocene (< 150 ky; 1 ky = 10^3 years) high sea level stands is based on ^{238}U-^{234}U-^{230}Th dating of corals. There is an apparent correlation between the ages of a number of coral terraces thought to represent high sea level stands and the

Division Contribution No. 4371 (557).

0012-821X/87/$03.50

times of high summer solar insolation in the northern hemisphere as calculated from known changes in the geometry of the earth's orbit and rotation axis [21–23]. This relationship is one of the major observations in support of the astronomical or Milankovitch theory of climate change [24] which states that the fluctuations in Pleistocene climate are caused by the changes in the distribution of solar energy received by the earth due to changes in the obliquity of the ecliptic, changes in the eccentricity of the earth's orbit and the precession of the earth's rotation axis.

Both of these important lines of investigation have been limited by (1) the analytical uncertainty obtainable by α-counting methods, and (2) the diagenetic changes of the host minerals. Studies of ^{238}U-^{234}U-^{230}Th-^{232}Th systematics in volcanics are critically dependent on the ability to determine the difference between the measured $^{230}Th/^{238}U$ activity ratio and unity. Yet, there appears to be some doubt as to whether any unaltered silicic volcanic rocks have $^{230}Th/^{238}U$ activity ratios measurably different from unity [12]. Similarly, the major issue in coral dating studies is whether ages of terraces thought to represent high sea level stands correspond to periods of high solar insolation in the northern hemisphere. Most coral terraces dated by ^{238}U-^{234}U-^{230}Th methods which are pertinent to the study of climatic fluctuations in the Pleistocene have ages between 70 and 150 ky. In this age range, a typical α-counting analysis gives a 2σ error of about ± 10 ky (see [25]). Since the time between successive peaks in the Milankovitch insolation curve is ~ 20 ky, if sea level highs correspond to Milankovitch insolation highs, then the ages of two successive terraces are barely resolveable at the 2σ level just considering analytical uncertainties. The time difference between a high point and an adjacent low point in the Milankovitch curve is ~ 10 ky. Therefore, a clear correlation between times of high insolation and ages of coral terraces representing high sea level stands cannot presently be made. For corals significantly older than 100 ky, ages of successive coral terraces cannot, in general, be resolved by α-counting.

We have therefore undertaken this study to examine the possibility of measuring ^{230}Th to high precision by isotope dilution mass spectrometry. We have recently shown that it is possible to routinely measure 5×10^9 atoms of ^{234}U to better than $\pm 5‰$ (2σ), 8×10^{12} atoms of ^{238}U to $\pm 2‰$ (2σ), and 3×10^{11} atoms of ^{232}Th to $\pm 20‰$ (2σ) using mass spectrometric methods [26–29]. The addition of high-precision ^{230}Th measurements to this group of nuclides would allow the application of ^{238}U-^{234}U-^{230}Th-^{232}Th systematics to a wide range of geologic problems. Among these is the potential to delineate the detailed chronology of events in the late Pleistocene and Holocene. The purpose of this study is: (1) to develop an accurate, high-precision technique to measure ^{230}Th in small amounts of coral by isotope dilution mass spectrometry; (2) to develop a procedure to separate U and Th from corals with high chemical yields and low procedural blanks; (3) to analyze ^{238}U, ^{234}U, ^{230}Th and ^{232}Th in a number of corals to determine the precision with which corals of different ages can be dated and compare these dates to those obtained by other methods; and (4) to use these techniques to date several corals thought to have grown during (a) high sea level stand(s) 120–150 ky ago and compare these ages to the time of the Milankovitch insolation high at 128 ky. The basic problem with the mass spectrometric determinations is the low level of ^{230}Th and the possible high ^{232}Th signal causing a contribution at mass 230. The more fundamental question of whether corals can be selected which represent truly closed systems must await more extensive studies.

2. Experimental methods

2.1. Instrumental procedure

Mass spectrometric procedures used in this laboratory for measuring small uranium samples [30,31] and for measuring ^{237}U [26] have been described earlier. The approach used here is virtually identical to the "isotopic composition" run described in the latter reference. We use a double spike with $^{233}U/^{236}U \approx 1$ and spike the sample so that $^{235}U/^{236}U \approx 10$. The measurements are carried out on the Lunatic I (LI) mass spectrometer using an electron multiplier with a gain of 4×10^3 in the analogue mode and an electrometer (Cary 401) with a 10^9 Ω feedback resistor [32]. Data are acquired in the sequence ^{236}U-^{235}U-^{234}U-^{234}U-^{233}U. Zeros are measured 0.5 mass units above and below each mass. Integration time for zeros

TABLE 1

Comparison between mass spectrometric and α-counting methods for measuring ^{230}Th and ^{234}U in a ~120 ky old coral

Method	Sample size	Number of ions or alpha particles measured/run		2σ uncertainty [a]		
		^{230}Th	^{234}U	$^{230}Th/^{238}U$	$^{234}U/^{238}U$	age (ky)
Mass spec.	200 mg coral	5×10^{6}	2×10^{6}	±2‰	±5‰	±1
α-counting	10 g coral	3×10^{3}	5×10^{3}	±40‰	±30‰	±10

[a] The α-counting uncertainties are taken from Harmon et al. [25] and are based on counting statistics.

and peaks are one second for all masses except ^{234}U. ^{234}U peaks are measured for four seconds and zeros for two seconds. Data acquisition takes ~ two hours and 100–200 ratios (50–100 cycles with two ^{234}U measurements/cycle) are measured. Data are acquired at filament temperatures of 1640–1800°C. The $^{234}U^{+}$ current ranges from 1500 to 3000 ions/s. The total number of ^{234}U ions collected in one run is $\sim 2\times10^{6}$. The main difference between the procedure used in this study and the one described in [26] is that 3×10^{10} atoms of ^{234}U are loaded on the filament instead of 5×10^{9} atoms. This has the effect of lowering the temperature at which data is acquired by ~ 50°C and increasing the length of time the beam remains at high intensity by about a factor of 2. Consequently, the errors in $^{234}U/^{238}U$ shown in Table 4 tend to be slightly lower than those from our previous study. The ionization efficiency (ions produced/atoms loaded) for this procedure is $U^{+}/U \sim 5\times10^{-4}$ due to large sample size.

All data sets of ten ratios are normalized using the power law (see [33]) and the mean $^{233}U/^{236}U$ ratio for that set of ten ratios. The isotopic ratios and deviations of these ratios are then reduced using the full double spike equations. All quoted errors are 2σ of the mean ($2\sigma_M$). $^{234}U/^{238}U$ ratios are calculated for normalized $^{234}U/^{235}U$ ratios and ^{238}U concentrations calculated from the normalized $^{235}U/^{236}U$ ratios using $^{238}U/^{235}U = 137.88$. For a single run, $2\sigma_M$ for the $^{234}U/^{238}U$ ratio is typically ±4 to 5‰ and for the ^{238}U concentration is typically ±2 to 3‰ (see Tables 1, 3, 4).

Measurement of the Th isotopes is also carried out on the LI spectrometer using the same detector system. The sample is spiked with a ^{229}Th tracer so that each run contains $\sim 2\times10^{11}$ atoms of ^{229}Th. The number of ^{230}Th atoms loaded on the filament ranges from 6×10^{8} for a 180 year old sample to 6×10^{10} for a sample of several hundred ky as shown in Table 2. Analogue scans of the Th spectrum for a young and old sample are shown in Figs. 1 and 2. At running conditions, the $^{229}Th^{+}$ current is $\sim 1\times10^{5}$ ions/s and the $^{230}Th^{+}$ current ranges from 4×10^{2} to 4×10^{4} ions/s. Data is acquired at filament temperatures of 1810–1870°C. The isotopes are measured in the sequence ^{229}Th-^{230}Th-^{230}Th-^{232}Th. Zeros are measured 0.5 mass units above and below each mass. Integration time for the ^{230}Th peaks is 4 seconds; for the ^{230}Th zeros and ^{229}Th peak, 2 seconds; and for the remaining peak and zeros, 1 second. Data acquisition takes ~ 40 minutes and 40–60 ratios (20–30 cycles with two ^{230}Th measurements/cycle) of $^{230}Th/^{229}Th$ are measured. The total number of $^{230}Th^{+}$ ions collected in a run ranges from 6×10^{4} for the 180-year sample to 6×10^{6} for the oldest sample. For the $^{230}Th/^{229}Th$ ratio, the value of $2\sigma_M$ for one run ranges from ±30‰ for the very young sample (180 years) to ±2‰ for samples ~ 100 ky old. These uncertainties are only a factor of 2–3 times the error

TABLE 2

Number of ^{230}Th atoms per analysis and weight of coral analyzed

Run	^{230}Th atoms $\times10^{-10}$	Coral weight (g)
TAN-E-lg	0.058	2.8
CWS-F-1	0.43	4.6
CH-8	3.2	4.1
AFS-12 A	2.4	0.25
AFS-12 B	3.8	0.39
AFS-12 C	2.7	0.28
E-L-3	2.3	0.26
E-T-2	2.2	0.28
VA-1	6.2	0.38

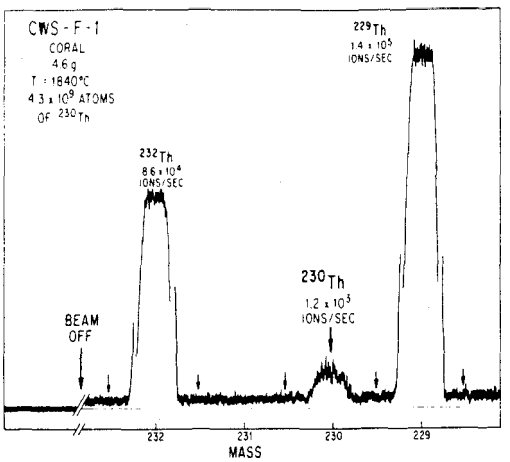

Fig. 1. Analogue scan of the Th spectrum for CWS-F-11 (845 years old) at a filament temperature of 1840°C. The sample was spiked with ^{229}Th. 4.3×10^9 atoms of ^{230}Th which had been extracted from 4.6 g of coral were loaded on the filament. The ionization efficiency was 0.8‰. Arrows show the position where zeros were measured. The background with the accelerating voltage on is slightly higher than the background with the accelerating voltage off due to the reflection of the ^{187}Re and ^{185}Re beams off the flight tube. The ^{230}Th abundance was determined to ±8‰ (2σ). Note the change in scale for ^{229}Th and ^{232}Th.

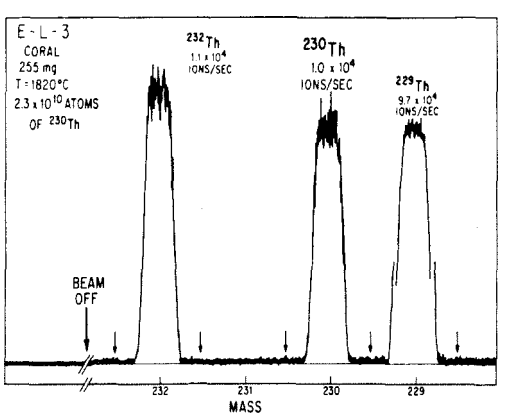

Fig. 2. Analogue scan of the Th spectrum similar to Fig. 1, but for a much older sample (E-L-3, 125.5 ky). 2.3×10^{10} atoms of ^{230}Th which had been extracted from 255 mg of coral were loaded on the filament. The ionization efficiency was 0.9‰ and the ^{230}Th abundance was determined to ±2‰. Note the change in scale for ^{229}Th.

due to counting statistics alone when the ions making up the background under the ^{230}Th peak and the counting statistics associated with the ^{229}Th peak are included in the calculation.

2.2. *Multiplier linearity and electrometer noise*

We have previously shown that the multiplier on the LI mass spectrometer is linear to ±2‰ for currents of up to 3×10^6 ions/s and isotopic ratios up to $\sim 10^2$ and that the response time of the electrometer is such that within one second after an ion beam is taken off the multiplier, the signal is $< 10^{-4}$ times the original signal [26,31]. For our Th measurements, the isotope ratios (^{229}Th/^{230}Th = 5–200) and ion currents (up to 1.6×10^5 ions/s) are not large enough to cause problems associated with electrometer response time or non-linearity problems that are significant. The noise level of the multiplier and amplifier under normal operating conditions is equivalent to ±12 ions/s where the uncertainty given is 2σ of the distribution for a series of 4-second noise measurements. The 2σ error for one ^{230}Th measurement including the background subtraction is ±17 ions/s. Since the ^{230}Th current is measured ~40 times in one run, the total error due to electrometer noise is $\pm 17/\sqrt{40} = \pm 3$ ions/s. For a ^{230}Th$^+$ current of 4×10^2 ions/s, this is about a quarter of the ±30‰ observed error. For larger samples, the error due to noise is smaller.

2.3. *Background characteristics*

Under normal operating conditions, the background under the Th spectrum is slightly higher than the background with the accelerating voltage off (cf. Figs. 1 and 2). This difference is typically ~150 ions/s and is due to the reflection of the ^{187}Re$^+$ and ^{185}Re$^+$ beams off the flight tube. In the vicinity of the ^{230}Th peak, the background due to the reflected peak is effectively linear. For larger (i.e. older) samples, the background current is only a few permil of the ^{230}Th$^+$ current and does not introduce significant errors. For smaller samples, the background current is >10% of the ^{230}Th$^+$ beam. This has the effect of lowering the precision of the ^{230}Th measurement slightly since the measurement of the ^{230}Th zero and the ^{230}Th peak are subject to the counting statistics associated with the ~150 ions/s. However, the Re beam is reasonably stable and does not change by

large amounts during the course of a run. Since a ^{230}Th zero is measured immediately before and immediately after each ^{230}Th peak measurement, we do not believe that significant inaccuracy or imprecision other than that associated with counting statistics is introduced by the background current.

2.4. Fractionation

Fig. 3 shows the change in the measured ^{229}Th/^{232}Th during the course of a spike calibration run. This shows that, not including the very end of the run, Th fractionates by a total range of only 1.5‰ per mass unit in the course of a run. This is much less than the ±2‰ error of the highest precision ^{230}Th measurements as shown by the "$+2\sigma$" and "-2σ" lines in Fig. 3. For the data reported here, ratios measured at the end of a run when the beam is decaying by more than 5%/minute are not included. Reproducible results for several spike calibration runs indicate that instrumental fractionation does not introduce errors larger than the ±2‰ error of the individual runs even for isotopes different in mass by 3 amu. Fractionation at the multiplier is corrected for by multiplying the measured ^{n}Th/^{m}Th ratio by $(n/m)^{1/2}$, where n and m are the mass numbers. It has been shown previously by measuring the same sample with the multiplier and collector, that this relationship adequately corrects for multiplier fractionation on the LI system [34].

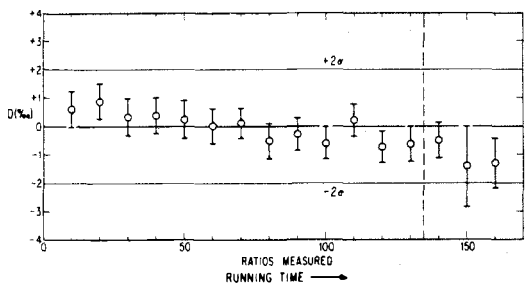

Fig. 3. This shows the measured ^{229}Th/^{232}Th ratio versus time for a spike calibration run. $D = \{[(^{229}\text{Th}/^{232}\text{Th})_{TEN}/(^{229}\text{Th}/^{232}\text{Th})_{GM}]^{1/3} - 1\} \times 10^3$ where the subscript TEN refers to the mean of a set of ten ratios and GM refers to the grand mean of all the ratios in the run. D is a measure of the deviation per mass unit of a given set of ten ratios from the grand mean in parts per thousand. The horizontal axis represents the time of data acquisition (~1 hour) and is scaled in cumulative ratios. The error bars for the individual points are $2\sigma_M$ for that set of ten ratios. The vertical dashed line represents the time that the beam began to decay by more than 5% per minute. Data to the right of this line is discarded. 10^{13} atoms of Th were loaded on the filament for this run. This is somewhat larger than typical filament loads for corals (10^{12} Th atoms). The horizontal lines labeled "$+2\sigma$" and "-2σ" represent the 2σ error in ^{230}Th/^{229}Th for high-precision coral runs. The total range of fractionation is well within these bounds, showing that error due to fractionation is small.

2.5. Ionization efficiency

The ionization efficiency for a number of Th runs on standards and Th separated from corals is shown plotted as a function of total Th loaded in Fig. 4. This shows that ionization efficiency decreases with increasing Th loaded on the filament using this approach. For the corals analyzed, total Th loads were $< 10^{12}$ atoms and ionization efficiencies were 0.7–1.3‰. As discussed below, corals have relatively high ^{230}Th/^{232}Th ratios (see Table 4), so for a fixed amount of ^{230}Th loaded on the filament, very little ^{232}Th is also loaded on the filament. Most geologic materials have ^{230}Th/^{232}Th ratios which are several orders of magnitude lower than corals, so for the same amount of ^{230}Th loaded, large amounts of ^{232}Th are also loaded. The relationship in Fig. 4 suggests that mass spectrometric ^{230}Th measurements on these materials would have significantly lower ionization efficiencies and, consequently, larger uncertainties than obtained here.

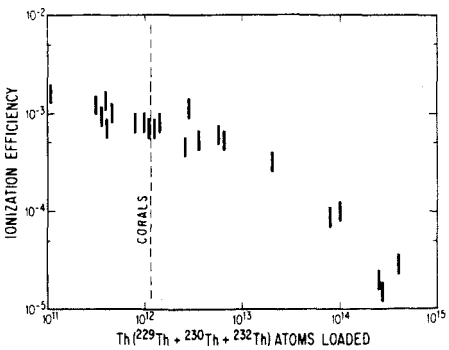

Fig. 4. This shows a log-log plot of the ionization efficiency vs. the total number of Th atoms loaded on the filament for corals and for standards. Ionization efficiency decreases with increasing Th loads. The coral runs all lie to the left of the dashed line marked "corals" and have ionization efficiencies of 0.7–1.3‰.

2.6. Spikes and standards

The ^{229}Th spike was obtained from Oak Ridge National Laboratory in solution in nitrate form. This was diluted with $1N$ HNO_3 and stored in a teflon bottle. Mass spectrometer runs to determine the isotopic composition of the spike showed that it was essentially pure ^{229}Th ($^{230}Th/^{229}Th < 2 \times 10^{-5}$ and the amount of ^{232}Th was indistinguishable from the filament loading blank, $^{232}Th/^{229}Th < 7 \times 10^{-4}$). Analogue scans showed that none of the U isotopes were present in appreciable amounts. A ^{232}Th standard solution was prepared (T. Wen, September 1976) from 99.998% pure ThO_2 powder (Johnson and Matthey) which was heated to 700°C, weighed, dissolved in a solution of $2.5N$ HNO_3 and $0.01N$ HF and stored in a 1-liter teflon bottle. This bottle has been weighed recently. Comparison with the original weight indicates that evaporative losses could not have increased the ^{232}Th concentration of the solution by more than 0.7‰ over the past ten years. The original ^{232}Th solution was diluted twice with $\sim 1N$ HNO_3 in 1985. The dilute solutions had volumes of 1 liter and 500 ml and were stored in tightly capped, nearly full teflon bottles. In isotopic composition, these solutions had $^{230}Th/^{232}Th = 6.8 \pm 0.2 \times 10^{-5}$ and $^{229}Th/^{232}Th < 10^{-5}$. The ^{229}Th spike was calibrated against the most dilute ^{232}Th standard solution. The ^{229}Th concentration of this spike is $(5.508 \pm 0.006) \times 10^{11}$ atoms/g (mean and $2\sigma_M$ for four experiments). The error for each experiment ranged from ± 0.9‰ to ± 2.0‰. None of four experiments gave a concentration which differed from the average value by more than 1.5‰.

As a further check, another ^{232}Th solution was prepared recently from a Th metal powder which was significantly less pure than the ThO_2 powder. An aliquot of this solution was mixed with a ^{229}Th tracer and the $^{232}Th/^{229}Th$ ratio was measured. The ^{229}Th concentration determined using the Th metal standard agreed to $\sim 1\%$ with that determined using the Th oxide standards and showed that processes such as adsorption of Th onto the walls of the bottle, or precipitation of Th salts, which would lower Th concentration, have not occurred to any significant extent for the Th oxide standard over the past ten years. U standards and spikes are as discussed by Chen and Wasserburg [31].

2.7. Chemical separation of U and Th

Procedures for purification of U and Th are similar to those described in [26]. Coral samples (with the exception of some of AFS-12 which was provided to us in powdered form) were prepared by breaking the sample into pieces several millimeters in diameter with a stainless steel chisel. These fragments were examined under a binocular microscope and any pieces that showed signs of secondary alteration were discarded. The remaining pieces were ultrasonically cleaned in distilled water twice. The large pieces were then rinsed individually in distilled water, dried and weighed. The fine pieces were discarded. Samples of 2.8–4.6 grams of young (< 10 ky) coral or ~ 500 mg of old (> 10 ky) coral were dissolved by first adding several milliliter of distilled water, then slowly adding concentrated HNO_3 over the course of ~ 1 hour. The solution was heated under a heat lamp for ~ 1 hour. This resulted in the oxidation of any remaining organic matter and changed the color of the solution from slightly brown to clear. The sample was then spiked and, in order to insure sample-spike equilibration, dried, fumed with concentrated $HClO_4$, and dried. It was then dissolved in $\sim 1N$ HCl and ~ 8 mg of Fe in chloride solution was added. The U and Th were then co-precipitated with Fe by the addition of ammonium hydroxide until the color of the solution changed from yellow to clear. The mixture was centrifuged and the supernate discarded. The residue was then rinsed twice with distilled water, dissolved in concentrated HNO_3, dried and redissolved in concentrated HNO_3 twice, dried and dissolved in 0.5 ml of $7N$ HNO_3. This solution was loaded on an anion exchange column (Dowex AG 1×8 resin) with a volume of 0.5 ml. Fe was eluted using $7N$ HNO_3. The Th fraction was then eluted with $6N$ HCl and the U fraction with $1N$ HBr. The U fraction was dried, dissolved with HNO_3, dried, dissolved in HNO_3, dried and dissolved in $0.1N$ HNO_3. An aliquot containing $\sim 3 \times 10^{10}$ atoms of ^{234}U (corresponding to ~ 70 mg coral) was loaded on a graphite-coated zone refined Re filament as described in [31]. The Th fraction was further purified by drying it down, dissolving it in HNO_3, drying it and dissolving it in 0.15 ml of $7N$ HNO_3. This solution was loaded on a column similar to the first column but with a volume of 0.15 ml. A similar elution scheme was

followed. The subsequent Th fraction was dried, dissolved in HNO_3, dried and dissolved in 0.1*N* HNO_3. For samples younger than 10 ky, the whole Th fraction was loaded, and for samples older than 10 ky, half the Th fraction (corresponding to 250–390 mg of coral) was loaded on a graphite-coated zone refined Re filament. The loading technique is similar to the U loading technique. For the complete procedure, the U yield is > 95% and the Th yield is 93–98%. The amount of U in the Th fraction is $< 10^{-5}$ times the total U processed.

2.8. Analytical blank

We use zone refined, highly annealed Re filaments (REMBAR Co., Inc.) that have been outgassed at ~ 2000°C for 2 hours. Examination of one batch of Re ribbon showed that outgassed filaments coated with graphite following our standard procedure produced $^{232}Th^+$ currents of 6×10^2 to 4×10^5 ions/s and $^{238}U^+$ currents of < 60 to 3×10^3 ions/s when heated to typical temperatures at which data were acquired. Since typical sample currents are 3×10^7 ions/s for ^{238}U and 8×10^4 ions/s for ^{232}Th, many of the $^{232}Th^+$ filament currents were unacceptably high. Outgassing for longer periods of time or at slightly higher temperatures did not appreciably lower the currents. A second batch of Re ribbon from the same supplier gave filament currents of < 60 to 1×10^4 for $^{232}Th^+$ and < 60 to 2×10^3 for $^{238}U^+$. Out of 53 filaments, all but three had $^{232}Th^+$ currents below 1×10^3 ions/s. Since occasionally, filaments in this batch have high $^{232}Th^+$ currents, as standard procedure, we check every filament in the mass spectrometer before loading a sample on it. Filaments with $^{232}Th^+$ currents higher than 10^3 ions/s are not used.

The total procedural blank including the filament blank is 1.2×10^{10} atoms of ^{238}U and 1.0×10^{10} atoms of ^{232}Th with upper limits of 9×10^6 atoms of ^{234}U and 6×10^6 atoms of ^{230}Th. The blanks were determined using standard mass spectrometer runs with digital data acquisition and standard integration times. Blank levels of ^{234}U are presumably ~ 10^{-4} times ^{238}U and levels of ^{230}Th around 10^{-5} times ^{232}Th. In order to avoid introducing ^{230}Th and ^{229}Th contamination from previous samples, all re-usable labware, including ion exchange columns, which come in contact with coral solutions are divided into two groups. One group is used for young corals (< 10 ky) which have low ^{230}Th concentrations and, when spiked, have low $^{230}Th/^{229}Th$ ratios, and the other group for old corals (> 10 ky) which have high ^{230}Th concentrations and higher $^{230}Th/^{229}Th$ ratios. The two groups of labware are cleaned and stored separately. Ion exchange resin is discarded after every use. Between samples, ion exchange columns are rinsed with 7*N* HNO_3 and distilled water, stored (in separate groups) in 7*N* HNO_3, and rinsed with 7*N* HNO_3 and distilled water before the next use.

2.9. Resolution of small differences in ^{230}Th abundance and time

For one run, the 2σ error in $^{234}U/^{238}U$ is ±4–5‰. The error in the ^{238}U abundance is ±2–3‰ and the error in the ^{230}Th abundance ranges from ±30‰ for the 180 year old sample (TAN-E-lg) to ±2‰ for a 123.1 ky old sample (AFS-12; see Tables 1, 3, 4). The error in $^{230}Th/^{238}U$ therefore ranges from ±30‰ to ±3‰. When the analytical errors in $^{234}U/^{238}U$ and $^{230}Th/^{238}U$ are propagated through the age equation (equation (1), discussed below), errors in age of ±5 years for TAN-E-lg and ±1.1 ky for AFS-12 A are calculated. Based on these errors, one would expect to be able to resolve the ages of two young (~ 200 year old) corals different in age by ~ 10 years and two old (~ 120 ky old) corals different in age by ~ 2 ky.

In order to confirm this age resolution estimate, we carried out the following experiment. About 3 g of AFS-12 were dissolved and the solution divided into five aliquots, four aliquots containing ~ 0.5 g of coral and the remaining aliquot kept in reserve. Known amounts of ^{230}Th from a ^{230}Th standard solution were added to three of the four aliquots. This increased the ^{230}Th concentrations in these aliquots by ~ 8‰, 16‰ and 32‰. This is equivalent to shifts in age of ~ 2, 4 and 8 ky. All four aliquots were then spiked, processed, and the Th isotopes measured as described above. The U isotopes were measured in one aliquot. The results are shown in Fig. 5 where the ^{230}Th abundance determined on the mass spectrometer is plotted against the gravimetrically determined ^{230}Th abundance. The ages corresponding to the ^{230}Th concentrations are also shown. These are calculated using equation (1) (see discussion below) and

182

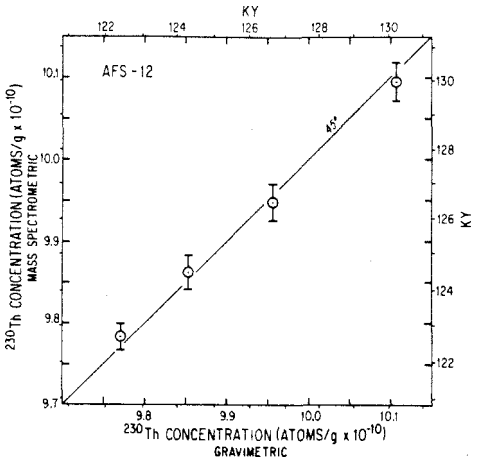

Fig. 5. This shows the mass spectrometrically determined ^{230}Th abundance (^{230}Th atoms/g) plotted vs. the gravimetrically determined ^{230}Th abundance for AFS-12 B and aliquots of AFS-12 B to which known amounts of ^{230}Th have been added. The axes are also scaled in ky using the measured ^{238}U abundance, ^{238}U/^{234}U ratio and equation (1). The error bars are $2\sigma_M$. None of the points deviate by more than 1.2‰ or 0.3 ky from a 45° line through the origin. The diagram shows that just considering the error in the ^{230}Th measurement, differences in age of < 2 ky are clearly resolvable for a coral ~ 120 ky old.

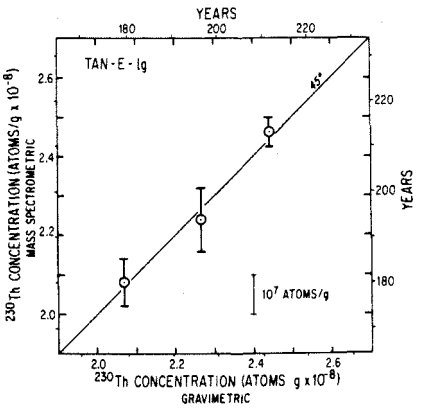

Fig. 6. This is similar to Fig. 5 but for a much younger coral (TAN-E-lg, 180 years). In addition to ^{230}Th atoms/g, the axes are also scaled in years. None of the points deviate from the 45° line by more than 12‰ or 2.4 years. The diagram shows that for corals ~ 200 years old, differences in ^{230}Th concentration of ~ 10^7 atoms/g, corresponding to differences in age of 17 years, are clearly quantitatively resolvable.

the results of the U analysis. The ^{230}Th concentration of the initial solution used in the calculation of the gravimetric ^{230}Th concentration is an average of the four ^{230}Th determinations after the known enrichments of ^{230}Th have been subtracted. All four points plot within 1.2‰ or 0.3 ky of a 45° line through the origin, indicating agreement between the mass spectrometric and gravimetric determinations will within the error of each individual measurement. Based on this experiment and assuming no error in the U analysis, it is clear that, for ~ 120 ky old corals, differences in age of 2 ky are analytically resolvable.

A similar experiment was performed to determine the age resolution for very young corals. About 15 g of TAN-E-lg was dissolved and the resulting solution divided into four aliquots. Three aliquots contained ~ 3 g of coral each, and the remainder was kept in reserve. ^{230}Th was added to two of the aliquots in order to increase the ^{230}Th concentration by 90‰ and 170‰, respectively. The number of ^{230}Th atoms added was 2×10^7 and 4×10^7. This corresponds to shifts in age of 17 and 33 years. The Th isotopes were measured in all three aliquots and the U isotopes in one aliquot. The results of this experiment are shown in Fig. 6. None of the points differ by more than 12‰ or 2 years from the 45° line, again well within the error of the individual measurements. This experiment shows that, for corals ~ 200 years old, differences in age of 17 years are clearly resolvable analytically.

3. Samples

We analyzed samples which had a variety of ages as well as samples which would provide information on the timing of the sea level high(s) at around 120 ky. Perhaps the most extensively studied coral terraces of this age are from Barbados [20–22], the Huon Peninsula in New Guinea [23,35] and islands in the New Hebrides Arc [36–38]. We have analyzed samples from Barbados and the New Hebrides as well as one coral from Hispaniola. Sample numbers, genus, species when known, locality, and references where more information concerning the samples can be found are listed in Table 3. TAN-E-lg, CWS-F-1 and CH-8 were provided to us by F.W. Taylor, AFS-12 (powder) by T.L. Ku, AFS-12 (rock fragment) and VA-1 by R.K. Matthews, and E-T-2 and E-L-3 by

TABLE 3

^{238}U and ^{232}Th concentrations in corals

Sample [a]	Genus and species	Locality	^{238}U (nmol/g) [b,c]	^{232}Th (pmol/g) [c,d]	($^{232}Th/^{238}U$) $\times 10^5$
TAN-E-lg	*Platygyra* –	Tangoa Is., S. of Santo Is., New Hebrides Arc (F.W. Taylor, written communication)	10.80 ± 0.04	0.083 ± 0.003	0.77 ± 0.03
CWS-F-1	*Platygyra* –	W. coast of Santo Is., New Hebrides Arc, (F.W. Taylor, written communication)	10.21 ± 0.01	0.147 ± 0.002	1.44 ± 0.02
CH-8	*Siderastua radians*	Canada Honda, shore of Lago Enriquillo, SW Dominican Republic [39]	9.68 ± 0.01	0.279 ± 0.002	2.88 ± 0.02
AFS-12 A	*Acropora palmata*	Rendezvous Hill, Christ Church Ridge, Barbados [20]	12.66 ± 0.02	1.40 ± 0.05	11.1 ± 0.4
B	–	–	12.62 ± 0.03	1.57 ± 0.03	12.4 ± 0.2
C	–	–	12.43 ± 0.03	1.37 ± 0.03	11.1 ± 0.2
E-T-2	*Oulophyllia crispa*	Port Havannah, Efate Is., New Hebrides Arc, [40]	9.75 ± 0.01	0.12 ± 0.03	1.2 ± 0.3
E-L-3	*Porites lutea*	Port Havannah, Efate Is., New Hebrides Arc, [40]	11.39 ± 0.03	0.12 ± 0.03	1.1 ± 0.3
VA-1	*Acropora palmata*	Hill View Terrace, St. George's Valley, Barbados [20]	13.37 ± 0.02	1.08 ± 0.02	8.1 ± 0.2
Open ocean surface water [e]	–		0.01383 ± 3	0.00051 ± 3	3.7 ± 0.2

[a] A, B and C indicate replicate analyses; for AFS-12, A and B represent different fractions of the same powder and C represents separate coral fragments.

[b] Calculated using $^{238}U/^{235}U = 137.88$.

[c] All errors are $2\sigma_M$. 1 nmol/g = 10^{-9} mol/g; 1 pmol/g = 10^{-12} mol/g.

[d] Corrected for the procedural blank of 0.02 ± 0.01 pmoles ^{232}Th; most of the error is due to the uncertainty in the blank correction.

[e] Atlantic surface water from [26].

A.L. Bloom. All samples have been previously dated by ^{14}C, $^{230}Th/^{234}U$ (α-counting) or U-He (see Table 5). Except for VA-1, all samples were shown by previous workers, using X-ray diffraction techniques, to contain less than 1% calcite. TAN-E-lg was alive when sampled and the portion which we analyzed represents the annual growth bands from 1804 to 1810. All samples grew in marine environments except possibly CH-8, which was collected along the shore of Lago Enriquillo, a lake on Hispaniola [39]. This sample is close to the base of a marine transgressive sequence. Based on faunal assemblages, it is thought that the body of water from which CH-8 grew was connected to the ocean. AFS-12 is from the reef crest facies of the Rendezvous Hill or Barbados III terrace which is thought to have formed during a high sea level stand and has an age of 129 ± 9 ky

($^{230}Th/^{234}U$, α-counting, 2σ; Ku, unpublished). E-T-2 and E-L-3 are from a terrace doublet on Efate Island in the New Hebrides Arc. E-T-2 is from the flower terrace and E-L-3 is from the upper terrace. Assuming that progressively higher terraces are older, E-L-3 would be the older of the two terraces. These have both been dated at 141 ± 16 ky (2σ, $^{230}Th/^{234}U$ (α-counting), [40]). They are thought to correlate with the terrace doublets of about the same age on the Huon Peninsula of New Guinea [36,40] and may correlate with a terrace doublet also of similar age on Loh Island in the New Hebrides [38]. It has been suggested that the double terraces in New Guinea represent two sea level highs ~ 125 ky and ~ 140 ky ago [41,42] (see [43]). The older of these two terraces would pre-date the nearest Milankovitch insolation high by some 10 ky and therefore could not be caused by this phenomenon. VA-1 (Hill View Terrace, Saint George's Valley, Barbados) has a U-He age of 520 ky [20] and was chosen in order to determine the isotopic characteristics of a very old sample. An extensive study [20] of these old terraces using U-He and ^{238}U-^{234}U-^{230}Th techniques has shown that many of the corals have $^{234}U/^{238}U$ initial values much higher than would be expected for a marine environment and some of them had $^{230}Th/^{234}U$ ratios slightly higher than the maximum possible value for a closed system.

4. Results

Our data for ^{238}U and ^{232}Th concentrations are shown in Table 3. ^{238}U concentrations in different corals are similar to those reported by previous workers. ^{232}Th concentrations vary by over an order of magnitude from 0.083 to 1.57 pmol/g and have errors of ±8‰ to ±250‰. The errors are largely due to the uncertainty in the blank correction (0.02 ± 0.01 pmoles ^{232}Th). Previous determinations of ^{232}Th in corals have not obtained such low values. The samples from Barbados (AFS-12 and VA-1) have distinctly higher ^{232}Th concentrations (1.08–1.57 pmol/g) than the other corals. $^{232}Th/^{238}U$ ratios are extremely low and range from 0.77×10^{-5} to 12.4×10^{-5}. These values are comparable to the $^{232}Th/^{238}U$ ratio of surface water in the open ocean (3.7×10^{-5}; [26,44–48]).

The isotopic data and the calculated ages are presented in Table 4. The $^{234}U/^{238}U$ atomic ratios have been reformulated into δ-notation, which denotes the fractional enrichment in $^{234}U/^{238}U$ relative to the $^{234}U/^{238}U$ ratio at secular equilibrium in parts per thousand. The observed value is given by $\delta^{234}U(0) = \{[(^{234}U/^{238}U)/(^{234}U/^{238}U)_{eq}] - 1\} \times 10^3$ where $(^{234}U/^{238}U)_{eq}$ is the atomic ratio at secular equilibrium (5.472×10^{-5}). The initial value is $\delta^{234}U(T)$ and is calculated using equation (2) (below). $^{230}Th/^{238}U$ atomic ratios have also been represented as activity ratios $[^{230}Th/^{238}U]_{act}$ by multiplying the $^{230}Th/^{238}U$ atomic ratio by $\lambda_{230}/\lambda_{238}$. The age is calculated from the ^{238}U-^{234}U-^{230}Th age equation (equation (1), below) using $\delta^{234}U(0)$ and $[^{230}Th/^{238}U]_{act}$.

Except for one sample, $\delta^{234}U(0)$ ranges from 103 for an older sample (E-T-2) to 152 for a younger coral (CWS-F-1). CH-8 has a distinctly lower $\delta^{234}U(0)$ (= 82) than the other samples. Errors are ± 4–6 δ-units. Except for CH-8 and VA-1, $\delta^{234}U(T)$ falls in a narrow range between 149 and 162. The range of these values is slightly higher but overlaps the range for present-day open ocean water of various depths (140–150; [26]). For CH-8, $\delta^{234}U(T) = 84$. For VA-1, $\delta^{234}U(T)$ is 530 using the U-He age (= 520 ky, [20]) and is much higher than the present seawater value. Not including VA-1, errors in $\delta^{234}U(T)$ range from ±4 to 9 δ-units and are somewhat larger than those for $\delta^{234}U(0)$.

$^{230}Th/^{232}Th$ atomic ratios vary from 0.0042 for the youngest coral (TAN-E-lg) to 1.2 for an older coral (E-L-3). These values are extremely high compared to most geologic materials ($^{230}Th/^{232}Th \sim 10^{-5}$). This is due to the extremely low $^{232}Th/^{238}U$ ratio in corals. The error in these values, ±9‰ to ±250‰, is due largely to uncertainty in the blank correction for ^{232}Th.

$^{230}Th/^{238}U$ atomic ratios range from 3.20×10^{-9} to 2.0144×10^{-5}, corresponding to activity ratios of 0.00190–1.1940. Errors range from ±30‰ for very low ratios to ±2‰ for higher ratios. VA-1 has $^{230}Th/^{238}U$ higher than the maximum possible value for closed system evolution from seawater, confirming observations by Bender et al. [20]. For the other samples, the ages and 2σ uncertainties in age have been calculated from equation (1), $\delta^{234}U(0)$ and $[^{230}Th/^{238}U]_{act}$ and are shown in Table 4. Replicate analyses have been

TABLE 4

U and Th isotopic composition of corals and seawater and coral ages [a]

Sample	$(^{234}U/^{238}U) \times 10^5$	$\delta^{234}U(0)$ [b,c]	$\delta^{234}U(T)$ [b,c]	$^{230}Th/^{232}Th$ [d]	$(^{230}Th/^{238}U) \times 10^5$	$[^{230}Th/^{238}U]_{act}$	Age [b,f]
TAN-E-lg	6.285 ± 31	149 ± 6	149 ± 6	0.0042 ± 2	0.00320 ± 9	0.00190 ± 5	180 ± 5 y
CWS-F-1	6.306 ± 22	152 ± 4	153 ± 4	0.0105 ± 2	0.01506 ± 13	0.00893 ± 8	845 ± 8 y
CH-8	5.920 ± 20	82 ± 4	84 ± 4	0.0465 ± 4	0.13415 ± 48	0.07951 ± 28	8,294 ± 44 y
AFS-12 A [g]	6.066 ± 22	109 ± 4	153 ± 6	0.116 ± 4	1.2811 ± 47	0.7593 ± 28	122.1 ± 1.1 ky
B	6.080 ± 35	111 ± 5	157 ± 7	0.103 ± 2	1.2874 ± 42	0.7631 ± 25	122.7 ± 1.3 ky
C	6.068 ± 25	109 ± 5	155 ± 6	0.117 ± 2	1.2957 ± 47	0.7680 ± 28	124.5 ± 1.3 ky
E-T-2	6.036 ± 22	103 ± 4	149 ± 6	1.1 ± 0.2	1.3179 ± 28	0.7811 ± 17	129.9 ± 1.1 ky
E-L-3	6.093 ± 26	113 ± 5	162 ± 7	1.2 ± 0.3	1.3071 ± 40	0.7748 ± 24	125.5 ± 1.3 ky
VA-1	6.136 ± 32	121 ± 6	-	0.249 ± 5	2.0144 ± 65	1.1940 ± 39	-
Open ocean water [h]	6.239 ± 26 to 6.292 ± 26	140 ± 5 to 150 ± 5	-	7×10^{-6} to 2×10^{-5}	3×10^{-5} to 7×10^{-5}	1×10^{-5} to 4×10^{-5}	-

[a] All errors are $2\sigma_M$; all isotope ratios are atomic ratios unless otherwise specified.

[b] $\lambda_{238} = 1.551 \times 10^{-10}$ y^{-1} [61]; $\lambda_{234} = 2.835 \times 10^{-6}$ y^{-1} [59,60]; $\lambda_{230} = 9.195 \times 10^{-6}$ y^{-1} [58].

[c] $\delta^{234}U = \{[^{234}U/^{238}U)/(^{234}U/^{238}U)_{eq}] - 1\} \times 10^3$ where $(^{234}U/^{238}U)_{eq}$ is the atomic ratio at secular equilibrium and is equal to $\lambda_{238}/\lambda_{234} = 5.472 \times 10^{-5}$. $\delta^{234}U(0)$ is the measured value. $\delta^{234}U(T)$ is the initial value calculated using the ^{238}U-^{234}U-^{230}Th age (equation (1)) and equation (2).

[d] Corrected for the ^{232}Th blank of 0.02 ± 0.01 pmoles; most of the error is due to the uncertainty of the blank correction.

[e] $[^{230}Th/^{230}U]_{act}$ is the activity ratio calculated by dividing $^{230}Th/^{238}U$ by the $^{230}Th/^{238}U$ atomic ratio at secular equilibrium; $(^{230}Th/^{238}U)_{eq} = \lambda_{238}/\lambda_{230} = 1.6871 \times 10^{-5}$.

[f] Age refers to the age of the sample in 1986; 1 ky = 10^3 years.

[g] A, B and C indicate replicate analyses; A and B are different fractions of the same powder; C is a rock fragment from the same sample.

[h] Values for the U isotopic composition and the ^{232}Th and ^{238}U abundances are from [26]; the ^{230}Th abundance is from surface water values in [55].

performed for AFS-12. Analyses "A" and "B" are from different splits of the same powder and "C" is from a separate rock fragment. All three analyses give $\delta^{234}U(0)$, $[^{230}Th/^{238}U]_{act}$ and age which are in excellent agreement within the error of the measurements. The ages which we obtained for E-L-3 and E-T-2 suggest that E-L-3 is younger than E-T-2. This is in apparent disagreement with the field evidence [40], which suggests that since E-L-3 is from the higher terrace, it should be older. The reason for this discrepancy is not apparent to us.

5. Discussion

5.1. The ^{238}U-^{234}U-^{230}Th age equation and the uncertainty in age

^{234}U and ^{230}Th are the longest lived intermediate daughters in a decay series that starts with ^{238}U and ends with ^{206}Pb. The ^{238}U decay series with only the nuclides pertinent to this discussion is shown below:

$$^{238}U \xrightarrow[6.446 \times 10^9 \text{ y}]{} {}^{234}Th \xrightarrow[34.8 \text{ days}]{} {}^{234}U \xrightarrow[352.7 \times 10^3 \text{ y}]{}$$

$$^{230}Th \xrightarrow[108.8 \times 10^3 \text{ y}]{} {}^{206}Pb$$

The times below the arrows are mean lives. The mean life of ^{238}U is several orders of magnitude longer than any of the intermediate daughters so that any closed system, regardless of the initial state, will approach a state of "secular equilibrium". In this state, the activities of all the intermediate daughters are the same and are equal to the ^{238}U activity. Any process which removes or adds nuclides in the decay chain will disrupt the equilibrium. The subsequent growth or decay of the intermediate nuclides toward a new equilibrium state can be used to date geological materials [14–17,49–54] ^{238}U-^{234}U-^{230}Th dating of corals is possible because of the extreme fractionation of U from Th in seawater ($^{232}Th/^{238}U$

is $\sim 10^5$ times lower than in igneous rocks). The $^{232}Th/^{238}U$ ratio in corals as shown in Table 3 is similar to that in seawater. The $^{230}Th/^{238}U$ ratio in seawater is similarly low. ^{230}Th measurements in surface water from the open ocean [55] indicate that this ratio is typically 3×10^{-10} to 7×10^{-10} or 2×10^{-5} to 4×10^{-5} times the equilibrium $^{230}Th/^{238}U$ ratio. If ^{230}Th does not fractionate greatly from ^{238}U during coral growth as appears to be the case from $^{232}Th/^{238}U$, then the initial $^{230}Th/^{238}U$ ratio must be negligible. Using this initial condition and the assumption that a coral remains a closed system with respect to U and Th, the equations for radioactive production and decay of ^{238}U, ^{234}U and ^{230}Th yield

Equation (1):

$$1 - \left[\frac{^{230}Th}{^{238}U}\right]_{act} = e^{-\lambda_{230}T} - \left(\frac{\delta^{234}U(0)}{1000}\right)\left(\frac{\lambda_{230}}{\lambda_{230} - \lambda_{234}}\right) \times (1 - e^{(\lambda_{234} - \lambda_{230})T})$$

(modified from Kaufman and Broecker, [17]).

Equation (2):

$$\delta^{234}U(T) = \delta^{234}U(0)e^{\lambda_{234}T}$$

where the λ's denote the decay constants and T is the age. Equation (1) is plotted in Fig. 7 which shows $[^{230}Th/^{238}U]_{act}$ plotted as a function of T and contoured in units of $\delta^{234}U(T)$. This shows that as T becomes large, $[^{230}Th/^{238}U]_{act}$ approaches unity. The second term on the right-hand side of the equation accounts for the fact that $\delta^{234}U$ in seawater and $\delta^{234}U(T)$ in corals are not equal to zero. Equation (1) shows that the age of a coral can be calculated if $\delta^{234}U(0)$, $[^{230}Th/^{238}U]_{act}$ and the decay constants are known. Equation (2) relates the observed $\delta^{234}U(0)$ to the initial state when the system was isolated with $^{230}Th = 0$.

In order to calculate the age accurately, accurate values for the decay constants must be known. Previous studies have used mean lives of 108,500 years for ^{230}Th and 357,800 years for ^{234}U, based on the studies of Attree et al. [56] and presumably Fleming et al. [57], respectively. We have chosen to use the more recent determinations of 108,750 $\pm$ 850 years (2σ; [58]) for the mean life of ^{230}Th

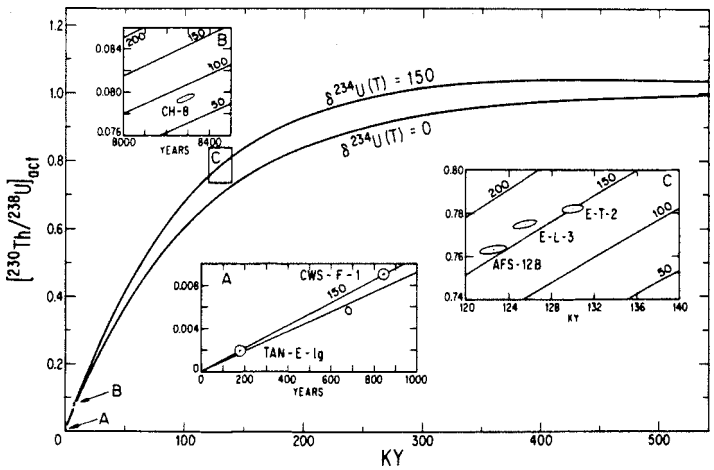

Fig. 7. This shows the change in $[^{230}Th/^{238}U]_{act}$ with time for different initial $\delta^{234}U$ values and is calculated assuming a closed system and assuming initial $^{230}Th = 0$ (equations (1) and (2)). $\delta^{234}U = 150$ is close to the present-day seawater value. Insets A, B and C are blowups of different areas of the graph. Note that the horizontal axes for A and B are scaled in years. All the contours are $\delta^{234}U(T)$ values. With the exception of VA-1 which cannot be plotted in this diagram, all the corals are plotted with their respective 2σ error ellipses. Note that for inset A, the analytical error is shown by the small black ellipses inside the open circles. The circles are drawn for clarity only. For insets B and C, the 2σ error is shown by the open ellipses and the mean value is represented by the centroid. With the exception of CH-8, which presumably grew in an environment restricted from the open ocean, all points lie on or close to the $\delta^{234}U(T) = 150$ line.

and 352,740 ± 710 years (2σ; [59,60]) for the mean life of ^{234}U. Within error, the earlier ^{230}Th value is the same as the more recent value, but the analytical uncertainty of the more recent value is much smaller. The value for ^{234}U is the average of the two 1971 references. These two values are different by 200 years. The 2σ error which we quote is from the latter reference. For ^{238}U, we use $(6.4464 \pm 0.0069) \times 10^9$ years (2σ; [61]).

The fractional errors in the decay constants are as follows: λ_{238}, ±1‰; λ_{234}, ±2‰; and λ_{230}, ±8‰. Errors in the decay constants will yield systematic errors in T. Errors in λ_{238} and λ_{234} are insignificant compared to our analytical errors for all T. For $\lambda_{230}T \ll 1$, λ_{230} is not an important term and does not introduce significant error in T. As T increases, λ_{230} becomes a more important term and the uncertainty in T increases. For T < 150 ky, the error in T due to error in λ_{230} is less than the error in T due to the analytical uncertainty. For T larger than 150 ky, the error in T due to error in λ_{230} is up to 1.5 times larger than the error due to analytical uncertainty. The error in years due to errors in λ's is ±0.4 for $T = 200$ years, ±2 for $T = 1000$ years, ±22 for $T = 10$ ky, ±800 for $T = 120$ ky, and ±17,000 years for $T = 300$ ky and is therefore insignificant compared to analytical error except at large T.

Uncertainties in T are also introduced by uncertainties in $\delta^{234}U(0)$ and $[^{230}Th/^{238}U]_{act}$. These uncertainties were the dominant source of error in earlier studies. We showed in the experimental method section that, based on the addition of a known quantity of ^{230}Th atoms, we could resolve the ages of two ~ 200 year old corals different in age by 17 years and could resolve the ages of two ~ 120 ky old corals different in age by 2 ky. We now examine the error in T, ΔT, introduced by analytical error, as a function of T. We have analyzed a number of corals of different ages. The calculated ages using equation (1) and the 2σ errors in age based on the propagation of the analytical errors in $\delta^{234}U(0)$ and $[^{230}Th/^{238}U]_{act}$ through equation (1) are listed in Tables 4 and 5 and plotted in Fig. 7. The coral data are also plotted on a $\Delta T/T$ versus T plot (Fig. 8). We have drawn an error envelope through these points. This envelope has been extrapolated to larger and smaller T using the following assumptions: For extrapolating to large T, we have assumed that the analytical uncertainty for older corals is the same as the analytical uncertainty for ~ 120 ky corals. This assumption is reasonable since the number of atoms/gram of ^{230}Th and ^{234}U for an infinite age coral are both within 50% of their values for a ~ 120 ky old coral. For extrapolating to T younger than 180 years, we have assumed that the fractional error is inversely proportional to the square

TABLE 5

Coral ages using different methods or techniques [a]

Sample	^{14}C [b] (conventional)	^{14}C [c] (corrected)	Ring counting	^{238}U-^{234}U-^{230}Th (α-counting)	^{238}U-^{234}U-^{230}Th (this study)
TAN-E-lg	270 ± 120 y (1)	30–70, 180–270, or 300–500 y	176–182 y (1)	–	180 ± 5 y
CWS-F-1	980 ± 120 y (1)	780–1010 y	–	–	845 ± 8 y
CH-8	8990 ± 120 y (2)	~ 10,000 y	–	–	8294 ± 44 y
AFS-12 A	–	–	–	129 ± 9 ky (3)	122.1 ± 1.1 ky
B				129 ± 9 ky (3)	122.7 ± 1.3 ky
C				129 ± 9 ky (3)	124.5 ± 1.3 ky
E-T-2	–	–	–	141 ± 16 ky (4)	129.9 ± 1.1 ky
E-L-3	–	–	–	141 ± 16 ky (4)	125.5 ± 1.3 ky

[a] All errors are 2σ. Ages refer to the ages in 1986 (C.E.). Numbers in parentheses refer to the following sources: (1) F.W. Taylor (written communication), (2) Taylor et al. [39], (3) Ku (unpublished), (4) Bloom et al. [40].

[b] ^{14}C ages are as reported by the sources in radiocarbon years using the 8033 year mean life; no corrections have been made for natural fractionation of carbon isotopes, the difference between $^{14}C/C$ in surface water and the atmosphere, or differences in initial $^{14}C/C$.

[c] ^{14}C ages have been corrected by us to dendroyears using the curves of Stuiver [68] for TAN-E-lg and CWS-F-1 and assuming a $^{14}C/C$ initial ratio from Klein et al. [69] for tree rings ~ 8000 years old. No corrections have been made for natural fractionation of carbon isotopes or the difference between $^{14}C/C$ in the surface water and the atmosphere.

188

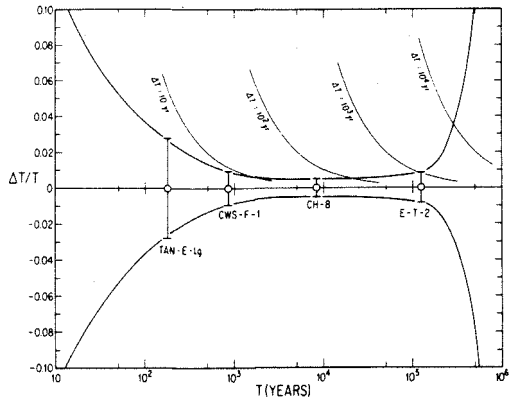

Fig. 8. This shows $\Delta T/T$ plotted versus time, where T is the age and ΔT is the 2σ error in age based on the propagation of analytical errors through equation (1). T is plotted on a log scale. Between 180 years and 129.9 ky, the error envelope is drawn through the observed values for several corals. The error envelope is extrapolated to younger and older T as described in the text. The lowest values of $\Delta T/T$ are at $\sim 10^4$ years and values of $\Delta T/T < 0.10$ can be obtained over the range $T = 15$ years to $T = 500{,}000$ years. Parts of the diagram are contoured in ΔT. The intersection of the $\Delta T = 10^4$ contour with the error envelope shows that $\Delta T < 10^4$ years for all $T < 3 \times 10^5$ years.

root of the number of ^{230}Th atoms per analysis. This error envelope shows that the smallest fractional errors in age of $\sim \pm 5‰$ are obtained for corals several thousand to several tens of thousands of years old. These samples are old enough to have enough ^{230}Th atoms for a high precision analysis (using small amounts of coral) yet are young enough ($\lambda_{230}T < 1$) to fall on the initial linear part of the $[^{230}\text{Th}/^{238}\text{U}]_{act}$ growth curve (see Fig. 7). The error envelope also shows that $\Delta T/T < 0.10$ for corals as young as 15 years old and as old as 500,000 years old. Corals as old as 600 ky have ages distinguishable from infinity at the 2σ level. Fig. 8 is also contoured in absolute error, ΔT. Examination of the $\Delta T = 10^4$ years contour shows that, for all $T < 300$ ky, $\Delta T < 10$ ky. If sea level highs are separated by ~ 20 ky, it follows that all coral terraces representing sea level highs which are younger than 300 ky have analytically resolvable ages.

The analyzed corals have previously been dated by the counting of coral growth rings, ^{14}C, and/or ^{238}U-^{234}U-^{230}Th using α-counting methods and are compared in Table 5. TAN-E-lg was dated by ^{14}C and by counting of growth rings (F.W. Taylor, written communication). It was determined using the latter method that the portion of the coral which we analyzed grew between 1804 and 1810 (176–182 years old). Our date of 180 ± 5 years (at the time the sample was analyzed, June 1986) is in excellent agreement with this result. TAN-E-lg, CWS-F-1 and CH-8 have all been dated by ^{14}C (F.W. Taylor, written communication, [39]). For CH-8, the corrected age has been given as an approximation without uncertainties because the precise correction at this time does not appear to be known. The corrected radiocarbon ages and our ages for TAN-E-lg and CWS-F-1 are consistent within the errors of the measurements. However, there is a substantial difference between the corrected ^{14}C age and our age for CH-8. The reality of this discrepancy requires serious comparison of both methods, particularly for samples older than 8000 years where the availability of samples dated by dendrochronology is limited. We note that the analytical precision of the ^{238}U-^{234}U-^{230}Th dates is several times higher than the ^{14}C dates.

AFS-12, E-T-2 and E-L-3 have been dated previously using the ^{238}U-^{234}U-^{230}Th method by α-counting. Our determinations agree with the earlier results at the 2σ level of uncertainty of the errors quoted. However, the uncertainties in the present study are around an order of magnitude smaller. It is clear from Table 1 that the main reason behind the improved precision is that many more ions can be measured by mass spectrometry than α-particles by counting decays. We measured $\sim 10^6$ ions of ^{230}Th or ^{234}U per run, whereas in a typical α-counting run, $\sim 10^3$ α-particles are measured. The sample size which we use (250 mg of coral) is also ~ 40 times smaller than the typical sample sizes used for α-counting.

5.2. *^{232}Th concentrations and $\delta^{234}U(T)$*

Our ^{232}Th determinations in corals are extremely low (Table 3). Because of the extremely low values and the long mean life of ^{232}Th, α-counting studies have often not reported ^{232}Th. Examination of the reported ^{232}Th concentrations (cf. [16,18,62–66]) shows that the typical detection limit in the α-counting studies is about 100 pmol/g and that values as high as 10^4 pmol/g have been measured. Thus, the previous values (with the

possible exception of [20]) are at least two orders of magnitude higher than the values which we report in Table 3. From an analytical standpoint, the low ^{232}Th concentrations found for corals mean that for a given amount of ^{230}Th loaded on the filament, relatively little ^{232}Th is also loaded on the filament. Thus, small amounts of total Th are loaded, ionization efficiency is high (see Fig. 4), and counting statistics for the ^{230}Th measurement are improved. The reliable determination of ^{232} Th also permits use of the ^{232}Th concentration as a geochemical tracer. From our results, it appears that $^{232}Th/^{238}U$ ratios in corals are about the same as open ocean surface water ([26]; Table 3), suggesting that these elements do not substantially fractionate from each other during coral growth. Substantial shifts in this ratio can therefore be used to indicate Th addition due to diagenesis (cf. [20]), metabolic effects, or growth from water with a different $^{232}Th/^{238}U$ ratio than open ocean water.

The precise $\delta^{234}U(T)$ values are sensitive indicators of alteration or the environment in which a coral grew. All samples, with the exception of CH-8 and VA-1, have $\delta^{234}U(T)$ values between 149 and 162. The range for open ocean water is $\delta^{234}U = 140$–150 [26]. Considering errors, $\delta^{234}U(T)$ for these samples is fully compatible with origin in a marine environment. This can be seen in insets "A" and "C" in Fig. 7 which show that these samples plot close to the $\delta^{234}U(T) = 150$ contour. Based on the $\delta^{234}U(T)$ values for the two youngest corals which are the least likely to have been altered, it appears that marine corals may initially have $\delta^{234}U$ values that are at the high end or possibly higher than our values for open ocean water, possibly reflecting near-shore waters. For VA-1, $\delta^{234}U(T) = 530 \pm 26$ (using the U-He age of 520 ky [20] for T). This is much higher than the seawater value and is clear evidence for diagenetic addition of ^{234}U, confirming previous observations [20]. CH-8 is thought to represent the initial stage of a marine transgression into the Enriquillo Valley [39]. However, the calculated $\delta^{234}U(T) = 84$ (see inset "B", Fig. 7) is distinctly different from seawater, and cannot represent closed system evolution from normal seawater. It is possible that the sample was diagenetically altered or that CH-8 grew in a body of water that was restricted from the ocean and had a different uranium isotopic composition than the ocean. As Lago Enriquillo is reasonably shallow ($\sim$ 20 m deep), limited exchange with sediments could produce significant changes in uranium isotopic composition.

5.3. The Milankovitch curve and ages of corals ~ 120 ky old

Milankovitch [24] has calculated curves of the summer solar insolation at various latitudes as a function of time (cf. recalculations by Berger [67]). The curve for 65°N is appropriate for the initial growth of continental glaciers (see Fig. 9). This curve has low values between 166 and 137 ky, rises a maximum at 128 ky, then drops to a low value at 116 ky. According to the Milankovitch Theory, the height of sea level as a function of time should have a shape similar to the insolation curve. The dates of coral terraces representing sea level highs, should have ages close to or slightly younger than the 128 ky peak. Two successive coral terraces in New Guinea [23,35] have given ages determined by α-counting to be $\sim$ 125 ky and $\sim$ 140 ky and have led to the idea that the sea level curve may have had a double peak with ages corresponding

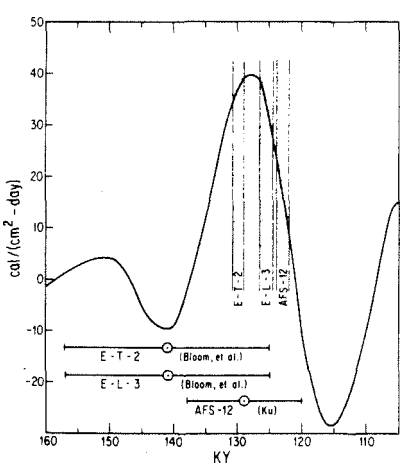

Fig. 9. The vertical axis represents the average solar insolation per day received at the top of the atmosphere at 65°N for the summer half year minus the present value. The curve is drawn for $T = 160$ ky to 105 ky and is taken from Berger [67]. The stippled bands represent the ages which we determined for E-T-2, E-L-3, and AFS-12. The error bars represent the ages of corals based on previous analyses (Bloom et al. [40]. Ku (unpublished)). The ages which we have determined agree with the earlier values at the 2σ level but are much more precise and lie specifically within the Milankovitch band.

to the terrace ages [41,42]. A sea level high at ~ 140 ky would pre-date the 128 ky insolation peak by more than 10 ky and could not be the result of Milankovitch forcing. Kaufman [43] has argued, based upon a statistical analysis of a large number of dates, that if there were two peaks, they could not have been separated by more than 7.5 ky and that both peaks must have ages no older than 129 ky. The precise ages of these terraces should resolve this issue which is critical to our thinking about the causes of the Pleistocene glaciations.

AFS-12, E-L-3 and E-T-2 were known from previous work to have ages between 120 and 160 ky and are thought to have grown during periods of high sea level. E-L-3 and E-T-2 are from the upper and lower terraces of a terrace doublet in the New Hebrides which may correlate with the New Guinea terrace doublet [36,40]. Assuming the corals have not been altered, the ages of the terraces can be compared to the age of the insolation high. This is shown in Fig. 9 along with previous age data. The earlier data showed that the ages were in the general vicinity of 120–160 ky. Our data show that the ages lie specifically within the Milankovitch band. The age of E-L-3 (129.9 ky) appears to agree almost exactly with the 128 ky insolation high with a hint that it might be 2 ky older than the maximum. E-T-2 (125.5 ky) and AFS-12 (123.1 ky) appear to postdate the maximum by as much as 5 ky. The ages of E-L-3, E-T-2 and AFS-12 support the idea that Pleistocene sea level highs are the result of Milankovitch forcing. The apparent high position of sea level at 129.9 ky (represented by E-T-2) would require that, as the insolation curve increases, the phase lag between the Milankovitch and the sea level curves be very small (~ 1 ky or less). The age of AFS-12 suggests that sea level was still high, 5 ky after the insolation peak, suggesting that, as the insolation curve decreases, the phase lag is significantly larger. From the spread in ages between E-T-2 and AFS-12, it appears that sea level was high for at least 7 ky during the last interglacial period. Our data do not preclude the possibility of a double sea level peak at ~ 120 ky, but suggest that if there is a double peak, both occurred specifically within the band and could be explained in a general way by the Milankovitch mechanism.

6. Conclusions

We have shown that it is possible to measure 6×10^8 ^{230}Th atoms to ±30‰ and 2×10^{10} ^{230}Th atoms to ±2‰ by isotope dilution mass spectrometry (2σ). This, coupled with the ability to measure 3×10^{10} ^{234}U atoms to ±5‰ and ^{238}U to ±2‰ [26], has allowed us to reduce significantly the analytical errors in ^{238}U-^{234}U-^{230}Th dating. This has allowed us to expand the time range over which useful age data on corals can be obtained to a range of a few years to ~ 500 ky. The uncertainty in age is ±5 years for a 180 year old coral (3 grams) and ±1 ky for a 123.1 ky old coral (250 mg). The ability to analyze small samples is very important with regard to studies of marine terraces. Reef forming corals are largely limited to the tropics. Solitary corals, however, grow in marine environments worldwide, and can be found in marine terraces of different latitudes, but only occur in small masses. Few marine terraces have yielded enough solitary coral for analysis by α-counting. The small sample size may also allow dating of materials such as foraminifera, clams and bones. Dating of these materials has been limited either by sample size requirements or sample alteration. The use of high dispersion mass spectrometers and ion counting detector systems will allow further refinement of these techniques, including extension to volcanics with high ^{232}Th contents. The precise measurements on corals which grew during sea level high(s) around 120 ky ago give ages which lie specifically within the 128 ky Milankovitch peak. Assuming closed system behavior, these ages support the idea that changes in Pleistocene climate are largely due to Milankovitch forcing.

Acknowledgements

We are particularly grateful to a number of our colleagues who have spent many years working on various aspects of coral terraces and coral dating and were willing to share their expertise. We enjoyed the sound advice and enthusiastic support of T.L. Ku and A.L. Bloom. F.W. Taylor and R.K. Matthews provided well-documented and characterized samples. We have benefited from discussions with Fairchild Broecker and P. Aharon. The reviewers, H.F. Shaw and W.S. Broecker, and the

editor, K.K. Turekian are thanked for constructive criticisms of the manuscript. Philosophical and technical advice from D.A. Papanastassiou is gratefully acknowledged. Funding for this work was specifically denied by the National Science Foundation. This work was possible through the support of the John D. MacArthur Fund using equipment supported by NASA grant No. NAG 9-43. Division Contribution No. 4371 (557).

References

1 R.E.M. Hedges, Radioisotope clocks in archaeology, Nature 281, 19, 1979.

2 F. Radicati di Brozolo, J.C. Huneke, D.A. Papanastassiou and G.J. Wasserburg, ^{39}Ar-^{40}Ar and Rb-Sr age determinations on Quaternary volcanic rocks, Earth Planet. Sci. Lett. 53, 445, 1981.

3 R.A. Bailey, G.B. Dalrymple and M.A. Lanphere, Volcanism, structure, and geochronology of the Long Valley Caldera, Mono County, California, J. Geophys. Res. 81, 725, 1976.

4 A.R. Gillespie, J.C. Huneke and G.J. Wasserburg, Eruption age of Pleistocene basalt from $^{40}Ar/^{39}Ar$ analysis of partially degassed xenoliths, J. Geophys. Res. 88, 4997, 1984.

5 M. Ivanovich and R.S. Harmon, Uranium Series Disequilibrium, 571 pp., Clarendon Press, Oxford, 1982.

6 B.L.K. Somayajulu, M. Tatsumoto, J.N. Rosholt and R.J. Knight, Disequilibrium of the ^{238}U series in basalt, Earth Planet. Sci. Lett. 1, 387, 1966.

7 V.M. Oversby and P.W. Gast, Lead isotope compositions and uranium decay series disequilibrium in recent volcanic rocks, Earth Planet. Sci. Lett. 5, 199, 1968.

8 S. Nishimura, Disequilibrium of the ^{238}U series in recent volcanic rocks, Earth Planet. Sci. Lett 8, 293, 1970.

9 C.J. Allègre and M. Condomines, Fine chronology of volcanic processes using ^{238}U-^{230}Th systematics, Earth Planet. Sci. Lett. 28, 395, 1976.

10 C.J. Allègre and M. Condomines, Basalt genesis and mantle structure studied through Th-isotopic geochemistry, Nature 299, 21, 1982.

11 S. Newman, R.C. Finkel and J.D. MacDougall, ^{230}Th-^{238}U disequilibrium systematics in oceanic tholeiites from 21°N on the East Pacific Rise, Earth Planet. Sci. Lett. 65, 17, 1983.

12 J.T. Bennett, S. Krishnaswami, K.K. Turekian, W.G. Melson and C.A. Hopson, The uranium and thorium decay series nuclides in Mt. St. Helens effusives, Earth Planet. Sci. Lett. 60, 61, 1982.

13 R.W. Williams, J.B. Gill and K.W. Bruland, Ra-Th disequilibria systematics: timescale of carbonatite magma formation at Oldoinyo Lengai volcano, Tanzania, Geochim. Cosmochim. Acta 50, 1249, 1986.

14 J.W. Barnes, E.J. Lang and H.A. Potratz, Ratio of ionium to uranium in coral limestone, Science 124, 174, 1956.

15 W.S. Broecker, A preliminary evaluation of uranium series inequilibrium as a tool for absolute age measurements on marine carbonates, J. Geophys. Res. 68, 2817, 1963.

16 D.L. Thurber, W.S. Broecker, R.L. Blanchard and H.A. Potratz, Uranium series ages of Pacific atoll coral, Science 149, 55, 1965.

17 A. Kaufman and W.S. Broecker, Comparison of ^{230}Th and ^{14}C ages for carbonate materials from lakes Lahontan and Bonneville, J. Geophys. Res. 70, 4039, 1965.

18 H.H. Veeh, $^{230}Th/^{238}U$ and $^{234}U/^{238}U$ ages of Pleistocene high sea level stand, J. Geophys. Res 71, 3379, 1966.

19 T.L. Ku, M.A. Kimmel, W.H. Easton and T.J. O'Neil, Eustatic sea-level 120,000 years ago on Oahu, Hawaii, Science 183, 959, 1974.

20 M.L. Bender, R.G. Fairbanks, F.W. Taylor, R.K. Matthews, J.G. Goddard and W.S. Broecker, Uranium series dating of the Pleistocene reef tracts of Barbados, West Indies, Geol. Soc. Am. Bull. Part I, 90, 577, 1979.

21 W.S. Broecker, D.L. Thurber, J. Goddard, T.L. Ku, R.K. Matthews and K.J. Mesollela, Milankovitch hypothesis supported by precise dating of coral reefs and deep sea sediments, Science 159, 297, 1968.

22 K.J. Mesolella, R.K. Matthews, W.S. Broecker and D.L. Thurber, The astronomical theory of climate change: Barbados data, J. Geol. 77, 250, 1969.

23 H.H. Veeh and J.M.A. Chappell, Astronomic theory of climate change: support from New Guinea, Science 167, 862, 1970.

24 M.M. Milankovitch, Canon of insolation and the ice age problem, Königlich Serbische Akademie, Beograd (English translation by the Israel Prog. for Sci. Translations, Washington, D.C., 1941).

25 R.S. Harmon, T.L. Ku, R.K. Matthews and P.L. Smart, Limits of U-series analyses: Phase I results of the Uranium-Series Intercomparison Project, Geol. 7, 405, 1979.

26 J.H. Chen, R.L. Edwards and G.J. Wasserburg, ^{238}U, ^{234}U, and ^{232}Th in seawater, Earth Planet. Sci. Lett. 80, 241, 1986.

27 J.H. Chen, G.J. Wasserburg, K.L. Von Damm and J.M. Edmond, Pb, U, and Th in hot springs on the East Pacific Rise at 21°N and Guaymas Basin, Gulf of California, Trans. Am. Geophys. Union 64, 724, 1983.

28 J.H. Chen and G.J. Wasserburg, $^{234}U/^{238}U$ and lead isotopic compositions in hot springs on the East Pacific Rise at 21°N, Geol. Soc. Am., Abst. Prog. 16, 469, 1984.

29 R.L. Edwards, J.H. Chen and G.J. Wasserburg, Precise measurements of $^{234}U/^{238}U$ in Pacific and Atlantic profiles, Geol. Soc. Am., Abst. Prog. 17, 572, 1985.

30 J.H. Chen and G.J. Wasserburg, A search for isotopic anomalies in uranium, Geophys. Res. Lett. 7, 275, 1980.

31 J.H. Chen and G.J. Wasserburg, Isotopic determination of uranium in picomole and subpicomole quantities, Anal. Chem. 53, 2060, 1981.

32 G.J. Wasserburg, D.A. Papanastassiou, E.N. Nenow and L.A. Bauman, A programmable magnetic field mass spectrometer with on-line data processing, Rev. Sci. Instrum. 40, 288, 1969.

33 G.J. Wasserburg, S.B. Jacobsen, D.J. DePaolo, M.T. McCulloch and T. Wen, Precise determination of Sm/Nd ratios, Sm and Nd isotopic abundances in standard solutions, Geochim. Cosmochim. Acta 45, 2311, 1981.

34 J.H. Chen and G.J. Wasserburg, The isotopic composition of silver and lead in the Cap York meteorite, Geochim. Cosmochim. Acta 47, 1725, 1983.

35 A.L. Bloom, W.S. Broecker, J.M.A. Chappell, R.K. Matthews and K.J. Mesolella, Quaternary sea level fluctuations on a tectonic coast: new $^{230}Th/^{234}U$ dates on the Huon Peninsula, New Guinea, Quat. Res. 4, 185, 1974.

36 G. Neef and H.H. Veeh, Uranium series ages and late Quaternary uplift in the New Hebrides, Nature 269, 682, 1977.

37 F.W. Taylor, B.L. Isacks, C. Jouannic, A.L. Bloom and J. Dubois, Coseismic and Quaternary vertical tectonic movements, Santo and Malekula Islands, New Hebrides Island Arc, J. Geophys. Res. 85, 5367, 1980.

38 F.W. Taylor, C. Jouannic and A.L. Bloom, Quaternary uplift of the Torres Islands, northern New Hebrides frontal arc—comparison with Santo and Malekula Islands, Central New Hebrides frontal arc, J. Geol. 93, 419, 1985.

39 F.W. Taylor, P. Mann, S. Valestro Jr. and K. Burke, Stratigraphy and radiocarbon chronology of a subaerially exposed Holocene coral reef, Dominican Republic, J. Geol. 93, 311, 1985.

40 A.L. Bloom, C. Jouannic and F.W. Taylor, Preliminary radiometric ages from the uplifted Quaternary coral reefs of Efate, appendix to R.P. Ash, J.N. Carney, and A. Macfarlane, Geology of Efate and offshore islands, New Hebrides Geol. Serv. Reg. Rep., 1978.

41 J. Chappell and H.H. Veeh, Late quaternary tectonic movements and sea level changes at Timor and Atauro Island, Geol. Soc. Am. Bull. 89, 356, 1978.

42 W.S. Moore, Late Pleistocene sea-level history, in Uranium Series Disequilibrium: Applications to Environmental Problems, M. Ivanovich and R.S. Harmon, eds., p. 481, Oxford University Press, London/New York, N.Y., 1982.

43 A. Kaufman, The distribution of $^{230}Th/^{234}U$ ages in corals and the number at last interglacial high-sea stands, Quat. Res. 25, 55, 1986.

44 C.A. Huh and M.P. Bacon, Thorium-232 in the eastern Caribbean Sea, Nature 316, 718, 1985.

45 A. Kaufman, The Th-232 concentration of surface ocean water, Geochim. Cosmochim. Acta 33, 717, 1969.

46 K.G. Knauss, T.L. Ku and W.L. Moore, Radium and thorium isotopes in the surface waters of the East Pacific and coastal S. California, Earth Planet. Sci. Lett. 39, 235, 1978.

47 W.S. Moore, The thorium isotope content of ocean water, Earth Planet. Sci. Lett. 53, 419, 1981.

48 M.P. Bacon and R.F. Anderson, Distribution of thorium isotopes between dissolved and particulate forms in the deep sea, J. Geophys. Res. 87, 2045, 1982.

49 W.D. Urry, The radio-elements in the water and sediments of the ocean, Phys. Res. 59, 479, 1941.

50 W.D. Urry, The radio-elements in non-equilibrium systems, Am. Jour. Sci. 240, 426, 1942.

51 C.S. Piggot and W.D. Urry, Radioactivity of ocean sediments. III. Radioactive relations in ocean water and bottom sediment, Am. Jour. Sci. 239, 81, 1941.

52 C.S. Piggot and W.D. Urry, Time relations in ocean sediments, Bull. Geol. Soc. Amer. 53, 1187, 1942.

53 H. Isaac and E. Picciotta, Ionium determination in deep sea sediments, Nature 171, 742, 1953.

54 T.L. Ku, The uranium series methods of age determination, Ann. Rev. Earth and Plan. Sci. 4, 347, 1976.

55 Y. Nozaki, Y. Horibe and H. Tsubota, The water column distributions of thorium isotopes in the western North Pacific, Earth Planet. Sci. Lett. 54, 203, 1981.

56 R.W. Attree, M.J. Cabell, R.L. Cushing and J.J. Pieron, A calorimetric determination of the half life of Th-230 and consequent revision of its neutron capture cross-section, Can. J. Phys. 40, 194, 1962.

57 E.H. Fleming, Jr., A. Ghiorso and B.B. Cunningham, The specific alphaactivities and half-lives of ^{234}U, ^{235}U, and ^{236}U, Phys. Rev. 38, 642, 1952.

58 J.W. Meadows, R.J. Armani, E.L. Callis and A.M. Essling, Half-life of ^{230}Th, Phys. Rev. C 22, 750, 1980.

59 M. Lounsbury and R.W. Durham, The alpha half-life of 234-U, in: Proc. Int. Conf. Chem. Nucl. Data Measurement and Applications, Canterbury, M.L. Hurrell, ed., p. 215, Inst. Civil Engineers, London, 1971.

60 P. de Bievre, K.F. Lauer, Y. le Duigou, H. Moret, G. Muschenborn, J. Spaepen, A. Spernol, R. Vaninbrouks, and Y. Verdingh, The half-life of 234-U, in: Proc. Int. Conf. Chem. Nucl. Data, Measurement and Applications, Canterbury, M.L. Hurrell, ed., p. 21, Inst. Civil Engineers, London, 1971.

61 A.H. Jaffey, K.F. Flynn, L.E. Glendenin, W.C. Bentley and A.M. Essling, Precision measurements of half-lives and specific activities of ^{235}U and ^{238}U, Phys. Rev. C 4, 1889, 1971.

62 T.L. Ku, Protactinium method of dating coral from Barbados Island, J. Geophys. Res. 73, 2271, 1968.

63 J.F. Marshall and B.G. Thom, The sea-level in the last interglacial, Nature 263, 120, 1976.

64 R.S. Harmon, R.M. Mitterer, N. Kriausakul, L.S. Land, H.P. Schwarcz, P. Garrett, G.J. Larson, H.L. Vacher and M. Rowe, U-series and amino acid racemization geochronology of Bermuda: implications for eustatic sealevel fluctuation over the past 250,000 years, Palaeogeogr., Palaeoclimatol., Palaeoecol. 44, 41, 1983.

65 R.E. Dodge, R.G. Fairbanks, L.K. Benninger and F. Maurrasse, Pleistocene sea levels from raised coral reefs of Haiti, Science 219, 1423, 1983.

66 B.L.K. Somayajulu, W.S. Broecker and J. Goddard, Dating Indian corals by U-decay-series methods, Quat. Res. 24, 235, 1985.

67 A.L. Berger, Long-term variations of caloric insolation resulting from the earth's orbital elements, Quat. Res. 9, 139, 1978.

68 M. Stuiver, A high precision calibration of the AD radiocarbon time scale, Radiocarbon 24, 1, 1982.

69 J. Klein, J.C. Lerman, P.E. Damon and E.K. Ralph, Calibration of radiocarbon dates: tables based on the consensus data of the Workshop on Calibrating the Radiocarbon Time Scale, Radiocarbon 24, 103, 1982.

Precise Timing of the Last Interglacial Period from Mass Spectrometric Determination of Thorium-230 in Corals

R. LAWRENCE EDWARDS, J. H. CHEN, T.-L. KU, G. J. WASSERBURG

The development of mass spectrometric techniques for determination of ^{230}Th abundance has made it possible to reduce analytical errors in ^{238}U-^{234}U-^{230}Th dating of corals even with very small samples. Samples of 6×10^8 atoms of ^{230}Th can be measured to an accuracy of ±3 percent (2σ) and 3×10^{10} atoms of ^{230}Th can be measured to an accuracy of ±0.2 percent. The time range over which useful age data on corals can be obtained now ranges from about 50 to about 500,000 years. For young corals, this approach may be preferable to ^{14}C dating. The precision with which the age of a coral can now be determined should make it possible to critically test the Milankovitch hypothesis concerning Pleistocene climate fluctuations. Analyses of a number of corals that grew during the last interglacial period yield ages of 122,000 to 130,000 years. The ages coincide with, or slightly postdate, the summer solar insolation high at 65°N latitude which occurred 128,000 years ago. This supports the idea that changes in Pleistocene climate can be the result of variations in the distribution of solar insolation caused by changes in the geometry of the earth's orbit and rotation axis.

FLUCTUATIONS IN CLIMATE RESULT IN CHANGES IN THE mass of water stored as ice in continental glaciers, which in turn cause changes in sea level. Because some species of coral grow very close to the sea surface, they can be used as indicators of the height of sea level in the past. The ^{238}U-^{234}U-^{230}Th-^{232}Th system has been used to delineate the absolute chronology of events in the last 150 ky (1 ky = 10^3 years) and has been applied to fossil corals to establish an absolute chronology for sea level changes (*1–3*). This approach has been particularly important in testing the astronomical theory of climate change which was formulated by Milankovitch (*4*). This theory states that the fluctuations in Pleistocene climate are caused by changes in the distribution of solar energy received by the earth due to changes in (i) the obliquity of the ecliptic, (ii) the eccentricity of the earth's orbit, and (iii) precession of the earth's rotation axis. On the basis of calculations from the orbital parameters, the summer solar insolation received at 65°N latitude was shown to be a function of time (*4*) and was viewed as a forcing function controlling the earth's climate. High values of summer insolation would favor deglaciation, low values would favor glaciation. The response of sea level height to orbital forcing can be modeled from the dynamics of the ocean, glacial growth and melting, and isostatic rebound. This is a particularly active area of research (*5, 6*).

The test of sea level height with time would depend on the accuracy of the orbital parameters and the accuracy of the sea level curve derived from the geologic record. If the insolation curve and the sea level curve were found to be identical, this would demonstrate that (i) the earth's climate responds to orbital forcing; (ii) the response shows no measurable phase lag; and (iii) of the possible curves that could be calculated from the orbital parameters, the summer solar insolation received at 65°N is the one that controls climate. Differences between the insolation curve and the sea level curve would indicate that at least one of these statements is not true.

Two approaches have been used to determine the height of sea level in the past. The ratio of ^{18}O to ^{16}O in seawater is a function of the fraction of water stored as ice in glaciers. Detailed measurements of ^{18}O/^{16}O as a function of depth in deep sea cores have provided a continuous record of climatic change over the past 10^6 years (*7, 8*). Spectral analysis of this record has provided convincing evidence that at least some of the variability in Pleistocene climate is the result of orbital forcing. However, the approach has been limited by the inability to independently assign an absolute chronology to this record.

A second approach is the dating of coral terraces. This does not provide a continuous record of sea level change but has the advantage that corals of appropriate age can be dated by ^{230}Th methods. An apparent correlation has been drawn between the ages of a number of coral terraces thought to have grown during periods of high sea level (interglacial and interstadial periods) and the times of high insolation (*1–3*). However, this approach has been limited by the analytical uncertainty of data obtainable with present methods, some discrepancies in results, and possible open-system behavior of corals with respect to uranium and thorium.

Analysis of ^{230}Th and ^{234}U has typically been done by α spectrometry. The precision with which a measurement can be made with this technique has practical limitations resulting from sample size and counting time. On the basis of our experience in analyzing 10^9 to 10^{10} uranium atoms by means of thermal ionization mass spectrometry (*9*), we have attempted to supplement the α-counting method with mass spectrometric measurements as a means of increasing precision and decreasing sample size. In order to compare this

R. L. Edwards is a graduate student in geochemistry, J. H. Chen is a senior scientist and member of the professional staff, and G. J. Wasserburg is the John D. MacArthur Professor of Geology and Geophysics in the Division of Geological and Planetary Sciences, California Institute of Technology, Pasadena, CA 91125. T.-L. Ku is a professor of geology in the Department of Geological Sciences at the University of Southern California, Los Angeles, CA 90089.

technique with previous methods, we have analyzed a number of corals that had been dated by ^{14}C, ^{238}U-^{234}U-^{230}Th (α counting), or counting of coral growth bands. Included among these samples is a series of corals that are thought to have grown during periods of high sea level 80 to 140 ky ago. These corals were chosen for analysis since the precise ages of these samples and their relation to the insolation curve would provide a critical test of the Milankovitch theory. The ^{238}U and ^{232}Th concentrations in a modern mollusk shell have also been measured as a means of assessing the suitability of this material for dating.

Systematics. ^{230}Th dating of corals is based on the decay of ^{238}U through a series of relatively short-lived intermediate daughters to ^{206}Pb. The pertinent nuclides in this decay chain are:

$$^{238}U \xrightarrow[6.446\times10^{9}\text{yr}]{} {}^{234}U \xrightarrow[352.7\times10^{3}\text{yr}]{} {}^{230}Th \xrightarrow[108.8\times10^{3}\text{yr}]{} {}^{206}Pb$$

where the numbers below the arrows are mean lives. For simplicity, the other short-lived intermediate daughters in the decay scheme have not been shown. The initial amount of ^{230}Th in corals can be calculated by multiplying the $^{230}Th/^{232}Th$ ratio of surface ocean water [see (*10, 11*)] by the ^{232}Th abundance in corals determined in our study. The calculated value is extremely low. It is equivalent to the amount of ^{230}Th generated by radioactive decay in about 1 year and can be taken to be zero. If we use this initial condition and assume that corals represent closed systems, the equations for radioactive production and decay can be solved.

$$1 - [^{230}Th/^{238}U]_{act} = e^{-\lambda_{230}T} - \left(\frac{\delta^{234}U(0)}{1000}\right)\left(\frac{\lambda_{230}}{\lambda_{230}-\lambda_{234}}\right)\left(1 - e^{(\lambda_{234}-\lambda_{230})T}\right) \quad (1)$$

$$\delta^{234}U(T) = \delta^{234}U(0)e^{\lambda_{234}T} \quad (2)$$

Equation 1 [modified from Kaufman and Broecker (*12*)] gives the age (T) as a function of the decay constants (λ) and the measured $^{234}U/^{238}U$ and $^{230}Th/^{238}U$ ratios. Equation 2 gives the initial $^{234}U/^{238}U$ ratio when the coral grew as a function of the measured $^{234}U/^{238}U$ ratio and T. For convenience, the $^{234}U/^{238}U$ ratio has been reformulated into δ notation. The present $\delta^{234}U$ value is

$$\delta^{234}U(0) = \{[(^{234}U/^{238}U)/(^{234}U/^{238}U)_{eq}] - 1\} \times 10^3$$

This represents the fractional deviation of the measured $^{234}U/^{238}U$ ratio from the $^{234}U/^{238}U$ value at secular equilibrium [$(^{234}U/^{238}U)_{eq}$] in parts per thousand. The initial $\delta^{234}U$ value when the system was isolated from seawater is given by $\delta^{234}U(T)$. The measured $^{230}Th/^{238}U$ atomic ratio has been represented as an activity ratio ($[^{230}Th/^{238}U]_{act}$) by multiplying the $^{230}Th/^{238}U$ atomic ratio by the ratio of the decay constants ($\lambda_{230}/\lambda_{238}$).

If $\delta^{234}U(T)$ is known, the equations represent two independent chronometers. We have chosen to use Eq. 2 not as a chronometer but as a means of calculating $\delta^{234}U(T)$ with the value of T determined from Eq. 1. If we assume that the uranium isotopic composition of seawater is constant with time, a difference between the calculated $\delta^{234}U(T)$ and the present seawater value (*11*) would indicate that the uranium in the coral was not derived via closed-system evolution from normal seawater. The calculated $\delta^{234}U(T)$ therefore provides an independent check of whether the coral has behaved as a closed system.

^{232}Th is not a nuclide in the decay chain shown above and does not appear in Eqs. 1 or 2. It has an extremely long mean life [2.0212×10^{10} years (*13*)] and can be considered stable over the time range considered here. Comparison of the $^{232}Th/^{238}U$ ratio in an old coral with the $^{232}Th/^{238}U$ ratio in modern corals would indicate whether substantial differential addition or leaching of ^{238}U or ^{232}Th had occurred subsequent to coral growth. Since the chemical properties of ^{230}Th and ^{232}Th are the same, knowledge of the $^{232}Th/^{238}U$ ratio provides another check of the closed-system assumption used in deriving Eq. 1.

Analytical procedures and samples. Detailed analytical procedures for measurement of the Th and U isotopes have been described (*11, 14*). In Table 1, we have listed, for each analysis, the amount of coral analyzed, the number of ^{230}Th atoms measured, and the precision of the ^{230}Th analysis at the 2σ level (2 standard deviations). This table shows that 3×10^{10} atoms of ^{230}Th can be measured to ± 2 ‰ (2σ) and that 6×10^8 atoms of ^{230}Th can be measured to ± 29 ‰ (2σ). The measurements have been verified with replicate analyses on standards and samples (Table 2). The accuracy of U and Th abundances are ultimately based on standard solutions with concentrations which are accurately known from gravimetry (*9, 14*).

Details about samples can be found in (*14*). Samples TAN-E-1g, CWS-F-1, and CH-8 have previously been dated by the ^{14}C method. Sample TAN-E-1g has also been dated by counting of coral growth bands. These samples were analyzed to determine the precision with which very young samples could be dated and to provide a comparison of the ages determined by mass spectrometry and those determined with the other methods. Sample CH-8 was collected along the shore of Lago Enriquillo, a lake in Hispaniola which was thought to be connected to the ocean at the time CH-8 grew (*15*). TAN-E-1g and CWS-F-1 are from nearshore marine environments.

Samples AFS-10, AFS-11, and AFS-12, AFM-20, and R-52 are from the Rendezvous Hill Terrace on Barbados (*16*), and E-T-2 and E-L-3 are from Efate Island, Vanuatu (*17*). Both islands are tectonically active and have been uplifted during the Pleistocene and Holocene. These samples are all thought to have grown during periods of high sea level during the last interglacial period and are known from previous ^{230}Th dating (α counting) to have grown between 110 and 140 ky ago (*17, 18*). Sample OC-51 is from the Worthing Terrace on Barbados (about 85 ky old) and FT-50 is from the Ventnor Terrace, also from Barbados (about 105 ky old) (*16*),

Table 1. Number of ^{230}Th atoms per analysis, mass of coral analyzed, and 2σ uncertainty in ^{230}Th abundance.

Run		10^{10} atoms of ^{230}Th (No.)	Coral mass (g)	2σ uncertainty* (‰)
TAN-E-1g		0.058	2.8	±29
CWS-F-1		0.43	4.6	±8
CH-8		3.2	4.1	±3
OC-51	A	4.4	0.41	±1
	B	3.8	0.34	±2
FT-50	A	4.2	0.41	±2
	B	2.1	0.20	±5
	C	3.5	0.33	±2
AFS-10		4.3	0.43	±3
AFS-11		4.4	0.41	±2
AFS-12	A	2.4	0.25	±3
	B	3.8	0.39	±2
	C	2.7	0.28	±2
AFM-20		3.0	0.28	±2
R-52		1.9	0.17	±3
E-L-3		2.3	0.26	±2
E-T-2	A	2.2	0.28	±2
	B	2.4	0.31	±2
VA-1		6.2	0.38	±3

*Errors are based on the standard deviations of the mean of about 60 isotope ratios measured in the course of a mass spectrometric run.

and are thought to have grown during interstadial periods. The Barbados and Vanuatu samples were analyzed in order to determine the precision with which relatively old corals could be dated, to compare these dates to previous results, and to compare the ages to the timing of the peaks in the 65°N insolation curve. Samples AFS-10, AFS-11 and AFS-12 are all from the same locality and were analyzed as a test of the closed-system assumption. Because of their stratigraphic assignment to the same reef crest and proximity to each other (*16*), they should have similar ages. If they were altered to different degrees, different apparent ages would be recorded by the ^{238}U-^{234}U-^{230}Th chronometer.

VA-1 is from one of the higher terraces in Barbados and has been dated by U-He methods as 520 ky old (*16*). This sample was analyzed to determine the isotopic characteristics of a very old sample. All the Barbados samples are of the species *Acropora palmata*, which is known to thrive near the crests of coral reefs and tends to live within about 2 m of the sea surface at low tide.

In addition to the coral samples (Table 1), we have also studied K-133, which is a portion of a giant clam (*Tridacna gigantus*) shell collected live from New Guinea in 1977. This was analyzed in order to determine the ^{238}U and ^{232}Th concentrations in a modern mollusk and assess the suitability of this material for ^{238}U-^{234}U-^{230}Th dating. The sample size was 2 g for the uranium analysis and 8 g for the Th analysis.

Measurements and analytical error. The ages (Table 2) have been calculated from Eq. 1. The errors in age (2σ) are based on the propagation of analytical errors. Our results demonstrate that very precise ages can be determined for corals 180 years old to 130 ky old (Fig. 1). Fractional errors in age ($\Delta T/T$) as small as 0.005 (at the 2σ level) can be obtained for corals that are about 10^4 years old. Fractional errors in age smaller than 0.1 can be obtained for corals with ages between 50 and 500,000 years.

The period of time that is pertinent to our test of the astronomical theory is about 130 ky ago. The error in age of a coral which is 130 ky old is about ±1 ky (Table 2 and Fig. 1). Since the difference between a high point and a low point on the 65°N insolation curve is about 10 ky, the error in age is small enough to allow a detailed comparison of the times of high sea level and the times of high summer insolation.

Except for CH-8 and VA-1, the $\delta^{234}U(T)$ values range from 149 to 174. This spread overlaps the range for open ocean water [140 to 150 (*11*)] but is somewhat higher. This may reflect the uranium isotopic composition of nearshore waters or possibly a small degree of alteration. Considering errors, however, the $\delta^{234}U(T)$ values are consistent with closed-system evolution from seawater and do not show clear evidence for any substantial diagenetic alteration. VA-1 has a $^{230}Th/^{238}U$ ratio higher than the maximum possible value for closed-system evolution from seawater, confirming previous observations (*16*), and does not permit an age to be calculated. If the U-He age [520 ky (*16*)] is used to calculate $\delta^{234}U(T)$, a value of 530 ± 26 is determined. This is much higher than the seawater value and is clear evidence for diagenetic addition of ^{234}U. For CH-8, the value of $\delta^{234}U(T)$ is 84, which is much lower than the seawater value. Although the possibility that this sample has been altered cannot be ruled out, it appears that this coral grew in a body of water that was restricted from the open ocean and that the low $\delta^{234}U(T)$ value reflects the isotopic composition of this body of water (*14, 15*).

The ^{232}Th values for corals (Table 1) range from 0.08 to 1.92 pmol/g. Because of the extremely low concentrations and the long mean life of ^{232}Th, α-counting studies have often not reported ^{232}Th. Examination of published ^{232}Th concentrations (*19*) shows that the typical detection limit is about 10^2 pmol/g, and values as high as 10^4 pmol/g have been reported. The earlier values are at least two orders of magnitude higher than those in Table 1. Our $^{232}Th/$

Table 2. U and Th isotopic composition and ages of corals. Reported errors are 2 standard deviations. Errors are based on 2 standard deviations of the mean of 60 to 300 isotope ratios measured during a mass spectrometric run.

Sample*	Locality*	^{238}U (nmol/g)	^{232}Th† (pmol/g)	$(^{232}Th/^{238}U)$ (10^5)‡	$\delta^{234}U(0)$§	$\delta^{234}U(T)$**	$[^{230}Th/^{238}U]^{\S\S}_{act}$	Age††
TAN-E-1g	Vanuatu	10.80 ± 0.04	0.083 ± 0.003	0.77 ± 0.03	149 ± 6	149 ± 6	0.00190 ± 5	180 ± 5 yr
CWS-F-1	Vanuatu	10.21 ± 0.01	0.147 ± 0.002	1.44 ± 0.02	152 ± 4	153 ± 4	0.00893 ± 8	845 ± 8 yr
CH-8	Hispaniola	9.68 ± 0.01	0.279 ± 0.002	2.88 ± 0.02	82 ± 4	84 ± 4	0.07951 ± 28	8294 ± 44 yr
OC-51 A	Barbados	17.05 ± 0.03	0.17 ± 0.02	1.0 ± 0.1	126 ± 5	161 ± 6	0.6307 ± 12	87.5 ± 0.6 ky
B		17.36 ± 0.03	0.15 ± 0.03	0.9 ± 0.2	126 ± 5	162 ± 6	0.6323 ± 17	87.9 ± 0.7 ky
FT-50 A	Barbados	13.93 ± 0.02	0.92 ± 0.02	6.6 ± 0.1	126 ± 5	173 ± 7	0.7357 ± 21	112.0 ± 1.0 ky
B		13.95 ± 0.02	0.92 ± 0.05	6.6 ± 0.4	127 ± 4	174 ± 6	0.7359 ± 37	111.8 ± 1.3 ky
C		13.97 ± 0.03	0.42 ± 0.03	3.0 ± 0.2	124 ± 5	170 ± 7	0.7353 ± 23	112.3 ± 1.1 ky
AFS-10	Barbados	12.82 ± 0.02	0.28 ± 0.02	2.2 ± 0.2	110 ± 4	157 ± 6	0.7728 ± 24	125.7 ± 1.2 ky
AFS-11	Barbados	13.67 ± 0.02	0.74 ± 0.02	5.4 ± 0.1	114 ± 6	161 ± 8	0.7653 ± 20	122.6 ± 1.5 ky
AFS-12 A	Barbados	12.66 ± 0.02	1.40 ± 0.05	11.1 ± 0.4	109 ± 4	153 ± 6	0.7593 ± 28	122.1 ± 1.1 ky
B		12.62 ± 0.03	1.57 ± 0.03	12.4 ± 0.2	111 ± 5	157 ± 7	0.7631 ± 25	122.7 ± 1.3 ky
C		12.43 ± 0.03	1.37 ± 0.03	11.1 ± 0.2	109 ± 5	155 ± 6	0.7680 ± 28	124.5 ± 1.3 ky
AFM-20	Barbados	13.46 ± 0.04	1.92 ± 0.04	14.3 ± 0.3	111 ± 4	160 ± 6	0.7852 ± 26	129.2 ± 1.4 ky
R-52	Barbados	13.98 ± 0.02	0.08 ± 0.06	0.6 ± 0.4	115 ± 6	165 ± 8	0.7846 ± 31	128.1 ± 1.7 ky
E-T-2 A	Vanuatu	9.75 ± 0.01	0.12 ± 0.03	1.2 ± 0.3	103 ± 4	149 ± 6	0.7811 ± 17	129.9 ± 1.1 ky
B		9.72 ± 0.01	0.10 ± 0.03	1.0 ± 0.3	106 ± 4	153 ± 6	0.7811 ± 12	129.2 ± 1.1 ky
E-L-3	Vanuatu	11.39 ± 0.03	0.12 ± 0.03	1.1 ± 0.3	113 ± 5	162 ± 7	0.7748 ± 24	125.5 ± 1.3 ky
VA-1	Barbados	13.37 ± 0.02	1.08 ± 0.02	8.1 ± 0.2	121 ± 6		1.1940 ± 39	
K-133	Huon Peninsula, New Guinea (mollusk)	(3.08 ± 0.08) $\times 10^{-4}$	0.249 ± 0.002	(8.08 ± 0.22) $\times 10^4$				
			Open ocean surface water‡‡					
		0.01383 ± 3	0.00051 ± 3	3.7 ± 0.2	140 ± 5 to 150 ± 5		1×10^{-5} to 4×10^{-5}	

*Further details on samples can be found in (*14–18*). A, B, and C indicate replicate analyses. For FT-50, A and B are different aliquots of the same dissolved rock fragment; C is a different rock fragment. For AFS-12, A and B are different fractions of the same powder and C is a different rock fragment. For E-T-2 and OC-51, A and B are different rock fragments. All samples are corals except for K-133 which is from a modern giant clam shell. †The ^{232}Th abundance has been corrected for the analytical blank of 0.02 ± 0.01 pmol. Most of the error in the ^{232}Th abundance is due to the error in the blank correction. ‡The numbers in this column represent the measured $^{232}Th/^{238}U$ ratio multiplied by 10^5. §The measured uranium isotopic composition calculated as described in text. **The initial uranium isotopic composition calculated from $\delta^{234}U(0)$, the ^{230}Th age, and Eq. 2. §§Calculated as described in text with decay constants from (*33, 36*). ††Calculated from Eq. 1; values for the decay constants are from references (*33–36*). ‡‡^{238}U, ^{232}Th, and $\delta^{234}U(0)$ are from (*11*). The ^{230}Th abundance is from surface water values in (*10*).

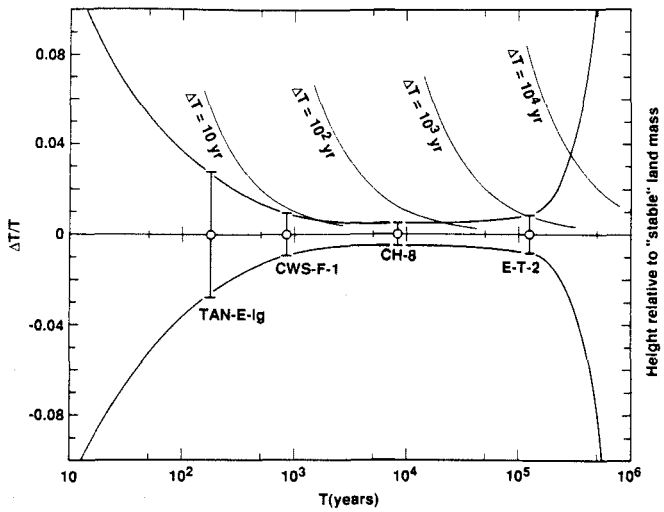

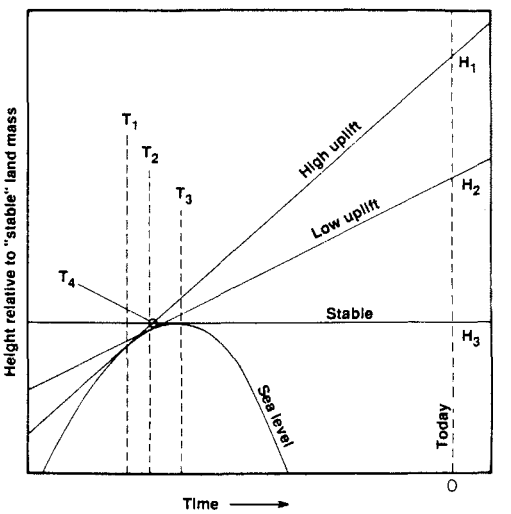

Fig. 1 (**left**). Fractional uncertainty in age ($\Delta T/T$) plotted as a function of time, where T is the age and ΔT is the 2σ error in age based on the propagation of analytical errors through Eq. 1. T is plotted on a log scale. Between 180 years and 129.9 ky, the error envelope is drawn through the observed values for several corals. The error envelope is extrapolated to younger and older T (assuming typical analytical errors). The lowest values of $\Delta T/T$ are at $\sim 10^4$ years and values of $\Delta T/T < 0.10$ can be obtained over the range $T = 15$ to 500,000 years. Parts of the diagram are contoured in ΔT. The intersection of the $\Delta T = 10^3$ year contour with the error envelope is at $T \sim 1.3 \times 10^5$ years and indicates that analytical error is small enough at $T \sim 10^5$ for a critical test of the astronomical theory. **Fig. 2** (**right**). Height relative to an arbitrary point on a tectonically stable land mass as a function of time. A rise and fall of sea level is represented by an arbitrary curve with negative curvature. The lines represent the change in height with time for a specific elevation at locations of high uplift, low uplift, and a tectonically stable locality. The specific elevation is the highest elevation at that locality which is covered by seawater and consequently the highest elevation at a given locality where corals could have grown. T_1, T_2, and T_3 represent coral ages. H_1, H_2, and H_3 are present heights of coral terraces. If the assumptions outlined in the text are valid, it may be possible to determine the rate of sea level rise as a function of time. Since both age and present height are measurable quantities, we can test whether the true scenario is consistent with the model.

^{238}U ratios range from 0.6×10^{-5} to 14.3×10^{-5}. These values are similar to the $^{232}Th/^{238}U$ value for open ocean surface water [$3.7 \pm 0.2 \times 10^{-5}$ (*6*)], suggesting that these elements do not fractionate substantially from each other during coral growth. Large shifts in this ratio can therefore be used to indicate Th or U addition during diagenesis or growth from water with $^{232}Th/^{238}U$ different from that found in the open oceans.

The ^{232}Th concentration of K-133 (a fragment of a modern giant clam shell) is 0.249 pmol/g, which is similar to the value for corals. However, the ^{238}U concentration is 3.08×10^{-4} nmol/g. This is about 10^2 times lower than the lowest previously reported values for a mollusk (*20*) and 4×10^4 times lower than the coral uranium content. The extremely large difference between giant clam and coral uranium contents indicates that these organisms have different mechanisms (or microenvironments) for incorporating uranium into their skeletons. Because of the low ^{238}U content, ^{238}U-^{234}U-^{230}Th dating of such a material would require a large sample. As giant clams have a mass of about 50 kg, large samples can be found. With the use of mass spectrometric techniques, such an analysis would, in principle, be possible. At secular equilibrium, 200 g of sample would contain 6×10^8 ^{230}Th atoms. With our techniques, this number of ^{230}Th atoms could be measured to an accuracy of ±3 percent (2σ) (Table 1). Although dating of such a sample is now technically feasible, it is clear from previous work (*20, 21*) that uranium in fossil mollusks is dominantly of diagenetic origin and that the process of uranium uptake must be understood before any serious attempt to date fossil mollusks can be made.

The ages calculated from replicate analyses of AFS-12, E-T-2, FT-50, and OC-51 agree within the 2σ error of the measurements. For these samples, replicate analyses were done on different fragments of the same hand specimen. The agreement between the replicate analyses is not only a demonstration of analytical reproducibility, but also shows that different fragments of the same hand specimen could not have been altered to varying degrees. The results are consistent with the closed-system assumption. The ^{230}Th age of AFS-11 agrees almost exactly with the ages determined from the three analyses of AFS-12. The age of AFS-10 appears to be slightly greater (1 to 2 ky) than that of AFS-11. Since these samples are from the same outcrop, they should have similar ages as is the case.

Age comparisons. The analyzed corals have previously been dated by other methods (Table 3). The younger samples have been dated by ^{14}C and reported in conventional radiocarbon years (*15, 22*) and as "corrected ages." For TAN-E-1g and CWS-F-1, the corrected ages were determined from the conventional ages with the use of the calibration curve of Stuiver (*23*). For CH-8, the corrected age has been given as an approximation since the precise value of the ratio of ^{14}C to C in the atmosphere at this time does not appear to be known. The corrected ^{14}C ages do not include adjustments for the natural fractionation of carbon isotopes or for the difference between $^{14}C/C$ in the atmosphere and surface waters. For TAN-E-1g, the corrected age is given by three time intervals since the conventional radiocarbon age intersects the calibration curve three times. TAN-E-1g was collected alive and it was determined from the counting of coral growth bands that the portion of the coral which we analyzed grew between 1804 and 1810 (*22*). The older samples had been dated by ^{238}U-^{234}U-^{230}Th with the use of α-counting techniques (*17, 18*).

Our date for TAN-E-1g of 180 ± 5 years (at the time the sample was analyzed, June 1986) is in excellent agreement with the age determined from counting of growth bands (176 to 182 years old). It also agrees with the corrected ^{14}C age. Since the conventional radiocarbon age intersects the calibration curve at three points, the corrected ^{14}C age includes three time intervals that span several

centuries. For CWS-F-1, the date determined by mass spectrometry agrees with the corrected ^{14}C date within errors. In this case, the conventional radiocarbon age intersects the calibration curve over only one range. For CH-8, there is a substantial difference between the mass spectrometric age and the corrected ^{14}C age. The reality of this discrepancy requires a more serious comparison of both methods, particularly for samples older than 8000 years, where the availability of samples dated by dendrochronology is limited.

For AFS-10, AFS-11, AFS-12, AFM-20, R-52, FT-50, OC-51, E-L-3, and E-T-2, the agreement between the mass spectrometrically determined ages and the earlier ages determined by α counting generally appears to be good at the 2σ level. The error in age, based on analytical errors, for the mass spectrometric measurements is five to ten times smaller than the error in age for the α-counting measurements.

Rate of sea level rise between 129 and 122 ky. The response of a coral reef relative sea level rise was first discussed by Darwin (*24*). He observed that reef-building corals thrive at water depths of less than 30 m and reasoned that if sea level were to rise, the reef must grow upward to remain near the sea surface or die. When sea level stops rising, the upward growth of the coral reef would stop. As sea level falls, the crest of the coral reef would remain as a subaerially exposed coral terrace. The age of the coral at the highest point of the terrace would represent the time at which sea level reached its highest elevation.

The situation at Barbados is more complicated. The Rendezvous Hill Terrace has present elevations of 27 to 61 m above sea level (*16*) (Table 4). Terraces of similar age (about 120 ky) in areas which may have been tectonically stable over the last 120 ky have elevations about 6 m above sea level (*25*). The difference in elevation between the Rendezvous Hill Terrace and the terraces from these areas is inferred to be due to tectonic uplift on Barbados that has occurred over the past 120 ky (*2*) (Table 4). The Barbados terraces must be the net result of two processes: fluctuations in sea level and tectonic uplift. This concept has been discussed by Mesollela *et al.* (*2*) for Barbados and by Bloom *et al.* (*26*) for New Guinea. Further discussion of the relation of reef morphology and zonation to sea level changes can be found in (*27, 28*).

Table 4. Present height, age, and average uplift rate of Barbados terraces.

Sample	Present height above sea level* (m)	Age (ky)	Rate of uplift† (m/ky)
AFS-11	30	122.6	0.20
AFS-12	30	123.1	0.19
AFS-10	30	125.7	0.19
R-52	37	128.1	0.24
AFM-20	55	129.2	0.38

*From topographic maps in reference (*16*); errors are about ±3 m. †Minimum uplift rates calculated as described in text.

It is necessary to distinguish between changes in the absolute height of sea level and tectonic displacements. Consider the following simple model. We assume that the sea level curve has negative curvature over a pertinent time range and that the rate of tectonic uplift at a given locality is constant (Fig. 2). The curve labeled "sea level" represents the change in sea level with time. The lines represent tectonic uplift for a specific elevation at localities with different uplift rates. The specific elevation is the one that intersects the sea level curve at the tangent point. This is the highest elevation that is covered by seawater and, consequently, is the highest elevation where a coral reef could have grown. The age of this coral records the time at which sea level was rising at the same rate as the land mass. For a "stable" land mass, this age (T_3) represents the time when sea level reached its maximum height. For a rising land mass, this age (T_1 or T_2) is older than the sea level maximum. The model

Table 3. Coral ages determined by different methods or techniques. Ages refer to the ages in 1986. Reported errors are 2σ. For ^{14}C and α counting, the errors are based on counting statistics. Errors in mass spectrometric ages are based on the standard deviation of the mean of 60 to 300 isotope ratios measured in the course of a mass spectrometric run.

Sample		^{14}C* (conventional) (years)	^{14}C† (corrected) (years)	Ring counting‡ (years)	^{238}U-^{234}U-^{230}Th§ (α counting) (ky)	^{238}U-^{234}U-^{230}Th (mass spectrometric)
TAN-E-1g		270 ± 120	30 to 70, 180 to 270, or 300 to 500	176 to 182		180 ± 5 years
CWS-F-1		980 ± 120	780 to 1010			845 ± 8 years
CH-8		8990 ± 120	~10,000			8294 ± 44 years
OC-51	A				85 ± 4	87.5 ± 0.6 ky
	B					87.9 ± 0.7 ky
FT-50	A				107 ± 7	112.0 ± 1.0 ky
	B					111.8 ± 1.3 ky
	C					112.3 ± 1.1 ky
AFS-10					123 ± 8	125.7 ± 1.2 ky
AFS-11					127 ± 9	122.6 ± 1.5 ky
AFS-12	A				129 ± 9	122.1 ± 1.1 ky
	B					122.7 ± 1.3 ky
	C					124.5 ± 1.3 ky
AFM-20	A				117 ± 8	129.2 ± 1.4 ky
	B				127 ± 9	
R-52	A				107 ± 6	128.1 ± 1.7 ky
	B				120 ± 9	
E-T-2	A				141 ± 16	129.9 ± 1.1 ky
	B					129.2 ± 1.1 ky
E-L-3					141 ± 16	125.5 ± 1.3 ky

*^{14}C ages are as reported in (*15, 22*) in radiocarbon years; the mean life of 8033 years was used; no corrections have been made for natural fractionation of carbon isotopes, the difference between $^{14}C/C$ in surface water and the atmosphere, or differences in initial $^{14}C/C$. †^{14}C ages have been corrected by us to dendroyears using the curves of Stuiver (*23*) for TAN-E-1g and CWS-F-1 and for CH-8, assuming a $^{14}C/C$ initial ratio from Klein *et al.* (*37*) for tree rings ~8000 years old. No corrections have been made for natural fractionation of carbon isotopes or the difference between $^{14}C/C$ in the surface water and the atmosphere. ‡From reference (*22*). §Ages from reference (*18*) except for E-T-2 and E-L-3 which are from reference (*17*).

predicts that older corals should have higher present heights ($T_1>T_2>T_3$ for $H_1>H_2>H_3$). By dating corals from localities with different uplift rates, one could, in principle, use this model to determine the rate of sea level rise as a function of time.

To use this approach, we must know the uplift rate at each locality. Exact uplift rates cannot be calculated from the present heights (H_1, H_2, H_3) and ages (T_1, T_2, T_3), but bounds can be placed on this rate. At the "high uplift" locality, the uplift rate is given by $(H_1 - H_3)/T_4$. T_4 is not known, but must lie between T_1 and T_3. Therefore, the uplift rate lies between $(H_1 - H_3)/T_1$ and $(H_1 - H_3)/T_3$.

For the Rendezvous Hill Terrace on Barbados, the corals with older ages have higher present heights as required by the model (Table 4). One of the Vanuatu samples does not meet this requirement. The Vanuatu samples have not been included in this analysis since their stratigraphic relationships are not clearly understood. Also listed are uplift rates calculated by subtracting 6 m (H_3) (*25*) from the present height (H_1 or H_2) and dividing by the age (T_1 or T_2). These are lower bounds on the uplift rate. Upper bounds could be calculated with the use of T_3. Mass spectrometric values for T_3 have not been obtained. Values for T_3 from α counting are, within error, the same as our values for T_1 and T_2 (*25*). Therefore, the minimum uplift rate is very close to the true uplift rate and is taken to represent this quantity.

If the assumptions used in deriving the above model are valid for the Barbados samples, then the uplift rate must be equal to the rate of sea level rise at the time of coral growth. It appears that the rate of sea level rise at 129 ky was about 0.4 m/ky, and between 126 and 122 ky the rate was about 0.2 m/ky. These rates of sea level rise suggest that sea level did not rise by more than 2 or 3 m between 129 and 122 ky. The extension of the present database to stable localities and localities with very high uplift rates should provide further insight into this problem.

The Milankovitch curve and the specific ages of corals. A histogram of our data for the Barbados and older Vanuatu samples (Fig. 3) shows three distinct age ranges. As the Barbados samples were collected from three distinct terraces, this would be expected. The Vanuatu samples apparently grew at the same time as the Rendezvous Hill corals from Barbados. The ages of these samples range from 130 to 122 ky. Analyses of one sample from the Ventnor Terrace and one sample from the Worthing Terrace on Barbados give ages of 112 ky and 87.7 ky, respectively. On the basis of the model for reef growth, the three age ranges should represent times when sea level was close to a maximum value but was still rising (at the rate of tectonic uplift).

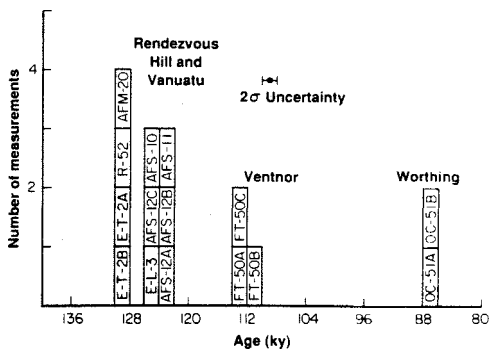

Fig. 3. The ages of corals from Barbados and Vanuatu. The typical 2σ error in age for each analysis is shown by the error bar. The Barbados samples are from three different terraces. The Vanuatu samples are stippled. These data suggest that the last interglacial period lasted from 130 ky to at least 122 ky ago and that interstadial periods occurred 112 and 87.7 ky ago. We have found no evidence for high sea level just prior to 130 ky ago.

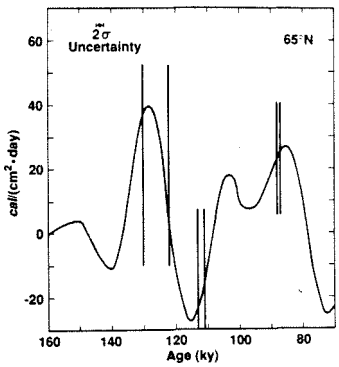

Fig. 4. The vertical axis represents the average solar insolation received at the top of the atmosphere at 65°N for the summer half year minus the present value. The curve is drawn for T = 160 ky to 70 ky (*29*). The stippled bands represent the ages shown in the histogram in Fig. 3. The oldest band represents the range of ages for a number of corals from the Rendezvous Hill Terrace in Barbados and from Vanuatu. The other bands represent the age and 2σ error in age for two individual samples from the Worthing and Ventnor terraces in Barbados. The error bars represent the typical 2σ errors in age for the mass spectrometric measurements. The oldest range of ages coincides with an insolation high and lends support to the Milankovitch hypothesis.

The three age ranges (Fig. 3) have been superimposed on a graph (Fig. 4) of the summer solar insolation received at 65°N latitude as a function of time [calculations by Berger (*29*)]. This curve has low values between 166 and 140 ky, rises to a very high value at 128 ky and drops to a very low value at 116 ky. It has maxima at 103 ky and 85 ky, then drops to a low value at 73 ky. The oldest range of coral ages occurs almost exactly at the time of the insolation maximum at 128 ky. The oldest corals in this range may have grown as much as 2 ky before the insolation high; the youngest in this range grew as much as 6 ky after the insolation high. Previous data, both geomorphic and radiometric (α counting) (*30*), have suggested the possibility that sea level was high about 140 ky ago. This would predate the 128 ky insolation peak by more than 10 ky and could not be the direct result of orbital forcing. We have found no evidence for high sea level 140 ky ago. Our oldest range of ages supports the idea that Pleistocene sea level highs can be the result of orbital forcing. The apparent high position of sea level 130 ky ago requires that, as the insolation curve increases, the phase lag between the insolation and sea level curves is small. The high position of sea level 6 ky after the insolation peak suggests that as the insolation curve decreases, the phase lag is significantly larger. From the range of ages, it appears that sea level was high for at least 8 ky during the last interglacial period.

The youngest coral (87.7 ky) grew about 2 ky before the insolation high at 85 ky. The apparent high position of sea level at this time could be the result of orbital forcing. However, the 112-ky-old coral grew 9 ky before the 103 ky insolation high. The high position of sea level at this time does not appear to coincide with an insolation high.

We conclude that the use of mass spectrometric techniques for the measurement of ^{230}Th and ^{234}U in corals permits a substantial increase in the range over which useful ages can be determined with the ^{238}U-^{234}U-^{230}Th system with a range from about 50 years to about 500 ky. The precision with which ages can be determined, based on analytical errors, is about five to ten times higher than by α-counting methods. The sample size requirement is about 30 times smaller. The precise determination of $\delta^{234}U$ and ^{232}Th will also permit a clearer evaluation of possible open-system behavior. The analyses on young corals suggest that this approach may be prefera-

ble to ^{14}C analysis for these materials. The basic problems of diagenesis and element remobilization will remain the fundamental problems that require study. Our precise measurements on corals that grew during the last interglacial period lie specifically within the 128-ky Milankovitch peak and support the idea that major changes in Pleistocene climate can be caused by orbital forcing. The age of a coral that grew during an interstadial period also supports this view. However, the age of a coral that grew during another interstadial period suggests that some changes in Pleistocene climate may be the result of other mechanisms. The ability to analyze small samples is very important with regard to studies of marine terraces. Reef-forming corals are largely limited to the tropics; however, solitary corals grow in marine environments worldwide, but only occur in small masses. Few terraces have yielded enough solitary coral for α-counting analysis. When the techniques outlined here are used, the small sample size will also allow dating of well-preserved solitary corals. If foraminifera could be dated, the absolute chronology for the $^{18}O/^{16}O$ record in deep sea sediments could be determined. The uranium concentration in foraminifera has been reported as 0.11 nmol/g (*31*). At secular equilibrium, 1 g of foraminifera contains 1.1×10^9 atoms of ^{230}Th, which could be measured to an accuraey of ±1 percent (2σ) by means of mass spectrometric techniques. These techniques have also been used in our laboratory to measure the concentrations of ^{230}Th (10^7 atoms per liter) and ^{232}Th in 1 to 3 liters of seawater (*11, 32*).

REFERENCES AND NOTES

1. W. S. Broecker *et al.*, *Science* **159**, 297 (1968).
2. K. J. Mesollela, R. K. Matthews, W. S. Broecker, D. L. Thurber, *J. Geol.* **77**, 250 (1969).
3. H. H. Veeh and J. M. Chappell, *Science* **167**, 862 (1970).
4. M. M. Milankovitch, *Canon of Insolation and the Ice Age Problem* (Königlich Serbische Akademie, Beograd, 1941), English translation by the Israel Program for Scientific Translations, Jerusalem, 1969.
5. W. T. Hyde and W. R. Peltier, *J. Atmos. Sci.* **42**, 2170 (1985).
6. W. R. Peltier, in *Irreversible Phenomena and Dynamical Systems Analysis in Geosciences*, C. Nicolis and G. Nicolis, Eds. (Reidel, Dordrecht, 1987), p. 399.
7. J. D. Hays, J. Imbrie, N. J. Shackleton, *Science* **194**, 1121 (1976).
8. J. Imbrie *et al.*, in *Milankovitch and Climate*, A. L. Berger, J. Imbrie, J. Hays, G. Kukla, B. Saltzman, Eds. (Reidel, Dordrecht, 1984), p. 269.
9. J. H. Chen and G. J. Wasserburg, *Anal. Chem.* **53**, 2060 (1981).
10. Y. Nozaki, Y. Horibe, H. Tsubota, *Earth Planet. Sci. Lett.* **54**, 203 (1981).
11. J. H. Chen, R. L. Edwards, G. J. Wasserburg, *ibid.* **80**, 241 (1986).
12. A. Kaufman and W. S. Broecker, *J. Geophys. Res.* **70**, 4039 (1965).
13. R. H. Steiger and E. Jäger, *Earth Planet. Sci. Lett.* **36**, 359 (1977).
14. R. L. Edwards, J. H. Chen, G. J. Wasserburg, *ibid.* **81**, 175 (1987).
15. F. W. Taylor, P. Mann, S. Valestro, Jr., K. Burke, *J. Geol.* **93**, 311 (1985).
16. M. L. Bender *et al.*, *Geol. Soc. Am. Bull. Part I* **90**, 577 (1979).
17. A. L. Bloom, C. Jouannic, F. W. Taylor, appendix to R. P. Ash, J. N. Carney, A. Macfarlane, *Geology of Efate and Offshore Islands, New Hebrides Geol. Surv. Regional Report* (1978).
18. T.-L. Ku, in preparation.
19. J. F. Marshall and B. F. Thom, *Nature (London)* **263**, 120 (1976).
20. W. S. Broecker, *J. Geophys. Res.* **68**, 2817 (1963).
21. A. Kaufman, W. S. Broecker, T.-L. Ku, D. L. Thurber, *Geochim. Cosmochim. Acta* **35**, 1155 (1971).
22. F. W. Taylor, written communication.
23. M. Stuiver, *Radiocarbon* **24**, 1 (1982).
24. C. R. Darwin, *The Structure and Distribution of Coral Reefs* (Smith and Elder, London, ed. 2, 1874).
25. T.-L. Ku, M. A. Kimmel, W. H. Easton, T. J. O'Neil, *Science* **183**, 959 (1974).
26. A. L. Bloom, W. S. Broecker, J. M. A. Chappell, R. K. Mathews, K. J. Mesollela, *Quat. Res.* **4**, 185 (1974).
27. R. K. Matthews, *ibid.* **2**, 368 (1972).
28. P. Aharon and J. Chappell, *Paleogeogr. Paleoclimatol. Paleoecol.* **56**, 337 (1986).
29. A. L. Berger, *Quat. Res.* **9**, 139 (1978).
30. W. S. Moore, in *Uranium Series Disequilibrium: Applications to Environmental Problems*, M. Ivanovich and R. S. Harmon, Eds. (Oxford Univ. Press, New York, 1982), p. 481.
31. T.-L. Ku, *J. Geophys. Res.* **70**, 3457 (1965).
32. A. J. Spivack, J. H. Chen, G. J. Wasserburg, *Trans. Am. Geophys. Union* **67**, 1066 (1986).
33. J. W. Meadows, R. J. Armani, E. L. Callis, A. M. Essling, *Phys. Rev. C* **22**, 750 (1980).
34. M. Lounsbury and R. W. Durham, in *Proceedings International Conference on Chemical Nuclear Data, Measurements and Applications*, M. L. Hurrell, Ed. (Institute of Civil Engineers, London, 1971), p. 215.
35. P. de Bievre *et al.*, *ibid.*, p. 21.
36. A. H. Jaffey, K. F. Flynn, L. E. Glendenin, W. C. Bentley, A. M. Essling, *Phys. Rev. C* **4**, 1889 (1971).
37. J. Klein, J. C. Lerman, P. E. Damon, E. K. Ralph, *Radiocarbon* **24**, 103 (1982).

38. We have benefited from the advice of and discussions with A. L. Bloom, F. W. Taylor, W. S. Broecker, R. K. Matthews, K. K. Turekian, and P. Aharon. We thank R. K. Matthews for the Barbados samples, A. L. Bloom for the older Vanuatu samples, F. W. Taylor for the younger Vanuatu and Hispaniola samples, P. Aharon for the giant clam sample, J. M. Edmond for suggestive discussions, and D. A. Papanastassiou for advice and support. Supported by the California Institute of Technology and NASA grant NAG 9-43 for equipment. The α-counting work was supported by NSF grant ATM-8514472 to T.-L.K. Division Contribution No. 4429 (564). This study was carried out at the Lunatic Asylum of the Charles Arms Laboratory.

12 December 1986; accepted 13 April 1987

HIGH PRECISION THORIUM-230 DATING OF CORALS USING THERMAL IONIZATION MASS SPECTROMETRY: APPLICATIONS TO PALEOSEISMOLOGY

by

R. Lawrence Edwards[1], F. W. Taylor[2], J. H. Chen[1] and G. J. Wasserburg[1]

[1] The Lunatic Asylum of the Charles Arms Laboratory, Division of Geological and Planetary Sciences, California Institute of Technology, Pasadena, California 91125

[2] Institute for Geophysics, University of Texas at Austin, Austin, Texas 78759

ABSTRACT

The recent development of mass spectrometric methods for determining ^{230}Th abundances reduces the analytical error in ^{230}Th ages of corals. Errors of ±3 yrs (2σ) for a 17 yr old coral, ±5 yrs at 180 yrs, ±44 yrs at 8,294 yrs, and ±1.1 ky at 123.1 ky (1 ky = 1,000 yrs) were obtained using these techniques. Within the error of the measurements, ^{230}Th ages agree with ages determined by counting of annual growth bands. These measurements indicate that the maximum amount of ^{230}Th incorporated into a coral skeleton during growth is equivalent to the amount of ^{230}Th generated by radioactive decay in <6 yrs. Using these techniques, we have dated two emerged corals from north Malekula Island and two from northwest Santo Island, Vanuatu. By analogy to partially emerged corals that were killed by coseismic uplift on Santo in 1973 (M_S = 7.5) and on Malekula in 1965 (M_S = 7.5), it appears that each pair of emerged corals was killed by an earlier coseismic uplift event. Pairs of emerged coral heads from each of the localities yield similar ^{230}Th ages. This demonstrates that each pair of corals died at the same time and is consistent with the idea that they were killed by the same event (presumed to be coseismic emergence). The ^{230}Th growth dates of the emerged corals (A.D. 1864±4 (2σ) and A.D. 1865±4 for Santo; A.D. 1729±3 and A.D. 1718±5 for Malekula) in conjunction with the dates of historical earthquakes yield recurrence intervals of 108 yrs for northwest Santo Island and 236 yrs for north Malekula Island. If a slip-predictable model is used, average uplift rates over the past few centuries are similar to uplift rates averaged over the past 6,126 yrs. It may be possible to extend this approach back in time and to other localities because coral features that represent paleoseismic events are preserved in the geologic record and we have the ability to recognize these features in the field. However, the difficulties in recognizing and sampling corals that represent paleoseismic uplifts become increasingly greater with increasing age.

INTRODUCTION

We have recently developed high precision mass spectrometric techniques to measure ^{230}Th and ^{234}U abundances in small amounts of coral (Edwards and others, 1987a, b). Use of these techniques reduces the analytical error in a ^{230}Th age, decreases the sample size required for an analysis, and increases the time range over which useful ages can be determined. The purpose of this note is to review the systematics and assumptions used in ^{230}Th dating, to

summarize the recent technical improvements in ^{230}Th measurements, and to examine situations where use of these techniques will have immediate impact in paleoseismologic studies.

SYSTEMATICS

^{230}Th dating of corals is based on the decay of ^{238}U through a series of intermediate daughters:

$$^{238}U \xrightarrow[6.446\times10^{9}\ yr]{} {}^{234}U \xrightarrow[352.7\times10^{3}\ yr]{} {}^{230}Th \xrightarrow[108.8\times10^{3}\ yr]{} {}^{206}Pb,$$

where the numbers below the arrows are mean lives and only the pertinent intermediate daughters are shown. The differential equations for radioactive production and decay can be solved for time as a function of the measured $^{234}U/^{238}U$ and $^{230}Th/^{238}U$ ratios if: (1) the initial $^{230}Th/^{238}U$ ratio, when the coral grew, is assumed to be zero, and (2) corals are assumed to be closed systems with respect to U and Th. The solutions are:

$$[^{230}Th/^{238}U]_{act} - 1 = [(\delta^{234}U(0)/1000)(\lambda_{230}/(\lambda_{230}-\lambda_{234})](1-e^{(\lambda_{234}-\lambda_{230})T}) - e^{-\lambda_{230}T} \quad (1)$$

and

$$\delta^{234}U(T) = \delta^{234}U(0)e^{\lambda_{234}T}. \quad (2)$$

Equation 1 (modified from Kaufman and Broecker, 1965) is used to calculate the ^{230}Th age. T is the age; the λ's are decay constants; $[^{230}Th/^{238}U]_{act}$ is the measured $^{230}Th/^{238}U$ atomic ratio times $\lambda_{230}/\lambda_{238}$; and $\delta^{234}U$ is the fractional enrichment of the $^{234}U/^{238}U$ ratio (at any given time) relative to the $^{234}U/^{238}U$ ratio at secular equilibrium in parts per thousand:

$$\delta^{234}U = [(^{234}U/^{238}U)(\lambda_{234}/\lambda_{238})-1](1000). \quad (3)$$

The value of $\delta^{234}U$ changes with time. The relationship between the present value $[\delta^{234}U(0)]$ and the initial value when the coral grew $[\delta^{234}U(T)]$ is given by equation 2. Equation 2 provides an independent test of the closed system assumption used in solving the radioactive decay equations. The initial uranium isotopic composition can be calculated using the age, T (from eq. 1) and the measured uranium isotopic composition. If the isotopic composition of uranium in seawater does not change with time, then differences between the calculated $\delta^{234}U(T)$ of the fossil coral and the present $\delta^{234}U$ value of seawater (Chen and others, 1986) would indicate open system behavior.

MEASUREMENT OF ^{230}Th AND ^{234}U BY THERMAL IONIZATION MASS SPECTROMETRY

^{230}Th ages of corals were first measured by Barnes and others (1956) using α-spectrometry to determine the $^{230}Th/^{238}U$ ratios. Thurber and others (1965) and Broecker and Thurber (1965) measured $^{234}U/^{238}U$ ratios as well as $^{230}Th/^{238}U$ ratios (again by α-spectrometry) and calculated ^{230}Th ages taking into account the fact that the $^{234}U/^{238}U$ ratio in seawater differs from the value at secular equilibrium (Thurber, 1962). Improvements in detector systems increased the resolution of α-spectra (see Rosholt, 1984) and obviated some of the problems associated with α-counting measurements, but major

improvements in the precision of ^{230}Th, ^{234}U and ^{238}U measurements (by α-spectrometry) have not been made since the pioneering work of Broecker and coworkers. This is because the precision of a measurement is limited by the number of atoms (or α-particles) that can be detected during a measurement. By α-spectrometry, only decaying particles can be detected. ^{230}Th has a mean life of ~ 10^5 yrs, so for a laboratory counting time of one week, only one out of 10^7 ^{230}Th atoms in a sample can be detected. In mass spectrometric measurements, ions are detected, and the precision of a measurement is limited by the fraction of ^{230}Th atoms that one can ionize. We have obtained ionization efficiencies of one out of 10^3 (Edwards and others, 1987a) for Th. For the same size sample, 10^4 times more atoms of ^{230}Th can be detected by mass spectrometric determination than by α-counting methods. Based solely on counting statistics, a ^{230}Th measurement by mass spectrometry should be about 10^2 times more precise than a ^{230}Th measurement (on the same size sample) by α-counting. Both methods of measurement have other sources of error (Harmon and others, 1979; Rosholt, 1984; Edwards and others, 1987a). Table 1 compares the methods and shows that, for a 120,000 yr old (120 ky) sample, the error in age is about an order of magnitude smaller and the sample size around fifty times smaller for mass spectrometric measurements.

TABLE 1.-- Comparison between mass spectrometric and α-counting methods for measuring ^{230}Th and ^{234}U in a ~ 120 ky old coral

Method	Coral sample size	Number of ions or alpha particles measured/run		2σ uncertainty[1]		
		^{230}Th	^{234}U	$^{230}Th/^{238}U$	$^{234}U/^{238}U$	Age(ky)
Mass spectrometry	200 mg	5×10^6	2×10^6	±2°/₀₀	±5°/₀₀	±1
α-counting	10 g	3×10^3	5×10^3	±40°/₀₀	±30°/₀₀	±10

[1] The α-counting uncertainties are taken from Harmon and others (1979) and are based on counting statistics. °/₀₀ indicates parts per thousand.

Table 2 shows samples that were dated by ^{14}C, counting of coral growth bands, ^{230}Th (α-counting) and ^{230}Th (mass spectrometric). The errors in the mass spectrometric ages, based on analytical errors, range from ±3 yrs (2σ) for a coral that is 17 yrs old to ±1.1 ky for samples that are around 120 ky old. Assuming typical analytical errors, we calculate that, for a 500 ky old sample, the error in age due to analytical uncertainty would be ±50 ky (2σ). Samples CWS-A, CWS-A-1d and TAN-E-1g were collected when the surface of the coral head was still alive, and their ages were determined from the counting of annual growth bands. For all three samples, the ^{230}Th ages and growth band ages agree within the error of the measurements (fig. 1). The ^{230}Th ages were calculated assuming that the initial amount of ^{230}Th incorporated into the coral skeleton was zero. The agreement between the ^{230}Th ages and the growth band ages indicates that this assumption is valid, within errors. For CWS-A,

the ^{230}Th age is three yrs older than the mean growth band age and the 2σ error is ±3 yrs, so the maximum amount of initial ^{230}Th incorporated into the skeleton is equivalent to the amount of ^{230}Th produced by radioactive decay in 6 yrs.

TABLE 2.-- Coral ages determined by different methods or techniques[1]

Sample[2]	^{14}C[3] (conventional) (yrs)	^{14}C[4] (corrected) (yrs)	Growth Bands (yrs)	^{238}U-^{234}U-^{230}Th[5] (α-counting) (ky)	^{238}U-^{234}U-^{230}Th[6] (mass spectrometric)
CWS-A	---	---	13-15	---	17±3 yrs
CWS-A-1d	---	---	49-51	---	54±5 yrs
TAN-E-1g	270±120	30-70, 180-270, or 300-500	176-182	---	180±5 yrs
CWS-F-1	980±120	780-1010	---	---	845±8 yrs
CH-8	8990±120	~10,000	---	---	8294±44 yrs
AFS-12 A	---	---	---	129±9	122.1±1.1 ky
B					122.7±1.3 ky
C					124.5±1.3 ky
E-T-2 A	---	---	---	141±16	129.9±1.1 ky
B					129.2±1.1 ky

[1] Ages refer to the ages in 1986. Reported errors are 2σ. For ^{14}C and α-counting, the errors are based on counting statistics. Errors in mass spectrometric ages are based on the standard deviation of the mean of 60-300 isotope ratios measured in the course of a mass spectrometric run.

[2] For AFS-12, A and B are different fractions of the same powder; C is a different fragment of coral. For E-T-2, A and B are different fragments of coral.

[3] ^{14}C ages are as reported by Taylor and others (1985) in radiocarbon years; the mean life of 8033 yrs was used; no corrections have been made for natural fractionation of carbon isotopes, the difference between $^{14}C/C$ in surface water and the atmosphere, or differences in initial $^{14}C/C$.

[4] ^{14}C ages have been corrected by us to dendroyears using the curves of Stuiver (1982) for TAN-E-1g and CWS-F-1 and for CH-8, assuming a $^{14}C/C$ initial ratio from Klein and others (1982) for tree rings ~ 8,000 yrs old. No corrections have been made for natural fractionation of carbon isotopes or the difference between $^{14}C/C$ in the surface water and the atmosphere.

[5] Ages from T.-L. Ku (written commun., 1986) except for E-T-2 which is from Bloom and others (1978).

[6] From Edwards and others (1987b) and R. L. Edwards (unpub. data).

For TAN-E-1g and CWS-F-1, the ^{230}Th age and ^{14}C age agree within the analytical errors (table 2). For TAN, however, the ^{14}C age has three ranges that span several centuries. This is because of changes in the initial $^{14}C/C$ ratio in the atmosphere with time. For CH-8, the ^{14}C and ^{230}Th ages do not agree. The reasons for this are unclear and the discrepancy emphasizes the importance of more detailed studies comparing ^{14}C and ^{230}Th ages.

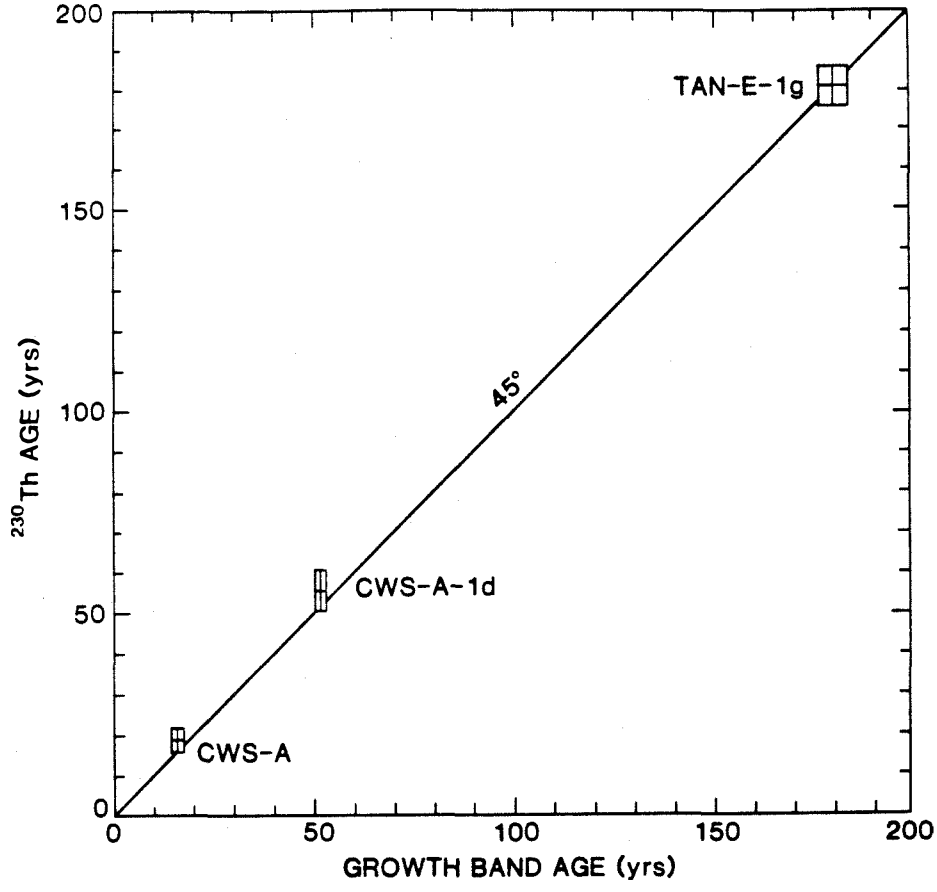

FIGURE 1.--^{230}Th age versus age determined by counting of annual growth bands. The error in the ^{230}Th age is 2σ and is based on analytical errors. The error in the growth band age is the range of ages in the sample which was analyzed. Boxes indicate the error limits of the age determinations.

Samples AFS-12 and E-T-2 are beyond the range of ^{14}C dating. The mass spectrometric ages agree with the α-counting ages but the errors for the mass spectrometric determinations are about an order of magnitude smaller. Replicate analyses of different fragments of AFS-12 and E-T-2 agree within analytical error. This indicates not only analytical reproducibility but also shows that different fragments of the same hand specimen could not have been altered to different degrees.

In summary, errors in ^{230}Th ages of corals due to analytical uncertainty are significantly lower when analysis is done by mass spectrometry instead of α-spectrometry. The error in mass spectrometric ^{230}Th ages are also lower than the errors in ^{14}C ages (due to analytical uncertainty). Mass spectrometric ^{230}Th ages have 2σ errors of ±3 yrs for a 17 yr old coral, ±5 yrs at 180 yrs, ±44 yrs at 8,294 yrs, ±1.1 ky at 123.1 ky, and an estimated error of ±50 ky at 500 ky. The sample size for the corals younger than 10 ky is ~ 3 g and for the 123.1 ky old sample, ~ 250 mg. For corals that grew during the past two centuries, ^{230}Th ages agree with ages determined from counting of growth bands. These measurements place an upper limit on the amount of initial ^{230}Th incorporated during coral growth (equivalent to the amount generated by radioactive decay in <6 yrs). This shows that the assumption that initial ^{230}Th is zero is valid. Future studies will address the validity of the assumption that corals can be chosen which have been closed with respect to U and Th exchange. The strongest evidence that diagenetic alteration is not a problem is the agreement between analyses of different fragments of the same sample (AFS-12 and E-T-2). This shows that different parts of the same hand specimen could not have been altered to different degrees.

APPLICATIONS IN PALEOSEISMOLOGY

Corals grow close to the sea surface. Therefore, the elevations and ages of fossil corals record changes in sea level with time. Apparent changes in sea level are caused by tectonic uplift (or subsidence), isostatic readjustments, and glacio-eustatic fluctuations in sea level. To the extent that eustatic and isostatic fluctuations in sea level (and apparent sea level) can be subtracted off, corals provide a record of tectonic movement. This approach has been used in a number of localities to determine uplift and subsidence rates averaged over ~ 10^5 yrs (see, for example, Moore and Fornari, 1984; Mesolella and others, 1969; Bloom, 1980).

There are two ways in which mass spectrometric ^{230}Th measurements will extend this approach. The first takes advantage of the ability to measure small samples. Reef-forming corals generally grow in the tropics. However, solitary corals grow in marine environments worldwide. Fossil solitary corals are only found in small masses in marine terraces. Therefore, dating by α-counting methods has only been possible in a few localities. Dating by mass spectrometric methods should extend this approach.

The second way takes advantage of the ability to date young corals (last several thousand years) very precisely. It may be possible to date corals which were killed by coseismic uplift and thereby date earthquakes. The ability to do this depends not only on the ability to date corals precisely, but also on the ability to identify fossil corals that were killed by coseismic uplift. The rest of this note will describe our results on samples from a specific locality where F. W. Taylor (unpub. data) found fossil corals presumed to have been killed by coseismic uplift.

Taylor and others (1987) examined partially emerged coral heads from Vanuatu. The tops of these coral heads were above sea level and were dead. The portions of the heads below sea level were still alive. The time of emergence and death of the upper part of a coral head could be determined by counting annual growth bands starting with the living portion of the coral. Using this approach, Taylor and others (1987) showed that the times of coral emergence correlated with the times of major earthquakes on northwest Santo Island (1973, M_S = 7.5) and north Malekula Island (1965, M_S = 7.5). The amount of emergence was 0.6 m on northwest Santo in 1973 and 0.8 m at the north Malekula locality in 1965.

At both localities, there are also completely emerged coral heads whose heights are 1.8 m above the highest living corals at northwest Santo and 1.3 m above the highest living corals on north Malekula. By analogy to the corals killed by coseismic uplift in 1965 and 1973, we considered the completely emerged corals also to have been killed by coseismic uplifts at earlier times. If this is true, then the ages of emerged coral heads at a given locality should be the same. We have dated the tops of two coral heads from each of the localities by ^{230}Th methods (table 3). At the northwest Santo locality, the growth dates of the two heads agree within analytical error (A.D. 1864±4, 1866±4), and at north Malekula, the dates of the two heads are similar to each other (A.D. 1729±3, 1718±4). The slight difference in growth date for the north Malekula locality is outside of analytical error and may be due to erosion of the outer (younger) part of the MAG coral head.

TABLE 3.-- ^{230}Th ages of emerged corals.

Sample	Island	Height[1] (m)	Date of growth (from ^{230}Th)[2] (yrs A.D.)
CWS-C	N.W. Santo	1.8	1866 ± 4
CWS-D-1[3]	N.W. Santo	1.8	1864 ± 4
CWS-D-2[3]	N.W. Santo	1.8	1868 ± 9
MAF	N. Malekula	1.3	1729 ± 3
MAG	N. Malekula	1.3	1718 ± 5

[1] Above the highest living corals at the same locality (F. W. Taylor, unpub. data).

[2] Determined by subtracting the ^{230}Th age from the date of analysis; dates are rounded to January 1 of the indicated year; reported errors are 2σ of the mean (R. L. Edwards, unpub. data).

[3] CWS-D-1 and CWS-D-2 are replicate analyses of the same coral.

The general agreement between growth dates of corals at a given locality is consistent with the idea that the heads were killed by coseismic uplift. The difference in growth dates between the north Malekula and northwest Santo corals indicates that they were killed by different events. The seismic recurrence interval at northwest Santo is (1973-1865) 108 yrs; the amount of uplift at this locality for the 1973 event was 0.6 m and for the 1865 event, 1.2 m. The uplift rate calculated by dividing 0.6 m by 108 yrs (slip-predictable model; see Shimazaki and Nakata, 1980) is 5.6 mm/y. The average uplift rate for the latter part of the Holocene can be estimated by dividing

the height of coral collected near the top of the Holocene terrace by its age. For northwest Santo, the average uplift rate over the past 6,126 yrs is 4.2 mm/y (see Taylor and others, 1987). Similarly, the seismic recurrence interval at north Malekula is (1965-1729) 236 yrs; the amount of uplift at this locality in 1965 was 0.8 m and in 1729, 0.5 m. The average uplift rate between 1729 and 1965 was 3.0 mm/y (slip-predictable), and the average rate over the last 6,126 yrs was 2.7 mm/y (Taylor and others, 1987). The similarity between short-term and long-term uplift rates at each locality suggests that, if a slip-predictable model is appropriate, uplift rates have been relatively constant throughout the Holocene and the total Holocene uplift can be accounted for by events similar to the 1965 and 1973 events.

In summary, the error in ^{230}Th ages (based on analytical errors) for corals ranges from ±3 yrs for a 17 yr old coral to ±1.1 ky for a 123.1 ky old coral. The correlation between growth band age and ^{230}Th age for living corals shows that initial ^{230}Th is less than the amount of ^{230}Th produced by radioactive decay in 6 yrs. Because of the precision with which the ages of corals can be measured, studies of paleoseismicity may be designed to use dating of corals for time control. The major problems are associated with the preservation of corals in the geologic record which represent paleoseismic events, the identification of such features in the field, and the determination of the depth at which the corals grew. In this note, we have described one instance where we believe identification of such a feature was possible.

ACKNOWLEDGMENTS

Discussions with D. A. Papanastassiou on various aspects of this project have been extremely helpful. We thank the Government of Vanuatu for assistance with fieldwork which was funded by NSF Grant EAR 79-19912 to F. W. Taylor. The age determinations were done in the Lunatic Asylum, supported by NASA Grant NAG 9-43. California Institute of Technology, Division of Geological and Planetary Sciences Contribution No. 4514 (593); University of Texas, Institute for Geophysics Technical Report No. 48.

REFERENCES CITED

Barnes, J.W., Lang, E.J., and Potratz, H.A., 1956, Ratio of ionium to uranium in coral limestones: Science, v. 124, p. 175-176.

Bloom, A.L., 1980, Late Quaternary sea level change on South Pacific coasts--A study of tectonic diversity, in Mörner, M.-A. ed., Earth Rheology, Isostasy and Eustasy: New York, N.Y., John Wiley & Sons, p. 505-516.

Bloom, A.L., Jouannic, C., and Taylor, F.W., 1978, Preliminary radiometric ages from the uplifted Quaternary coral reefs of Efate, appendix to Ash, R.P., Carney, J.N., and MacFarlane, A., Geology of Efate and offshore islands: New Hebrides Geological Survey Report, p. 47-49.

Broecker, W.S., and Thurber, D., 1965, Uranium series dating of corals and oolites from Bahaman and Florida Key limestones: Science, v. 149, p. 58-60.

Chen, J.H., Edwards, R.L., and Wasserburg, G.J., 1986, ^{238}U, ^{234}U, and ^{232}Th in seawater: Earth Planetary Science Letters, v. 80, p. 241-251.

Edwards, R.L., Chen, J.H., and Wasserburg, G.J., 1987a, ^{238}U-^{234}U-^{230}Th-^{232}Th systematics and the precise measurement of time over the past 500,000 years: Earth Planetary Science Letters, v. 81, p. 175-192.

Edwards, R.L., Chen, J.H., Ku, T.-L., and Wasserburg, G.J., 1987b, Precise timing of the last interglacial period: Science, v. 236, p. 1547-1553.

Harmon, R.S., Ku, T.-L., Matthews, R.K., and Smart, P.L., 1979, Limits of U-series analyses--Phase I, results of the Uranium-Series Intercomparison Project: Geology, v. 7, p. 405-409.

Kaufman, A., and Broecker, W.S., 1965, Comparison of ^{230}Th and ^{14}C ages for carbonate materials from lakes Lahontan and Bonneville: Journal Geophysical Research, v. 70, p. 4039-4054.

Klein, J., Lerman, J.C., Damon, P.E., and Ralph, E.K., 1982, Calibration of radiocarbon dates--Tables based on the consensus data of the Workshop on Calibrating the Radiocarbon Time Scale: Radiocarbon, v. 24, p. 103-122.

Mesolella, K.J., Matthews, R.K., Broecker, W.S., and Thurber, D.L., 1969, The astronomical theory of climate change--Barbados data, Journal Geology, v. 77, p. 250-274.

Moore, J.G., and Fornari, D.J., 1984, Drowned reefs as indicators of the rate of subsidence of the island of Hawaii: Journal Geology, v. 92, p. 752-759.

Rosholt, J.N., 1984, Isotope dilution analyses of U and Th in geologic samples using ^{236}U and ^{229}Th: Nuclear Instruments Methods, v. 223, p. 572-576.

Shimazaki, K., and Nakata, T., 1980, Time-predictable recurrence model for large earthquakes: Geophysical Research Letters, v. 7, p. 279-282.

Stuiver, M., 1982, A high precision calibration of the A.D. radiocarbon time scale: Radiocarbon, v. 24, p. 1-26.

Taylor, F.W., Jouannic, C., and Bloom, A.L., 1985, Quaternary uplift of the Torres Islands, northern New Hebrides frontal arc--Comparison with Santo and Malekula Islands, central New Hebrides frontal arc: Journal Geology, v. 93, p. 419-438.

Taylor, F.W., Frohlich, C., Lecolle, J., and Strecker, M., 1987, Analysis of partially emerged corals and reef terraces in the Central Vanuatu Arc--Comparison of contemporary coseismic and non-seismic with Quaternary vertical movements: Journal Geophysical Research, v. 92, p. 4905-4933.

Thurber, D., 1962, Anomalous $^{234}U/^{238}U$ in nature: Journal Geophysical Research, v. 67, p. 4518-4520.

Thurber, D.L., Broecker, W.S., Blanchard, R.L., and Potratz, H.A., 1965, Uranium-series ages of Pacific atoll coral: Science, v. 149, p. 55-58.

Earth and Planetary Science Letters, 72 (1985) 389–404
Elsevier Science Publishers B.V., Amsterdam – Printed in The Netherlands

[6]

The age and emplacement of obducted oceanic crust in the Urals from Sm-Nd and Rb-Sr systematics

R. Lawrence Edwards and G.J. Wasserburg

The Lunatic Asylum of the Charles Arms Laboratory, Division of Geological and Planetary Sciences, California Institute of Technology, Pasadena, CA 91125 (U.S.A.)

Received July 23, 1984
Revised version received December 20, 1984

The Urals contain a 2000 km belt of mafic-ultramafic bodies. The Sm-Nd and Rb-Sr systematics of two of these bodies, the Kempersai Massif in the South Ural Mountains and the Voykar-Syninsky Ophiolite Complex in the Polar Ural Mountains have been examined. These data confirm the hypothesis that these bodies represent fragments of pre-collision oceanic crust and establish constraints on the nature and timing of events in the Uralian Orogeny. Two Kempersai gabbros define Sm-Nd internal isochrons of 397 ± 20 My and 396 ± 33 My with $\epsilon_{Nd}(T) = +8.7 \mp 0.6$ and $+8.4 \mp 1.3$, respectively. Whole rock samples of pillow basalt, diabase, gabbros, troctolite, and a metasediment give Sm-Nd values which lie on this isochron indicating that these rocks are genetically related and have an igneous crystallization age of 397 My. Whole rock samples of Voykar-Syninsky diabase, gabbros, and clinopyroxenite give Sm-Nd values which lie on or within ~ 1 ϵ-unit of this isochron indicating an age and $\epsilon_{Nd}(T)$ virtually identical to those of Kempersai. $\epsilon_{Nd}(T)$ for the Kempersai and Voykar-Syninsky mafic samples range from +7.3 to +9.0 with an average value of +8.4. This indicates that the Urals ophiolites are derived from an ancient depleted mantle source and are most plausibly pieces of the oceanic crust and lithosphere. The fact that a metasediment has the same ϵ_{Nd}(397 My) as the other samples indicates derivation from an oceanic source with negligible continental input. $\epsilon_{Nd}(T)$ for the massifs is ~ 1.5 ϵ-units lower than the average for modern MORBs. This may be due to the differential evolution of the MORB source over the past 397 My and in conjunction with data for other ophiolites and Mesozoic MORB suggests that over the past 750 My the source for MORB has evolved at a rate less than or equal to its rate of evolution averaged over the age of the earth. Initial $^{87}Sr/^{86}Sr$ ratios are highly variable ranging from $\epsilon_{Sr}(T) = -25.2$ for a gabbro to +70.3 for a highly serpentinized harzburgite. This reflects the effects of seawater alteration which is particularly strong on ultrabasic rocks. We conclude that the long belt of mafic-ultramafic rocks in the Urals, which includes the Kempersai and Voykar-Syninsky Massifs, represents segments of Siluro-Devonian oceanic crust. Our igneous age for Kempersai in conjunction with other age constraints suggest that these segments of oceanic crust formed at least 80 My before the collision that produced the Urals.

1. Introduction

Ophiolite belts around the world tend to be concentrated near present-day continental margins. However, particularly in Eurasia, ophiolites belts also occur in orogenic belts interior to continents. A striking example is the linear trend of mafic-ultramafic bodies in the Ural Mountains which traverse the Eurasian from north to south. These bodies typically have dimensions, in map view, of tens to hundreds of kilometers and in overall structure are nappes [1,2]. It has been hypothesized that they represent fragments of oceanic crust that pre-date the continent-continent collision which created the Urals and are in suture zones between these continental blocks [1–4].

We have examined the Sm-Nd and Rb-Sr isotopic characteristics of two of these bodies, the Kempersai Massif and the Voykar-Syninsky Mas-

Division Contribution No. 4016 (460).

0012-821X/85/$03.30

sif. Kempersai outcrops in the South Ural Mountains. The Voykar-Syninsky Massif lies on the same linear trend of mafic-ultramafic bodies 2000 km to the north in the Polar Urals. The purpose of this study is: (1) to investigate whether the Nd and Sr isotope systematics of Kempersai and Voykar-Syninsky are consistent with the hypothesis that this belt of mafic-ultramafic rocks represent fragments of old oceanic crust, (2) to determine the igneous crystallization age of these massifs using Sm-Nd mineral and whole rock isochrons and compare this age with other constraints on the age of the collision that produced the Urals, (3) to determine whether the rock units in the massifs are genetically related and to determine the isotopic signatures of the mantle sources, (4) to establish some constraints on the nature and history of the continental collision.

2. Geology

Reviews of the geologic and tectonic relationships in the Urals are presented by Ivanov [5] and Hamilton [6]. Details of the geologic relationships of the Kempersai and Kharbarny Massifs are presented by Lennykh et al. [2,3] and Burtman et al. [7]. Geologic relationships of the Voykar-Syninsky Massif are discussed by Efimov et al. [8], Savelyev and Savelyeva [9,10], and Page et al. [11]. Much of the following discussion is taken from these references. The Urals are composed in large part of folded eugeoclinal and miogeoclinal Paleozoic rocks (Fig. 1). This fold belt runs north-south for ~ 2000 km, is roughly 250 km wide and is bounded by continental blocks. To the west lies the Russian Craton. To the east lies the Kazakhstan block, except in the extreme northern Urals where the Siberian block lies immediately east of the fold belt. The location of the boundary between these two blocks in the vicinity of the Urals is not known because it is obscured by Mesozoic and Cenozoic sediments. A traverse across the Urals from west to east shows the following lithologies and structures. The Russian Craton is covered with Mesozoic and Cenozoic platform sediments. To the east and stratigraphically below the platform sediments are upper Paleozoic and Triassic

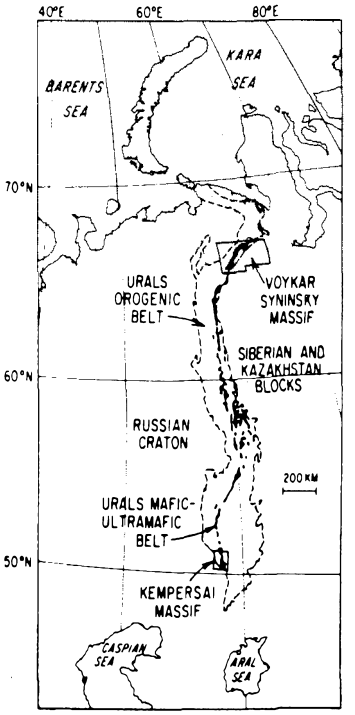

Fig. 1. Map of central Eurasia showing the position of the Urals fold belt. The linear belt of ultramafic rocks in the Urals is shown in black. Included in this belt are the Kempersai and Voykar-Syninsky Massifs, other similar ultramafic bodies, and 11 Alaskan-type concentrically zoned ultramafic bodies which outcrop in the Central Urals (after [42]).

molasse. Further east are folded upper Proterozoic and Paleozoic miogeoclinal sediments of the Russian Platform. The structure of the miogeocline is dominated by westward directed thrust faults [6]. The miogeocline is bounded to the east by the Main Uralian Fault Zone which separates it from the eugeocline to the east. The Main Uralian Fault is a zone (20 km wide) of highly sheared schists. Along the fault zone and immediately to the west of it is a linear belt of ultramafic rocks, serpentinites, and associated gabbroic rocks [12,6]. The Kempersai and Voykar-Syninsky Massifs make up part of this belt which is the main subject of this paper. Immediately east of the Main Uralian Fault Zone is a belt of folded eugeoclinal sediments and volcanics of Precambrian to Carbonif-

erous age. These are intruded by granitoids of middle to upper Paleozoic age. East of the eugeocline, the rocks of the Urals fold belt are obscured by Cenozoic and Mesozoic sediments of the West Siberian Lowlands. These sediments have an average thickness of ~ 3 km [6]. If there is an eastern miogeocline in the Urals associated with the Kazakhstan block, it lies beneath these sediments and is topographically much deeper than the western miogeocline associated with the Russian block. Thus, there is a fundamental asymmetry in the Urals.

The Kempersai Massif is the southernmost of the linear trend of mafic-ultramafic bodies (Figs. 1, 2). Kempersai is a 35 km by 70 km body which outcrops on the western slope of the South Ural Mountains just west of the Main Uralian Fault Zone. It includes one of the great chromite deposits of the world, the Donsai Chromite Mine. Kempersai is thrust over serpentine melange which in turn lies on top of cherts, volcanoclastics, and volcanics. These rocks are in turn thrust over

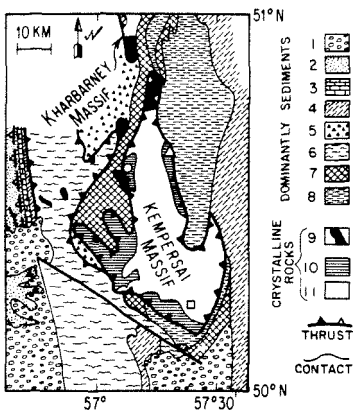

Fig. 2. Geologic map of the Kempersai Massif, the southern tip of the Kharbarney Massif and the surrounding area. Sample localities are indicated with open symbols: ○ = UR-2 to UR-11b; △ = UR-24 to UR-29; □ = UR-33 to UR-35 (after [42–45, 12]). *1* = Mesozoic and Cenozoic platform cover; *2* = C-Tr molasse; *3* = C shelf deposits; *4* = D-C graywacke, flysch; *5* = S-D continental slope deposits; *6* = S cherts, diabase, and spilites; *7* = O diabase, tuffs, and conglomerates; *8* = Є-O terrigenous sediments, volcanics, sandstones, and siltstones; *9* = ultramafics, gabbros, undifferentiated; *10* = gabbros and metagabbros; *11* = harzburgite and dunite.

Paleozoic miogeoclinal sediments of the Russian Platform (Fig. 2). The direction of transport of all these units is inferred to be from the east since there is no obvious source area in the Russian craton to the west. A K-Ar age of 404 My for a Kempersai amphibolite has been reported [13]. Much of what is known about field relations at Kempersai is inferred from the Kharbarney Massif, a body which is similar to Kempersai and outcrops just to the north of it. Kharbarney, like many of the mafic-ultramafic complexes in the Urals, is an allochthonous nappe [1]. The core of the anticline is made up dominantly of serpentinized harzburgite. The limbs are composed of a variety of mafic rocks. This nappe is thrust over serpentine melange, and cherts and volcanoclastics which are themselves thrust over Paleozoic miogeoclinal deposits of the Russian Platform. The section at Kharbarney [7] has at its base over 800 m of harzburgite with dunite and olivine chromite pods, typically highly serpentinized. Above this are clinopyroxenite and hornblendite lenses up to 50 m thick. On top of this are over 1000 m of gabbroic rocks often metamorphosed to amphibolites, then 300–500 m of medium- to fine-grained amphibolites. The top of the unit is composed of over 1100 m of diabases and volcanics metamorphosed to greenschists. The section at Kempersai is similar but also contains volcanogenic sediments. Much of the gabbroic portion of the Kempersai section is troctolite. Kempersai is an antiform similar to Kharbarney. The mafics on the eastern overturned limb of the antiform are amphibolites whereas those on the western limb are often unmetamorphosed except for uralitisation and saussuritisation [2].

The Voykar-Syninsky Massif outcrops on the east slope of the Polar Ural Mountains (Figs. 1, 3). With dimensions of ~ 300 km by ~ 70 km it is the largest of the mafic-ultramafic bodies in the Urals. It is extremely well exposed and preserved. Serpentinization is minimal. The structure of the area is dominated by thrust sheets which have been transported from the southeast to the northwest and lie on top of Eocambrian through Upper Carboniferous miogeoclinal sediments of the Russian Platform. The thrust sheets are made up of, from northwest to southeast, Devonian flysch and

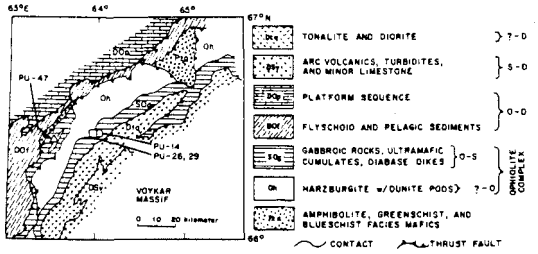

Fig. 3. Geologic map of the northeast portion of Voykar-Synin-sky Massif and vicinity. Sample locations are indicated with open symbols (after Page et al. [11] where a complete geologic map can be found). O = Ordovician; S = Silurian; D = Devonian.

pelagic sediments, the ophiolite complex, tonalite and diorite, and Silurian and Devonian island arc rocks. A minimum age of 375 My for gabbro and diabase dikes from the eastern edge of the massif has been reported [14] from K-Ar dating of a cross-cutting tonalite. K-Ar ages ranging from 400 to 470 My have also been reported for gabbros of the ophiolite complex [15]. The ophiolite complex is dismembered and is made up of several thrust sheets. The westernmost and structurally lowest sheet is dominantly made up of gabbroic rocks metamorphosed to amphibolite facies. Interlayered with the metagabbros are metamorphosed clinopyroxenites, wehrlites, and dunites. The base of this sheet is a cataclasized schist of gabbroic composition metamorphosed to blueschist facies. Structurally above this sheet is a sheet composed dominantly of tectonized harzburgite 4–6 km thick [8]. Locally bodies of dunite and associated chromite-rich pods are present within the harzburgite. Directly above the harzburgite are cumulate dunites, wehrlites, pyroxenites and gabbros. Up section these are replaced by gabbros and metagabbros. Above this is a sheeted diabase dike complex locally intruded by coarse-grained hornblende gabbros and plagiogranites.

3. Samples and analytical procedures

Kempersai samples were collected along traverses across the eastern and western limbs of the anticline and from the Donsai Chromite Mine in the ultramafic core of the anticline (see Fig. 2 for sample locations). Voykar-Syninsky samples were collected by Norman Page during traverses of the area sponsored by IGCP Project 39 [14]. Sample numbers correspond to sample numbers in Page et al. [11] where further descriptions of these samples can be found. Locations for the Voykar-Syninsky Massif samples are shown in Fig. 3. Petrographic descriptions of all samples may be obtained from the authors. Samples were analyzed for Sm, Nd, Rb, and Sr concentrations and $^{143}Nd/^{144}Nd$ and $^{87}Sr/^{86}Sr$ ratios using mass spectrometry and isotope dilution.

Samples from the Kempersai Massif include a number of mafic rocks in various states of alteration, a number of highly serpentinized ultramafic rocks, and a metasediment. Samples were chosen so that all the major rock types were represented and so that samples in different states of alteration were measured. The analyzed mafic rocks are: UR-3, a pillow basalt; UR-5, a troctolite; UR-11b, a pegmatitic gabbro; UR-24, a gabbro; and UR-25, a diabase. Of these, the sample which appears petrographically most altered is UR-3 pillow basalt. The mafic sample which petrographically shows the least evidence for metamorphism and alteration is UR-24 gabbro. UR-24 has primary igneous plagioclase, clinopyroxene, and olivine. The only evidence for metamorphism are coronal structures around olivine which is successively rimmed by a corona of orthopyroxene, then a corona of amphibole + spinel. This sample was chosen in order to obtain an internal Sm-Nd isochron because of its lack of alteration and because it represents the major rock type in the mafic portion of Kempersai. The ultramafic samples are UR-2, a serpentinized harzburgite; UR-33, a serpentinite; UR-34, a hornblende-chromite ore; and UR-35, a serpentine-chromite ore. These samples are all highly serpentinized and have little or no primary olivine remaining. UR-2 is typical of the harzburgite which is the major ultramafic rock type at Kempersai. UR-35 is typical of the ore at the Donsai Chromite Mine. UR-34 occurs as a very minor vein rock in the ore body. It is a chromian hornblende-chromite rock. The hornblende contains 2.5 wt.% Cr_2O_3 which is extremely high. UR-29 is the only metasediment collected. It

has been metamorphosed to amphibolite facies and comes from the top of the section. It is predominantly hornblende and quartz. The protolith is presumably volcanoclastic. This sample was chosen to put constraints on the nature of the sedimentary basin in which it was deposited.

Samples from the Voykar-Syninsky Ophiolite Complex include major mafic rock types and a clinopyroxenite. Analyzed samples are PU-14, a gabbro; PU-26, a gabbro; PU-29, a diabase; and PU-47, a clinopyroxenite. PU-26 appears petrographically more altered than PU-14. PU-29 is from a sheeted dike complex. PU-47 is a clinopyroxenite dike intruded into harzburgite.

Analysis proceeded as follows. For whole rock samples, 10 to 40 grams of rock was chiseled from the clean interior of each sample; this was crushed with a cleaned stainless steel mortar and passed through a 300 μm sieve. For all whole rock samples (except UR-35), the following procedures were followed. 500–1000 mg of the crushed powder was dissolved in HF and $HClO_4$. A small aliquot was spiked to determine rough Sm, Nd, Rb, and Sr concentrations. Using these concentrations, the bulk of the solution was then optimally spiked. For higher concentration samples ($> \sim 0.5$ ppm Nd), an aliquot corresponding to ~ 100 mg was passed through our standard ion exchange columns [16,17]. After chemical separation, Sm, Nd, and Sr concentrations were determined more accurately. Rb was not rerun and consequently the Rb concentrations have larger errors. However, because of the low Rb/Sr ratios, negligible error is introduced into initial $^{87}Sr/^{86}Sr$ values. For lower concentration samples ($< \sim 0.5$ ppm Nd) the same procedure was followed except that in place of the first ion exchange column we used a similar column with higher capacity. An aliquot corresponding to 400 mg of sample was passed through this column. In samples UR-34 and UR-35, an insoluble residue of chromite remained after HF-$HClO_4$ dissolution. We have proceeded under the assumption that no significant fractionation of Sm/Nd and Rb/Sr between solution and chromite residue occurred during dissolution. Further details of the techniques are given by Eugster et al. [16], Papanastassiou and Wasserburg [18], Papanastassiou et al. [19], DePaolo [17], and Wasserburg et al. [20].

UR-35 contains only 6.2 ppb Nd. Special chemical separation techniques were required to separate out enough Nd for the mass spectrometer run without introducing large blank corrections. This sample is the lowest concentration rock sample for which $^{143}Nd/^{144}Nd$ ratios have been measured to an accuracy of several parts in 10^5. Details of the special chemical separation procedures used are given by Ngo and Wasserburg (in preparation).

For UR-11b, mineral separates were obtained by both handpicking and magnetic separation yielding plagioclase and clinopyroxene separates over 99% pure. For UR-24, the clinopyroxene and plagioclase separates were better than 99.9% pure. The olivine in UR-24 is rimmed successively by orthopyroxene, then hornblende with small spinel inclusions. A 99.9% pure handpicked sample of orthopyroxene-amphibole grains was also obtained. Mineral separates were washed in acetone and distilled water and dried. Chemical separation and mass spectrometric procedures for the mineral separates were identical to those used for whole rock samples.

4. Results

Our results are shown in Tables 1 and 2 and Figs. 4–8. Following DePaolo and Wasserburg [21,22] the Nd isotopic data has been represented in ϵ notation which gives the fractional deviation of the $^{143}Nd/^{144}Nd$ ratio from a chondritic reservoir (CHUR) in parts per 10^4. The initial isotopic composition at time T (the crystallization age) is: $\epsilon_{Nd}(T) \approx \epsilon_{Nd}(0) + Q_{Nd} f^{Sm/Nd} T$. Here $f^{Sm/Nd} = [(^{147}Sm/^{144}Nd)_M/(^{147}Sm/^{144}Nd)_{CHUR}] - 1$. Model system parameters are: $(^{143}Nd/^{144}Nd)^0_{CHUR} = 0.511847$; $(^{147}Sm/^{144}Nd)_{CHUR} = 0.1967$; $Q_{Nd} = 25.13\ AE^{-1}$. $(^{143}Nd/^{144}Nd)_M$ is the ratio in the sample. For Sr, $(^{87}Sr/^{86}Sr)^0_{UR} = 0.7045$, $(^{87}Rb/^{86}Sr)^0_{UR} = 0.0827$ and $Q_{Sr} = 16.67\ AE^{-1}$ [22,23,20].

Concentration data (Table 1) show that each of the four elements analyzed vary by several orders of magnitude. The serpentine-rich ultramafic rocks (UR-2, UR-33, UR-35) have Nd concentrations ranging from less than a ppb (UR-2) to several

394

TABLE 1

Rb, Sr, Nd and Sm concentrations (ppm) in Urals ophiolites

	Rb	Sr	Sm	Nd
Kempersai Massif				
Mafics				
UR-3 basalt	19.3	147	2.95	8.22
UR-5 troctolite	0.368	74.4	0.0386	0.114
UR-11b peg gabbro-WR	0.489	90.8	0.314	0.607
-CPX			1.14	1.94
-PLAG			0.123	0.403
UR-24 gabbro-WR	0.0407	136	0.315	0.784
-CPX	–	–	1.68	3.18
-AM + OPX	–	–	0.176	0.565
-PLAG	–	–	0.0952	0.473
UR-25 diabase	0.182	113	3.15	9.00
UR-29 metasediment	1.19	208	4.82	13.58
Ultramafics				
UR-2 serpentinized harzburgite	0.113	3.24	0.0000801	0.000566
UR-33 serpentinite	0.0240	1.54	–	–
UR-34 hbld-chr ore	0.269	62.9	0.853	3.36
UR-35 serp-chr ore	0.00318	0.730	0.00209	0.00622
Voykar Massif				
PU-14 gabbro	1.01	86.4	0.0835	0.191
PU-26 gabbro	0.110	118	0.198	0.452
PU-29 diabase	0.134	139	2.31	6.21
PU-47 clinopyroxenite	0.0417	7.24	0.206	0.352

WR = whole rock; CPX = clinopyroxene mineral separate; PLAG = plagioclase; AM + OPX = amphibole + orthopyroxene; hbld-chr = hornblende-chromite ore; serp-chr = serpentine chromite ore; peg gabbro = pegmatitic gabbro.

ppb (UR-35). The other samples, generally of mafic composition, have Nd concentrations orders of magnitude higher ranging from several hundred ppb (UR-5) to several ppm (UR-29). The serpentine-rich ultramafics have Sr concentrations ranging from sub-ppm levels (UR-35) to a few ppm (UR-2) whereas the other samples generally have Sr concentrations of tens to hundreds of ppm. Sm/Nd ratios and Rb/Sr ratios show consistent trends for most samples. $f^{Sm/Nd}$ for most samples are positive whereas $f^{Rb/Sr}$ values are generally negative (see Table 2). Whole rock $f^{Sm/Nd}$ values range up to +0.799 (PU-47) and whole rock $f^{Rb/Sr}$ values range down to −0.99 (UR-24).

To establish the crystallization age of Kempersai, we analyzed mineral separates from UR-24 gabbro and UR-11b pegmatitic gabbro (see Figs. 4 and 5). Clinopyroxene, plagioclase, an orthopyroxene + amphibole mineral separate and whole rock data for UR-24 define a linear array in an Sm-Nd evolution diagram (Fig. 4). None of the four points deviates by more than 0.15 ϵ-units from a best fit line through the data points as shown in the inset in Fig. 4. This is well within analytical error. Nd concentrations (Table 1) and Sm/Nd ratios (Table 2) for the three mineral separates in UR-24 are fully compatible with what one would expect for equilibrium fractionation of Nd and Sm between these 3 phases: $C^{Nd}_{PLAG} < C^{Nd}_{AMPHIBOLE} < C^{Nd}_{CPX}$ and $[Sm/Nd]_{PLAG} < [Sm/Nd]_{AMPHIBOLE} < [Sm/Nd]_{CPX}$. We therefore conclude that the linear array shown in Fig. 4 represents an isochron. A best fit line through the four points using the regression routine of Williamson [24] gives an age of 397 ± 20 My and an initial $\epsilon_{Nd} = +8.68 \mp 0.56$. Clinopyroxene, plagioclase, and whole rock data for UR-11b pegmatitic gabbro also define a linear array (Fig. 5). All of the three data points lie within 0.1 ϵ-units of a best fit line. Again, Sm and Nd fractionate

TABLE 2

Sm-Nd and Rb-Sr isotopic data from Urals ophiolites

Samples	$\frac{^{143}Nd}{^{144}Nd}$ [a]	$\frac{^{147}Sm}{^{144}Nd}$ [b]	$f^{Sm/Nd}$	$\frac{^{87}Sr}{^{86}Sr}$ [c]	$\frac{^{87}Rb}{^{86}Sr}$ [d]	$f^{Rb/Sr}$	$\epsilon_{Nd}(T)$ [e]	$\epsilon_{Sr}(T)$ [e]
Kempersai Massif								
UR-3 pillow basalt	0.512339 ± 13	0.2172	+0.104	0.70706 ± 5	0.380	+3.59	+8.6 ± 0.3	+12.6 ± 0.7
UR-5 troctolite	0.512316 ± 19	0.2034	+0.034	0.70241 ± 4	0.0143	−0.83	+8.8 ± 0.4	−24.2 ± 0.6
UR-11b peg gabbro-WR	0.512571 ± 24	0.3126	+0.589	0.70274 ± 4	0.0156	−0.81	+8.3 ± 0.4	−19.6 ± 0.6
-CPX	0.512691 ± 21	0.3564	+0.812	-	-	-	+8.4 ± 0.4	-
-PLAG	0.512244 ± 31	0.1845	−0.062	-	-	-	+8.4 ± 0.6	-
UR-24 gabbro-WR	0.512409 ± 19	0.2430	+0.235	0.70226 ± 3	0.000866	−0.99	+8.6 ± 0.4	−25.2 ± 0.4
-CPX	0.512611 ± 21	0.3203	+0.629	-	-	-	+8.6 ± 0.4	-
-AM + OPX	0.512275 ± 18	0.1879	−0.045	-	-	-	+8.8 ± 0.4	-
-PLAG	0.512093 ± 17	0.1217	−0.381	-	-	-	+8.6 ± 0.3	-
UR-25 diabase	0.512301 ± 39	0.2120	+0.078	0.70363 ± 9	0.00468	−0.94	+8.1 ± 0.8	−6.1 ± 1.3
UR-29 metasediment	0.512352 ± 19	0.2145	+0.090	0.70413 ± 4	0.0165	−0.80	+9.0 ± 0.4	0.0 ± 0.6
UR-2 serpentinized harzburgite	-	0.0857	−0.565	0.70956 ± 5	0.102	+0.23	-	+70.3 ± 0.7
UR-33 serpentinite	-	-	-	0.70801 ± 16	0.0451	−0.45	-	+52.8 ± 2.3
UR-34 hbld-chr ore	0.511951 ± 20	0.1536	−0.219	0.70490 ± 3	0.0124	−0.85	+4.2 ± 0.4	+11.3 ± 0.4
UR-35 serp-chr ore	0.512155 ± 18	0.2036	+0.035	0.70801 ± 5	0.0126	−0.85	+5.7 ± 0.4	+55.4 ± 0.7
Voykar-Syninsky Massif								
PU-14 gabbro	0.512432 ± 21	0.2648	+0.346	0.70407 ± 6	0.0337	−0.59	+8.0 ± 0.4	−2.2 ± 0.9
PU-26 gabbro	0.512400 ± 21	0.2647	+0.346	0.70356 ± 3	0.00269	−0.97	+7.3 ± 0.4	−6.9 ± 0.4
PU-29 diabase	0.512355 ± 19	0.2250	+0.144	0.70459 ± 5	0.00280	−0.97	+8.5 ± 0.4	+7.7 ± 0.7
	0.512371 ± 27	0.2250	+0.144	-	-	-	+8.8 ± 0.5	-
PU-47 clinopyroxenite	0.512706 ± 25	0.3538	+0.799	0.70394 ± 4	0.0166	−0.80	+8.8 ± 0.5	−2.7 ± 0.6

[a] Errors are 2σ of the mean. $^{143}Nd/^{144}Nd$ is normalized to $^{146}Nd/^{142}Nd = 0.636151$. Nd was measured as NdO^+ and corrected to Nd metal values using $^{18}O/^{16}O = 0.00211$ and $^{17}O/^{16}O = 0.00387$ (for details see [20]).

[b] 2σ error is smaller than ± 2‰.

[c] Errors are 2σ of the mean. $^{87}Sr/^{86}Sr$ is normalized to $^{86}Sr/^{88}Sr = 0.1194$.

[d] 2σ error is smaller than ± 1%.

[e] Errors are based on analytical uncertainty and do not include errors from the age correction; $\epsilon(T)$ values are calculated using 397 My.

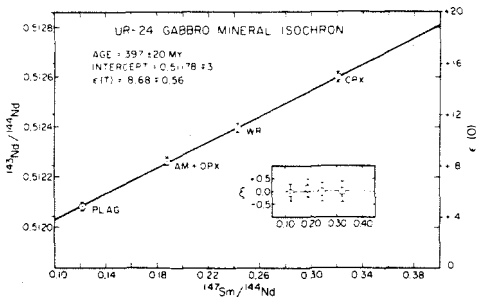

Fig. 4. Sm-Nd evolution diagram showing the internal isochron for UR-24 gabbro. The inset shows a blow-up of the deviations of the data points from a best fit line and shows that the data points are colinear well within analytical error. Error bars are 2σ of the mean.

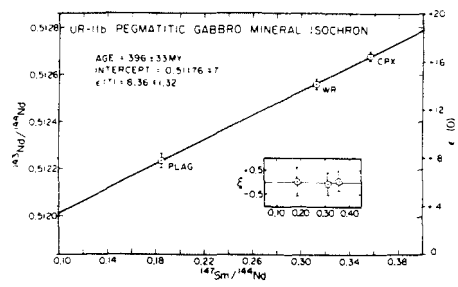

Fig. 5. Sm-Nd evolution diagram showing the internal isochron for UR-11b pegmatitic gabbro. The inset shows a blow-up of the deviations of the data points from a best fit line and indicates that the data points are colinear well within analytical error.

between clinopyroxene and plagioclase as expected for equilibrium fractionation ($C^{Nd}_{PLAG} < C^{Nd}_{CPX}$ and $[Sm/Nd]_{PLAG} < [Sm/Nd]_{CPX}$). We conclude that the linear array for UR-11b also represents an isochron which gives an age of 396 ± 33 My and an initial $\epsilon_{Nd} = +8.36 \mp 1.32$. The Sm-Nd internal isochron ages for UR-24 and UR-11b are essentially identical.

The Kempersai whole rock Sm-Nd data (Fig. 6) include values for every major mafic rock type in the sequence, as well as UR-29 metasediment, UR-35 serpentine chromite rock, and UR-34 hornblende-chromite vein. Within analytical error, the mafic rocks and the metasediment all plot on the 397 My reference isochron indicating that these rock units are genetically related and formed 397 My ago from an isotopically homogeneous reservoir with $\epsilon_{Nd}(397\ My) = +8.68$. Two samples, UR-34 and UR-35 from the Donsai Chromite Mine, lie off the 397 My reference isochron (circles in Fig. 8). UR-34 with 3.36 ppm Nd gives an $\epsilon_{Nd}(397\ My) = +4.1$ and UR-35 which has only 6.2 ppb Nd gives an $\epsilon_{Nd}(397\ My) = +5.7$. The Voykar-Syninsky Massif whole rock Sm-Nd data are shown in Fig. 7. Samples PU-47 clinopyroxenite and PU-29 diabase plot on the reference isochron determined for Kempersai. Samples, PU-14 gabbro and PU-26 gabbro lie slightly below the reference isochron by ~ 1 ϵ-unit. Thus the Voykar-Syninsky Massif samples have approximately the same $\epsilon_{Nd}(T)$ and age as UR-24 and the other Kempersai samples but clearly show evidence for slight heterogeneities in $\epsilon_{Nd}(T)$ and/or age.

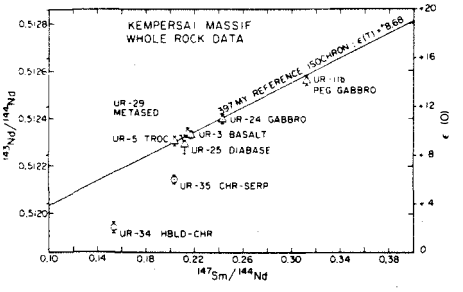

Fig. 6. Kempersai Massif whole rock data plotted on an Sm-Nd evolution diagram. Triangles are mafic rocks and the metasediment. Circles are ultramafics from the Donsai Chromite Mine.

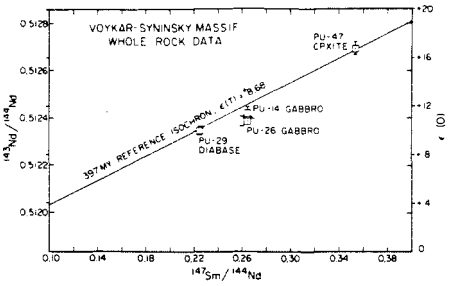

Fig. 7. Voykar-Syninsky Massif whole rock data plotted on an Sm-Nd evolution diagram showing general but not exact agreement with Kempersai results.

The whole rock Rb-Sr data for all samples is plotted in Fig. 8 along with a 397 My reference isochron. The Rb-Sr data exhibit none of the coherence of the Sm-Nd results and have clearly been disturbed. Initial $^{87}Sr/^{86}Sr$ ratios vary from 0.70225 ± 4 for UR-24 gabbro to 0.70900 ± 5 for UR-2 harzburgite. The serpentine-rich ultramafics (circles in Fig. 10) tend to have higher ϵ_{Sr} than the mafic members of the suite. The petrographically more altered mafic rocks have higher ϵ_{Sr} than the mafic samples which appear little altered.

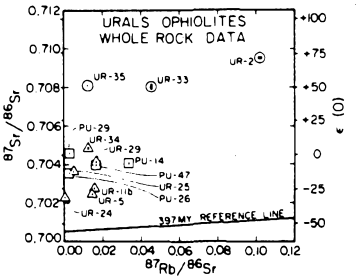

Fig. 8. Rb-Sr evolution diagram with the Urals ophiolite data points measured in this study. Circles are serpentine-rich ultramafic rocks from Kempersai. Triangles are the remaining samples from Kempersai. Squares are the Voykar-Syninsky Massif samples. One sample (UR-3 pillow basalt) has a high Rb/Sr ratio and plots off this diagram ($^{87}Sr/^{86}Sr = 0.70706$, $^{87}Rb/^{86}Sr = 0.380$). 2σ errors are the size of the black rectangle for each data point.

5. Discussion

The Kempersai data are plotted on an initial ϵ_{Nd} vs. ϵ_{Sr} diagram in Fig. 9. The Voykar-Syninsky Massif samples and the Kempersai mafic rocks and metasediment define a trend which we will refer to as the Urals Mafic Trend. In this trend ϵ_{Sr} varies from -25.2 to $+12.6$ while ϵ_{Nd} remains essentially constant. Thus the Nd isotope systematics show an amazing coherence for samples collected 2000 km apart and in various degrees of alteration. They all record essentially the same $\epsilon_{Nd}(T)$ (between $+7.3$ and $+9.0$) indicating that these rocks are genetically related. The avarage initial $\epsilon_{Nd} = +8.4$. This indicates that the Urals ophiolites are derived from an ancient depleted mantle source and are most plausibly pieces of the oceanic crust and lithosphere. Some of the Sr data supports this view.

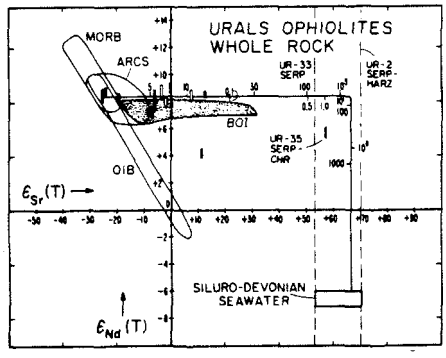

Fig. 9. ϵ_{Sr} vs. ϵ_{Nd} diagram with all data points measured in this study. Kempersai data are represented by solid symbols and Voykar-Syninsky data by open symbols. The uncertainty in ϵ_{Nd} is represented by the length of the data points. Uncertainty in ϵ_{Sr} is less than the width of the data points. ϵ_{Nd} for Siluro-Devonian seawater is from Shaw and Wasserburg [46] and ϵ_{Sr} from Veizer and Compston [47] and Burke et al. [48]. A mixing curve between rock and seawater is shown. Numbers above and to the right of the mixing curve are water-rock ratios for mafic rocks. Numbers below and to the left of the curve are for serpentine-rich ultramafics. The parameters used are: for unaltered mafic rock $\epsilon_{Nd} = +8.4$, $\epsilon_{Sr} = -25.2$, Nd = 0.784 ppm, Sr = 136 ppm; for unaltered ultramafic rock, the same ϵ values, Nd = 6.22 ppb, Sr = 0.730 ppm; for seawater $\epsilon_{Nd} = -6.0$, $\epsilon_{Sr} = +66.3$, Nd = 3×10^{-6} ppm; Sr = 8.5 ppm. *BOI* = Bay of Islands Ophiolite Complex; *ARCS* = field for oceanic arcs; *OIB* = ocean island basalts.

To compare ϵ_{Nd}(397 My) for Urals ophiolites with present-day analogues, we need to correct for the differential evolution of the source relative to CHUR. To do this we need the $f^{Sm/Nd}$ for the source and a model for how this source has evolved. The average $f^{Sm/Nd}$ for the mafic igneous rocks which we analyzed is $+0.23$ which agrees well with a value for oceanic crust of $+0.22$ determined from the Samail Ophiolite [25], from the Bay of Islands Ophiolite [26], and from arguments relating the Rb-Sr systematics of modern MORBs to their Sm-Nd systematics [27]. The value for the ophiolite section is similar to the value for the Urals ophiolite source since mineral-melt distribution coefficients for Sm and Nd are so small for most plausible upper mantle minerals [28], that even small percentages of partial melt, in equilibrium with a solid residue, effectively scavenge almost all of the Nd and Sm. Therefore $f^{Sm/Nd}$ for the source is approximately equal to $f^{Sm/Nd}$ for the Urals ophiolite magmas ($+0.22$). To calculate how ϵ_{Nd} for the source has changed over the past 397 My, we use the two models for the evolution of the source for MORBs investigated by Jacobsen and Wasserburg [27] as guides. For purposes of discussion we assume that the source for MORBs has evolved at a constant rate. In Model I the mass of the source increases through geologic time while the f-values for this reservoir remain constant. The equation defining the change in ϵ_{Nd} for the MORB source is $\epsilon_{Nd}(0) \approx \epsilon_{Nd}(T) + Q_{Nd} f^{Sm/Nd}[\langle \tau_0 \rangle - \langle \tau_T \rangle]$ (modified from Jacobsen and Wasserburg [27], eq. 21b). Here $\langle \tau_0 \rangle$ and $\langle \tau_T \rangle$ are the average age of the source today and at time T respectively. For $\epsilon_{Nd}(397) = +8.4$ and $f^{Sm/Nd} = +0.22$, this gives $\epsilon_{Nd}(0) = +9.5$. This lies squarely within the range of modern MORB and at the upper end of the range for modern oceanic arcs. In Model II the mass of the source for MORBs is constant, while $f^{Sm/Nd}$ for this reservoir has increased throughout geologic time from a starting value of $f^{Sm/Nd} = 0$. For Model II the appropriate equation is $\epsilon_{Nd}(0) = \epsilon_{Nd}(T) + Q_{Nd}\langle f^{Sm/Nd} \rangle T$ (modified from Jacobsen and Wasserburg [27], eq. 54). $\langle f^{Sm/Nd} \rangle$ is the time weighted average f-value over the period of time T to 0. If we assume that over the past 397 My $f^{Sm/Nd}$ has increased at the average rate of change for $f^{Sm/Nd}$ since fractionation from CHUR,

then $\epsilon_{Nd}(0) = +10.8$. This value lies in the upper part of the range for modern MORB and just above the range for modern oceanic arcs.

Over the last five years Sm-Nd data for a number of Phanerozoic and late Precambrian ophiolites and for Mesozoic MORB have been obtained. This growing body of data may place important constraints on the evolution of the source of MORBs through geologic time. These data are presented in Fig. 10. Also shown for reference are two possible models for the evolution of the source for MORB through geologic time. These are Models I and II from Jacobsen and Wasserburg [27], with the added stipulation that the source for MORB has evolved at a constant rate over the age of the earth. One would expect a certain amount of scatter in the data plotted in Fig. 10. There are two reasons for this scatter. First, there are slight heterogeneities in ϵ_{Nd} ($\sim \pm 2$ ϵ-units) for modern MORB. Old MORB should have similar heterogeneities. Second, not all ophiolites represent material generated at a mid-ocean ridge. Inclusion of ophiolitic material not representative of MORB would cause scatter below the "true" MORB curve. Nevertheless, the data appear to show some trends. In general ϵ_{Nd} for ophiolites is less than ϵ_{Nd} for modern MORB. This is consistent with the progressive evolution of the MORB source from CHUR through time.

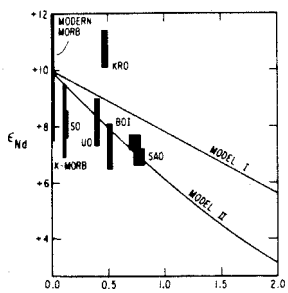

Fig. 10. Data for the Urals ophiolites, other ophiolites and Cretaceous MORB are plotted on an ϵ_{Nd} vs. T diagram. Also shown are two possible models for the evolution of the MORB source. These are Models I and II from Jacobsen and Wasserburg [27]. *SO* = Samail Ophiolite [29]; *K-MORB* = Cretaceous MORB [49]; *UO* = Urals ophiolites (this study); *KRO* = Kings River Ophiolite (Shaw, personal communication); *BOI* = Bay of Islands Ophiolite [26]; *SAO* = Saudi Arabian ophiolites [50].

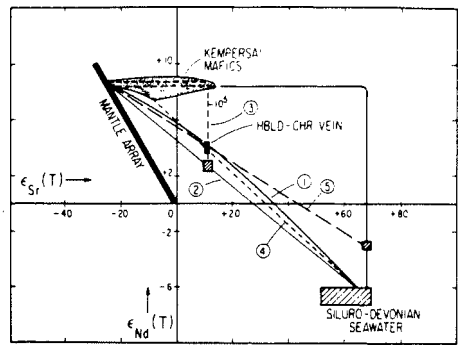

Fig. 11. ϵ_{Nd} vs. ϵ_{Sr} diagram showing the mixing model for UR-34 hornblende chromite vein rock. See text for details.

Most of the data also plot below the "Model I" curve in Fig. 11 and appear to define a steeper slope (~ 4 ϵ-units/AE). Thus if the MORB source has evolved according to Model I then the rate of evolution of the MORB source over the past 750 My has been slower than the average over the age of the earth. Most of the data plot on the "Model II" curve. If the MORB source has evolved according to Model II, the data is consistent with a rate of evolution for the past 750 My equal to the average rate over the age of the earth.

As opposed to the Sm-Nd systematics which in general appear to show closed system behavior, the Rb-Sr systematics are clearly disturbed. This is evident in Fig. 8 as well as in Fig. 9. In the latter plot, for rocks of the Urals Mafic Trend, ϵ_{Sr} varies by ~ 40 ϵ-units. The rock with the lowest $\epsilon_{Sr} = -25.2$ (UR-24) has a depleted mantle Sr signature consistent with the Nd data and lies on the mantle array. It is also petrographically the least altered sample. In general, samples which show little evidence for alteration have low ϵ_{Sr} whereas those that are extensively altered have high ϵ_{Sr}. This indicates that radiogenic Sr has been introduced during the alteration process. Assuming that the Kempersai mafic trend is due to two-component mixing and that one component is unaltered rock ($\epsilon_{Nd}(T) = +8.4$, $\epsilon_{Sr}(T) = -25.2$), candidates for the second component are limited. The second reservoir must have the following properties: (1) it must have ϵ_{Sr} greater than or equal to the highest ϵ_{Sr} sample and (2) it must either have ϵ_{Nd} equal to

+8.4 or have a very much higher Sr/Nd ratio than unaltered Urals ophiolite rocks. The best candidate is a hydrothermal fluid derived from Siluro-Devonian seawater.

Fig. 9 shows a mixing line between the sample least radiogenic in Sr and Siluro-Devonian seawater assuming complete closed system exchange between rock and seawater [29, eq. 1]. Water-rock (W/R) ratios were calculated for two cases. In the first case, the Nd and Sr concentrations are for typical mafic rock (e.g. UR-24). In the second, the concentrations are for Urals serpentinites (e.g. UR-35). All rocks in the Urals Mafic Trend plot on the calculated mixing line. The highest W/R is ~ 15 for a pillow basalt. This is far lower than $W/R \sim 10^5$ which is required for an appreciable shift in ϵ_{Nd}. For the ultramafic rocks the situation is different. Because their Nd concentrations are much lower, hydrothermal alteration causes shifts in ϵ_{Nd} at much lower water-rock ratios. UR-35 has $\epsilon_{Nd} = +5.7$ and $\epsilon_{Sr} = +55.4$ and plots on our mixing line at $W/R \sim 400$. This result appears to be an extreme example of exchange "over the top" of the mixing curve. The data on UR-35 taken in conjunction with those in the mafic trend appear to be explained semi-quantitatively by seawater hydrothermal interactions which have altered both the Nd and Sr systematics. Two other highly serpentinized rocks, a harzburgite and a dunite are shown in Fig. 9. Because of their extremely low Nd concentrations only ϵ_{Sr} was determined. The ϵ_{Sr} for both rocks is close to Siluro-Devonian seawater values. These data along with the arguments presented above strongly suggest that seawater is the agent of serpentinization. All samples discussed so far plot on a mixing curve between unaltered Urals ophiolite rocks and Siluro-Devonian seawater or are compatible with such a model. The mafics plot on the low ϵ_{Sr} part of the mixing line and the ultramafics plot on the high ϵ_{Sr} part of the mixing curve. However, one sample (UR-34) lies far off the mixing line. This is a hornblende-chromite vein rock which has $\epsilon_{Nd} = +4.2$ and $\epsilon_{Sr} = +11.3$. The low ϵ_{Nd} value is particularly enigmatic. Either this rock originally had a lower ϵ_{Nd} than the rest of the unit or ϵ_{Nd} has decreased after crystallization. Since there is no other evidence for primary initial ϵ_{Nd} different from ~ +8, we pursue the second possibility (Fig. 11). All possibilities involve mixing of highly evolved hydrothermal fluids derived from seawater with fresh seawater or seawater that has had only very limited interaction with the oceanic crust. Based on Sr concentrations measured in fluids coming out of mid-ocean ridge hydrothermal vents [30–33], we assume that the generation of hydrothermal fluids from seawater involves no net change in Sr concentration. Similar measurements for Nd indicate that Nd concentrations may greatly increase during this process [34,33]. In our first model we allow Nd concentrations to increase during the generation of the hydrothermal fluid. Seawater is considered to equilibrate isotopically with unaltered ophiolite with an increase in Nd concentration during this process. This hydrothermal fluid mixes with fresh seawater along trajectory 1 (Fig. 11) generating a new hydrothermal fluid with the isotopic composition of UR-34. This composition is reached when the Nd concentration in the first hydrothermal fluid is 1.8 times that of seawater and the ratio of the first hydrothermal fluid to seawater ratio is 0.7. We consider the veins represented by UR-34 to precipitate directly out of this solution. This requires 8×10^5 g of water for each gram of rock precipitated. In our second model, we assume Nd concentrations remain constant during the generation of a hydrothermal fluid. Seawater that has equilibrated with unaltered Urals ophiolite rock mixes with fresh seawater along trajectory 2 (Fig. 11) generating a new hydrothermal fluid which migrates along fractures and exchanges with unaltered Urals ophiolite rock (trajectory 3) creating a solution out of which the veins precipitate. This requires a water-rock ratio of 7×10^5 to generate the solution and 10^6 g of solution for every gram of rock precipitated. Variations of this model are shown by trajectories 4 and 5. Trajectory 4 is a mixing curve between seawater and a hydrothermal fluid which has not completely equilibrated with rock. Trajectory 5 is a mixing curve between a completely equilibrated hydrothermal fluid and seawater which has exchanged only slightly with the ophiolite. In both of these cases veins (such as UR-34) are considered to precipitate directly out of solution and require 10^6 g of water for each

gram of rock precipitated. All of these models require fairly large water/rock ratios. These ratios are plausible, however, for a minor rock type that occurs in veins and may represent precipitates from a solution.

6. Age relationships

Sm-Nd mineral isochrons for UR-24 and UR-11b define ages of 397 ± 20 My and 396 ± 33 My respectively. The fact that most whole rock data for both the massifs fall on this isochron indicates that this represents the igneous crystallization age of the complexes. Both the initial ϵ_{Sr} and initial ϵ_{Nd} show that the igneous rocks from Kempersai and Voykar-Syninsky were derived from an old depleted source. We interpret these observations to mean that these massifs represent sections of oceanic crust. We now compare the crystallization age of this piece of oceanic crust with the age of the collision that produced the Urals (Table 3). Constraints on the age of collision come from paleomagnetic data on major tectonic blocks surrounding the Urals and from geologic observations. We first discuss the paleomagnetic data. Using apparent polar wander paths and paleobiogeographic data, Scotese et al. [35], Smith et al. [36] and Scotese [37] estimated the relative positions of major continental blocks throughout Paleozoic time (see Fig. 12). The bulk of the Soviet data used by these workers was collected by

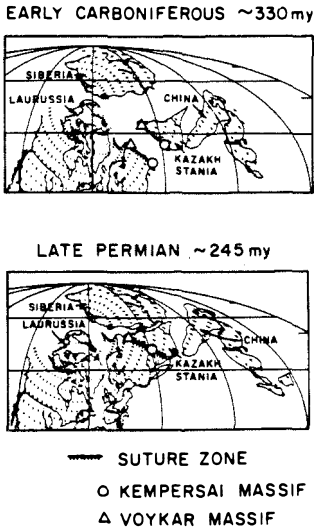

Fig. 12. The positions of Laurussia, Kazakhstania, and Siberia in the early Carboniferous are shown in the upper box. The open circle depicts the future location of Kempersai. The open triangle depicts the future Voykar-Syninsky Massif. The same continents are shown in the lower box but in the late Permian immediately after the collision of Kazakhstania and Laurussia (after Scotese et al. [35]).

Khramov et al. [38]. Typical reported errors at the 95% confidence level for paleomagnetic poles are about 10°. These studies show that in the early Paleozoic, the portion of Eurasia north of the Tethys suture was made up of three major independent blocks: Siberia, Kazakhstania, and

TABLE 3

Age constraints on Urals ophiolites and the Uralian Orogeny

Event	Age	Method
Igneous crystallization of the Kempersai Massif	397 ± 20 My	Sm/Nd internal isochron (this study)
Age of the collision between Kazakhstan and Laurussia	Upper Carboniferous (320 My) to Permian (245 My) [a]	paleomagnetic polar wander paths [35,36,38]
Change from dominantly marine sedimentation to dominantly terrestrial sedimentation in the Urals	Carboniferous/Permian boundary (286 My) [a]	stratigraphic [40]
Cessation of major deformation	by Upper Permian (258 My) [a]	structural-stratigraphic [40]

[a] The paleomagnetic, stratigraphic and structural-stratigraphic age constraints are reported as periods and epochs. We have assigned absolute ages to these epochs (in parentheses) using the geologic time scale of Palmer [41].

Laurussia (Fig. 12). Laurussia is now immediately west of the Urals. Kazakhstania is immediately east of the southern Urals. Siberia is probably immediately east of the extreme northern Urals. The location of the boundary between Kazakhstania and Siberia just east of the Urals is unknown because it is obscured by Mesozoic and Cenozoic cover. Apparent polar wander paths for Siberia and Laurussia are clearly distinct for the early Paleozoic through the lower Devonian. Data for Kazakhstania are lacking for the early Paleozoic, but its lower Devonian pole position is distinct from those of Siberia and Laurussia [35, appendix]. By upper Devonian time, pole positions for Siberia and Laurussia are separated by ~ 20°. This is at the limit of resolution of the data and it is not clear whether these blocks are separated by an ocean or have collided and are a coherent tectonic block [39]. Kazakhstan, however, at this time, still has a pole position which is distinct from the other two blocks. A similar relationship holds for the lower Carboniferous. Poles for Siberia and Laurussia are ~ 15° apart whereas the pole for Kazakhstan is more than 30° from each of these poles. By the late Carboniferous the poles for the three blocks are separated from each other by 15–20°. Late Permian and Triassic poles for the three blocks are within 12° of each other, essentially the same, well within errors of ~ 10° for each pole. Given these data, the following scenario emerges. This is essentially the picture presented by Scotese et al. [35] (see Fig. 12). For the early Paleozoic through the early Devonian, the three blocks were clearly separate. From the late Devonian to the early Carboniferous, Siberia and Laurussia were probably close to each other but still separate. Kazakhstania was clearly separate from the other two. By the late Carboniferous, all three blocks were close to each other. By the late Permian, the blocks had collided and large scale relative motion between the blocks ceased. A conservative interpretation of the paleomagnetic data would be that Laurussia and Siberia collided between the upper Devonian (~ 370 My) and upper Permian (~ 245 My) and that Kazakhstania and Laurussia collided sometime between the upper Carboniferous (~ 320 My) and upper Permian (~ 245 My).

Geologic constraints on the collision age are consistent with the paleomagnetic constraints. These constraints are derived from some basic observations on the structure and stratigraphy of sediments preserved in the Urals [40]. Marine sediments dominate the sedimentary record during the early and middle Paleozoic through the Carboniferous. In the Permian, however, sedimentation was dominantly terrestrial. In the Lower Permian, thick sequences of fluvial conglomerates are developed. These observations are consistent with the presence of a Paleozoic marine basin between Kazakhstania and Laurussia into the Carboniferous. This basin closed by the Permian, creating mountains from which the Permian conglomerates were derived. Pre-Permian sediments in the Urals are folded whereas Upper Permian and younger sediments are either unfolded or only weakly folded. This suggests that the collision that produced the Urals was over by the end of Permian time. A summary of age constraints is presented in Table 3. The igneous crystallization age for Kempersai is clearly older than the age of the collision between Kazakhstania and Laurussia estimated from paleomagnetic data, and the age of the closing of the marine basin between the two blocks, estimated from stratigraphic and structural observations. There is a gap between our crystallization age and the age of the collision of ~ 80 to ~ 150 My depending on the choice of a collision age. Thus, Uralian ophiolites were either obducted onto the Laurussian continental margin as young oceanic crust or were obducted as relatively old oceanic crust during the collision.

7. Obduction model

Our model for the obduction of the Urals ophiolites (Fig. 13) is based on the following three points: (1) ϵ_{Nd} for the metasediment on top of the Kempersai section suggests that there was essentially no input of continental materials into the oceanic basin on top of Kempersai; (2) Kempersai and Voykar-Syninsky presently sit on top of the miogeoclinal sediments of the Laurussian continental margin and clearly must have been transported from the east; (3) we assume that obduc-

402

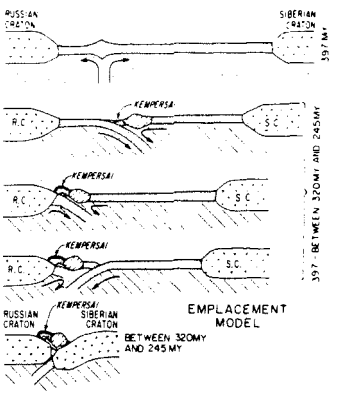

Fig. 13. Obduction model for Urals ophiolites. See text for details.

tion is due to continental underthrusting. The metasediment gives $\epsilon_{Nd} = +9.0$, plots on the Urals Mafic Trend, and the 397 My isochron. This is strong evidence for the protolith coming from an oceanic environment with an age similar to the Urals ophiolites. It is also strong evidence for a lack of continental input into the basin. We assume this result is representative of sediments in the ocean basin above Kempersai and Voykar-Syninsky. This suggests that the ocean basin above the Urals ophiolites was bounded on at least one side by an oceanic terrain such as an island arc. In the present geometry of the Urals, there is no candidate for an arc to the west of the belt of Urals ophiolites, so the arc must have been to its east. The simplest geometry for the ocean basin before obduction must have been from west to east: Laurussian continent, ocean basin containing Kempersai and Voykar-Syninsky, island arc, ocean basin, Kazakhstanian continent. Assuming that continental underthrusting is the mechanism for obduction, we propose the following tectonic history: crystallization occurs at a mid-ocean ridge at 397 My. As the basin starts closing due to subduction from west to east, the future Kempersai and Voykar-Syninsky become part of a fore arc basin. They are obducted onto the Laurussian continental margin due to continental underthrusting. The eastern part of the basin begins to close until Kazakhstania collides with Laurussia sometime between 320 and 245 My ago. The Urals ophiolite belt is preserved in its present position on top of Laurussian continental margin sediments.

8. Conclusions

The conclusions are as follows:

(1) Basic and ultrabasic rocks from Kempersai and Voykar-Syninsky have initial $\epsilon_{Nd}(397\ My) = +8.4$ indicating derivation for an ancient depleted mantle source.

(2) The high ϵ_{Nd}, the ϵ_{Sr} data, and the association of rock types confirms the hypothesis that Kempersai and Voykar-Syninsky represent sections of obducted oceanic crust. These data strongly support the interpretation that the linear belt of mafic-ultramafic complexes along the 2000 km length of the Urals represent samples of Paleozoic oceanic crust.

(3) The Sr isotopic data and the correlation with ϵ_{Nd} indicate extensive alteration by seawater. The ultrabasics with low Nd and Sr concentration show the largest effects of this. Seawater is the agent of uralitisation and saussuritisation in the mafics and the agent of serpentinization in the ultramafics.

(4) Sm-Nd systematics give a 397 ± 20 My crystallization age for Kempersai. This age is consistent with paleomagnetic and geologic age constraints on the age of the collision that produced the Urals. The crystallization age is ~ 80–150 My older than the collision age.

(5) The isotopic composition of a metasediment indicates negligible contribution from continental sources indicating that the Urals ophiolites were associated with an oceanic arc.

(6) $\epsilon_{Nd}(T)$ for the Urals ophiolites in conjunction with Nd data for other ophiolites and Mesozoic MORB suggest that over the past 750 My the MORB source has evolved at a rate less than or equal to its rate of evolution averaged over the age of the earth.

Acknowledgements

The authors wish to thank N.A. Bogdanov and V.L. Barsukov for arranging the field trip to

Kempersai in the fall of 1979 as a part of bilateral scientific exchange. Our knowledge of the southernmost Urals was greatly enhanced by discussions and intellectual discourse with our colleagues A.A. Efimov, N.V. Puchkov, V.R. Schmeliov, N.A. Paneyakh, S.F. Sobolev, S.F. Karpenko, A.A. Marakushev and Galina N. Savelyeva. We hope that this modest effort may provide a token of thanks for the extraordinary opportunity in the field. Robert G. Coleman served as traveling companion and hammer thrower as well as omnipotent ophiolist. He continued to provide valuable discussion on his area of expertise as well as reference material and hospitality to the senior author. N.J (no period) Page generously provided well documented samples which he had collected from the Voykar-Syninsky Ophiolite Complex, shared with us his first-hand knowledge of the geology of the area, and provided reference material that was otherwise unobtainable. This project has benefited from numerous discussions with H.F. Shaw and D.A. Papanastassiou. We thank H.H. Ngo for unselfishly and patiently sharing his time and expertise on chemical procedures. This work has been supported by NSF grant No. EAR83-12882 and an NSF Graduate Fellowship to R.L.E. The functioning laboratory in which this work was carried out was supported by NASA grant No. NAG9-43. Contribution No. 4016 (460).

References

1 A.S. Perfiliev and S.V. Ruzhentsev, Structural position of gabbro-ultrabasic complexes in folded belts, Geotectonics 7, 130, 1973.

2 V.J. Lennykh, A.S. Perfiliev and V.N. Puchkov, Peculiarities of the internal structure and metamorphism of alpine-type ophiolite massifs in the Urals, Geotectonics 12, 255, 1978.

3 V.J. Lennykh, A.S. Perfiliev and V.N. Puchkov, The internal structure and metamorphism of alpine type ophiolitic massifs of the Urals, in: Ophiolites of the Canadian Appalachians and Soviet Urals, IGCP Project 39–Ophiolites, Dep. Geol., Memorial Univ. Newfoundland, Rep. 8, 141, 1979.

4 S.N. Ivanov, A.S. Perfiliev, V.N. Puchkov, S.V. Ruzhentsev and S.G. Samygin, The tectonic position of ophiolites in the Urals, in: Ophiolites of the Canadian Appalachians and Soviet Urals, IGCP Project 39—Ophiolites, Dep. Geol., Memorial Univ. Newfoundland, Rep. 8, 109, 1979.

5 S.N. Ivanov, A.S. Perfiliev, A.A. Efimov, G.A. Smirnov, V.M. Necheukhin and G.B. Fershtater, Fundamental features in the structure and evolution of the Urals, Am. J. Sci. 275-A, 107, 1975.

6 W. Hamilton, The Uralides and the motion of the Russian and Siberian platforms, Geol. Soc. Am. Bull. 81, 2553, 1970.

7 V.S. Burtman, Y.Y. Moldavantsev, A.D. Perfiliev, S.S. Shults, Oceanic crust of the Variscides in the Urals and Tien Shan, Sov. Geol. 3, 23, 1974.

8 A.A. Efimov, V.I. Lennykh, V.N. Puchkov, A.A. Savelyev, G.N. Savelyeva and R.G. Jaseva, Guidebook for excursion, ophiolites of the Polar Urals, in: 4th Field Conference, Moscow, Aug. 1–15, 1978, N.A. Bogdanov, ed., p. 95, 1978.

9 A.A. Savelyev and G.N. Savelyeva, Ophiolites of the Voykar-Syn'insk Massif, Geotectonics 11, 427, 1977.

10 A.A. Savelyev and G.N. Savelyeva, Ophiolites of the Voykar Massif, Polar Urals, in: Ophiolites of the Canadian Appalachians and Soviet Urals, IGCP Project 39—Ophiolites, Dep. Geol., Memorial Univ. Newfoundland, Rep. 8, 127, 1979.

11 N.J Page, P.J. Aruscavage and J. Haffty, Platinum-group elements in rocks from the Voykar-Syninsky ophiolite complex, Polar Urals, USSR, Miner. Deposita 18, 443, 1983.

12 S.S. Gorokhov and V.A. Sharfman, Main Uralian Fault in the southern Urals, Dokl. Akad. Nauk SSSR 149, 38, 1962.

13 V.N. Pavlov, G.G. Kravchenko and I.I. Chuprynina, Khromity Kempersayskgo plutona (Chromites of the Kempersai Pluton), Moscow, 1968.

14 N.A. Bogdanov, B.A. Morgan and N.J Page, Ophiolite complex traversed, Geotimes, p. 22, 1979.

15 A. Knipper, Ophiolite belt of the Urals, IGCP Project "Ophiolites", International Atlas of Ophiolites, Geol. Soc. Am., Map Chart Ser. MC-33, sheet 3, scale 1:250,000, 1979.

16 O. Eugster, F. Tera, D.S. Burnett and G.J. Wasserburg, The isotopic composition of gadolinium and neutron-capture effects in some meteorites, J. Geophys. Res. 75, 2753, 1970.

17 D.J. DePaolo, Study of magma sources, mantle structure, and the differentiation of the earth using variations of $^{143}Nd/^{144}Nd$ in igneous rocks, 360 pp., Ph.D. Dissertation, California Institute of Technology, 1978.

18 D.A. Papanastassiou and G.J. Wasserburg, Rb-Sr ages and initial strontium in basalts from Apollo 15, Earth Planet. Sci. Lett. 17, 324, 1973.

19 D.A. Papanastassiou, D.J. DePaolo and G.J. Wasserburg, Rb-Sr and Sm-Nd chronology and genealogy of basalts from the Sea of Tranquility, Proc. 8th Lunar Sci. Conf., p. 1639, 1977.

20 G.J. Wasserburg, S.B. Jacobsen, D.J. DePaolo, M.T. McCulloch and T. Wen, Precise determination of Sm/Nd ratios: Sm and Nd isotopic abundances in standard solutions, Geochim. Cosmochim. Acta 45, 2311, 1981.

21 D.J. DePaolo and G.J. Wasserburg, Nd isotopic variations and petrogenetic models, Geophys. Res. Lett. 3, 249, 1976.

22 D.J. DePaolo and G.J. Wasserburg, Inferences about magma sources and mantle structure from variations of $^{143}Nd/^{144}Nd$, Geophys. Res. Lett. 3, 743, 1976.

23 S.B. Jacobsen and G.J. Wasserburg, Sm-Nd isotopic evolution of chondrites, Earth Planet. Sci. Lett. 50, 139, 1981.

24 J.M. Williamson, Least squares fitting of a straight line, Can. J. Phys. 46, 1845, 1968.

25 M.T. McCulloch, R.I. Gregory, G.J. Wasserburg and H.P. Taylor, Sm-Nd, Rb-Sr and $^{18}O/^{16}O$ isotopic systematics on an oceanic crustal section: evidence from the Samail Ophiolite, J. Geophys. Res. 86, 2721, 1981.

26 S.B. Jacobsen and G.J. Wasserburg, Nd and Sr isotopic study of the Bay of Islands Ophiolite Complex and the evolution of the source of midocean ridge basalts, J. Geophys. Res. 84, 7429, 1979.

27 S.B. Jacobsen and G.J. Wasserburg, The mean age of crustal and mantle reservoirs, J. Geophys. Res. 84, 7411, 1979.

28 F.A. Frey, D.H. Green and S.D. Roy, Integrated models of basalt petrogenesis: a study of quartz tholeiites to olivine melilites from SE Australia utilizing geochemical and experimental petrological data, J. Petrol. 19, 463, 1978.

29 M.T. McCulloch, R.I. Gregory, G.J. Wasserburg and H.P. Taylor, A neodymium, strontium, and oxygen isotopic study of the Cretaceous Samail Ophiolite and implications for the petrogenesis and seawater-hydrothermal alteration of oceanic crust, Earth Planet. Sci. Lett. 46, 201, 1980.

30 F. Albarède, A. Michard, J.F. Minster and G. Michard, $^{87}Sr/^{86}Sr$ ratios in hydrothermal waters and deposits from the E. Pacific Rise at 21°N, Earth Planet. Sci. Lett. 55, 229, 1981.

31 J.M. Edmond, K.L. Von Damm, R.E. McDuff and C.I. Measures, Chemistry of Hot Springs on the East Pacific Rise and their effluent disposal, Nature 297, 187, 1982.

32 K.L. Von Damm, Chemistry of submarine hydrothermal solutions at 21°N, East Pacific Rise and Guaymas Basin, Gulf of California, 240 pp., Ph.D. Thesis, MIT/WHOI, WHOI-84-3, 1983.

33 D.J. Piepgras and G.J. Wasserburg, Strontium and neodymium isotopes in hot springs on the East Pacific Rise and Guaymas Basin, Earth Planet. Sci. Lett. 72, in press.

34 A. Michard, F. Albarède, G. Michard, J.F. Minster and J.F. Charlon, Rare-earth elements and uranium in high-temperature solutions from East Pacific Rise hydrothermal vent field (13°N), Nature 303, 795, 1983.

35 C.R. Scotese, R.K. Bambach, C. Barton, R. Van der Voo and A.M. Ziegler, Paleozoic base maps, J. Geol. 87, 217, 1979.

36 A.G. Smith, A.M. Hurley and J.C. Briden, Phanerozoic Paleocontinental World Maps, 102 pp., Cambridge University Press, Cambridge, 1981.

37 C.R. Scotese, An introduction to this volume: paleomagnetism and the assembly of Pangea, in: Plate Reconstruction from Paleozoic Paleomagnetism, R. Van der Voo, C.R. Scotese and N. Bonhommet, eds., Am. Geophys. Union, Geodyn. Ser. 12, 1, 1984.

38 A.N. Khramov, G.N. Petrova and D.M. Pechersky, Paleomagnetism of the Soviet Union, in: Paleoreconstruction of the Continents, M.W. McElhinny and D.A. Valencio, eds., Am. Geophys. Union/Geol. Soc. Am., Geodyn. Ser. 2, 177, 1981.

39 E. Irving, Drift of the major continental blocks since the Devonian, Nature 270, 304, 1977.

40 D.V. Nalivkin, Geologiya SSSR, 813 pp., Izdat, Akad. Nauk SSSR, Moscow, 1962.

41 A.P. Palmer, The Decade of N. American Geology 1983 Geologic Time Scale, Geology 11, 503, 1983.

42 G. Choubert and A. Faure-Muret, Geologic World Atlas, 1:10,000,000, sheet 10, Unesco, Paris, 1976.

43 A.V. Peive, S.N. Ivanov, A.S. Perfiliev and V.M. Necheuhlin, Tectonic map of the Urals, 1:1,000,000, 5 sheets, Academy of Sciences of the USSR, Moscow, 1976.

44 A.P. Markovsky, Geologic map of Eurasia, sheets 2, 6, and 9, 1:5,000,000, Ministry of Geology of the USSR, Moscow, 1975.

45 N.P. Kheraskov, The Ebeta Overthrust, South Urals, Geotectonics 5, 214, 1971.

46 H.F. Shaw and G.J. Wasserburg, Sm-Nd in marine carbonates and phosphates: Implications for Nd isotopes in seawater and crustal ages, submitted to Geochim. Cosmochim. Acta, 1984.

47 J. Veizer and W. Compston, $^{87}Sr/^{86}Sr$ composition of seawater during the Phanerozoic, Geochim. Cosmochim. Acta 38, 1461, 1974.

48 W.H. Burke, R.E. Denison, E.A. Hetherington, R.B. Koepnick, H.F. Nelson and J.B. Otto, Variation of seawater $^{87}Sr/^{86}Sr$ throughout Phanerozoic time, Geology 10, 516, 1982.

49 B.-M. Jahn, J. Bernard-Griffiths, R. Charlot, J. Cornichet and F. Vidal, Nd and Sr isotopic compositions and REE abundances of Cretaceous MORB (Holes 417D and 418A, Legs 51, 52 and 53), Earth Planet. Sci. Lett. 48, 171, 1980.

50 S. Claesson, J.S. Pallister and M. Tatsumoto, Samarium-neodymium data on two late Proterozoic ophiolites of Saudi Arabia and implications for crustal and mantle evolution, Contrib. Mineral. Petrol. 85, 244, 1984.

APPENDIX C: ABSTRACTS

The Precise Dating of Holocene and Pleistocene Corals from Mass Spectrometric Determination of ^{230}Th and ^{234}U

R. L. EDWARDS, J. H. CHEN and G. J. WASSERBURG (Div. of Geological and Planetary Sciences, California Institute of Technology, Pasadena, California 91125)

The absolute chronology of the late Pleistocene high sea level stands is based on the dating of uplifted coral terraces using the ^{238}U-^{234}U-^{230}Th system. This chronology has been used in support of the Milankovitch theory. However, this approach has been limited by the analytical uncertainty associated with α-counting measurements. We have therefore developed techniques to measure the ^{230}Th and ^{234}U abundances in corals by isotope dilution mass spectrometry. This has allowed us to significantly reduce the analytical errors in ^{238}U-^{234}U-^{230}Th dating and greatly reduce the sample size. The time range over which useful age data on corals can be obtained ranges from fifty years to ~500ky. Routine analysis on 250mg of coral (~120ky) has an error of ±1ky (2σ) and should allow a critical evaluation of the Milankovitch hypothesis. The age determined on a young coral is 180±5yr which agrees with the age from counting of growth bands and suggests that this approach may be preferrable to ^{14}C analysis for these materials. We found that ^{232}Th contents of these corals were extremely low (0.083 to 1.57 pmoles/g) and were more than two orders of magnitude lower than previous values.

Ages with high analytical precision were determined for several corals from Barbados (123.1±1.1ky) and the New Hebrides (125.5±1.3ky and 129.9±1.1ky) that grew during the last interglacial. These ages lie specifically within or slightly postdate the Milankovitch insolation high at 128 ky and support the idea that the dominant cause of Pleistocene climate change is Milankovitch forcing. The apparent high position of sea level at 129.9ky would require that, as the insolation curve increases, the phase lag between the Milankovitch and sea level curves is small. The youngest age is ~5ky after the insolation peak and suggests that, as the insolation curve decreases, the phase lag is larger.(563)

PRECISE MEASUREMENTS OF $^{234}U/^{238}U$ AND U CONCENTRATIONS IN PROFILES OF PACIFIC AND ATLANTIC WATERS.

EDWARDS, R. Lawrence, CHEN, James H. and WASSERBURG, G. J., Lunatic Asylum, Division of Geological and Planetary Sciences, California Institute of Technology, Pasadena, CA 91125.

High precision measurements of $^{234}U/^{238}U$ ratios and U concentrations in profiles of Atlantic (10 m to 4280 m; 7°44'N, 40°43'W) and Pacific (surface to 4900 m; 14°41'N, 160°01'W) waters have been made in order to determine the degree of heterogeneity of these parameters in the open ocean. The measurements were made possible by the development of mass spectrometric techniques to measure $^{234}U/^{238}U$ to ± ~ 5°/₀₀ (2σ) and U concentrations to ± 2°/₀₀ with 2-5 x 10^9 atoms of ^{234}U. A ^{233}U–^{236}U double spike is used to correct for instrumental mass fractionation. The average $^{234}U/^{238}U$ for 4 samples from the Pacific profile is 144 ± 4°/₀₀ higher than the equilibrium atomic $^{234}U/^{238}U$ ratio (5.47 x 10^{-5}). The average for 5 samples in the Atlantic profile is identical (144 ± 4°/₀₀). A comparison of $^{234}U/^{238}U$ values for samples above and below the thermocline shows similar homogeneity. U concentrations normalized to 35°/₀₀ salinity are the same within ~ 1% (3.215 ± 6 to 3.257 ± 6 ppb) but clearly show variation greater than the ± 2°/₀₀ error. The reason for this fine scale variation requires further investigation. Our data suggest that $^{234}U/^{238}U$ in the open ocean is homogeneous to within ~ 8°/₀₀. This is consistent with the long residence time of U and the long ^{234}U half life compared to the residence time of water in the deep ocean.

Similar measurements on marine pore fluids which can easily be done using our technique should provide constraints on the U flux across the sediment–water interface.

New Timekeepers of Earth Surface Processes in the Pleistocene and Holocene

J. H. CHEN, R. L. EDWARDS, and G. J. WASSERBURG
(Lunatic Asylum, Caltech, Pasadena, CA 91125)

Over the past four decades, there have been many studies of the nuclides in the ^{238}U decay chain, as a means of studying the mobility and transport of actinide elements in nature and addressing dating schemes for a variety of geological processes. While the theoretical aspects of these techniques are well-developed, analytical techniques have centered on the α-counting of ^{234}U and ^{230}Th. It is well-known that measuring all the available nuclides in a sample as compared to counting only the decaying atoms can result in a substantial increase in sensitivity. Such increases in sensitivity are the basis of much of the work now done by accelerator mass spectrometry (^{14}C, ^{10}Be). Previous studies from the laboratory in an effort to search for isotopic anomalies in $^{238}U/^{235}U$ from meteorites have shown that, using mass spectrometric techniques, it is possible to routinely measure this ratio on samples of $\sim 10^{-9}$g of uranium (containing 2×10^{10} ^{235}U atoms) to a precision of ±2°/₀₀ (2σ). We have recently extended these techniques to routinely measure 5×10^{9} atoms of ^{234}U to better than ±5°/₀₀ and 2×10^{10} ^{230}Th atoms to ±2°/₀₀₀. We applied the new mass spectrometric techniques to the study of ^{234}U and ^{232}Th concentrations in seawater. Small samples of 10mℓ seawater for $^{234}U/^{238}U$ and 250mℓ for ^{232}Th yield high precision data ($^{234}U/^{238}U$ to 5°/₀₀) for short data acquisition times of ~1 hr. We also have very precisely dated fossil corals and obtained useful ages between a few years and ~500k.y. The uncertainty in age, based on analytical errors, is ±5y for a 200-year-old coral and ±1k.y. at ~120k.y. This method has greatly reduced the uncertainty associated with conventional α-counting techniques and is performed on much smaller samples. We have obtained highly precise dates for the high sea stands that occurred ~120k.y. ago from coral reefs at several localities in the Pacific and Atlantic. These data are essential to the rigorous testing of the Milankovitch hypothesis of climate variation. (#596)

Sm-Nd and Rb-Sr Systematics of the Kempersai Ultramafic Complex, South Ural Mountains, USSR

R. L. EDWARDS and G. J. WASSERBURG (both at the Calif. Inst. of Tech., Pasadena, CA 91125)

Orogenic belts formed during continent-continent collisions often contain a long linear belt of mafic-ultramafic bodies. We examined the Rb-Sr and Sm-Nd isotopic systematics of one of these suites, the Kempersai Ultramafic Complex, Ural Mtns., USSR, in order to evaluate the hypothesis that these bodies represent fragments of oceanic crust. Sm-Nd systematics for 3 samples give a whole rock and internal isochron age of 377±23 My and an initial $\varepsilon_{Nd} = +8.9 \mp 0.76$. We interpret this as representing the original igneous age. The high initial ε_{Nd} clearly demonstrates the oceanic affinity of the complex and shows derivation from an ancient depleted mantle. Initial ε_{Nd} is ~ 1εu higher than the Bay of Islands Ophiolite Complex (Jacobsen & Wasserburg 1979). The measured $^{87}Sr/^{86}Sr$ in 2 samples give 0.70241±4 and 0.70274±4 corresponding to initial $\varepsilon_{Sr} = -24.5$ and -19.9. This is consistent with the depleted mantle source inferred from the Nd data. For a pillow basalt initial $\varepsilon_{Nd} = +8.6 \pm 0.25$ and measured $^{87}Sr/^{86}Sr = 0.70706 \pm 5$ corresponding to an initial $\varepsilon_{Sr} = +14.1$. This implies contamination by seawater. Initial $\varepsilon_{Nd} = +3.5 \pm 0.39$ for hornblende in a chromite ore from the ultramafic portion of the suite is significantly lower than the initial ε_{Nd} defined by the other samples. Measured $^{87}Sr/^{86}Sr = 0.70490 \pm 3$ corresponding to initial $\varepsilon_{Sr} = +11.0$. Exchange with a metasomatic fluid other than seawater is inferred with large fluid/rock ratios required. We conclude that the Kempersai Ultramafic Complex does represent a segment of oceanic crust. It appears that this segment of crust was formed ~ 100 My before it was obducted during the collision that produced the Urals. Assuming these conclusions may be generalized, our data strongly support the interpretation that the linear belt of mafic-ultramafic complexes along the 2000 km length of the Urals represent samples of Paleozoic oceanic crust. Div. Cont. # 3886 (439).

Sm-Nd AND Rb-Sr SYSTEMATICS OF THE KEMPERSAI AND VOYKAR MASSIFS: EVIDENCE FOR A BELT OF OBDUCTED OCEANIC CRUST IN THE URAL MOUNTAINS, USSR

EDWARDS, R. Lawrence and WASSERBURG, G.J., Div. Geol. and Planet. Sci., California Institute of Technology, Pasadena, Ca 91125

The Urals contain a 2000 km belt of mafic-ultramafic bodies which is represented, in large part, by a series of allochthonous nappes which span Eurasia. We examined the Sm-Nd and Rb-Sr systematics of the Kempersai Massif in the S. Ural Mts. and the Voykar Massif in the Polar Urals. This study confirms the hypothesis that these bodies represent fragments of pre-collision oceanic crust and establishes constraints on the nature and timing of events in the Uralian Orogeny. Two Kempersai gabbros define Sm-Nd internal isochrons of 397±20 MY and 396±33 MY with $\varepsilon_{Nd}(T) = +8.7\mp0.6$ and $+8.4\mp1.3$. Six Kempersai whole rock samples including every major mafic rock type and a metasediment give Sm-Nd values which lie on this isochron. We interpret this age as the original igneous age of Kempersai. Four whole rock samples including the major mafic rock types from the Voykar Massif give Sm-Nd values which lie on or within ~ 1εu of this isochron. This suggests that the crystallization age and $\varepsilon_{Nd}(T)$ is virtually identical to that of Kempersai. The uniform and high $\varepsilon_{Nd}(T) = +8.4$ is consistent with an oceanic affinity for the massifs and shows derivation from an ancient depleted mantle. The fact that a metasediment lies on the isochron indicates its derivation from an oceanic source with negligible continental input. On an ε_{Nd}-ε_{Sr} diagram, ε_{Nd} is constant for the mafics from the two massifs but ε_{Sr} values for the mafics and ultramafics range from -25.2 to +71.1. We interpret the high ε_{Sr} values as being due to exchange of material from an ancient depleted mantle source with seawater. We conclude that the long belt of mafic-ultramafic rocks in the Urals, which includes the Kempersai and Voykar Massifs, represents segments of Siluro-Devonian oceanic crust. Our igneous age for Kempersai in conjunction with other age constraints suggests that these segments of oceanic crust formed ~ 120 MY before the collision that produced the Urals. Div. Cont.#4114(489)

R. LAWRENCE EDWARDS and G.J. WASSERBURG, California Institute of Technology, Pasadena, CA USA

Sm-Nd AND Rb-Sr ISOTOPIC SYSTEMATICS OF THE KEMPERSAI ULTRAMAFIC COMPLEX, SOUTH URAL MTS., USSR

Orogenic belts formed during continent-continent collisions often contain a long linear belt of mafic-ultramafic bodies. In the Urals this belt is represented, in large part, by a series of allochthonous nappes which span the Eurasian continent from the Kempersai Ultramafic Complex in the S. Ural Mountains to the Voykar Massif in the Polar Urals (Ivanov et al, 1979; Ruzhentsev and Samygin, 1979; Savelyev and Savelyeva, 1979; Lennykh et al, 1979; Burtman et al, 1973). Through the courtesy and cooperation of the Academy of Sciences of the USSR, we were able to collect samples from the Kempersai Ultramafic Complex. We examined the Rb-Sr and Sm-Nd isotopic systematics of Kempersai in order to evaluate the hypothesis that these mafic-ultramafic bodies represent fragments of pre-collision oceanic crust.

The Kempersai Massif is a 35 km by 70 km nappe with a harzburgite-rich ultramafic core and limbs composed of troctolite, gabbro, diabase, pillow basalt, and metasediments. Mineral separates from a pegmatitic gabbro define an Sm-Nd internal isochron of 385±32 My and an initial ϵ_{Nd}=+8.5∓1.3. Six whole rock samples including every major mafic rock type and the metasediment, give Sm-Nd values which lie on this isochron. We interpret this age as the original igneous age. The uniform and high initial ϵ_{Nd} is consistent with an oceanic affinity for the complex and shows derivation from an ancient depleted mantle. Initial ϵ_{Nd} is ~1 ϵ unit higher than the Bay of Islands Ophiolite Complex (Jacobsen and Wasserburg, 1979). The fact that the metasediment lies on the isochron, indicates derivation from an oceanic source with negligible continental input.

On an ϵ_{Nd}-ϵ_{Sr} diagram, ϵ_{Nd} values for the mafics are constant ~+8.5, but ϵ_{Sr} values are variable. The measured $^{87}Sr/^{86}Sr$ in three of the mafic samples are 0.70241±4, 0.70274±4, and 0.70225±3 corresponding to initial ϵ_{Sr} = -19.4, -19.9 and -25.7. This is consistent with the depleted mantle source inferred from the Nd data. The other mafic samples have more radiogenic $^{87}Sr/^{86}Sr$ values that range up to a measured $^{87}Sr/^{86}Sr$ of 0.70706±5 for a pillow basalt. This corresponds to an initial ϵ_{Sr} = +14.1. We interpret these radiogenic values as being due to seawater contamination and calculate a water-rock ratio for the pillow basalt of ~30.

Samples collected from the ultramafic portion of the suite have also been examined. A highly serpentinized olivine-chromite ore with a Nd concentration of 6.2 ppb, has an initial ϵ_{Nd} = +5.7 and a measured $^{87}Sr/^{86}Sr$ = 0.70824±71 corresponding to initial ϵ_{Sr} = +47.7. We suggest that mixing with seawater has disturbed both the Sm-Nd and Rb-Sr systems and calculate a water-rock ratio of ~250. A highly serpentinized harzburgite and a serpentinized dunite have measured $^{87}Sr/^{86}Sr$ = 0.70956±5 and 0.70801±16 corresponding to initial ϵ_{Sr}=+65.4 and +52.7. These values are consistent with our hypothesis of seawater contamination and suggest that seawater is the agent of serpentinization in these rocks. Nd and Sr isotopic characteristics of a hornblende-chromite vein suggest local metasomatism by highly evolved fluids.

We conclude that the Kempersai Ultramafic Complex does represent a segment of oceanic crust. In order to generalize these results, we are investigating the Voykar Massif in the Polar Urals to see if it exhibits similar isotopic characteristics. Our igneous age for Kempersai, in conjunction with paleomagnetic and geologic age constraints, suggest that this segment of oceanic crust was formed ~100 My before the collision that produced the Urals. Assuming these conclusions may be generalized, our data strongly support the interpretation that the linear belt of mafic-ultramafic complexes along the 2000 km length of the Urals represent samples of Paleozoic oceanic crust.

Div. Cont. #3966 (451)